DISS. ETH NO. 24669

ELECTROCHEMICAL DURABILITY MONITORING IN REINFORCED CONCRETE

A thesis submitted to attain the degree of

DOCTOR OF SCIENCES of ETH ZURICH

(Dr. sc. ETH Zurich)

presented by

YURENA SEGUÍ FEMENIAS

M.Sc. Industrial Engineering, Universitat Politècnica de Catalunya (UPC)

born on 11.01.1987

citizen of Spain

accepted on the recommendation of

Prof. Dr. Bernhard Elsener, examiner

Prof. Dr. Ueli Angst, co-examiner

Prof. Dr. Rob Polder, co-examiner

2017

ACKNOWLEDGEMENTS

The Swiss National Science Foundation (SNF) is kindly acknowledged for financing this work. The Swiss Federal Laboratories for Materials Science and Technology (EMPA) is also appreciated for certain laboratory equipment used in this work.

Many people have contributed to this work. First of all, I would like to thank my main thesis supervisor, Bernhard Elsener, for accepting me as PhD student; sharing with me his wide knowledge; and providing valuable technical, professional, and personal advice through these years. I also want to express my gratitude to my thesis co-supervisor, Ueli Angst, for his excellent and caring guidance. Both Bernhard Elsener and Ueli Angst placed enormous confidence in my work and greatly contributed to it with many valuable discussions and inspiring inputs. I would also like to thank them for their unconditional support over the years, which turned into a truly rewarding experience for myself.

I have also benefited a lot from former members of my research group, Francesco Caruso and Prannoy Suraneni, who provided valuable input to my work. Francesco Caruso has been a true mentor in questions related to chemistry and laboratory work. I want to thank Prannoy Suraneni for his profound support and for the numerous very inspiring discussions and insightful remarks.

I also want to thank all the members of the PCBM research group for creating a wonderful working environment. First, I would like to thank Robert Flatt, for being an excellent leader of this group, both at a professional and at a personal level, and for giving me first the opportunity to be a part of it. I also want to acknowledge Andrea Louys, Heinz Richner, Andreas Reusser and Köbi Scherrer, for their important contribution to the beautiful atmosphere we have in this research group. I am grateful to Sara Mantellato for her unconditional friendship and support over the years, providing many meaningful experiences. I also want to thank Timothy Wangler, for his advice, both technical and personal, and specially for his personal support. I should also thank Asel Maria Aguilar, for our valuable inspiring conversations about life, and for being part of my family in Switzerland. I must also thank Ana Vallejo and Thibault Demoulin, for our “games nights” and sports events, which turned into fun experiences and a solid friendship. I also want to acknowledge Marta Palacios, Ylenia Praticò, Matteo Stefanoni, Giulia Gelardi, Federica Boscaro, and Carolina Boschmann for their special help and support.

I would also like to acknowledge my friends in Switzerland outside of ETH. In particular, I want to thank Simone Von Ah, Marco Vario, Alexis Leibbrandt, Nenad Tripic, Shut-ting Wang, Yurate Plyushkyavichyute, and Felicia Constandopoulos for being part of my family in Switzerland. I am also grateful to my friends from Spain, particularly to Emma Martínez, Joan Noguera, Bibiana Siscart, Núria Farrerons, Marta Cudeiro, Ares Sanjuan, and Tonia Prats, for always providing special moments.

I specially want to thank Tim Schöler: my best friend, my mentor, my inspiration, and my partner in so many aspects of my life. I want to thank you for constantly reminding me of the things that are essential in life. This work would have not been the same without you.

Finally, I want to thank my family for their support over the years and for making many sacrifices to give me all possible choices and opportunities in life. I specially want to thank my father, who has been the most hard working person I have ever known; this work has also been possible because of him.

ABSTRACT

Corrosion of the steel reinforcement is one of the most widespread degradation mechanisms in reinforced concrete structures. In addition to loss in serviceability and structural damage, corrosion costs constitute a major part of the costs of the infrastructure. To tackle this issue, maintenance and repair of structures should be performed at early ages; this requires information on pH and chloride content of the concrete pore solution and on the corrosion state of the steel. Potentiometric measurements between pH or chloride sensors and a reference electrode are the basis for this, but accurate potential measurements are difficult because reference electrodes to be embedded in concrete are affected by changes in pH and chloride concentration. In addition, while chloride sensors (e.g. Ag/AgCl ion-selective electrodes) are state of the art, a long-term stable pH sensor to be embedded in concrete is not available.

In this thesis, an electrode system to be embedded in concrete, composed of several chloride sensors (Ag/AgCl ISEs) and pH sensors (Iridium/Iridium oxide (IrO_x) electrodes) has been developed and tested. The results showed that Ag/AgCl ISEs and IrO_x electrodes allow monitoring the chloride concentration and the pH respectively in concrete in-situ over time. This is only possible when the measured sensors potentials are corrected for diffusion potentials arising between the sensors and the reference electrode due to gradients in chloride concentration and/or pH. For this task, an algorithm has been developed. Additionally, when applying the correction for the diffusion potentials, the sensors can be used as reference electrodes.

The new pH sensors operate reliably in a pH range of 9 to 13.5 with an accuracy of ± 0.5 pH units, in this work up to ca. 2 years in alkaline solutions and 6 months in concrete. The sensors allowed for the first time to follow carbonation (4% CO_2, 65% RH) of mortar samples made of Ordinary Portland Cement (w/c 0.5). It was found that the pH of the pore solution first decreases to about 12.5 (region of the $Ca(OH)_2$ buffer), remains constant at that pH for a long time and drops rapidly to about pH 9 afterwards. Whereas the time to reach pH 9 coincides with the usual tests of the carbonation front with indicators sprayed on the freshly split concrete surface, the time to reach the “early carbonation front” of pH 12.5 is reached about 3 times faster.

The possibility to continuously monitor pH (and chloride concentration) in the concrete pore solution is a result of high scientific relevance that has implications in corrosion of steel in concrete. Scientifically, the kinetics of carbonation can now be studied in detail because information about the pH of the pore solution can be obtained continuously and non-destructively. This will also allow studying the carbonation of new blended cements with a reduced clinker content. It is expected that the time during which the pH remains constant at ca. 12.5 can be related to the buffer capacity of concrete. A drop of the pH to 12.5 in “un-carbonated” concrete has severe implications on chloride induced corrosion: a pH decrease from 13.5 to 12.5 at the reinforcement means that the chloride threshold to induce pitting corrosion is about ten times lower. This could not be verified so far because on site investigations only provide the chloride content but not the pH – and laboratory tests usually are too short to reach significant carbonation. It might be that one of the causes of the wide scatter in the “critical chloride content” could be the variable pH at the reinforcement level that was not measured.

ZUSAMMENFASSUNG

Die Korrosion der Stahlbewehrung ist einer der häufigsten Schadensmechanismen von bewehrten Betonbauten. Neben einer abnehmenden Gebrauchstauglichkeit und den entstehenden Schäden an der Konstruktion führt Korrosion zu großen Kosten in der Infrastruktur. Um diesem Problem entgegen zu wirken, sollte die Planung von Instandhaltung und –setzung auf Informationen zum pH-Wert und zum Chloridgehalt der Porenlösung im Beton und zum Korrosionszustand des Stahls beruhen. Die Grundlage dazu sind potentiometrische Messungen zwischen pH- bzw. Chloridsensoren und einer Referenzelektrode. Exakte Messungen sind jedoch schwierig, da die Referenzelektroden ebenfalls einbetoniert sind und deshalb von Aenderungen des pH-Werts und des Chloridgehalts beeinflusst werden. Hinzu kommt, dass zwar Chloridsensoren (z.B. Ag/AgCl ionenselektive Elektroden) Stand der Technik sind, aber zur Zeit keine langzeitstabilen pH-Sensoren zur Anwendung im Beton existieren.

Im Zuge dieser Doktorarbeit wurde ein Elektrodensystem, bestehend aus verschiedenen pH-Sensoren (Iridium/Iridium oxide (IrO_x) und Chloridsensoren (Ag/AgCl ISEs), zur Anwendung in Beton entwickelt und getestet. Die Ergebnisse zeigen, dass die hier verwendeten Sensoren es ermöglichen, den Chloridgehalt bzw. den pH-Wert im Beton über die Zeit zu messen. Dies ist nur möglich wenn die an den Sensoren gemessenen Potentiale um die zwischen der Referenzelektrode und den Sensoren auftretenden Diffusionspotentiale, entstehend aufgrund des unterschiedlichen Chloridgehalts und/oder pH-Werts, korrigiert werden. Zu diesem Zweck wurde ein iterativer Algorithmus entwickelt. Eine wichtige Folgerung ist, dass potentiometrischen Messungen ohne Korrektur des Diffusionspotentials zu fehlerhaften Ergebnissen führen würden. Des Weiteren können durch die vorgenommene Korrektur die Sensoren als Referenzelektroden genutzt werden.

Die neuen pH-Sensoren funktionieren zuverlässig in einem pH-Bereich von 9 bis 13.5 mit einer Genauigkeit von ± 0.5. Dies wurde in der vorliegenden Doktorarbeit über 2 Jahre in alkalischen Lösungen und 6 Monate in Beton getestet. Die eingebauten Sensoren erlaubten erstmals die Kinetik der Karbonatisierung (4% CO_2, 65% RH) von Mörtelproben aus herkömmlichen Portlandzement (w/z 0.5) zu erfassen. Dabei zeigte sich, dass der pH-Wert in der Porenlösungen des Betons zunächst auf etwa 12.5 (im Bereich des $Ca(OH)_2$ Puffers) absinkt, dann für längere Zeit konstant auf diesem pH-Niveau bleibt, um anschließend stark abzufallen auf ca. pH 9. Die gemessene Zeit um einen pH-Wert von etwa 9 zu erreichen

stimmt überein mit den üblichen Tests für die Karbonatisierungstiefe, bei denen Indikatorenlösungen direkt auf die Oberfläche von frisch gespaltenem Beton appliziert werden. Ein pH Wert von 12.5 (“frühe Karbonatisierung”) wurde ungefähr 3-mal schneller erreicht.

Die Möglichkeit, den pH-Wert (und den Chloridgehalt) in Porenlösungen von Beton kontinuierlich überwachen zu können, ist von großer wissenschaftlicher Relevanz und hat auch Auswirkungen auf die Korrosion der Bewehrung in Beton. Für die Forschung bedeutet dies, dass der Karbonatisierungprozess jetzt genauer untersucht werden kann, da die bis dato immer fehlende Information über den pH-Wert der Porenlösung nun kontinuierlich und ohne destruktiven Eingriff verfügbar ist. Das erlaubt es nun insbesondere die Karbonatisierung von Beton mit neuen Zementmischungen mit reduziertem Klinkeranteil zu untersuchen. Es wird erwartet, dass die Verweildauer bei etwa pH-Wert 12.5 mit dem der Pufferkapazität des Zements korreliert. Der Abfall des pH-Werts auf 12.5 in „unkarbonatisiertem“ Beton hat grosse Auswirkungen auf die chlorid-induzierte Korrosion: eine pH-Wert Reduktion von 13.5 auf 12.5 unmittelbar an der Stahlbewehrung bedeutet, dass der tolerierbare Chloridgehalt, um Lochfrasskorrosion auszulösen, etwa 10-mal geringer ist. Dies konnte bisher nicht nachgewiesen werden, da Untersuchungen auf der Baustelle nur den Chloridgehalt, nicht aber den pH-Wert messen konnten – in Labortests hingegen ist der Untersuchungszeitraum meist zu kurz, um signifikante Karbonatisierung zu erreichen. Möglicherweise ist diese Variation des pH Wertes an der Bewehrung einer der Gründe für die grosse Streuung des „kritischen Chloridgehalts“ im Stahlbeton“.

TABLE OF CONTENTS

APPENDICES

This thesis includes the following six appended documents, composed by five papers and one appendix.

Paper I:

Ag/AgCl ion-selective electrodes in neutral and alkaline environments containing interfering ions

Y. Seguí Femenias, U. Angst, F. Caruso, B. Elsener (2015)

Materials and Structures 49, 2637–265. doi: 10.1617/s11527-015-0673-8.

Paper II:

Monitoring chloride concentrations in concrete by means of Ag/AgCl ion-selective electrodes

Y. Seguí Femenias, U. Angst, B. Elsener (2015)

In *ICCRRR - International Conference on Concrete Repair, Rehabilitation and Retrofitting*, Leipzig

Paper III:

Monitoring pH in corrosion engineering by means of thermally-produced iridium oxide electrodes

Y. Seguí Femenias, U. Angst, B. Elsener (2017)

Materials and Corrosion, 1-13. doi: 10.1002/maco.201709715.

Paper IV:

PH-monitoring in mortar with thermally-oxidized iridium electrodes

Y. Seguí Femenias, U. Angst, B. Elsener (2017)

RILEM Technical Letters (submitted)

Paper V:

Durability monitoring of reinforced concrete

Y. Seguí Femenias, U. Angst, B. Elsener (2017)

In *SMAR 2017 - International Conference on Smart Monitoring, Assessment and Rehabilitation of Civil Structures*, Zürich (accepted)

Appendix:

Sensor system embedded in mortar exposed to chloride and CO_2 ingress

SYMBOLS AND ABBREVIATIONS

Symbol	Meaning	Usual dimensions
a	Activity	-
Ag/AgCl/sat.KCl	Silver/silver chloride/saturated potassium chloride (reference electrode) ca. +199 mV vs. standard hydrogen electrode	
C–S–H	Calcium silicate hydrates	
CH	Portlandite	
E	Electrochemical potential	V
E^0	Standard electrode potential	V
E_0	Electrode equilibrium potential	V
E_{corr}	Corrosion potential	V
ESEM	Environmental scanning electron microscopy	
F	Faraday constant	96 485 $C \cdot mol^{-1}$
I	Current	A
i	Current density	$A \cdot m^{-2}$
i_{corr}	Corrosion current density (corrosion rate)	$A \cdot m^{-2}$
ISE	Ion-selective-electrode	
$K_{i,j}$	Selectivity coefficient	-
K_{sp}	Solubility product	-
OCP	Open Circuit Potential	
OPC	Ordinary Portland Cement	
R	Molar gas constant	8.314 $J \cdot mol^{-1} \cdot K^{-1}$
RE	Reference electrode	
RH	Relative humidity	%
SCE	Saturated Calomel Electrode (reference electrode) ca. +244 mV vs. standard hydrogen electrode	
SEM	Scanning electron microscopy	
SHE	Standard Hydrogen Electrode	
SCMs	Supplementary Cementicios Materials	
T	Temperature	K
u	Ionic mobility	$cm^2 \cdot V^{-1} s^{-1}$
w/c	Water-to-cement ratio	-
WE	Working electrode	

1 INTRODUCTION

Reinforced concrete is one of the most common materials used in civil engineering worldwide. It is used in the construction of transportation structures, e.g., bridges, tunnels, parking garages, etc., and in many public and private buildings. The main benefits of this material are the wide availability of the raw materials required for its fabrication, the relative low costs compared to other materials (e.g., metals), and the overall good durability of the built structures.

Reinforced concrete structures are subjected to many degradation processes. Among them, corrosion of the reinforcing steel is considered as the major cause of degradation of concrete structures in many parts of the world [1]. Owing to the high alkalinity provided by the cement hydration products (pH 12.5-13.5), steel reinforcement is protected from corrosion by an oxide layer, i.e., the passive film, formed on its surface. However, this passive layer can become unstable due to the carbonation of the cement paste or in the presence of chlorides. Carbonation is the reaction of the alkaline constituents in the concrete pore solution with carbon dioxide from the environment, which leads to a decrease of the alkalinity of the concrete. Chlorides may be present in the raw materials, e.g., chloride-contaminated cement or when using sea-dredged aggregates, or they can penetrate at later stages when the structure is exposed to chloride-bearing environments, such as seawater or deicing salts. Both processes can lead to the breakdown of the passive layer and result in corrosion initiation. Corrosion of the steel reinforcement leads to the loss of rebar cross section and to a decrease in the load-bearing capacity of the structure and in many cases, in spalling of the concrete cover. This will affect both serviceability and safety of the structure.

In addition to the structural damage, dealing with corrosion is very costly and has a major impact on the economies of industrial countries. At present, inspection and maintenance costs of reinforced concrete structures have grown to such extent that they constitute a major part of the costs of the infrastructure [2, 3], e.g., traffic delay costs due to inspection and maintenance of concrete infrastructures have been estimated to be between 15 and 40% of the construction costs [2]. In fact, the annual costs related to corrosion constitute a significant part of the gross national product in the OECD (Organization for Economic Cooperation and Development) countries. For example, cost of corrosion was estimated to ca. 3% of U.S. Gross Domestic Product (GDP) in 1998 [4]. That year, approximately 15% of the existing bridges were found structurally deficient, primarily due to corrosion of steel reinforcement, resulting in

a rehabilitation cost for bridge decks of $3.2 billion [4]. In 2013, the global cost of corrosion was estimated to be 3.4% of the global GDP. In Switzerland, the annual costs for repair and maintenance of the national highway system increased from ca. SFr. 250 in 1995 to ca. 770 millions in 2010 [5]; form these costs, corrosion of the reinforcing steel is a significant contributor [6].

Corrosion detection methods are usually based on routine visual inspections of structures [3, 7]. This approach usually allows identifying the location where damage takes place, but not necessarily at the right time, i.e., corrosion is usually detected when a significant amount of damage has developed and the costs of repair are high [3, 8]. It is estimated that savings between 15 and 35% of the corrosion cost could be obtained if good and appropriate practice maintenance are applied at early ages [8]. Damage detection at early ages would allow, for example, optimization of concrete repairs, scheduling of building inspections and maintenance programs, and the minimization of traffic delays. Additionally, maintaining structural safety would be significantly improved.

Monitoring systems based on embedded sensors are the basis for early detection of corrosion. This approach allows obtaining continuous information at certain specific locations in a non-destructive manner, providing advance warning for corrosion. In this context, sensors to monitor pH and chloride concentration of the pore solution are especially important, as the (invisible) ingress of aggressive substances can be continuously monitored and the risk of corrosion initiation determined. With this information, remedial actions can be taken well before damage appears and corrosion onset can be delayed [3]. Additionally, the data obtained could also be used as input for service life prediction models, resulting in a further improvement of corrosion prediction and protocols for the condition assessment of structures.

Many of the current corrosion monitoring techniques are based on the measurement of the electrochemical potential of the reinforcing steel in concrete compared to that of a reference electrode. Thus, various attempts to develop embeddable reference electrodes for concrete have been made. Some of these approaches provided satisfactory results for certain applications but most of the existing electrodes exhibit potential drifts, derived from changes in chloride concentration and pH, to the extent that even relatively tolerant applications (e.g. monitoring steel potential) may be impaired under certain conditions [9]. Sensors to monitor chlorides and pH in concrete have also been developed. Most of the current methods are based on a potentiometric measurement, where stability requirements for the reference

potential are particularly high and must be satisfied over long periods of time, e.g. at least for several decades, as the processes leading to corrosion initiation are slow. At present, no embeddable reference electrode exists that fulfills the desired stability criteria that allow the application of these sensors in the field.

This thesis contributes to developing long-term stable sensors to be embedded in concrete. Based on the obtained results, an electrode system based on several embedded pH and chloride sensors is proposed. An algorithm is developed that allows obtaining reliable long-term electrode potential response, together with pH and chloride profiles over time. The application of the proposed electrode system is expected to improve many aspects related to durability of reinforced concrete. In particular, this electrode system improved corrosion monitoring and allowed obtaining a better inside on the mechanism of carbonation.

2 OBJECTIVES

The main objective of this thesis is to develop an embeddable electrode system that is able to provide a long-term stable reference potential and to accurately monitor changes in pH and chloride concentration in reinforced concrete structures.

2.1 Long—term stable embeddable reference electrode system

The current embeddable reference electrodes for field use have been proven to be accurate on the long-term only when the pH and the chloride concentration remain relatively constant. When the pore solution composition changes, potential drifts that are difficult to recognize occur, mainly due to diffusion potentials. This leads to measurement errors that impair the correct interpretation of the results obtained, for example, with potentiometric sensors.

The present project aims at developing an embeddable reference electrode system that is able to provide a long-term stable reference potential in concrete, even if the pH or the chloride concentration are changing. The proposed solution is based on the combination of chloride and pH sensors embedded at different depths. The potential measurement between the different sensors allows identifying changes in chloride concentrations and pH at the different locations. As a result, the diffusion potentials established between the electrodes can be calculated and the electrode potential can be correctly evaluated. This requires an algorithm.

2.2 Monitoring free chloride concentration of the concrete pore solution

To detect changes in the chloride content in concrete, reliable chloride sensors are needed. Ag/AgCl ion-selective electrodes (ISEs), i.e., electrodes that exhibit a potential response as a function of the activity of chloride ions, are already used in-situ. However, it is not known how the presence of interfering species (e.g. sulfides, hydroxides) or the concrete alkaline environment in absence of chlorides affect the sensor response.

This work aims at improving the understanding of chloride ion-selective electrodes when embedded in concrete. This involves the identification and evaluation of the main error sources, such as the long-term stability in alkaline environments and the sensitivity to interfering ions that may be present in concrete and in chloride-bearing environments.

2.3 Monitoring pH of the concrete pore solution

The reference electrode potential may be affected by changes in pH. However, a non-destructive method for monitoring the pH of the pore solution does not yet exist. To tackle this issue, thermally oxidized iridium (IrO_x) electrodes are produced in this work. These electrodes shall be prepared and used as pH sensors embedded in concrete. To achieve this aim, the production protocol, conditioning, and potential response of these electrodes in alkaline solutions of different pH is studied. Additionally, the pH of the pore solution shall be monitored during exposure of the cement paste to CO_2 ingress(carbonation).

3 THEORETICAL BACKGROUND

3.1 Concrete

Concrete is a material composed of aggregates (sand and gravel) and the reaction product of cement and mixing water, i.e., the *cement paste*. Additionally, reinforcing steel bars are usually embedded in concrete in order to improve the mechanical properties of the material, e.g., the tensile strength and ductility.

The reaction between cement and water is termed *cement hydration* and it leads to the transformation of the initially fluid cement paste into a solid, which gains strength over time. The transformation from fluid to solid is known as *setting*, whereas the subsequent strength gain is known as *hardening*. The nature of the porosity (see sections 3.1.3 and 3.1.4) and composition of the cement paste determine most of the properties of the hardened concrete and thus, the durability and performance of the material.

3.1.1 Cement hydration

Cements are finely ground inorganic powders that set and develop strength by reacting with water. The main cement used in civil engineering is known as Ordinary Portland Cement (OPC) [10, 11].

The chemical composition of Portland cement is complex, and it consists of various oxides [10, 11]. The four main phases of the clinker are tricalcium silicate, $3CaO{\cdot}SiO_2$ (C_3S in cement notation); dicalcium silicate, $2CaO{\cdot}SiO_2$ (C_2S in cement notation); tricalcium aluminate, $3CaO{\cdot}Al_2O_3$ (C_3A in cement notation); and tetracalcium ferroaluminate, $4CaO{\cdot}Al_2O_3Fe_2O_3$ (C_4AF in cement notation). Other components, such as sodium and potassium oxides, are present in small and variable amounts. Additionally, calcium sulfate (usually in the form of gypsum, $CaSO_4{\cdot}2H_2O$, $C\bar{S}H_2$ in cement notation) is added to control the rate of hydration of the aluminate phases.

Hydration of the calcium silicate phases leads to two products: calcium hydroxide (also known as portlandite, denoted CH in cement notation), and calcium silicate hydrate (C–S–H in cement notation). Portlandite occupies 20-25% of the volume of solids of fully hydrated Portland cement paste and it does not contribute significantly to the strength, but its presence is very important because it contributes, together with NaOH and KOH, to the high pH of the pore solution, e.g., in the rage of pH 13-14 [10-15]. Portlandite is additionally the main source

of the alkali reservoir at pH≈12.5. C–S–H is an amorphous gel-like substance with variable chemical composition. It is the phase with the highest contribution to the strength development [10, 11]. Hydration of the aluminate phases in the presence of gypsum leads to two broad classes of products [10, 11]: Aft, that denotes the family of minerals referred to as aluminate ferrite tri-sulfate; and AFm, that denotes the family of minerals referred to as aluminate ferrite monosulfate.

3.1.2 Blended cements

Blended cements are obtained by blending Portland cement with particular mineral admixtures. As a result, the CO_2 emissions associated with the production of Portland cement can be significantly decreased [16, 17]. The most common mineral admixtures, also called supplementary cementitious materials (SCMs), currently used are [10, 11]:

- *Pozzolanic Materials*: they can be either natural, like pozzolana, or artificial, like fly ash and silica fume. They are mainly glassy siliceous materials that may contain aluminous compounds and a low amount of lime (calcium hydroxide). The reaction between pozzolanic materials, calcium hydroxide (provided mainly by the hydration of Portland cement), and water is known as the *pozzolanic reaction* and the main product of this reaction is C–S–H. The result is a material with a lower content of calcium hydroxide and a higher amount of C–S–H, compared to OPC. In addition, pozzolanic additions usually provide a denser cement microstructure with smaller pore sizes;

- *Ground Granulated Blast Furnace Slag (GGBFS):* it is a byproduct of the production of iron. Like Portland cement, it is composed of lime, silica, and alumina, although in different proportions compared to OPC. This admixture acquires hydraulic properties if it is quenched. Its presence refines the pore structure of the cement paste;

- *Limestone*: it is obtained from the fine grinding of limestone and it contains a high amount of calcium carbonate $CaCO_3$. It has a filler effect when used in cement, especially when finely ground, e.g., particles smaller than cement grains. Its reactivity is very limited.

Cement paste obtained with addition of these mineral admixtures differs considerably from pastes with Ordinary Portland Cement. These admixtures usually lead to a denser paste microstructure and lower alkalinity (see section 3.3.5) [10, 11].

Classification

According to the European standard EN 197-1 [18], the following cement types can be distinguished:

- CEM I (*Portland cement*): it contains at least 95% of Portland clinker;
- CEM II (*Portland-composite cements*): it contains additions up to 35% of another constituent (GGBFS, pozzolanic materials, limestone, etc.);
- CEM III (*blast furnace cement*): it contains 36–95% of blast furnace slag;
- CEM IV (*pozzolanic cement*): it contains 11–55% of pozzolanic materials;
- CEM V (*composite cement*): it contains simultaneous addition of slag (18–50 %) and pozzolanic materials (18–50 %).

Other types of Cement

Other types of cement than those described above also exist for special uses. These are, for instance: low heat cements, calcium aluminate cements, sulfate-resisting cements, expansive cements, quick setting cements, white or coloured cements, etc. [11].

3.1.3 Pore structure

The cement paste formed by the hydration reactions contains interconnected pores of different sizes [11, 19]. The volume of hydrates is lower than the cumulated volume of cement and water (*chemical shrinkage*); this difference in volume leads to the formation of pores. Upon mixing of cement and water, water fills the space between cement particles but as hydration proceeds, hydration products fill this space, reducing the volume of pores and their connectivity.

Depending on the size, pores can be divided into gel, capillary, and macro pores [11, 19]. Gel pores correspond to the interlayer spacing within C–S–H and they are a few nanometers in size. Capillary pores correspond to the volume fraction of cement paste filled with excess water that can evaporate upon contact of the concrete with the atmosphere. The size of the capillary pores ranges from ca. 10 nm to a few μm and it mainly depends on the water-to-cement ratio (w/c) and the degree of hydration. Macro pores usually correspond to entrapped air bubbles or voids originating from incomplete compaction during concrete mixing and

casting. The dimensions of these pores can be up to a few millimeters in size. Additionally, cracks are also likely to be present in concrete structures, for example, owing to static or dynamic loads; as the result of thermal gradients during the hardening stage; due to drying or autogeneous shrinkage, etc.

Finally, it should be noted that the porosity of cement paste may differ from one concrete to another. One of the reasons for that is the variation in cement paste properties between bulk paste and the zone adjacent to the aggregates, i.e., the interfacial transition zone [20], or at the interface between reinforcing steel and cement paste [21, 22].

3.1.4 Durability aspects

Gases (e.g. CO_2) and liquids (e.g. water, in which various ions can be dissolved) can ingress through the pores of concrete. In this context, the *permeability of concrete* can be defined as the extent to which transport of liquids and gases occur.

It is believed that gel pores do not contribute significantly to transport processes. In contrast, permeability increases markedly and non-linearly with an increase in the number of capillary pores and their connectivity, since the transport of aggressive agents becomes facilitated [19, 23]. As the capillary pore system loses its connectivity, the rate of transport becomes more limited, as it is more controlled by the small gel pores.

In this context, the denser microstructure provided by blended cements [10] compared to Ordinary Portland Cement may be beneficial for durability aspects, such as the ingress of aggressive agents that lead to corrosion initiation (see 3.3.6 sections and 3.3.10).

3.2 Electrochemical aspects of electrodes

3.2.1 Electrode potential

When an *electrode*, i.e., a material (not necessarily metallic) through which current can flow or on which an electrochemical reaction can take place, is immersed in an *electrolyte*, i.e., a solution which contains dissolved ions, a phase boundary at the electrode-electrolyte interface forms. An electrical double layer is then formed between the electrons in the electrode and the ions in the electrolyte. This charge separation gives rise to an electric potential difference across the double layer, called electrode potential E, which can be measured versus a reference electrode (section 3.2.7).

It is often the case that an electrochemical reaction is associated with the process described above, i.e., the species that constitute the electrode undergo either an oxidation or a reduction reaction, termed *half-cell reaction*. As an example, the two possible half-cell reactions for a metal Me (electrode) can be written as:

- *Oxidation reaction*: loss of electrons or increase in the oxidation state:
  $Me \rightarrow Me^{z+} + ze^-$ (1)

- *Reduction reaction*: gain of electrons or decrease in the oxidation state:
  $Me^{z+} + ze^- \rightarrow Me$ (2)

At standard conditions (temperature of 25°C, pressure of 1 bar, and concentration of 1 mol·L^{-1} of species involved in the half-cell reaction, i.e., Me^{z+} in the example), the electrode potential is termed *standard electrode potential* and it is usually designated by E^0. The series of standard potentials can be found in literature [24, 25].

For other conditions, the electrode potential and can be calculated with the Nernst equation:

$$E = E^0 + \frac{RT}{zF} \ln \frac{a_{\mathrm{ox}}}{a_{\mathrm{red}}} \quad (3)$$

where R is the gas constant (8.314 J·mol^{-1}·K^{-1}), T is the temperature (K), F is the faraday constant (96.485·10^3 C·mol^{-1}), a_{ox} is the activity of the oxidized species (species that increase the oxidation state), and a_{red} is the activity of the reduced species (species that reduce the oxidation state).

3.2.2 Pourbaix diagram

The pH is an important variable of aqueous solutions, since hydrogen or hydroxide ions are involved in many electrochemical reactions of metals. On this basis, the *Pourbaix diagram* is a graphical representation of the thermodynamically stable compounds of a metal immersed in an aqueous solution as a function of the electrode potential, pH, and concentration of metal ions in the electrolyte.

Pourbaix diagrams can be found for many aqueous electrochemical systems in the literature. Fig. 1 shows the Pourbaix diagram for the case of iron in water (for iron concentration of 10^{-6} mol·L^{-1} and 25°C) [26].

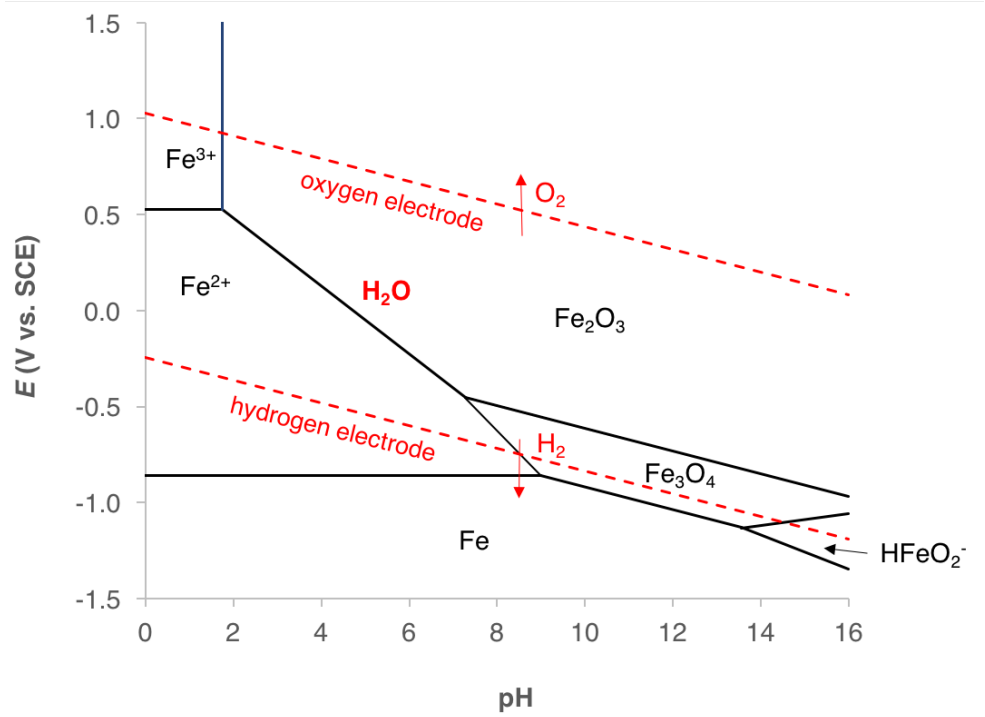

Fig. 1 Pourbaix diagram for iron in water (for iron concentration of 10^{-6} mol·L^{-1} and 25°C). In this case, only Fe, Fe_3O_4, Fe_2O_3 are considered as solid products. After [26].

The dashed red lines in Fig. 1 represent the hydrogen and oxygen electrodes. Between these lines, water is stable (region of natural environments) and it partially dissociates into H^+ and OH^-. Above the *oxygen electrode line*, O_2 evolution takes place. Below the *hydrogen electrode line*, H_2 evolution takes place. These reactions and the corresponding Nernst equation are:

Hydrogen electrode:

$H_2 + H_2O \rightarrow 2H^+ + 2e^-$ (4)

$E_{H_2/H^+}\,(\mathrm{mV\ vs.\ SCE}) = -0.244 - 0.059pH$ (5)

Oxygen electrode:

$4OH^- \rightarrow O_2 + 2H_2O + 4e^-$ (6)

$E_{OH^-/O_2}(\mathrm{mV\ vs.\ SCE}) = 1.026 - 0.059pH$ (7)

From Fig. 1, it can be seen that at potential values below ca. -0.9 V vs. SCE, iron is in a condition of *immunity*, whereas at potentials above this value, iron has the tendency to oxidize (anodic reaction). For the potential values comprised within the hydrogen and oxygen electrode lines, i.e., potential range when water is stable, iron oxidizes; thus, when immersed

in water, steel will dissolve (in acidic/neutral conditions) or form iron oxides (in alkaline conditions).

3.2.3 Electrode kinetics

In practice, it is useful to know in which circumstances a thermodynamically possible reaction is feasible and at which rate it takes place. The reaction velocity is usually expressed as the reaction electrical *current I* per unit of area*, i.e.,* the *current density i* (considered positive for oxidation reactions and negative for reduction reactions).

The reaction kinetics are usually studied with the potential-current density relationship (*polarization curve*) or with the potential-logarithm of current density relationship (*Evans diagram*).

Polarization curve

In this case, the electrode potential *E* is plotted versus the current density *i*. The intercept of this curve is at the *equilibrium potential* (or *reversible potenti*al) E_0, i.e., the potential at which the rate of the oxidation and reduction reactions are equal, resulting in a net zero-current density associated with the electrode. Fig. 2 shows a schematic representation of a polarization curve (red line) of a metal; obtained as the sum of the individual oxidation and reduction reactions curves (black lines).

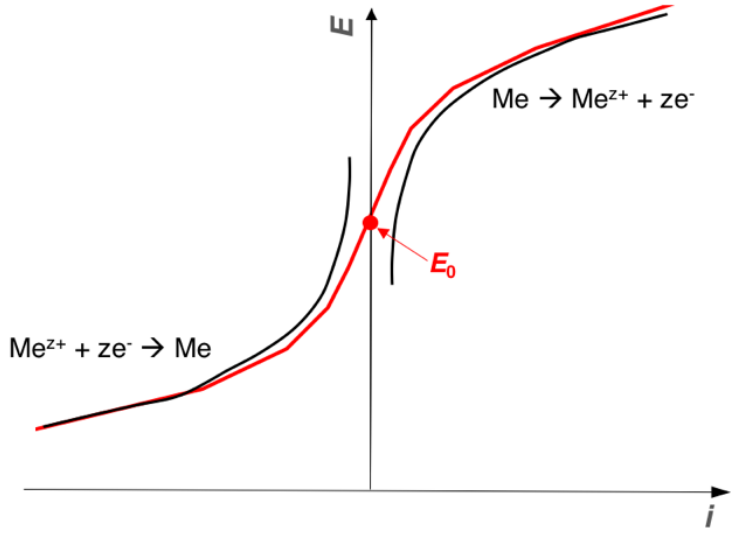

Fig. 2 Schematic representation of a polarization curve of a metal with the indicated equilibrium potential E_0. The polarization curve (red line) is the sum of the individual curves corresponding to the oxidation and reduction reactions (black lines).

Evans diagram

In the Evans diagram, the electrode potential E is plotted versus $\log|i|$. Fig. 3 shows a schematic representation of an Evans diagram of a metal.

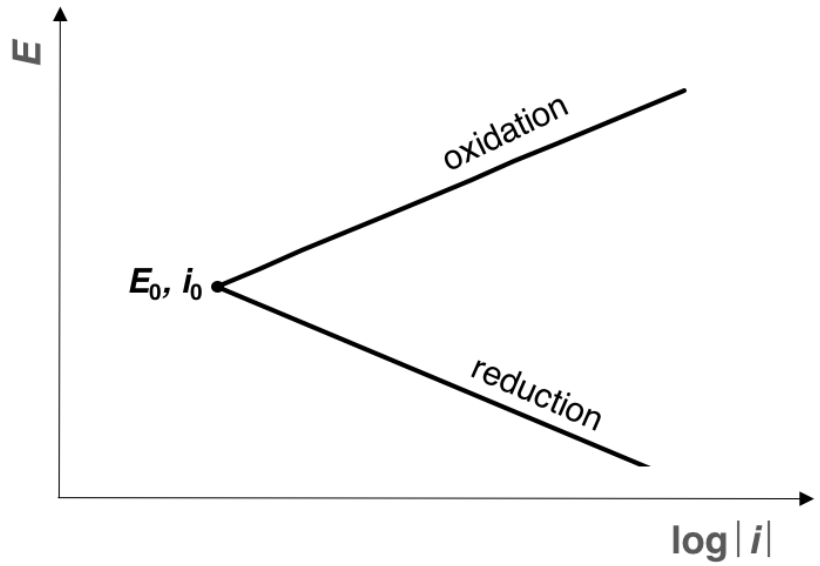

Fig. 3 Schematic representation of an Evans diagram of a metal

In this plot, two straight lines can be differentiated, each one corresponding to the oxidation and reduction reactions of the metal. The slope of the oxidation and reduction lines is termed *Tafel slope*, and it may be different for the two reactions. The point of intersection of the respective oxidation and reduction lines corresponds to the equilibrium potential E_0 and the value of current density at which these lines intersect is called the *exchange current density* i_o.

Mixed potential

An electrochemical cell is composed of at least one *cathode* (where a reduction reaction takes place) and at least one *anode* (where an oxidation reaction takes place). The cell potential ΔU_{cell} is then calculated as the difference between the equilibrium potentials E_0^{anode} and E_0^{cathode} of the anodic and cathodic reactions respectively:

$$\Delta U_{\text{cell}} = E_0^{\text{anode}} - E_0^{\text{cathode}} \quad (8)$$

Based on the laws of thermodynamics, two situations are possible [24, 27, 28]:

- When $\Delta U_{\text{cell}} = 0$, the two half-cells are in equilibrium (at the anodic and cathodic equilibrium potentials);

- When $\Delta U_{cell} > 0$ ($E^0_{cathode} > E^0_{anode}$), a spontaneous cell reaction takes place. In this case, the cell is at a potential, called *mixed potential* $E_{mixed\ potential}$ (different from the equilibrium potential), with a non-zero current associated to the electrode.

Due to the principle of electroneutrality, the current density i for the anodic and cathodic reactions should be equal ($i_{anode}=i_{cathode}$), assuming equal surface area for both anode and cathode. By imposing this condition, the working conditions (i and $E_{mixed\ potential}$) of a spontaneous cell can be determined. Fig. 4 shows a schematic representation of an Evans diagram for a spontaneous cell reaction. It can be observed that the intersection point between the anodic and cathodic curves corresponds to the cell mixed potential $E_{mixed\ potential}$.

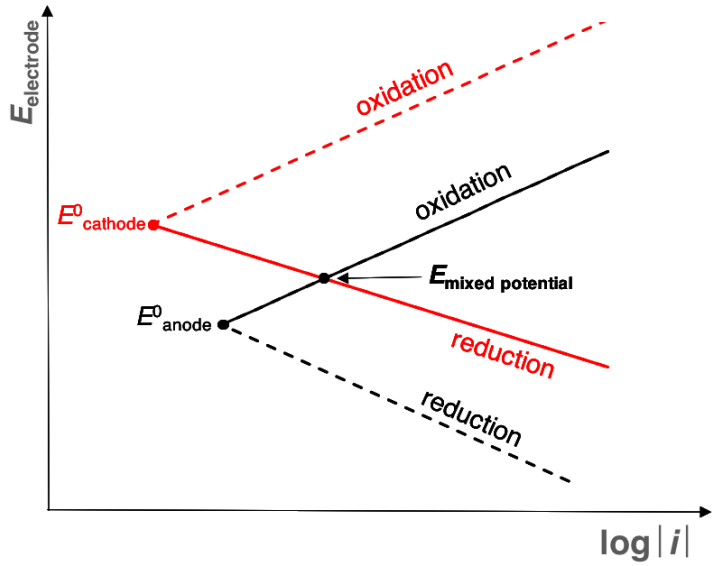

Fig. 4 Schematic representation of an Evans diagram for a spontaneous cell reaction. The intersection point between the anodic and cathodic curves correspond to the cell mixed potential $E_{mixed\ potential}$.

From Fig. 4, it can be seen that the potential at the anode and at the cathode is the same and equal to the mixed potential ($E_{anode} = E_{cathode} = E_{mixed\ potential}$). It should be noted that this equality is only valid when anodic and cathodic reactions happen at the same place, i.e., this concept cannot be applied, for instance, to chloride-induced corrosion (section 3.3.7).

3.2.4 Potentiometric measurement

In a potentiometric measurement, the *working electrode* (WE) is the electrode on which the electrochemical reaction of interest (electrode reaction) takes place. The potential of the working electrode cannot be determined absolutely and it must be referred to the potential of

another electrode with known and fixed potential, i.e., the *reference electrode* (RE), that must be placed in the same electrolyte.

Potentiometric measurements are usually performed with an instrument called voltmeter, which has a high input impedance, resulting in a very small current flowing in the measuring circuit. In general, this current is too small to interfere with the measurement and the potential measured ($E_{measured}$) is expressed as the difference between working electrode potential (E_{WE}) and the reference electrode potential (E_{RE}):

$$E_{\text{measured}} = E_{\text{WE}}(\text{vs. RE}) = E_{\text{WE}} - E_{\text{RE}} \quad (9)$$

A schematic representation of the set-up of a potentiometric measurement is shown in Fig. 5.

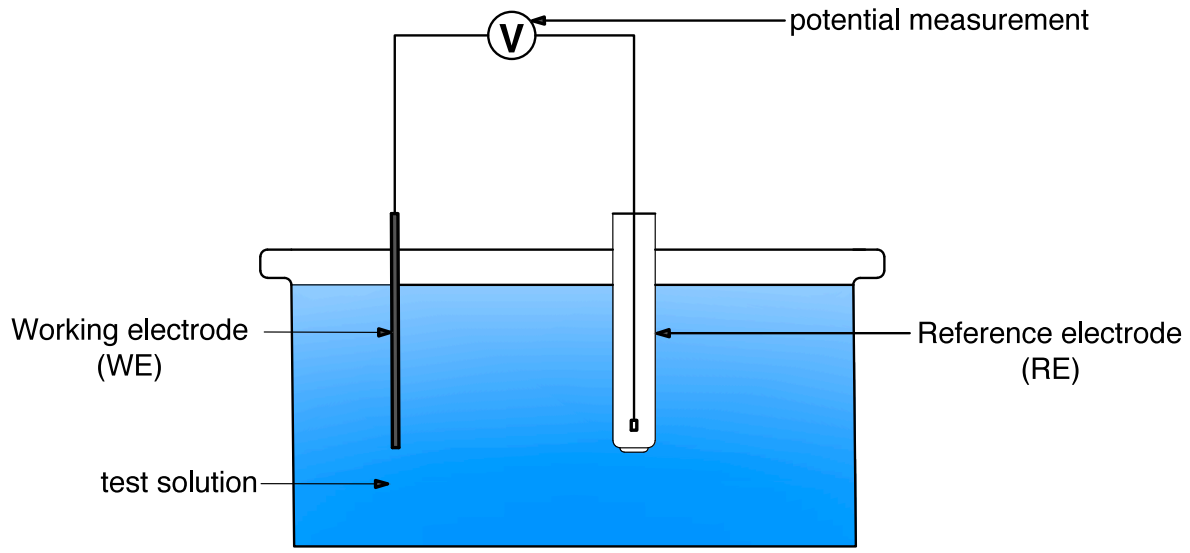

Fig. 5 Schematic representation of the set-up of a potentiometric measurement

If the reference electrode cannot be placed near to the working electrode, the potential measured can be affected by the *ohmic drop* (also termed *IR drop*), i.e., potential drop caused by the solution resistance against current flow. The IR drop is usually small for most electrolytes, but it can become important for low-conductivity solutions [29]. In order to solve this problem, the reference electrode can be placed near the surface of the working electrode by means of a Luggin-Haber capillary [29].

Potential scale and conversion

By definition, the electrode potential is referred to the standard hydrogen electrode (SHE), which is universally adopted as the primary standard reference electrode, i.e., the zero-point of the electrochemical potential scale.

In potentiometric measurements, other types of reference electrodes are generally used (see section 3.2.7); thus, the potentials must often be converted. The conversion from the potential value measured with one reference electrode (E_{WE} (vs. RE_1)) to the value measured with another reference electrode (E_{WE} (vs. RE_2)) is a simple operation:

$$E_{\mathrm{WE}}(\mathrm{vs.\,RE_1}) + E_{\mathrm{RE_1}}(\mathrm{vs.\,SHE}) = E_{\mathrm{WE}}(\mathrm{vs.\,RE_2}) + E_{\mathrm{RE_2}}(\mathrm{vs.\,SHE}) \quad (10)$$

The electrochemical potential of the available electrodes versus the standard hydrogen electrode (E_{RE} (vs. SHE)) can be found in literature [24, 25].

3.2.5 Open circuit potential

The *open circuit potential* (OPC) is the potential at which the net current is zero, i.e., the total anodic current is equal to the total cathodic current. The potential measured in a potentiometric measurement $E_{measured}$ is the open circuit potential.

For the specific case of corrosion in concrete, the open circuit potential is equal to the corrosion potential E_{corr} (section 3.3.3, Fig. 9) and to mix potential $E_{mix\ potential}$ (Fig. 4) when the anodic and cathodic currents are equal, i.e., when anodic and cathodic reactions happen at the same place. However, if anodic and cathodic reactions are spatially separated, e.g., in most cases for chloride-induced corrosion (section 3.3.7)., the open circuit potential is comprised somewhere in between the potential of the anode and the potential of the cathode.

3.2.6 Diffusion potential

Whenever two electrolytes of different compositions come into contact, ionic diffusion takes place across the boundary as a consequence of the concentration difference. Due to the different ionic mobilites of the involved species, some ions move faster than others, leading to a charge separation. As a result, an electrical potential originates, termed diffusion potential $E_{diffusion}$, which decelerates the fast-moving ions and accelerates the slower ions. This process is known as *migration*. In the end, a steady state is reached in which the involved ions are transported by a combination of migration and diffusion.

The diffusion potential $E_{\text{diffusion}}$ can be calculated with the Henderson equation [25]:

$$E_{\text{diffusion}} = \frac{RT\sum\frac{|z_i|}{z_i}u_i\left(c_i^{\beta}-c_i^{\alpha}\right)}{F\sum|z_i|u_i\left(c_i^{\beta}-c_i^{\alpha}\right)}\ln\frac{|z_i|u_ic_i^{\alpha}}{|z_i|u_ic_i^{\beta}} \quad (11)$$

where α and β denote the two solutions with different composition, u_i is the ionic mobility ($cm^2 \cdot V^{-1}s^{-1}$), and c_i ($mol \cdot L^{-1}$) is the concentration of the species involved.

A schematic representation of a diffusion potential established between two electrolytes with different concentration (in the example, different sodium hydroxide concentrations) is shown in Fig. 6.

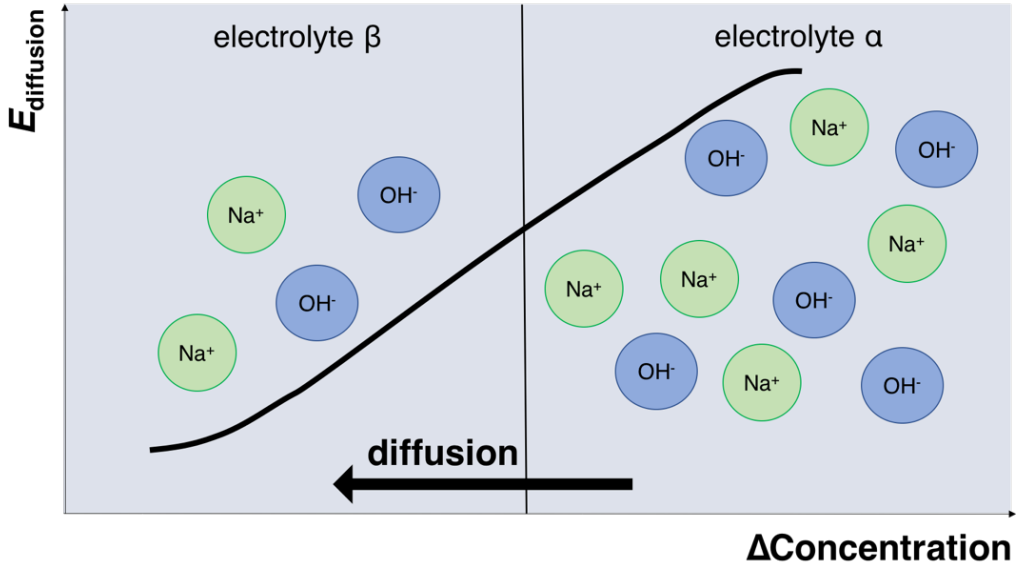

Fig. 6 Schematic representation of a diffusion potential established between two electrolytes as a function of the difference in concentration between them (in this case, different sodium hydroxide concentrations).

In concrete, diffusion potentials can be present due to internal concentration gradients, such as differences in pH or chloride content [30-33]. Diffusion potentials in the order of hundreds of mV have been reported [33-35], where pH gradients have the highest impact due to the high mobility of OH^- in aqueous solution [25].

Cement paste is considered to have permselective properties, i.e., the electrically charged surfaces of the pore walls interact with the diffusing ions, affecting the ion transport [34, 36]. A consequence of this is that the above-mentioned diffusion potentials become larger. However, Angst et al. [37] reported that porous Portland cement mortar with w/c = 0.6 did not

show significant permselective behavior. This effect may be then restricted for denser cements pastes, e.g., with lower water-to-cement ratios [34, 36-38].

Diffusion potentials can arise while performing potentiometric measurements in concrete, as a consequence of the differences in concentration at the interface between the concrete pore solution and the internal solution of the reference electrode [9, 31, 32, 39]. Additionally, diffusion potentials are likely to be a serious error source [32, 39, 40] for the application of ion-selective electrodes in concrete (see section 6.2.1).

3.2.7 Reference electrodes

A reference electrode is an electrode that ideally exhibits a stable, well-defined, reversible and reproducible electrochemical potential response. In this context, stable means that the potential response is fixed and it does not change even if the composition of the test solution changes; reversible means that the potential response should always return to its equilibrium (see sections 3.2.1 and 3.2.3) after a small transient perturbation, e.g., polarization, and reproducible means that the same potential must be obtained if the electrode is constructed with the same electrode/solution combinations.

The most commonly used reference electrodes are listed below, arranged by basic working principle [41-43]:

- *First kind*

These electrodes consist of a metal Me immersed in a solution containing cations of this metal Me^{z+} [41-43]. The potential is then determined by the following redox equilibrium:

$$Me^{z+} + ze^{-} \leftrightarrow Me \qquad (12)$$

The electrode potential is calculated with the Nernst equation (Eq. (3)).

An example of a reference electrode of the first kind is the copper/copper sulphate reference electrode ($Cu/CuSO_4$).

- *Second kind*

These electrodes consist of a metal Me covered with a sparingly soluble salt containing cations of this metal Me^{z+}. This system is immersed in a solution containing the anions of the salt [41-

43]. A typical example of reference electrode of the second kind is the Ag/AgCl/KCl reference electrode. In this case, the metal (Ag) is covered with solid AgCl and immersed in a solution containing KCl. The equilibrium is then established between the following interfaces:

1. The metal and its cation in the sparingly soluble salt. For the example of the Ag/AgCl/ KCl electrode, the following reaction takes place:

$$\mathrm{Ag} \leftrightarrow \mathrm{Ag^+} + \mathrm{e^-} \tag{13}$$

2. The anion of this salt and the anion in solution. For the example of the Ag/AgCl/ KCl electrode, the following solubility equilibrium is established:

$$\mathrm{AgCl} \leftrightarrow \mathrm{Ag^+} + \mathrm{Cl^-} \tag{14}$$

The activities of silver and chloride ions are then related through the solubility product of silver chloride $K_{\mathrm{sp\_AgCl}}$:

$$K_{\mathrm{sp\_AgCl}} = a_{\mathrm{Ag^+}}\, a_{\mathrm{Cl^-}} \tag{15}$$

The amount of silver and chloride ions dissolved in solution is fixed for a given concentration of KCl, as a result of the low solubility of AgCl. Consequently, the activity of the silver ions in the electrode is also fixed, so the electrode exhibits a stable and defined potential response. Combining Eqs. (3) and (15), the potential of the electrode $E_{\mathrm{Ag/AgCl/KCl}}$ can be calculated as:

$$E_{\mathrm{Ag/AgCl/KCl}} = E^0_{\mathrm{Ag/Ag^+}} + \frac{RT}{F}\ln K_{\mathrm{sp\_AgCl}} - \frac{RT}{F}\ln a_{\mathrm{Cl^-}} \tag{16}$$

Another common reference electrode of the second kind is the saturated calomel electrode (SCE). In this case, Hg is covered with Hg_2Cl_2 and immersed in saturated KCl solution. As the salt concentration of the internal electrolyte is fixed, all the SCEs have the same electrochemical potential value at the same temperature. Ag/AgCl/KCl electrodes, on the other hand, exist with a variety of KCl concentrations and their electrode potentials vary accordingly (see Table 1).

Electrodes of the second kind are generally more accurate. However, it should be noted that the solubility of KCl is especially sensitive to changes in temperature, which in turn affects the potential of the electrode [25, 41].

- *Third kind / Redox*

Reduction-oxidation electrodes (redox electrodes) consist of an inert metal (usually Pt) immersed in a solution containing a substance present in two different oxidation states, e.g., Fe^{3+}/Fe^{2+} [41-43]. The metal merely acts as a medium for the transfer of electrons between the oxidized (Ox) and reduced (Red) forms. The potential is then determined by the following redox equilibrium:

$$\mathrm{Ox} + ze^{-} \leftrightarrow \mathrm{Red} \tag{17}$$

The electrode potential is calculated with the Nernst equation:

$$E_{\mathrm{Ox/Red}} = E^{0}_{\mathrm{Ox/Red}} + \frac{RT}{zF} ln \frac{a_{\mathrm{Ox}}}{a_{\mathrm{Red}}} \tag{18}$$

More complicated redox equilibriums exist based on the same working principle, as for example the quinhydrone electrode [42].

Design of reference electrodes

For a reference electrode to exhibit a fixed and stable potential, it is important that the composition of the internal electrolyte is not changed; thus, it must be well separated from the test solution. For that, the internal electrolyte is placed in the *electrode compartment*, which is then connected to the test solution through the *liquid junction*. The liquid junction is a porous plug or membrane that acts as an ionic conductor but also as a physical barrier to minimize leaking. Electrodes of the first kind may be particularly affected by leakage [41].

As a consequence of the gradient in chemical composition across the liquid junction, i.e., difference in chemical composition between internal electrolyte and test solution, a diffusion potential (section 3.2.6) arises at the junction, i.e., the *liquid junction potential* $E_{\text{liquid junction}}$. The liquid junction potential adds arithmetically to the measured potential (Eq. (9)) when a reference electrode described in this section is used:

$$E_{\mathrm{measured}} = E_{\mathrm{WE}}(\mathrm{vs.\,RE}) + E_{\mathrm{liquid\,junction}} = E_{\mathrm{WE}} - E_{\mathrm{RE}} + E_{\mathrm{liquid\,junction}} \tag{19}$$

Fig. 7 shows a schematic depiction of a reference electrode design with the indicated liquid junction potential established between the internal electrolyte (electrolyte β in section 3.2.6) and the test solution (electrolyte α in section 3.2.6).

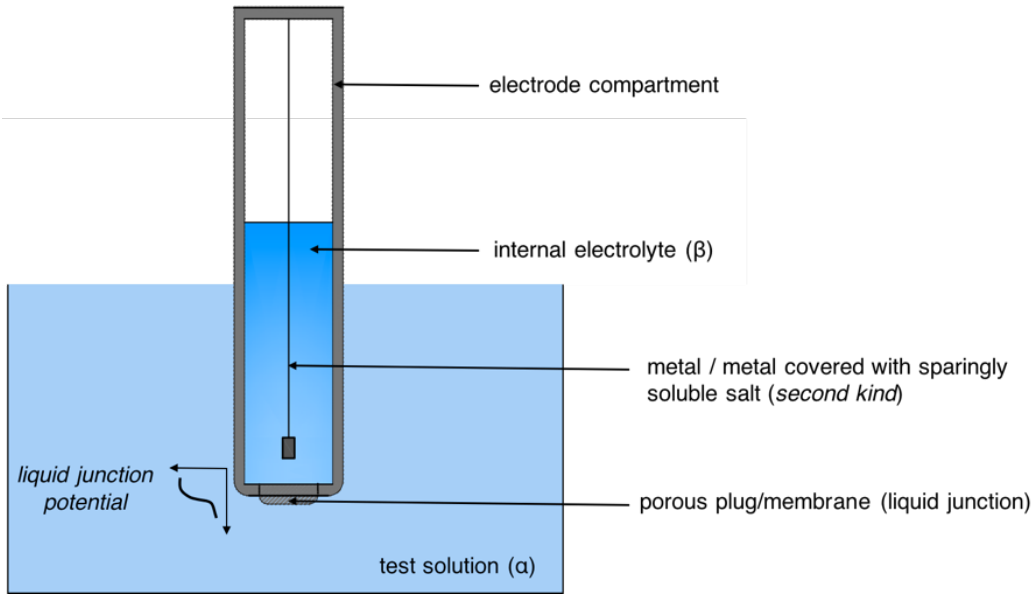

Fig. 7 Schematic depiction of a reference electrode design

Potential scale

Table 1 reports the main features (composition and concentration of internal electrolyte) and the potentials of the most commonly used reference electrodes.

Table 1 Reference electrode potentials vs standard hydrogen electrode (SHE) at 25°C

Reference electrode	Internal electrolyte		Potential (mV vs. SHE)
	Composition	Concentration	
$Cu/CuSO_4$	$CuSO_4$	1.27 mol·L^{-1} (saturated)	318
SCE	KCl	4.16 mol·L^{-1} (saturated)	244
Ag/AgCl/KCl	KCl	4.16 mol·L^{-1} (saturated)	199
		4 mol·L^{-1}	200
		1 mol·L^{-1}	235
		0.6 mol·L^{-1}	250
		0.1 mol·L^{-1}	288
		0.01 mol·L^{-1}	343

3.2.8 Ion-selective electrodes (ISEs)

An ion-selective electrode (ISE) is a type of electrode capable of selectively measuring the activity of a particular ionic species, i.e., the *primary ion* [41, 43-46].

ISEs are composed of an inner reference electrode (based on the ones described in section 3.2.7), placed in an electrolyte (internal electrolyte) containing the ion of interest at a constant activity. This system is separated from the test solution by a thin (insoluble) membrane. Once the ISE is immersed in the test solution, processes based on ion-exchange or ion transport between the primary ion and the membrane components take place at the solution-membrane interfaces (both at the inner electrolyte-membrane interface and test solution-membrane interface) until equilibrium is established [41, 43-46]. If the primary ion concentration on each side of the membrane was equal, the potential difference across the membrane would be zero. Otherwise, a membrane potential, that depends on the activity of the ion of interest, develops.

The membrane potential can be obtained from the potential measurement between the internal ISE reference electrode and an external reference electrode. Since the activity of the primary ion in the internal electrolyte is constant, the potential response of the ISE (E_{ISE}) can be expressed as a function of the activity of the target ion in the test solution [41, 43-46]:

$$E_{ISE} = k' + \frac{\mathrm{R}T}{z_{\mathrm{i}}\mathrm{F}} \ln a_{\mathrm{i}} \qquad (20)$$

where z_{i} is the charge of the primary ion, a_{i} is the activity of the primary ion, and k' (V) is a constant that depends on the type and composition of ISE [45].

Eq. (20) is written based on the assumption that the ISE responds only to the ion of interest. However, the ISE may also be sensitive to other ions and its potential response also depend on them. This interference is traditionally considered with the selectivity coefficient, $K_{\mathrm{i,j}}$ (with j standing for the interfering species) included in the Nikolsky-Eisenman equation:

$$E_{\mathrm{ISE}} = k' + \frac{\mathrm{R}T}{z_{\mathrm{i}}\mathrm{F}} \ln\left(a_{\mathrm{i}} + \sum\left(K_{\mathrm{i,j}} \cdot a_{\mathrm{j}}^{\,z_{\mathrm{i}}/z_{\mathrm{j}}}\right)\right) \qquad (21)$$

where a_{j} is the activity of the interfering ionic species.

Depending on the nature of the membrane material used, ISEs can be divided into four main groups: glass, liquid, solid, and gas electrodes [41, 43-46].

- *Glass electrodes*

The most common glass electrode is the pH electrode [41, 44, 46]. It consists of a thin, pH-sensitive glass membrane and an internal reference electrode (usually a SCE or a Ag/AgCl/KCl reference electrode, section 3.2.7) immersed in a dilute hydrochloric acid solution. Once the electrode is immersed in the solution whose pH is to be measured, equilibrium establishes across the glass membrane with respect to hydrogen ions. The overall mechanism of the response is complex and it is attributed to the replacement of sodium ions in the glass by protons [45].

In this case, the ISE potential is proportional to the pH:

$$E_{\mathrm{ISE}} = k' + 0.059pH \qquad (22)$$

The accuracy of these electrodes decreases in highly acidic or highly alkaline media [45, 46]. To overcome this problem, glass membranes with different compositions have been proposed [25, 44]. Additionally, changes in the chemical composition of the glass membrane (along with changes in the internal electrolyte) lead to electrodes sensitive to ions other than hydrogen, including Na^+, NH_4^+, Li^+, K^+, etc. [44].

- *Liquid electrodes*

These type of ISEs are based on water-immiscible liquid substances impregnated in a polymeric membrane [46]. The internal reference electrode is usually a Ag/AgCl/KCl reference electrode (section 3.2.7), which is immersed in a solution containing a chloride salt of the primary ion. For the ISE to respond to the ion of interest, an ion-exchanger or ionophore is dissolved in the viscous liquid membrane. The ion-exchanger or ionophore is a neutral "carrier" molecule that extracts the target ion at the solution-membrane interface, so the membrane potential is established.

A common liquid membrane ISE is the calcium-selective electrode. Other ISEs based on liquid membranes are used to detect Mg^{2+}, ClO_4^-, K^+, NO_3^-, etc [25, 44-46].

- *Solid electrodes*

In this case, the membrane consists of single crystals, polycrystalline pellets, or mixed crystals of salts, usually of low solubility [41, 43-46]. It is also possible to find internal solution-free

ISEs, where the electrode consists of a metal coated with a sparingly soluble salt (membrane), which contains the metal cations and the ion of interest.

These electrodes usually respond to those ions that are components of the active membrane material. When immersed in solutions containing the ion of interest, the salt forming the membrane will either dissolve or precipitate, causing changes at the membrane-test solution interface, so the membrane potential develops. The behavior of these electrodes is thus basically determined by the solubility of the salt forming the membrane. Because of that, most of the interfering species in this type of electrodes are ions that can form components of low solubility with the ions forming the membrane.

ISE based on solid membranes are used to detect F^-, Br^-, I^-, Cl^-, etc. [25, 46]. In this work, a chloride ISE with solid membrane is used to monitor chloride concentrations in concrete (papers I, II, V and Appendix).

- *Gas-Sensing Electrodes*

These devices include a glass pH-electrode protected from the test solution by a polymer diaphragm. Between the glass membrane and the diaphragm, there is a small volume of electrolyte. Small molecules of gas can penetrate the diaphragm and interact with the trapped electrolyte, resulting in reactions that change the pH, so the pH-electrode responds to it [25].

A common gas-sensing electrode based on this working principle is the Clark oxygen electrode [46].

3.2.9 Metals and metal/metal oxides – pseudo-reference electrodes

The essential difference between a true reference electrode (as defined in 3.2.7) and a pseudo-reference electrode is the lack of thermodynamic equilibrium in the latter case [25, 41, 43]. As a consequence, the potential response is in some cases not defined but these electrodes can exhibit potentials approximately constant under certain conditions [43].

In most cases, pseudo-reference electrodes consist of a piece of metal or metal/metal oxides, i.e., metal substrate coated with metal oxides.

These electrodes have been generally developed to be used as pH sensors. Examples of metals used for this application are Sn, W, Fe, Ir, Os, Ag, Cu, Zn, etc. [47]. However, their use

is limited to a narrow pH range and the potential response often depends on the anions present in solution. Experience with metal/metal oxides has been slightly more successful [47-49], such as the use of the palladium-palladium oxide electrode [48, 49], the antimony electrode [43, 47], or the iridium/iridium oxide (IrO_x) electrode [50-57]. Among them, iridium/iridium oxide (IrO_x) electrodes have performed specially well in aqueous solutions over wide range of pH and temperature [50-57]. The potential response of these electrodes is also reported to be insensitive to the oxygen content in solution [51, 52].

The main difference between the IrO_x pH-electrode and the traditional glass pH-electrode is related to the pH-sensing mechanism. In glass pH-electrodes, the mechanism is determined by the equilibrium established across the glass membrane with respect to the activity of hydrogen ions (see section 3.2.8), whereas the IrO_x electrode response is determined by a redox reaction. Theoretically, the potentiometric response of iridium oxide to pH is governed by the transition between two oxidation states, Ir(III) and Ir(IV) [26]. The properties of these electrodes are known to be dependent on fabrication methods and conditions used [58], which results in a high variability in the reported potential-pH responses [50, 52-54, 56, 57, 59-63]. It is suggested that this issue is because the IrO_x electrode is originally covered by a layer of anhydrous oxide, but after immersion in aqueous solution hydration develops, resulting in a potential shift for different immersion times. Once a stable hydrated oxide film is formed, the potential shift stops [64, 65].

In this work, IrO_x electrodes produced by thermal oxidation are used to monitor the pH of the concrete pore solution (papers III-V and Appendix).

3.2.10 Non-potentiometric sensors

- *Fibre optic sensors*

Fibre optic sensors are based on the transmission of light (originating from a laser or any superluminescent source) via an optical fiber and its conversion into an electrical signal [66, 67].

A typical fibre optic sensor system consists of a fibre-optic cable connected to a sensor/detector. The fibre optic cable consists of a glass or plastic core, surrounded by a layer made of cladding material, usually protected from physical damage by a coating. The difference in the index of refraction between the core and the cladding layer enables the total reflection of light, which is then transmitted from the cable to the sensor/detector, where the

light energy is converted into an electrical signal. The basic structure of an optical fibre is shown in Fig. 8a, whereas the basic working principle of an optical fibre, i.e., total internal reflection, is shown in in Fig. 8b.

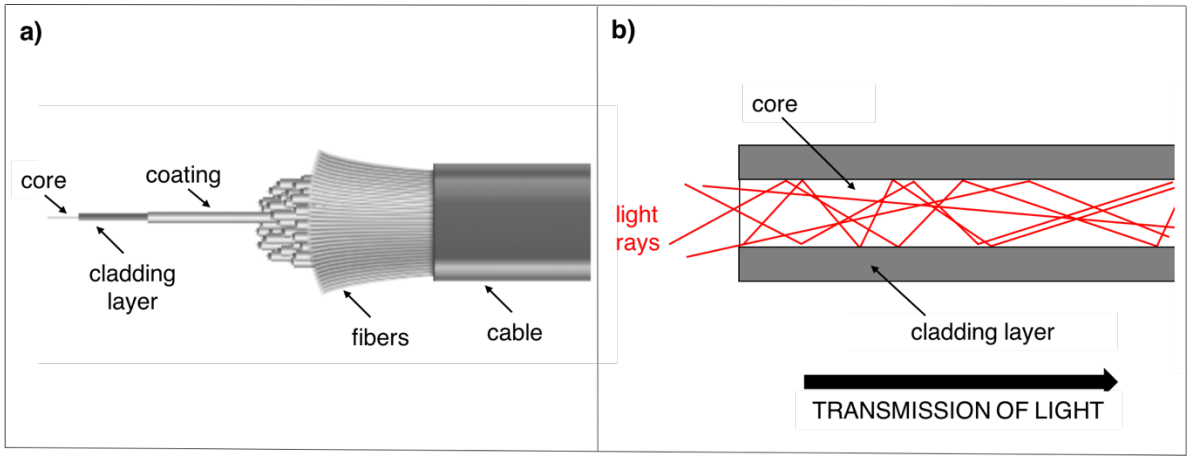

Fig. 8 (a) Basic structure of an optical fibre (b) Working principle of an optical fibre (total internal reflection) [67].

Depending on the application, a fibre optic sensor can be classified as follows [67]: physical sensors (used to measure physical properties, such as temperature, stress, etc.), chemical sensors (used for pH measurements, gas analysis, etc.), and bio-medical sensors (used to measure blood flow, glucose content, etc.).

Several fibre-optic pH sensors have been developed. In this case, measurements are performed in a similar way but the cladding is composed by a material, e.g. organic dye, whose optical properties (absorbance, reflectance, fluorescence, energy transfer, refractive index, etc.) are changed by the chemical of interest (the hydrogen ions). Most of the reported fibre optic pH-sensors exploit different indicator dyes, which cause changes in the absorption spectrum of the test solution, e.g. color, as a function of pH. These changes are then converted into electrical signals [68-73].

- *Sensor systems based on coulometric measurements*

In a coulometric method, the change of the concentration of the electroactive substance is measured in dependence on the current passed through the cell. A common technique for that is the coloumetric titration [27].

A common type of sensor for this type of measurements is the ion sensitive field effect transistor (ISFET) [74], which consists of a potentiometric sensor with an integrated

impedance converter; when the concentration of the ion of interest changes, the current through the transistor will change accordingly, and provide an output potential that is a function of the concentration of the ion of interest.

There are a number of works based on the combination of an ISFET with a reference electrode that have been used to determine the pH in solution [75-77].

3.3 Corrosion of steel embedded in concrete

3.3.1 Corrosion process

In the case of metallic materials, the term corrosion usually stands for the electrochemical reaction of the metal with its environment (e.g., oxygen). For steel embedded in concrete, the corrosion reaction can formally be split up into the following half-cell reactions:

Oxidation reaction (dissolution of iron):

$$Fe \rightarrow Fe^{2+} + 2e^{-} \quad (23)$$

Reduction reaction (oxygen reduction, for neutral and alkaline electrolytes):

$$H_2O + ½O_2 + 2e^{-} \rightarrow 2OH^{-} \quad (24)$$

The dissolved iron Fe^{2+} usually reacts with the OH^{-} ions, forming $Fe(OH)_2$. The overall reaction is then written as follows:

$$Fe + H_2O + ½O_2 \rightarrow Fe(OH)_2 \quad (25)$$

The corrosion product $Fe(OH)_2$ is usually further oxidized to Fe_3O_4 or Fe_2O_3, commonly known as rust [78]. The transformation of metallic iron to rust leads to the deterioration of the reinforced concrete structure, i.e., by decreasing its load capacity, and may cause severe damage to a structural component or the whole system. This corrosion state is referred to as *active state*.

3.3.2 Passivity

From Fig. 1, it can be seen that in alkaline aqueous media, steel forms iron oxides. In this case, the metal itself is thermodynamically not stable and is always associated with (minimal) anodic dissolution. However, the resulting corrosion products are not dissolved in water or loosely present on the surface (rust); they form a compact and adhesive oxide layer, i.e., the

passive layer. These are known as *conditions of passivity* and the interval of potentials associated with it is known as *passivity range*.

The passive layer is a few nanometers thick and it acts as a kinetic barrier at the metal/electrolyte interface. As a consequence, further dissolution is inhibited, i.e., dissolution rate of iron is negligible (≈0.1 μm year) [7].

Typical metals and alloys that owe their corrosion resistance to passivation are high-alloyed steels, aluminum alloys, titanium, and also normal steel in alkaline media (e.g. steel in concrete). However, the passive layer can also be a weak spot in passive metals; if the passive layer is damaged or destroyed (e.g. due to exposure to chloride, see section 3.3.7), high corrosion rates can occur locally [7].

3.3.3 Kinetics of corrosion

The rate at which anodic and cathodic reactions occur depends on the Fe/Fe^{2+} electrode and the oxygen electrode. From their cathodic and anodic polarization curves, the corrosion conditions, i.e., corrosion potential E_{corr} and corrosion current density i_{corr}, can be determined [7].

The anodic (for the Fe/Fe^{2+} electrode) and cathodic (for the oxygen electrode) polarization curves in active and passive state are schematically depicted in Fig. 9a and Fig. 9c respectively, and related to the Pourbaix diagram in Fig. 9b.

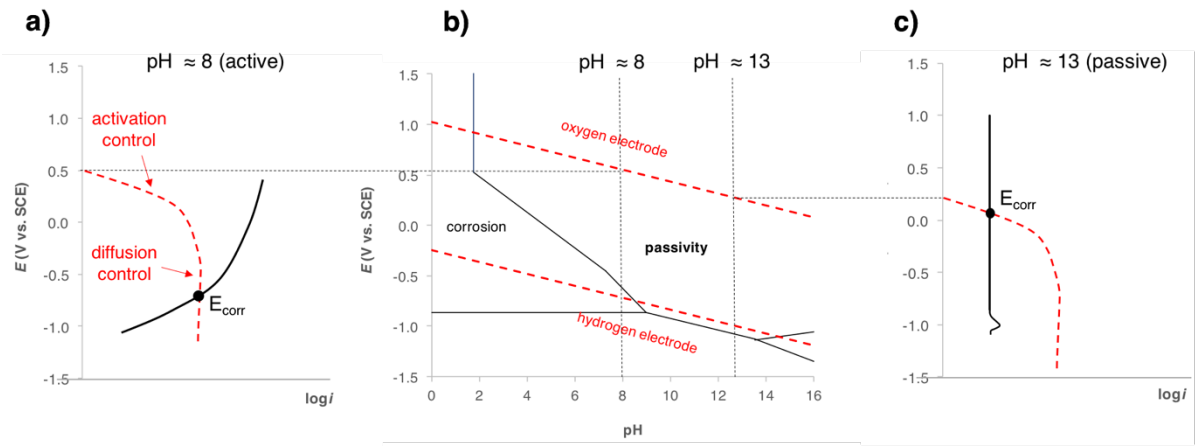

Fig. 9 (a) Schematic representation of the anodic (solid black line) and cathodic (red dotted line) polarization curves in active state (at pH ≈8); (b) simplified Pourbaix diagram for iron with indicated zones of passivity and corrosion when immersed in water; (c) schematic representation of the anodic (solid black line) and cathodic (red dotted line) polarization curves in passive state (at pH ≈13).

The effect of the pH of the electrolyte can clearly be seen in Fig. 9a and Fig. 9c. A large range of passivity is visible at high pH (Fig. 9c), where the current density associated to the anodic curve (iron dissolution) is very low, almost independent on the potential. In contrast, the logarithm of the anodic current density increases with the potential at low pH values (for example below pH 9, Fig. 9a). Additionally, the reaction rate of the cathodic half-cell reaction increases with declining potentials to more negative values [7].

Differences in the shape of the cathodic and anodic curves can also be seen. When the polarization curves plotted in the Evans diagram are straight lines (with Tafel slopes, as defined in section 3.2.3), the reaction kinetics are under *activation control*, i.e., all the involved species are available at the electrode surface and the reaction rate is determined by charge transfer at the electrode/electrolyte interface. In contrast, the reaction kinetics are under *diffusion control* when the consumption of the species involved in the half-cell reaction is faster than the rate at which they are provided at the electrode/electrolyte interface. In this case, the polarization curve becomes a vertical line. Both situations (activation and diffusion control) are indicated in Fig. 9a for the cathodic reaction (oxygen reduction). Both the cathodic reaction involving hydrogen evolution (acid media) and the anodic dissolution of a metal often proceed under activation control, whereas oxygen reduction is typically under diffusion control in concrete [29].

3.3.4 Carbonation-induced corrosion

In moist environments, acid gases, such as CO_2 or SO_2 can react with the alkaline components dissolved in the concrete pore solution (mainly sodium and potassium hydroxides) and with the solid hydration products (such as $Ca(OH)_2$ or C–S–H) in the cement paste, resulting in a decrease of the pH of the pore solution. In this regard, the main reaction of interest is between CO_2 and $Ca(OH)_2$, as it is more rapid compared to the other cement phases. This reaction, i.e., *carbonation* reaction, takes place in aqueous solution and can schematically be written as:

$$CO_2 + Ca(OH)_2 \rightarrow CaCO_3 + H_2O \qquad (26)$$

The main consequence of carbonation is that the pH of the pore solution drops from its initial value of pH 13-14, to values approaching neutrality. In these conditions, the steel in humid carbonated concrete corrodes as if it was in contact with water. The corrosion rate is usually ≤ 100 μm/y [7].

3.3.5 Factors affecting carbonation resistance of Portland and blended cements

The rate of penetration of CO_2 in concrete and the corrosion propagation associated with it depend on a number of factors, such as CO_2 concentration, exposure conditions, material composition, and material properties [7, 79-82]. The main parameters are described below.

The water-to-cement ratio (w/c) is one of the major factors when considering concrete durability. In the context of corrosion, a decrease in the w/c ratio leads to a decrease in the permeability of the concrete, resulting in a slower corrosion propagation [7, 79-81]. Similarly, appropriate curing is a major parameter in the resistance against corrosion propagation, as it provides better hydration and denser structure [79-81]. The corrosion rate in carbonated concrete is significantly increased in the presence of chlorides [7, 79, 82], despite the fact that that the pH of the pore solution may increase during chloride binding [83]. Additionally, presence of mineral admixtures also has an important effect on the carbonation resistance, as they modify both pore structure and chemical composition of the pore solution, e.g. alkalinity. This is discussed in detail in the next subsection.

Type of cement

The pH of the pore solution in Ordinary Portland Cement is determined by the dissolved phases in the pore solution. Owing to the presence of Portlandite ($Ca(OH)_2$) and specially to the dissolved alkaline phases, such as NaOH and KOH, the pH of the pore solution lies in the range pH 13-14 [10-15]. In this context, Portlandite is responsible for the alkali reservoir at pH≈12.5 [84, 85]. If mineral admixtures are used, the Portlandite content is decreased due to the partial replacement of OPC with these admixtures; if pozzolanic mineral admixtures are used, the Portlandite content is additionally decreased due to its consumption in the pozzolanic reaction. A decrease in the Portlandite content can result in a slight decrease of the pH of the pore solution and in a reduction in the carbonation resistance due to the decreased buffer capacity provided by this phase.

Additions of 10-20% of silica fume and fly ash can cause a reduction in the pH of the pore solution up to 0.7 pH units, with silica fume having the highest impact [86-89]. The presence of these mineral admixtures results in a lower carbonation resistance despite providing a denser microstructure compared to OPC [81, 90, 91]. The pH of the pore solution is also decreased in cements containing blast furnace slag, i.e., CEM III [92, 93]; in this case, use of ground-granulated blast-furnace slag was observed to exhibit faster carbonation [93], but shallower *carbonation depth* [93, 94], i.e., thickness of carbonated concrete with pH≈9, due to

the modified denser microstructure compared to OPC. In practice, use of ground-granulated blast-furnace slag cements does not suppose any problem with respect to reinforcement corrosion for cover depths in the usual range of civil engineering structures [93]. If cements other than OPC are used, such as of calcium aluminate cements, the chemical composition can be significantly modified [95], leading in some cases to higher carbonation rates [96].

The pH values obtained with blended cements are generally not reduced to levels that prevent the formation of the passive layer (Fig. 1) but in many cases, carbonation resistance is decreased. Nevertheless, when the material is well-designed and cured properly, the lower alkalinity and decreased buffer capacity of these cements could be compensated by the denser microstructure of their cement pastes [7, 94, 97, 98].

3.3.6 Penetration of carbonation

According to Tuutti [99], the service life of reinforced concrete structures can be divided into initiation and propagation stages. The initiation stage describes the time before corrosion initiation, i.e., the time until the carbonation front reaches the reinforcement and steel is depassivated. The propagation stage is the period after depassivation when active corrosion takes place.

In order to take preventive measures before corrosion starts (propagation stage), the prediction of the penetration of carbonation (initiation stage) is essential. For that, often the parabolic formula is used [7, 81, 91]:

$$d = K\sqrt{t} \qquad (27)$$

where d is carbonation depth (mm), t is time (years), and K is a parameter termed carbonation coefficient (mm/years$^{1/2}$), which depends on time, type of material, and exposure conditions [7, 91, 97].

Other carbonation models have been and are being developed [98-103]. These models usually consist of complex nonlinear systems of differential equations based on the diffusion of CO_2 through the concrete. For these models, experimental data is usually needed, both for the determination of the input parameters and for the validation of the model itself. For that, detailed knowledge of pH-profiles as a function of time is especially important.

3.3.7 Chloride-induced corrosion

Halides can attack and locally destroy the passive layer that protects steel from corrosion [104, 105]. In this regard, chloride attack is particularly important as chlorides are present in many environments, e.g., seawater and deicing salts.

In contrast to general corrosion processes, e.g., carbonation-induced corrosion (section 3.3.4), where corrosion occurs homogeneously over the entire metal surface, the local breakdown of the passive layer leads to localized corrosion. The potential at which the passive layer is locally destroyed is called pitting potential E_{pit} and the morphology of the attack, consisting of a small cavity formed on the steel surface, is referred to as *pit*.

The geometry of the pit imposes some restrictions in terms of mass transport. For example, oxygen diffusion into the pit is usually slower than its depletion through the cathodic reaction. Consequently, areas no longer protected by the passive film act as local anodes with respect to surrounding still passive areas where the cathodic reaction takes place.

Once corrosion has initiated, a very aggressive environment is produced inside the pits. Chlorides, being negatively charged ions, migrate to the anodic region, where the positively charged iron ions (Fe^{2+}) are produced. In addition, the dissolved iron ions hydrolyse. A possible reaction is [106]:

$$Fe^{2+} + H_2O \rightarrow FeOH^- + H^+ \qquad (28)$$

The electrolyte in the pit is acidified (Eq. (28)) so repassivation is avoided. In contrast, the passive film in the cathodic area is strengthened due to chloride migration to anodic zones and alkalinity production in the cathodic reaction (see Eq. (24)). As a result, both anodic and cathodic behaviors of the respective active and passive zones are stabilized and a macrocell is established, i.e., the anodic and cathodic reactions are spatially separated.

To maintain electroneutrality, negatively charged ions (anions) present in the pore solution migrate to the pit, while positively charged ions (cations) migrate to the exterior bulk solution. In neutral or alkaline water, e.g. concrete pore solution, hydroxide ions also migrate to the pit, preventing a fall in pH in the area around it. Due to the presence of an ohmic resistance, the potentials at the anode and at the cathode are not equal, as energy is dissipated by this ionic current passing the resistance in the electrolyte.

Fig. 10 schematically summarizes the chloride-induced corrosion process of steel embedded in concrete.

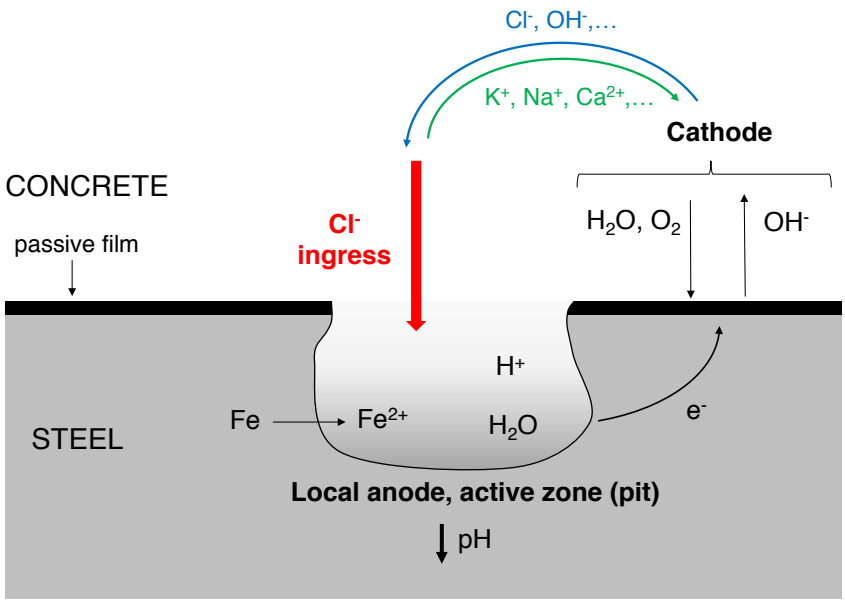

Fig. 10 Schematic representation of the chloride-induced corrosion process of steel embedded in concrete

Corrosion caused by chloride penetration can reach rates up to 1 mm/y, i.e., 10 times faster than carbonation-induced corrosion (section 3.3.4) [7].

3.3.8 Critical chloride content

Initiation of pitting corrosion takes place when the chloride content at the surface of the reinforcement reaches a *threshold value* (or *critical chloride content*). The critical chloride content is usually expressed as percentage of chlorides by mass of cement.

When exposed to the atmosphere, the risk of corrosion initiation for non-carbonated concrete structures made of OPC is traditionally considered low for chloride contents below 0.4% by mass of cement and high for contents above 1% by mass of cement [7, 107]. These values are only indicative, as the critical chloride content depends on numerous factors [12, 105, 107-111]. The main factors are described in the next paragraphs.

The risk of corrosion initiation increases as the Cl^-/OH^- ratio rises above a certain value [15, 22, 112, 113] but there is also a great variability in the reported critical chloride to hydroxide ratios [22, 110], as it depends on several parameters, e.g., type of cement. The most famous reference in this regard is the one by Hausmann [113], that suggested a critical chloride to hydroxide ratio of $Cl^-/OH^-=0.6$.

The influence of blended cements with additions of pozzolana or blast furnace slag on the chloride threshold is subject to controversy; while some authors reported that these cements exhibit lower critical chloride contents [82, 114, 115], others [116] indicated that this depends on other factors, such as the free chloride content, total chloride content, and the Cl^-/OH^- ratio. For sulfate-resisting cements with low C_3A content, the critical chloride content seems to be lower than for Ordinary Portland Cement [7].

Presence of voids (air voids, crevices, or microcracks) may weaken the layer of cement hydration products deposited at the steel/concrete interface, favoring the local acidification required for propagation of pits (section 3.3.7). In contrast, solid hydration products on the steel surface protect the steel from chloride attack [21, 22, 110].

The exposure conditions of the structure also influence the chloride threshold. For example, when the moisture content of concrete is near the saturation level, the transport of oxygen is hindered, resulting in a chloride threshold up to one order of magnitude greater than for structures exposed to the atmosphere [7].

3.3.9 Chloride binding capacity

In concrete, chlorides can be found in three different forms [83]: chemically bound (e.g., Friedel's salt), physically adsorbed (e.g., adsorbed on C–S–H), and dissolved in the pore solution, i.e., *free chlorides* [83]. The relation between free chloride ions and bound chlorides (including both chemically bound and physically adsorbed) is described in the *chloride binding isotherms* reported in literature [117, 118].

It is generally assumed that only the chlorides that are freely dissolved in the pore solution interact with the steel and lead to depassivation. *Chloride binding capacity* is thus an important property, which depends on the cement mineralogical composition, microstructure, pH of the pore solution, temperature, chloride salt, etc. [14, 15, 22, 83, 107, 112, 119-121]. Generally, binders with higher amounts of aluminate phases, e.g., C_3A and C_4AF, have a higher binding capacity [122-124], as these phases form Friedel's salt [125]. In contrast, a decrease in the alkalinity of the pore solution may lower the binding capacity due to the increase in the solubility of Friedel's salt [87, 120]. The microstructure of the material is also important, as denser cement matrix may increase the adsorption of chloride ions on the C–S–H [83, 107, 111].

Nevertheless, it should be noted that bound chlorides can (at least) partially be released as soon as the pH drops [83, 99, 107, 110], as for example if the concrete carbonates (section 3.3.4) [83, 99, 107, 110]. Additionally, chlorides may also be released (or less chlorides will be bound) in the presence of sulfates, e.g. in seawater [83].

Chloride binding in blended cements

Binding capacity of cements with low content of aluminate phases is lower than those with a higher content of these phases [83, 120, 126]. Because of this, CEM V has a lower chloride binding capacity compared to OPC. In contrast, cements bended with slag and fly ash have higher binding capacities than OPC [119, 120, 126, 127]; this is likely due to the presence of Al_2O_3 phase in these admixtures, which contributes to the formation of Friedel's salt [83, 107]. In fact, CEM III, has a higher resistance against chloride-induced corrosion, probably due to the increased binding capacity [125]. Finally, the addition of silica fume decreases the chloride binding capacity [87, 119, 120].

In conclusion, blended cements may tolerate higher total chloride content despite the overall lower chloride threshold (see section 3.3.8) due to the increased binding capacity.

3.3.10 Penetration of chlorides into concrete

As previously mentioned, the service life of reinforced concrete structures can be divided into initiation and propagation stages [99]. In the case of chloride-induced corrosion, the initiation stage is the time until a certain concentration of chlorides (critical chloride content) reaches the reinforcement and the steel is depassivated. Knowledge of the kinetics of chloride transport into concrete is thus essential for the assessment of the service life of the structure.

Chloride transport in concrete is a complex process that comprises the following mechanisms: capillary suction, diffusion, permeation, and migration. Nevertheless, chloride profiles in concrete are traditionally modelled with the following equation based on Fick's second law of diffusion:

$$C(x,t) = C_0 + (C_S - C_0)\left(1 - \mathrm{erf}\left[\frac{x}{2\sqrt{D_a(t)\cdot t}}\right]\right) \quad (29)$$

where $C(x,t)$ is the chloride concentration (mol·L^{-1}) at depth x (m) and time t (s), C_0 is the initial chloride content in concrete (mol·L^{-1}), C_s is the chloride content at the exposed surface (mol·L^{-1}), and D_a (m^2·s^{-1}) is the apparent diffusion coefficient.

The apparent diffusion coefficient D_a is obtained from fitting experimental data and it mainly depends on exposure conditions, time, and material. The time-dependence of D_a is usually expressed with the following equation:

$$D_a(t) = D_0 \left(\frac{t_0}{t}\right)^n \quad (30)$$

where D_0 ($m^2 \cdot s^{-1}$) is a reference apparent diffusion coefficient at a reference time t_0, and n is the age factor, which is a constant depending on the type of cement.

The diffusion model described above provides relatively good results but it is mainly based on empirical data and relies on simplified assumptions, e.g., chloride transport is based on purely diffusion. In order to provide more accurate results, other models have been developed, where the cement microstructure and age of the material are specially considered [77, 128-130]. These models include other processes, such as chloride binding, migration of ions, electrical interactions between different ionic species, etc. Data of chloride profiles for different types of cement and exposure conditions are important, both for the determination of the input parameters and for the validation of the model itself.

3.3.11 Factors affecting the corrosion potential E_{corr} of steel

The corrosion potential E_{corr} (section 3.3.3) depends on several parameters, such as pH, chloride content, oxygen content, type of cement, etc. [7].

When exposed to the atmosphere and in the passive state, the reinforcement generally has a corrosion potential between +100 and -200 mV vs. SCE [7]. However, when concrete is saturated with water, the diminished supply of oxygen to the steel surface can bring the potential down to values below- 400 mV vs. SCE and it may even reach values below -900 mV SCE when oxygen is totally lacking [7].

The presence of chloride ions in concrete leads to changes in the anodic polarization curve and reduces the passivity range. As a result, the corrosion potential can be below -500 mV vs. SCE in concrete with a high content of chlorides [7].

Experience shows that the corrosion potential depends on the moisture content in concrete, with more positive values being measured in dry concrete [7]. When the moisture content decreases, the ohmic drop must be additionally taken into account. In this case, the potential

of the steel has an intermediate value between the anodic and cathodic potentials, within the range of 0 to -600 mV vs. SCE.

Additionally, the type of cement replacement may also influence the corrosion potential, e.g. lower potentials were registered in slag cement [131].

It can thus be deduced that the measurement of the potential of the reinforcing steel does not necessarily indicate whether it is in the passive or active state. The chloride concentration and the pH at the steel/concrete interface are in this regard the two most important parameters to determine the corrosion state of the reinforcement, as they are directly related to the stability and breakdown of the passive film and the posterior corrosion initiation (see sections 3.3.4 and 3.3.7). Coupling data of steel potential, chloride concentration and pH is thus especially useful in to order to asses reliably the corrosion state of the steel reinforcement in concrete.

4 STATE-OF-THE-ART

This section gives an overview on the available embeddable sensors for concrete to be used as reference electrode, chloride sensor and pH sensor. The advantages and limitations of the different sensors are discussed.

4.1 Requirements of embeddable sensors for concrete

Overall, sensors to be embedded in concrete must fulfill the following requirements:

- Be long-term stable in highly alkaline environment (ideally for several decades as it may take many years until the carbonation front and/or sufficient concentration of chlorides reach the reinforcement);
- Response time up to a few days is sufficient for the desired application, as the processes leading to changes in pH and chloride concentrations are relatively slow;
- Be insensitive to oxygen, as different oxygen contents can be found for different exposure conditions; thus, this could lead to measurement errors;
- They should not introduce harmful species into the concrete (e.g. chlorides);
- Have low or no polarizability, and in case of accidental polarisation the sensors should return to their original potential (for potentiometric sensors);
- Have a low impedance in order not to compromise the sensitivity of the instruments used for potentiometric measurement (for potentiometric sensors);

Other requirements for embeddable sensors for concrete depend on the specific application. In the next section, the requirements of sensors to be used as reference electrode and as pH and chloride sensors are described. Note that these requirements apply to potentiometric sensors because other types of sensors are not investigated in this study (for reasons that will become clear in the state of the art).

4.1.1 Requirements of reference electrodes

The stability criteria of the potential response depend on the application. For corrosion monitoring purposes, the electrode potential should be stable, but a drift on the long-term (in the order of years) in the range of a few tens of millivolts might be acceptable, as steel corrosion is usually accompanied by a potential change of hundreds of millivolts [7]. In this case, the electrode does not have to exhibit a well-defined reversible potential, since for these applications, relative potentials (e.g. with respect to time) are more important than absolute

values. Thus, electrodes other than the reference electrodes defined in section 3.2.7 are, in principle, valid. In contrast, for the potential measurement of ion-selective electrodes, e.g. Ag/AgCl ISE used as chloride senor, a potential drift of the order of 10-20 millivolts can significantly affect the accuracy of the measurement [32, 39, 40, 132]. For the same reasons, if a metal/metal oxide, e.g., IrO_x electrode, is used as a pH sensor, a potential drift of ca. 20-30 mV would lead to measurement errors of ca. 0.5 pH units. Thus, in this case it is important that the reference electrodes have well-defined potentials and exhibit very low potential drifts, e.g. <1 mV/year.

Reference electrodes must be insensitive to changes in their environment (mainly to pH and to chloride concentration) as corrosion initiation is usually accompanied by changes in chloride content and/or pH and this could lead to the misinterpretation of the results.

Finally, it should be noted that concrete structures can be subjected to different exposure conditions, e.g. seasonal changes, which can lead to variable humidity and temperature conditions. Reference electrodes should ideally be independent on humidity and temperature. However, the potential response of most of electrodes depends on temperature [9, 41-46, 132]; thus, data should be available to make the appropriate corrections.

4.1.2 Requirements of chloride and pH sensors

As indicated in section 4.1.1, a potential drift of the order of 10– 20 millivolts significantly affects the accuracy of the response when ion-selective electrodes and metal/metal oxides are used as chloride and pH sensors respectively. It is thus important that these sensors have well-defined and reversible potential responses and exhibit very low potential drifts (e.g. <1 mV/year). Additionally, the sensors used for the measurement of pH and chloride concentration must be insensitive to species other than pH and chloride respectively.

Finally, the sensors responses should ideally be independent on changes in humidity and temperature. As most of the existing sensors are, at least, dependent on temperature [9, 41-46, 132], data to make the corresponding corrections should be available.

4.2 Long—term stable embeddable electrodes

4.2.1 Reference electrodes

Studies performed on reinforced concrete indicate that reference electrodes of the second kind (described in section 3.2.7) are relatively stable on the long term [9, 133]. A study carried

out over 10 years with embedded Ag/AgCl/KCl electrodes in concrete showed that these electrodes exhibit stable potential response on the long-term [133]. However, the performance of these electrodes can be impaired due to diffusion potentials at the liquid junction (liquid junction potential) [9, 31, 32, 39]. Despite the existence of models to predict the magnitude of diffusion potentials (see section 3.2.6), its quantification may become difficult, as the knowledge of the exact chemical composition of the concrete pore solution is needed and this is not straightforward, especially in field conditions. Moreover, the pore solution composition can drastically change because of carbonation and/or chloride ingress (see sections 3.3.4 and 3.3.7); thus, the liquid junction potential is also changed. In this case, the quantification of the liquid junction potential becomes impossible unless pH and chloride contents are monitored.

4.2.2 Pseudo reference electrodes

The manganese dioxide electrode (MnO_2) is one of the most widely used embeddable reference electrode for concrete [133-136]. A major advantage is the good long-term stability of these electrodes, e.g., at least up to 10 years [133-135].

This electrode is designed as a double junction electrode containing an inner NaOH solution of pH 13.5 [9]. Compared to SCE and Ag/AgCl/KCl electrodes (section 3.2.7), the liquid junction potential error is significant, e.g., the potential response of this electrode can increase by 30mV when the pH of the test solution decreases from pH 13.5 to pH 12.5 [9]. If the pH of the concrete pore solution remains constant at pH≈13.5, this problem is insignificant and it may be argued that these electrodes are suitable for monitoring the potential of reinforcing steel in the case of chloride-induced corrosion. However, the interpretation of the measured steel potential with these electrodes may then become difficult for example, when the cement paste carbonates. Moreover, deviations in the electrode potential were observed in chloride contaminated concrete [133].

Many metals, such as zinc, lead, stainless steel, platinum, gold, palladium, nickel, magnesium, magnesium alloys, titanium, etc. have also been tested but most of them generally show instability in the short term [134]. Although they are not currently in common use, lead and zinc have been used as reference electrodes in concrete [9, 134]. These materials exhibit a potential response as a consequence of corrosion reactions, i.e., mixed potentials [9]. Laboratory tests with zinc embedded in concrete have shown unstable and fluctuating potentials. Lead has a more stable electrochemical behavior in concrete in comparison to zinc,

but its potential response is not completely well-defined [9]. Additionally, there is a general concern because of the sensitivity of these electrodes to oxygen and pH [9].

Studies based on graphite and metal/metal oxides [9, 64, 133, 137] indicate that these electrodes are generally highly sensitive to pH changes and that graphite is moreover highly sensitive to the oxygen concentration.

Activated carbon pseudo-reference electrode seems to provide better stability compared to the existing metal and metal oxide pseudo-reference electrodes. However, at chloride concentrations higher than 0.5 mol·L^{-1}, the OCP of this electrode is reported to decrease about 12mV/decade [138]. This could lead to problems when high chloride concentrations are expected.

4.2.3 Electrode system

From sections 4.2.1 and 4.2.2, it can be seen that there is no reference electrode that meets the desired requirements of long-term stability and insensitivity to environmental changes. In this context, a promising suggestion was indirectly made in a doctoral thesis published in 1997 [139], where it was proposed to embed a combination of different electrodes that are sensitive to different environmental parameters (particularly pH and chloride). The individual potential changes of the electrodes would allow identifying the changes in the individual environmental parameters. The idea was unfortunately not further developed.

In this context, Dong et al. [140] later developed a multifunctional sensor for in situ and non-destructive monitoring corrosion, based on a reference electrode (MnO_2 electrode) combined with a pH sensor (Ti/IrO_2 electrode) and a chloride sensor (Ag/AgCl ion-selective electrode). The main advantage of this approach would be the improved interpretation of corrosion potential data, as corrosion potential largely depends on the chemical environment (section 3.3.11). However, as indicated in section 4.2.2, the potential response of the MnO_2 electrode is affected by pH changes and thus, the reliability of the potential response of this electrode could be seriously compromised, for example when cement paste carbonates. To solve this problem, the potential drift of the MnO_2 electrode caused by pH changes should be evaluated and its potential response corrected accordingly. The authors however, did not consider this aspect.

4.3 Sensors to monitor chloride concentrations in solution

4.3.1 Chloride ion-selective electrodes (ISE)

Measurement of chloride concentrations in concrete by means of embedded sensors is traditionally done with Ag/AgCl ion-selective electrodes (ISEs) [39, 141-145]. This is a well-established method in laboratory conditions; but attempts of in situ use of Ag/AgCl ISEs in concrete have also been made. These chloride sensors show good long-term stability and sensitivity to chloride ions [39, 141-144] but their performance may be impaired by the presence of interfering ions [13, 39, 146-149]. In concrete, problems may arise in presence of mid-high concentrations of sulfide ions, as for example, in slag cement. This aspect is further discussed in papers I and II.

Another factor that may impair the performance of these sensors is the absence or low content of chlorides in highly alkaline environments. In this case, the AgCl membrane may transform into Ag_2O [150] and the sensor response may then be influenced by the pH. Nevertheless, it has been reported that the sensors are able to recover fast as soon as they come into contact with chlorides [39, 151]. More research is however needed regarding the long-term stability (in the order of years) of the Ag/AgCl ISE membrane in absence of chlorides and exposed to highly alkaline environments.

In order to improve the performance of ion-selective electrodes, several variations in the composition of these electrodes have also been made in the last years. A promising solution has been made by Karthick et al. [152]. The approach is based on an Ag/AgCl ion-selective electrode coated with a polymeric membrane. This approach would prevent the membrane transformation into Ag_2O when exposed to alkaline environments, without compromising the performance of the sensors. In fact, this type of Ag/AgCl ISEs seems to provide better stability compared to the non-coated ones. However, studies with these Ag/AgCl ISEs when embedded in concrete do not exist.

4.3.2 Other sensors

In section 4.3.1, chloride determination is based on a potentiometric measurement between the Ag/AgCl ISE and a reference electrode. However, a long-term stable reference electrode for concrete still does not exist (section 4.2). In order to solve this problem, Abbas et al. [153, 154] proposed a method based on a chronopotentiometric approach. In chronopotentiometry, the potential of an electrode is measured while a current pulse is applied. In this case, a galvanostatic pulse is applied to an Ag/AgCl ISE, which initiates a faradaic reaction depleting

the Cl^- ions near the sensor surface. One approach would consist of measuring the Ag/AgCl ISE potential against another electrode and relating it to the chloride concentration [154]; whereas another approach would consist of measuring the time needed to completely deplete the chloride ions near the sensor surface, which is a function of the chloride concentration [153]. In both cases, a reference electrode is needed but it only needs to provide a stable potential during the measurement time, i.e., in the order of seconds; thus, any metal wire or pseudo-reference electrode could be used. Despite the advantage that no long-term stable reference electrode is needed, this method may present several limitations. For example, the response obtained is not stable at high pH and very low chloride concentrations; high current is needed for high chloride contents, which can in turn degrade the Ag/AgCl ISE membrane; the Ag/AgCl ISE membrane can also be degraded due to the interaction of other ions, e.g., hydroxide ions, after chlorides are depleted at the sensor; long-term stability of these sensors has not been addressed, studies in concrete are lacking, etc. In order to avoid the degradation of the Ag/AgCl ISE membrane due to the applied electric current, the authors proposed a system with a separated sensing electrode (chloride sensor) and actuating electrode (actuator). In this case, a constant current is applied to the actuator, which will cause changes in the chloride concentration that can be determined with the sensing electrode. This proposal would avoid the degradation of the Ag/AgCl ISE membrane derived from the electric current applied. However, the other limitations would still remain [155].

A few works based on the use of fibre optic sensors to determine chloride concentrations in concrete have been made [156, 157] but they present some limitations. McPolin et al. [156] observed that the measurement of chloride concentration was biased by a reaction involving chlorides and sensor components; this reaction is irreversible and thus the functionality of the sensor was impaired. It was thus concluded that the sensors required further development. Tang et al. [157] reported better results, where the studied sensors exhibited high sensitivity, good accuracy, e.g., concentration fluctuations below 0.3% after 72 hours, and promising preliminary results in concrete. Despite the promising results, long-term stability studies should be extended to much longer times, i.e., in the order of months to years, as the registered drifts could lead to serious measurement errors on the long-term. Therefore, fibre optic sensors to determine chloride concentrations need to be further developed to be used in concrete.

4.4 Sensors to monitor pH in the concrete pore solution

There is currently no well-established sensor to measure pH in the concrete pore solution. In this regard, the most challenging requirement concerns the long-term stability in strongly alkaline conditions. Different sensors have been developed for this purpose; among them metal oxides and fibre optic sensors have been tested in concrete [158].

4.4.1 Fibre optic sensors

Fibre optic sensors present some advantages, such as low price and overall chemical stability. However, most of the currently available fibre optic sensors present severe limitations for the application in concrete [69-73, 156, 159, 160]: the pH-range that they can accurately measure is very narrow (e.g., the reported results are usually within a range of 2 pH units), the measured pH may be inaccurate in some cases due to leaching effects, these sensors usually present chemical instability at high pH values, and very few studies exist where pH>13 has been measured.

A promising solution was suggested by Nguyen et al. [71], who proposed a fibre optic pH sensor that could provide a reliable and reproducible response over a pH range of 10-13. In this case, the sensors were tested several times for about 20 months. Between measurements, the sensors were stored and thus, data on continuous immersion in alkaline solution is not available. Additionally, studies in concrete are lacking. It is believed that before using the sensors in concrete, the long-terms stability when continuously immersed in alkaline solution should be investigated.

Only a few studies have been performed with fibre optic sensors in concrete. Basheer et al. [160] reported fibre optic sensors that were able to reliably measure pH values between ca. pH 9-13 in solution. However, the life-span was too short for the desired application and when tested in concrete, the sensors were only able to provide a reliable response during the first minutes of cement hydration because the pH presumably exceeded the upper limit of the sensor (pH 13). McPolin et al. [156] embedded a fibre optic pH sensor in a carbonated mortar specimen and monitored pH fluctuations until 18 months. No data was reported regarding the reliability of the measured pH or while cement paste was carbonated, i.e., pH changes in the pore solution were not monitored. Habel et al. [159] tested fibre optic sensors embedded in concrete structures but the pH range measured was limited to pH<13. While the results were satisfactory, no data regarding the long-term stability (in the order of several years) exist and additionally, the authors indicated that problems could arise in relatively dry environments.

In conclusion, the performance of fibre optic sensors overall presents severe limitations for the application in concrete, especially in terms of life span and pH range covered. Additionally, results in terms of long-term stability and accuracy of the potential response when embedded in concrete are lacking.

4.4.2 Potentiometric sensors – metal/metal oxides

Concerning the use of potentiometric sensors as pH sensors, the IrO_x electrodes showed promising results in terms of high stability in a broad pH range, i.e., from pH 1-2 up to pH 13 [50-58]; accuracy [50-58]; and insensitivity to oxygen in solution [51, 52].

Regarding the performance of these sensors in concrete, only two studies have been reported. Du et al. [149] measured pH fluctuations, i.e., pH range measured between 12.5 and 13.5, over 60 days at the interface between reinforcing steel and mortar when the mortar sample was exposed to chloride ingress. Dong et al. [140] used an iridium oxide electrode (formed on a Ti substrate, i.e., Ti/IrO_2 electrode) to monitor the pH while a concrete sample was exposed to dry/wet cycles over 250 days. In this case, the pH measured ranged between 11.5 and 13.5.

From the reported works with embedded IrO_x electrodes, it can be deduced that despite the promising results, there are many aspects that were not investigated: long-term exposure, i.e., experiments were limited to <1 year; potential response at pH<11, i.e., pH measured was always >11.5; and pH evolution while cement paste is carbonated, which would be the main desired outcome. Additionally, the accuracy of the pH obtained with these sensors was not validated with another method, e.g. pH-indicator spraying test. Thus, experience in concrete needs to be further developed. These aspects are studied in papers III, IV, and V.

Finally, it should be noted that since IrO_x electrodes are potentiometric sensors, a long-term stable reference electrode would be needed.

5 METHODS USED

In this section, the most important features of the main experimental techniques used in this work are summarized.

5.1 Potential measurement

The potential of the electrodes used in this work was measured according to the set-up shown in Fig. 5. The potential measurements between the working electrode and the reference electrode were performed with a PGSTAT 30 Autolab potentiostat/galvanostat (Metrohm Autolab, Utrecht, the Netherlands) with high input impedance (100 GΩ).

When the electrodes were immersed in solution, their potential was measured against the silver/silver chloride/saturated potassium chloride (Ag/AgCl/sat. KCl) reference electrode (+0.199 V vs. SHE). A Luggin capillary was used to avoid contamination derived from the contact between test solution and electrolyte of the reference electrode. For the tests with electrodes embedded in mortar, the silver/silver chloride/saturated potassium chloride (Ag/AgCl/sat. KCl) reference electrode was used as external reference electrode for the calibration of the embedded electrodes. This external reference electrode was placed on the specimen surface and simulated pore solution (0.15 mol·L^{-1} NaOH 0.2 mol·L^{-1} KOH and sat. $Ca(OH)_2$) was used to establish electrolytic contact. A Ag/AgCl ion-selective electrode was used as internal embedded reference electrode. This electrode exhibits a stable and well-defined potential response for a known concentration of chlorides; this electrode was thus embedded in mortar containing known content of chlorides so the reference potential was fixed and stable.

5.2 Microscopic image analysis

5.2.1 Optical microscope analysis

The optical microscope uses visible light and a system of lenses to produce magnified images of the samples to be analyzed. The light can be either transmitted through the sample (usually for samples with a thickness of about 30 μm) or reflected from the sample surface (usually for thicker samples). Optical microscopes can be very simple but there are also many complex microscopes designs aiming to improve the resolution. In this regard, the stereoscopic microscope is an optical microscope in which the light is reflected from the sample surface and it has a resolution of a few μm. In the present work, images of the sensors used were obtained with Leica M60 stereoscopic microscope.

5.2.2 Scanning electron microscope (SEM) analysis

A scanning electron microscope (SEM) is a type of electron microscope that produces images of a sample by scanning its surface with a focused beam of electrons [161, 162]. The electrons beam interacts with the atoms in the sample, typically to a depth of ca. 1 μm, producing various signals, of which the two most often used are backscattered electrons and secondary electrons. When the electrons enter the sample, they might lose all their energy or might be deviated so they will leave the sample (backscattered electrons). Secondary electrons are outer shell electrons that are hit by the electron beam and ejected from the atom.

A detector within the SEM collects both backscattered and secondary electrons in order to form the image. In this context, topographic contrast arises because the number of backscattered and secondary electrons depends on the angle between beam and local surface. The resolution in this case is of a few nm.

The main limitation of conventional SEM microscopes is that they require that the studied samples are under vacuum. In the case of concrete or cement paste, this implies that the microstructure and some properties may be altered. To solve this issue, an environmental scanning electron microscope (ESEM) is normally used, which allows study of samples in a low-vacuum and high relative humidity environments [162].

In this work, the cross section of the produced IrO_x electrodes was studied with a quanta 200 3D (FIB) environmental scanning electron microscope by FEI.

5.3 Carbonation depth (pH indicator)

A pH indicator is a chemical compound that changes its color depending on the pH of the solution or surface with which it is in contact. This technique has been widely used for the determination of carbonation depth in concrete, i.e., depth at which the pH gradient meets a selected pH value (e.g. pH≈9 in concrete). The method consists of spraying the indicator solution on freshly exposed concrete surfaces, thus, it requires destructive testing. The carbonation depth is then usually determined from the average (together with the standard deviation) of several measurements of the depth of color change.

The most common indicators used in concrete are phenolphthalein (color change at pH≈9), and thymolphthalein (color change at pH≈10) [163]. Other indicators that can be used in concrete are indigo carmine (color change at pH≈12.6), tropaeolin O (color change at pH≈12),

or a combination of phenolphthalein and thymolphthalein (color change at pH≈11) [163]. The accuracy of this method is roughly one pH unit. In the present work, a thymolphthalein solution was used to determine the carbonation depth.

5.4 Acid digestion/potentiometric titration method for chloride determination

In general, the methods used for the determination of the total chloride content (usually in % by cement weight) of a mortar (or concrete) sample are based on the homogenization of a representative dry sample of mortar (or concrete) powder and the subsequent dissolution of it in acid. The total chloride content is then measured by various methods, such as titration or spectrophotometry.

In the present work, the analysis of the total chloride content was performed with a method based on the acid digestion of mortar powder followed by potentiometric titration with silver nitrate solution, based on the EN 14629 standard [164]. The extraction procedure was the following: about 3 gr of powdered mortar (with mix proportions cement/water/sand 1: 0.5: 2) were mixed with 20 mL of 5 mol·L^{-1} nitric acid. This solution was stirred for 10 minutes; then 40 mL of deionized water were added and this solution was stirred again for 3 minutes (at 85-95°C). Afterwards, ammonia solution was added until a pH between 3 and 5 was reached. Potentiometric titration was next performed. Silver nitrate solution (0.1 mol·L^{-1}) was added incrementally so the chloride ions would precipitate as silver chloride. At each step, the potential of the filtrate was measured with a chloride ion-selective electrode. This allowed the endpoint, which is the amount of silver nitrate required to precipitate all chloride ions, to be determined.

There is a certain degree of uncertainty associated to the total chloride content analyzed with this method. For example, the aggregate fraction and size can introduce a certain degree of variability in the results, as specimens may be too small to be representative of bulk concrete [165]. In this case, samples consisted of mortar with aggregate size <1 mm and thus, the error arising from this is minimum.

Finally, it should be noted that sulfides are known to interfere with the determination of chloride content [166]. Blast furnace slag aggregates and cements contain sulfide in concentrations that can produce erroneously high test results. To eliminated this interference, treatment with hydrogen peroxide, as described in [167], should be used.

6 DISCUSSION

This project proposes an electrode system composed of several Iridium/Iridium oxide (IrO_x) electrodes and several Ag/AgCl ion-selective electrodes, embedded in concrete at different locations. The approach is based on the potentiometric measurements between all the embedded electrodes. An algorithm was developed that allows associating any potential change of the individual electrodes with the specific environmental change, i.e., pH and chloride concentration, and obtaining a well-defined potential response at all times, i.e., a reference potential. The most important aspects of this proposal are discussed here.

6.1 Long—term stable embeddable electrode system

This thesis proposes an electrode system to be embedded in concrete, composed of several Ag/AgCl ISEs and several Iridium/Iridium oxide (IrO_x) electrodes. A schematic representation of this electrode system is shown in Fig. 11.

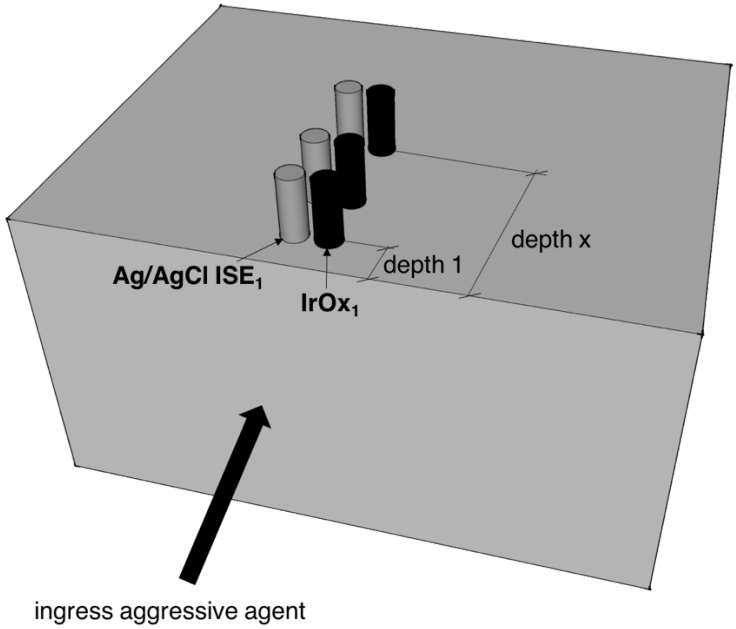

Fig. 11 Schematic representation of the electrode system composed of several IrO_x electrodes and several Ag/AgCl ISEs embedded at different cover depths

In this thesis, it has been shown that the potentiometric response of an IrO_x electrode $E_{\mathrm{IrO_x}}$ is dictated by the pH of the pore solution (paper III) and independent on the chloride content (Appendix): $E_{\mathrm{IrO_x}} = f(pH)$. On the other hand, the potentiometric response of an AgCl ion-selective electrode $E_{\mathrm{Ag/AgCl\ ISE}}$ is determined by the chloride concentration in the pore solution

(papers I and II) and independent on the pH (papers I-II, Appendix): $E_{\mathrm{Ag/AgCl\ ISE}} = f(\mathrm{Cl^-})$. Therefore, the studied IrO_x electrodes and Ag/AgCl ion-selective electrodes can successfully be used as pH and chloride sensors respectively. In order to do that, the potential of the Ag/AgCl ISEs and IrO_x electrodes must be measured and converted into chloride concentration and pH respectively. This is only possible if diffusion potentials arising between these electrodes and the reference electrode are taken into account. In this work, an algorithm is developed (section 6.3) that enables separating electrodes potentials from diffusion potentials.

In a potentiometric measurement, the potential of the working electrode (Ag/AgCl ISE and IrO_x electrodes) is referred to the potential of another electrode with known and fixed potential, i.e., the reference electrode (see section 3.2.4). The Ag/AgCl ISEs and IrO_x electrodes proved to exhibit a well-defined and long-term stable potential for known conditions chloride concentration and pH respectively. Thus, when pH and chloride concentration at a given electrode location are known, both Ag/AgCl ISEs and IrO_x electrodes can be used as reference electrode.

Section 6.1.1 summarizes the main conclusions on the use of the Ag/AgCl ion-selective electrode as chloride sensor and discusses its use as reference electrode. Section 6.1.2 gives an overview on the use of the IrO_x electrode as pH sensor and discusses its use as reference electrodes.

6.1.1 Ag/AgCl ion-selective electrode as chloride sensor and as reference electrode

The Ag/AgCl ISEs exhibit a well-defined potential response for a given concentration of chlorides with an accuracy of ca. ±0.05 mol·L^{-1}, independent on the pH (see papers I-II). The *detection limit* of chloride ion, i.e., minimum detectable chloride concentration, in aqueous neutral solution is <0.002 mol·L^{-1} (paper I) and <0.01 mol·L^{-1} at pH≈14 according to Angst et al. [39].

At low concentration of chlorides, i.e., below the detection limit, the potential response of this electrode is not well-defined (papers I-II) and it should not be used as reference electrode. Nevertheless, absence of chlorides does not impair the functionality of the Ag/AgCl ISE as chloride sensor, since upon chloride arrival, this electrode exhibits the potential response expected from the calibration curve, e.g., in this work, the Ag/AgCl ISEs exhibited a stable

potential response for 60 days after being exposed to chloride-free alkaline solutions for ca. 60 days (paper I-II).

The Ag/AgCl ISE should neither be used as chloride sensor nor reference electrode in presence of sulfides due to the interference caused by this ion, e.g., the potential response of the Ag/AgCl ISEs was affected by sulfide concentrations >0.006 mol·L^{-1} in presence of 0.01 mol·L^{-1} of chlorides. This interference is likely more pronounced for lower chloride concentrations (papers I-II).

It can thus be concluded that the Ag/AgCl ISEs can successfully be used to monitor chloride concentrations in concrete (paper V and Appendix) and when the chloride concentration is known, they can also be used as reference electrodes (paper V and Appendix).

6.1.2 IrO_x electrode as pH sensor and as reference electrode

The IrO_x electrodes produced in this work exhibited a stable and defined potential response to pH for almost 2 years exposed to alkaline solution (paper III) and for about 6 months when embedded in concrete (papers IV-V). From the obtained results, it was concluded that they can be used to monitor pH with a maximum error of 0.5 pH units at least over a range of pH 9-13.5. The potential response of the IrO_x electrodes is additionally independent on both oxygen content (paper III) and chloride content (Appendix). Thus, the IrO_x electrodes can also be used as reference electrodes if the pH is known.

It is important to note that upon immersion in aqueous solution, the potential of IrO_x electrodes shifts during the first months but after sufficient immersion time, i.e., conditioning for ca. 3-4 months (paper III), in alkaline solution the IrO_x electrodes exhibit a drift-free potential response. It was also observed that each produced IrO_x electrode responds slightly different (paper III); thus, it is recommended that pre-calibration of each IrO_x electrode is performed before use.

Finally, it should be noted that concrete structures are subjected to exposure conditions that can lead to variations in humidity, e.g., wet-dry, cycles, and temperature. The IrO_x electrode performed well in a relatively dry environment (65% RH, paper IV) but since the oxide layer formed on the iridium substrate is likely hydrated, the potential response of this electrode in drier environments needs to be studied. The effect of temperature on the electrode response also needs to be addressed in further work.

6.2 Diffusion potentials

In concrete, diffusion potentials will arise due to pH gradients when the concrete carbonates and/or due to chloride concentration gradients when chloride ingresses the concrete. As indicated in section 3.2.6, diffusion potentials in the order of hundreds of mV have been reported in concrete [33-35]. Therefore, the correction of the measured electrode potential with respect to the diffusion potential is especially important, as will be illustrated in this section.

Fig. 12a shows the diffusion potential established between a solution β (Fig. 6) without chlorides and solution α (Fig. 6) with chloride concentration ranging from 0 until 5 mol·L^{-1}. In this case, both solutions have pH≈13.5. Fig. 12b shows the diffusion potential established between a solution β with pH≈13.5 and solution α with pH ranging from 11 until 13. In this case, both solutions are chloride-free. The diffusion potential is calculated with Eq. (11) for two types of alkaline solutions, one containing NaOH and the other containing KOH so the effect of the counter ion (Na^+, K^+) can be evaluated. For the calculation, ionic mobilities of the involved ions (Na^+, K^+, Cl^-, and OH^-) are taken from [25].

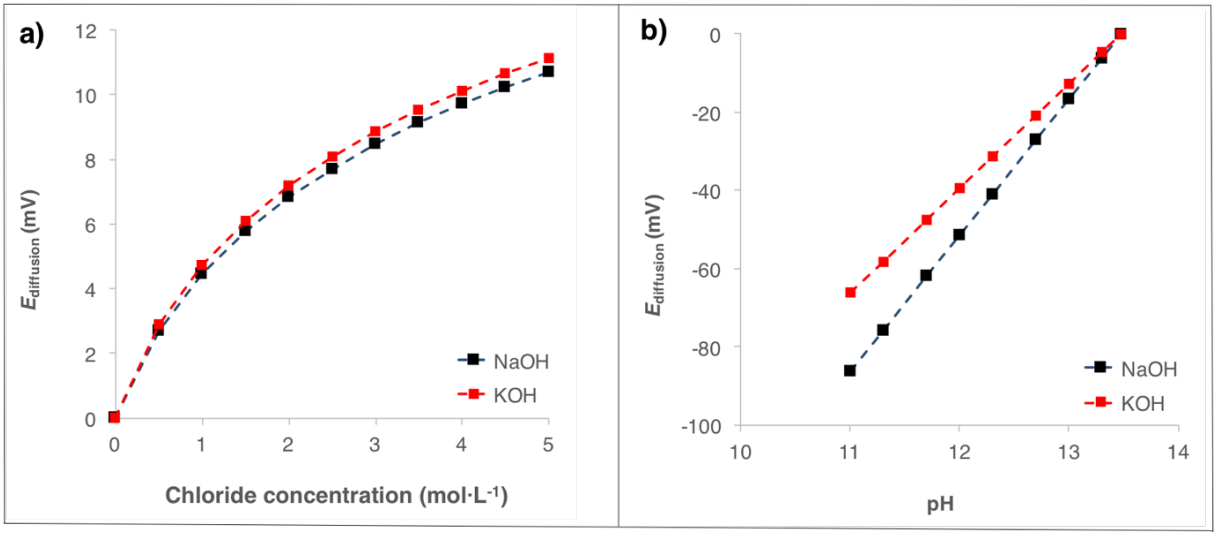

Fig. 12 (a) Diffusion potential established between a solution β without chlorides and solution α with chloride concentration ranging from 0 until 5 mol·L^{-1}. Note that both solutions have pH≈13.5 and that $E_{diffusion}$ is plotted as a function of the chloride concentration of the solution α (b) Diffusion potential established between a solution β with pH≈13.5 and solution α with pH ranging from 11 until 13. Note that both solutions are chloride-free and that $E_{diffusion}$ is plotted as a function of the pH of the solution α. In both cases, the diffusion potential is calculated with Eq. (11) for two types of alkaline solutions, one containing NaOH and the other containing KOH.

From Fig. 12, it can be seen that the diffusion potential increases with the difference in chemical composition between the solutions involved, where the pH has the highest impact, reaching values up to ca. 60 mV for a gradient of 2 pH units.

Diffusion potentials differ depending on the ions dissolved in solution, i.e., differences in the calculated diffusion potentials can be observed between the NaOH and KOH solutions despite having the same pH (Fig. 12). The largest difference in the calculated diffusion potential between the NaOH and KOH solutions is of 20 mV for a gradient of 2 pH units. This potential difference corresponds to <0.5 pH units in the response of the studied pH sensors (compare section 6.2.1) and it is comprised within the accuracy range of this electrode (paper III). Nevertheless, it should be noted that often pore solutions are a mixture of NaOH and KOH, thus deviations in the calculated diffusion potentials due to differences in the exact composition of the pore solution are expected to be lower in most of cases, compared to the results shown in this section. Consequently, diffusion potentials in the pore solution would change with respect to the results shown in Fig. 12 but it is considered that they will not compromise significantly the reliability of the sensors proposed in this work.

Due to the exact pore solution composition being unknown, especially as carbonation of the cement paste proceeds, NaOH solution has been considered for the calculation of diffusion potentials in this work, i.e., Na^+ is considered as a charge balance to the OH^- concentration that will change as cement paste carbonates.

6.2.1 Effect of diffusion potentials on the potentiometric response of Ag/AgCl ISE and IrO_x electrodes

Diffusion potentials add arithmetically to the measured potential $E_{measured}$ between the working electrode and the reference electrode (Fig. 5). Fig. 13 shows a schematic representation of the measured potential $E_{measured}$ between a pH or chloride sensor (working electrode) and a reference electrode in presence of a diffusion potential due to pH and/or chloride gradients in concrete.

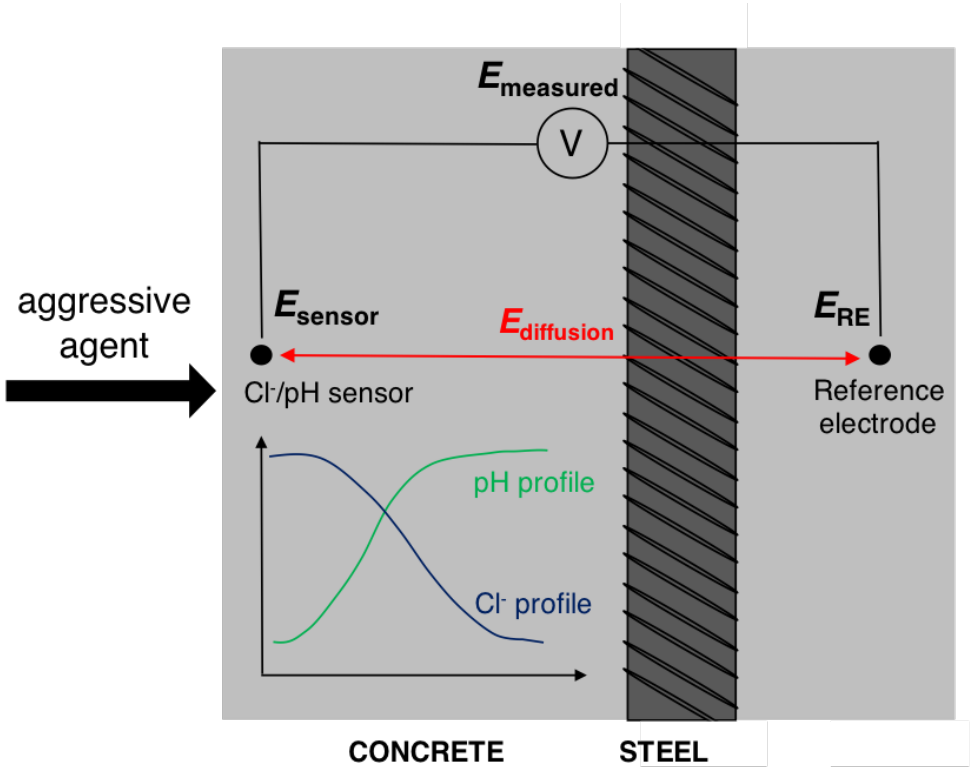

Fig. 13 Schematic representation of the measured potential $E_{measured}$ between a pH or chloride sensor and a reference electrode in presence of a diffusion potential due to pH and/or chloride gradients in concrete.

The measured potential $E_{measured}$ is written as:

$$E_{\text{measured}} = E_{\text{sensor}}(\text{vs. RE}) + E_{\text{diffusion}} = E_{\text{sensor}} - E_{\text{RE}} + E_{\text{diffusion}} \quad (31)$$

where E_{sensor} is the potential response of the pH or chloride sensor (working electrode).

The effect of the diffusion potential on the accuracy of pH and chloride concentration obtained with the studied pH and chloride sensors can be illustrated with a simple calculation. From the calibration curves of the Ag/AgCl ISE (papers I-II) and considering a theoretical $E_{\text{IrO}_x} - pH$ slope of -0.059 mV/pH for the IrO_x electrode (paper III), the chloride concentration and pH are respectively obtained for two cases: a) the measured potential is corrected for the diffusion potential ($E_{\text{sensor}} = E_{\text{measured}} + E_{\text{RE}} - E_{\text{diffusion}}$); b) the measured potential is not corrected for the diffusion potential ($E_{\text{sensor}} = E_{\text{measured}} + E_{\text{RE}}$). For this calculation, it is assumed that the electrolyte at the reference electrode location contains 0 mol·L^{-1} of chlorides and has pH≈13.5. The results are reported in Table 2. Note that the diffusion potential is calculated according to Eq. (11) considering NaOH solution as electrolyte and NaCl as chloride salt (ionic mobilities of the involved ions are taken from [25]).

Table 2. Example of pH and chloride concentrations determined with IrO_x electrodes and Ag/AgCl ISEs respectively for two cases: a) the measured potential is corrected for the diffusion potential (corrected potential; b) the measured potential is not corrected for the diffusion potential (uncorrected potential). For this calculation, it is assumed that the electrolyte at the reference electrode location contains 0 $mol \cdot L^{-1}$ of chlorides and has pH≈13.5

a) Corrected potential		**b) Uncorrected potential (calculated if $E_{measured} = E_{sensor} - E_{RE}$)**		
Cl^- ($mol \cdot L^{-1}$)	**pH**	**Cl^- ($mol \cdot L^{-1}$)**	**pH**	**$E_{diffusion}$ (mV)**
2	≈13.5	≈1.6	≈13.4	5.53
0.01	≈11	≈0.09	≈11.9	≈-52
0.1	≈11	≈0.35	≈11.5	≈-30

From Table 2, it can clearly be seen that corrections for the diffusion potentials are essential, especially for pH gradients; for example, a pH gradient of 2.5 units (between pH 13.5 and pH 11) can lead to errors in the chloride and hydroxide concentrations of one order of magnitude if the measured potentials are not corrected accordingly. In comparison, diffusion potentials due to chloride gradients are relatively low at pH ≈13.5 but can significantly increase in presence of both chloride and pH gradients. Thus, relying on the experimentally measured potentials would lead, in most of cases, to the misinterpretation of the results. In conclusion, correction of the measured potentials for the diffusion potentials is essential when determining the individual electrodes potentials.

6.3 Algorithm for determination of reference potential, pH and chloride concentration

In order to determine the pH and chloride concentration, the potential of the IrO_x electrodes and Ag/AgCl ISEs must be measured and converted into chloride concentration and pH respectively. This is only possible if diffusion potentials arising between the electrodes due to differences in chloride concentration and/or pH have been taken into account (section 6.2.1). In this section, an algorithm is developed that enables separating electrodes potentials from diffusion potentials.

From the set-up presented in Fig. 11, the potential of any electrode (Ag/AgCl ISE or IrO_x electrode) can be measured versus any other embedded electrode (Ag/AgCl ISE or IrO_x electrode used as reference electrode, see sections 6.1.1and 6.1.2) and calculated with Eq. (31). As an example, Fig. 14 shows different possible potential measurements between 4 embedded electrodes (two Ag/AgCl ISEs and two IrO_x electrodes) assuming one-dimensional ingress of aggressive agent, i.e., the chloride concentration and pH for the electrodes embedded at depth x (or y) are the same. In Fig. 14, the arrows show the

potential measurement performed, where the arrow end indicates the working electrode (and the arrow begin the reference electrode).

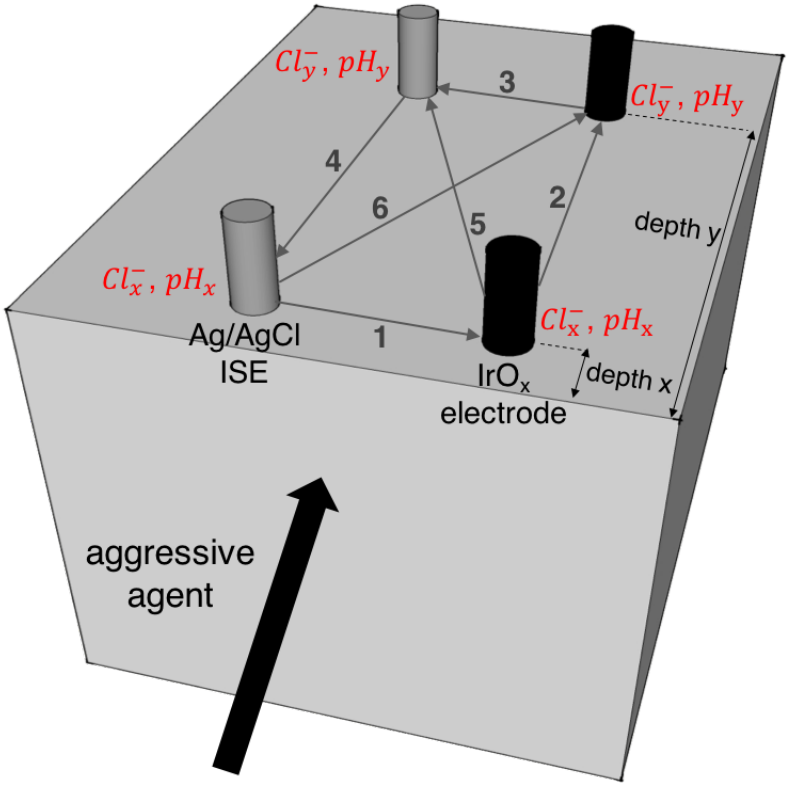

Fig. 14 Potential measurements between 4 embedded electrodes (two Ag/AgCl ISEs and two IrO_x electrodes) assuming one-dimensional ingress of aggressive agent. The arrow shows the potential measurement performed, with the arrow end indicating the working electrode (and the arrow begin the reference electrode). The parameters to be calculated are indicated in red.

The potential measured between the different combinations of electrodes shown in Fig. 14 can be written as:

$$E_{\text{measured 1}} = E_{\text{IrO}_x}(pH_x) + E_{\text{diffusion}}(Cl_x^-, pH_x, Cl_x^-, pH_x) - E_{\text{Ag/AgCl ISE}}(Cl_x^-) \quad (32)$$

$$E_{\text{measured 2}} = E_{\text{IrO}_x}(pH_y) + E_{\text{diffusion}}(Cl_y^-, pH_y, Cl_x^-, pH_x) - E_{\text{IrO}_x}(pH_x) \quad (33)$$

$$E_{\text{measured 3}} = E_{\text{Ag/AgCl ISE}}(Cl_y^-) + E_{\text{diffusion}}(Cl_y^-, pH_y, Cl_y^-, pH_y) - E_{\text{IrO}_x}(pH_y) \quad (34)$$

$$E_{\text{measured 4}} = E_{\text{Ag/AgCl ISE}}(Cl_x^-) + E_{\text{diffusion}}(Cl_x^-, pH_x, Cl_y^-, pH_y) - E_{\text{Ag/AgCl ISE}}(Cl_y^-) \quad (35)$$

$$E_{\text{measured 5}} = E_{\text{Ag/AgCl ISE}}(Cl_y^-) + E_{\text{diffusion}}(Cl_y^-, pH_y, Cl_x^-, pH_x) - E_{\text{IrO}_x}(pH_y) \quad (36)$$

$$E_{\text{measured 6}} = E_{\text{IrO}_x}(pH_y) + E_{\text{diffusion}}(Cl_y^-, pH_y, Cl_x^-, pH_x) - E_{\text{Ag/AgCl ISE}}(Cl_x^-) \quad (37)$$

There is only one solution of pH and chloride profiles that will fulfill all the combination of equations (Eqs. (32)-(37)); thus, solving this equation system will lead to the determination of pH and chloride concentration at each electrode location. For that, an iterative calculation procedure must be used (see example in section 6.3.1). The previously obtained chloride concentration and pH at a given location would be useful input data.

The proposed equation system (Eqs. (32)-(37)) is in this case over-determined. This is considered beneficial, as it will allow detecting the impairment of an individual electrode without compromising the functionality of the whole electrode system. In order to improve the robustness of this electrode system (in case an electrode fails), it is recommended that several electrodes are embedded at the same depth.

It should be noted that Eqs. (32)-(37) are based on the assumption that one-dimensional ingress of aggressive agent occurs. This may not be the case in real field conditions; in that case, 8 parameters (pH and chloride concentration for each of the 4 embedded electrodes) need to be determined but only 6 equations (Eqs. (32)-(37)) are available for that, leading to an under-determined equation system. This can be easily solved by embedding more electrodes (as suggested earlier in this section), e.g., for 6 embedded electrodes, 12 parameters need to be determined (pH and chloride concentration for each of the 6 embedded electrodes) but 15 equations will be available (over-determined system).

To facilitate the calculations, these equations could be implemented and run in a computer program, given the condition that the sum of errors needs to be minimized. Once this equation system is solved, electrode and diffusion potentials are separated. Despite the added calculation time, this approach presents the advantage that chloride and pH profiles can be obtained even if chloride and pH conditions are changing over time at each electrode location. Additionally, as the pH and chloride concentration are obtained at each electrode location, the electrode potential response will be well defined; thus, any embedded electrode can be used as reference electrode (sections 6.1.1 and 6.1.2).

6.3.1 Example of application of the algorithm

In this section, an example of the algorithm used for the determination of pH and chloride concentrations is presented.

To facilitate the calculations, in this example it is assumed that the pH and chloride concentration at the reference electrode location (Cl^-_{RE}, and pH_{RE}) are known, i. e, the potential of the reference electrode E_{RE} is known and well-defined (for both Ag/AgCl ISE and IrO_x electrode, sections 6.1.1 and 6.1.2) and that the ingress of aggressive agent is one-dimensional. The chloride and pH concentrations at depth "x" (Cl^-_x, and pH_x) can be then calculated with the potential responses of an Ag/AgCl ISE and IrO_x electrode embedded at this depth (Fig. 14). Based on Eqs. (31)-(37), the potential response of these electrodes is:

$$E_{\mathrm{IrO}_x}(pH_x) = E_{\mathrm{measured}}\,(\mathrm{IrO}_x \text{ vs. RE}) - E_{\mathrm{diffusion}}(Cl^-_{\mathrm{x}}, pH_{\mathrm{x}}, Cl^-_{\mathrm{RE}}, pH_{\mathrm{RE}}) + E_{\mathrm{RE}} \quad (38)$$

$$E_{\mathrm{Ag/AgCl\ ISE}}(Cl^-_{\mathrm{x}}) = E_{\mathrm{measured}}\,(\mathrm{Ag/AgCl\ ISE}_x \text{ vs. RE}) - E_{\mathrm{diffusion}}(Cl^-_{\mathrm{x}}, pH_{\mathrm{x}}, Cl^-_{\mathrm{RE}}, pH_{\mathrm{RE}}) + E_{\mathrm{RE}} \quad (39)$$

Owing to the to the interdependence of pH_x, Cl^-_x, $E_{\mathrm{IrO}_x}(pH_x)$, $E_{\mathrm{Ag/AgCl\ ISE}}(Cl^-_x)$, and $E_{\mathrm{diffusion}}(Cl^-_{\mathrm{x}}, pH_{\mathrm{x}}, Cl^-_{\mathrm{RE}}, pH_{\mathrm{RE}})$, no closed solution can be given and an iterative calculation procedure is proposed. With this calculation, the chloride concentration and pH can be obtained at different exposure times, i.e., *time step*. As indicated earlier in this section, the calculated chloride concentration and pH at a given location in the previous time step are useful input data. This iterative calculation is then comprised by the following steps:

1. The potential of the IrO_x electrode embedded at depth "x" ($E_{\mathrm{IrO}_x}(pH_x)$ is calculated with Eq. (38). The diffusion potential $E_{\mathrm{diffusion}}(Cl^-_{\mathrm{x}}, pH_{\mathrm{x}}, Cl^-_{\mathrm{RE}}, pH_{\mathrm{RE}})$ is calculated with the pH and chloride concentration obtained in the previous time step. For the first time step, it is assumed that $E_{\mathrm{diffusion}}(Cl^-_{\mathrm{x}}, pH_{\mathrm{x}}, Cl^-_{\mathrm{RE}}, pH_{\mathrm{RE}}) \approx 0$;

2. The value of pH in this iteration "*i*" ($pH_{x,i}$) is determined from the calibration curve of the IrO_x electrode;

3. The diffusion potential $E_{\mathrm{diffusion}}(Cl^-_{\mathrm{x}}, pH_{\mathrm{x}}, Cl^-_{\mathrm{RE}}, pH_{\mathrm{RE}})$ is calculated with the pH value calculated in the current iteration ($pH_{x,i}$) and with the chloride concentration obtained in the previous iteration (in the first iteration, the chloride concentration is obtained from the previous time step, assuming $Cl^-_x \approx 0$ for the first iteration of the first time step);

4. The potential of the Ag/AgCl ISE embedded at depth "*x*" $E_{\mathrm{Ag/AgCl\ ISE}}(Cl^-_x)$ is calculated with Eq. (39);

5. The chloride concentration in this iteration "*i*" ($Cl^-_{x,i}$) is determined from the calibration curve of the Ag/AgCl ISE electrode;

6. The calculated pH_x and Cl^-_x are evaluated: if the pH difference between two consecutive iterations become < 0.1 pH units and the chloride concentration difference between two consecutive iterations become < 0.01 mol·L^{-1}, the iterative calculation is finished. Other criteria are also possible;

7. If the criteria condition is not fulfilled, $E_{\text{diffusion}}(Cl^-_x, pH_x, Cl^-_{RE}, pH_{RE})$ is calculated and another iteration step is done.

Fig. 15 summarizes the algorithm used to determine the chloride concentration (Cl^-_x) and pH (pH_x) at an IrO_x electrode and at a Ag/AgCl ISE embedded at depth "x", assuming known pH and chloride concentration (pH_{RE} and Cl^-_{RE}) at the location of the reference electrode (IrO_x electrode or Ag/AgCl ISE).

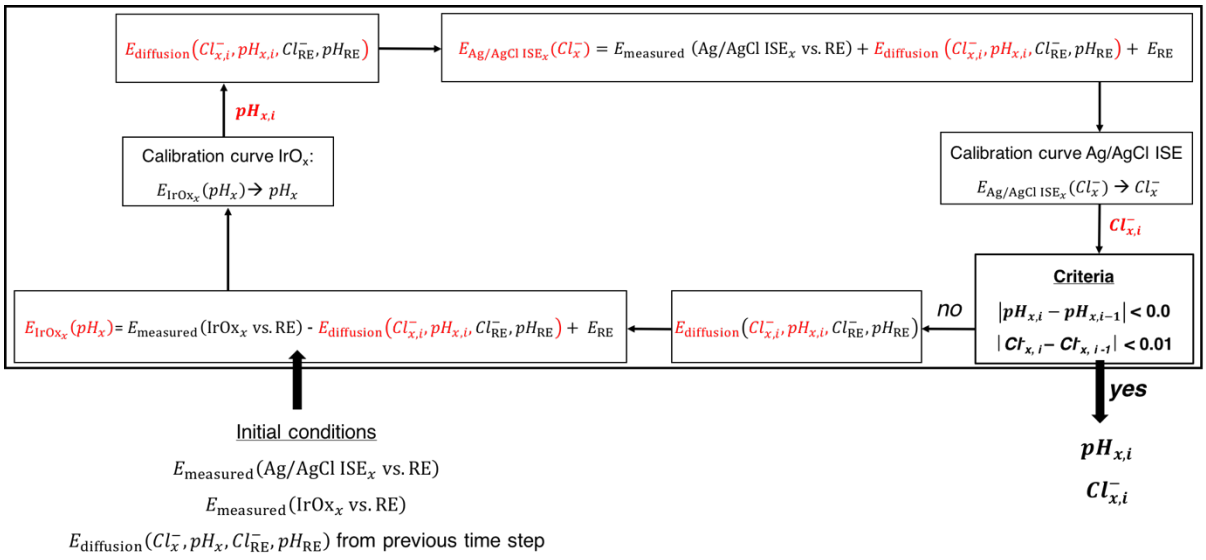

Fig. 15 Algorithm used to determine the chloride concentration (Cl^-_x) and pH (pH_x) at an IrO_x electrode and at an Ag/AgCl ISE embedded at depth "x", assuming known reference electrode potential E_{RE} and known pH and chloride concentration (Cl^-_{RE}, pH_{RE}) at the reference electrode location. The parameters changed in this calculation are indicated in red. The calculated pH and chloride concentration in each iteration ($pH_{x,i}$ and $Cl^-_{x,i}$) are specifically indicated in the diagram.

Note that the algorithm is analogous when pH and chloride concentrations at the reference electrode location are unknown and when the ingress of aggressive agent is not one-dimensional.

6.3.2 Measurement of steel potential

The simple measurement of steel potential does not necessarily indicate whether the reinforcement is in the passive or active state (section 3.3.11) but coupling data of steel potential, chloride profiles, and pH profiles would provide a good insight in that regard.

As indicated earlier in this section, once the conditions of pH and chloride concentration at each electrode location are known, any embedded electrode can be used as reference electrode (sections 6.1.1 and 6.1.2). Thus, the steel potential can be measured versus any of the embedded electrodes. The measured steel potential is:

$$E_{\text{measured}}(\text{steel vs. RE}) = E_{\text{steel}} + E_{\text{diffusion}}(Cl^-_{\text{steel}}, pH_{\text{steel}}, Cl^-_{\text{RE}}, pH_{\text{RE}}) - E_{\text{RE}} \quad (40)$$

where $E_{\text{measured}}(\text{steel vs. RE})$ is the measured steel potential versus any embedded electrode used as RE, $E_{\text{RE}}$is the reference electrode potential, Cl^-_{RE} and pH_{RE} are the respective chloride concentration and pH at the reference electrode location, and Cl^-_{steel} and pH_{steel} are the respective chloride concentration and pH at the steel surface.

The pH and chloride concentration at the steel surface must be known in order to evaluate the diffusion potential and calculate the steel potential correctly (Eq. (40)). The easiest solution to this is to embed (at least) one electrode as close as possible to the steel surface so diffusion potentials between this electrode and the steel reinforcement would be minimized. This electrode can also be used as reference electrode to determine the steel potential:

$$E_{\text{measured}}(\text{steel vs. RE}) \approx E_{\text{steel}} - E_{\text{RE}} \quad (41)$$

Note that Cl^-_{steel} and pH_{steel} can anyway be determined when pH and chloride profiles are calculated with the electrode system proposed in this thesis if (at least) one electrode is placed close to the steel surface, i.e., chloride pH conditions at the location of this electrode are Cl^-_{steel} and pH_{steel}

6.3.3 Electrode system with reference electrode

The simplest way to determine pH and chloride profiles with the algorithm proposed in this thesis is when the conditions of pH and chloride concentration at one electrode location are constant over time. This will simplify significantly the calculations.

In the electrode system shown in Fig. 14, it is suggested to embed some electrodes at a very

high cover depth, where, even after decades, the pH and the chloride concentration remain unaffected. These electrodes can then be considered reference electrodes. The values of pH and chloride concentration can then be obtained from a potential measurement performed with an external reference electrode, following the procedure described in section 2.2.1 of the Appendix for the chloride sensor (analogous for the determination of pH with an IrO_x electrode). In order to minimize errors arising from diffusion potentials between external and internal reference electrodes, it is important that this calibration is performed within the first days after casting, i.e., before the structure is exposed to the ingress of aggressive agents.

It is also recommended that more than one electrode is embedded at the high cover depth. This will allow increasing the robustness of the measurement and ensure the electrode system functionality in case one of the internal reference electrodes is impaired.

Nevertheless, it should be underlined that even if the pH and the chloride concentration would change at the reference electrode location, the functionality of the electrode system would be unaffected and that having an embedded reference electrode is mainly beneficial to reduce the calculation time.

6.3.4 Practical example of application of the algorithm

In this section, the algorithm proposed for the calculation of pH and chloride concentrations is applied to the results obtained from a mortar sample subjected to one-dimensional chloride ingress. This mortar sample had embedded IrO_x electrodes, steel bars and Ag/AgCl ISEs.

In this experiment, the mortar sample was put in contact with synthetic pore solution (0.2 $mol \cdot L^{-1}$ KOH, 0.15 $mol \cdot L^{-1}$ NaOH and sat. $Ca(OH)_2$) containing chlorides. The aim of this experiment was to study the behavior of the IrO_x electrodes under chloride ingress. The calculations were simplified by assuming that diffusion potentials were only due to chloride gradients and that the pH remained constant. In this section, the complete algorithm, where both chloride and pH gradients are considered is applied to the measured potentials of the electrodes (Ag/AgCl ISEs and IrO_x electrodes) versus the embedded internal reference electrode (Ag/AgCl ion-selective electrode embedded in a mortar containing chlorides, section 2.2.1 of the Appendix).

The main features of the set-up are shown in Fig. 16. More details on the experimental set-up can be found in section 2.2.1 of the Appendix.

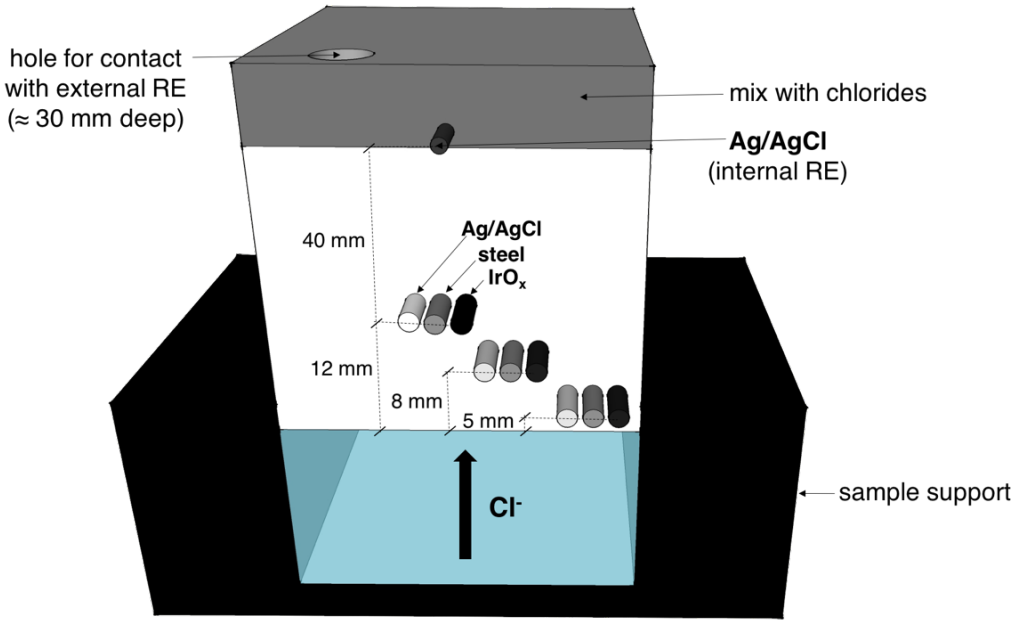

Fig. 16 Main features of the set-up used to monitor chloride ingress with embedded Ag/AgCl ISEs, IrO_x electrodes and steel rods at 5, 8 and 12 mm depth. All the surfaces were coated with epoxy resin with the exception of the surface of chloride ingress.

Fig. 17a shows the chloride concentration as a function of exposure time to chloride ingress at each depth (5, 8 and 12 mm). As a comparison, the results obtained under the assumption of constant pH gradients are also plotted. Fig. 17b shows the calculated pH as a function of exposure time to chloride ingress at each depth (5, 8 and 12 mm).

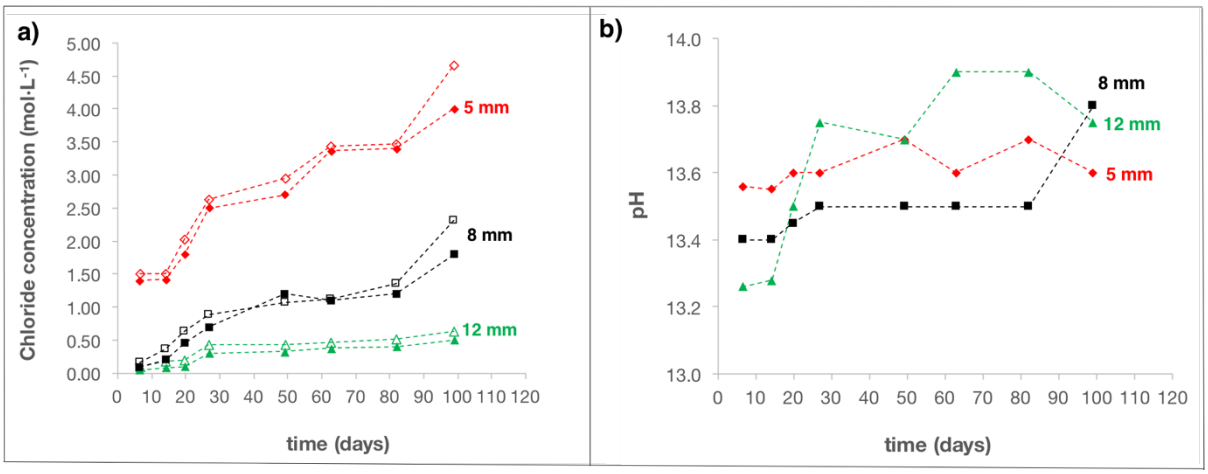

Fig. 17 (a) Chloride concentration as a function of exposure time to chloride ingress at each depth (5, 8 and 12 mm), calculated with the algorithm described in section 6.3.3 (filled markers). As a comparison, the results obtained under the assumption of constant pH are also plotted (empty markers) (b) pH as a function of exposure time to chloride ingress at each depth (5, 8 and 12 mm), calculated with the algorithm described section 6.3.3.

From the results presented in Fig. 17a, it can be seen that the chloride concentration increased with time and that this increase is markedly higher at shallower depths. The obtained results are in good agreement with the calculated chloride concentrations obtained with the simplified algorithm (neglecting pH gradients). This is because the pH of the exposure solution containing chlorides was similar to the internal pore solution, thus not giving rise to significant pH gradients. It should be noted that these results correspond to a very specific situation under unrealistic conditions; in reality, both pH and chloride gradients would be expected, where the correction regarding diffusion potentials becomes very important (section 6.2).

The pH increased over time up to ca. 0.4 pH units for the electrodes embedded at 8 and 12 mm depths (Fig. 17b). It is believed that this pH increase may be caused by chloride binding, as suggested in [15], that occurred as chlorides penetrated the mortar sample. This pH increase was not observed for the electrode embedded at the shallowest depth (5 mm). The chloride concentrations at this depth are considerably higher and it is believed that the binding capacity was practically used up during the first days of exposure to chloride ingress. Thus, this pH increase may have happened before the first potential measurement was performed and it was not detected. In fact, the calculated pH at this depth is initially higher than the calculated pH at the two other depths. More experiments should be performed to confirm this hypothesis.

Validation of the results

In order to validate both the electrode system and the results obtained, the potential difference between different combination of electrodes ($\mathrm{Ag/AgCl\ ISE_{5\ mm}}$ vs. $\mathrm{Ag/AgCl\ ISE_{12\ mm}}$, $\mathrm{IrO_{x_{5\ mm}}}$ vs. $\mathrm{Ag/AgCl\ ISE_{12\ mm}}$, $\mathrm{Ag/AgCl\ ISE_{5\ mm}}$ vs. $\mathrm{Ag/AgCl\ ISE_{12\ mm}}$, and $\mathrm{IrO_{x_{5\ mm}}}$ vs. $\mathrm{Ag/AgCl\ ISE_{12\ mm}}$) is both measured and calculated for 8 different exposure times to chloride ingress (shown in Fig. 17). The calculated potential ($E_{\mathrm{calculated}}$) is obtained with Eqs. (38)-(39) with the pH and chloride concentrations obtained at each time step.

Fig. 18 shows the potential measurements performed for calculating the pH and chloride concentration at each depth and the potential measurement performed for the mentioned validation.

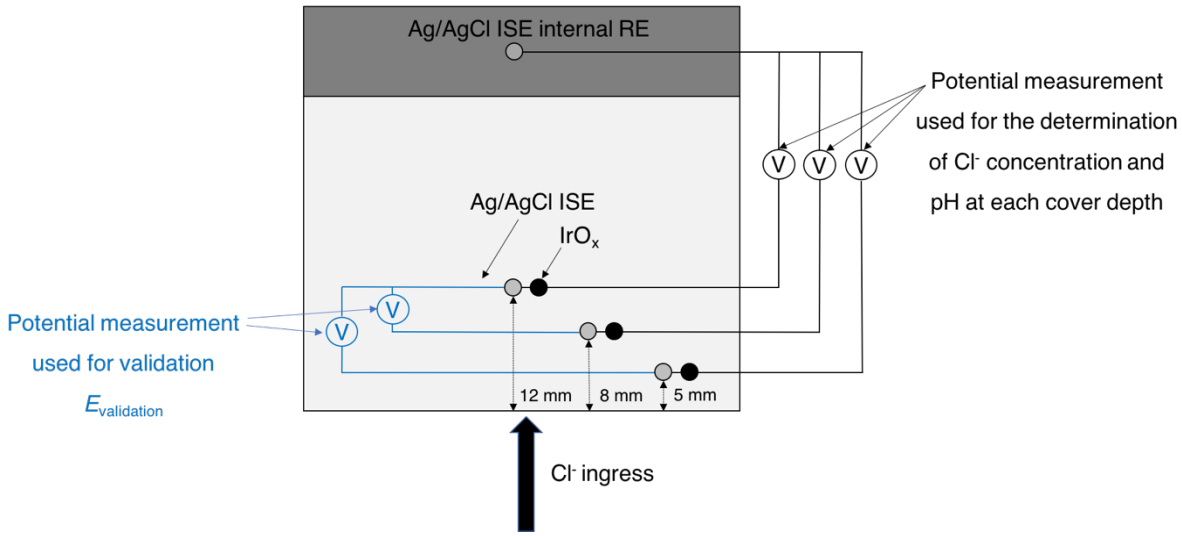

Fig. 18 Potential measurements performed for calculating the pH and chloride concentration at each depth and potential measurement performed for the validation of both electrode system and obtained results.

Fig. 19 shows the average of the potential difference ΔE between the potential measurement used for this validation ($E_{validation}$) and the calculated potential ($E_{calculated}$) between the same combination of electrodes. The average of this potential difference is obtained from the calculated potential differences at 8 different exposure times to chloride ingress (between 6 and 99 days of exposure to chloride ingress, see Fig. 17). The working electrode in each case ($\mathrm{Ag/AgCl\ ISE_{5\ mm}}$, $\mathrm{E_{IrOx_{5\ mm}}}$, $\mathrm{Ag/AgCl\ ISE_{5\ mm}}$, and $\mathrm{IrO_{x_{5\ mm}}}$) is indicated in the graph.

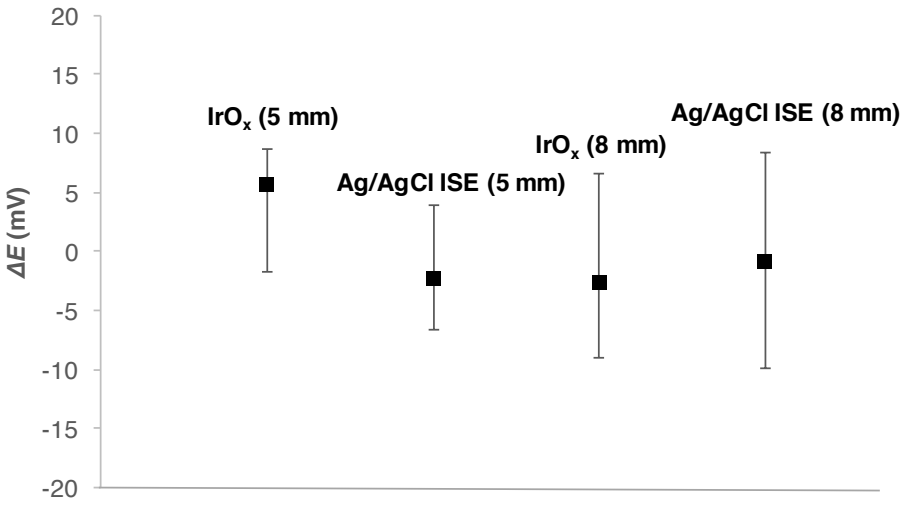

Fig. 19 Average of the potential difference ΔE (from 8 individual calculations) between the potential measurement used for this validation ($E_{validation}$ in Fig. 18) and the calculated potential ($E_{calculated}$), according to Eqs. (38)-(39), between the same combination of electrodes. The working electrode in each case is indicated in the graph. The error bars represent the potential range between the maximum and minimum calculated ΔE.

From the results shown in Fig. 19, it can be seen that differences between measured and calculated potentials are always <0.01 V. This scatter in the obtained results is likely due to simplifications made in the calculations, e.g., assumption of linear concentration gradients in the Henderson equation, NaOH solution is used to simulate the concrete pore solution when calculating diffusion potentials, permselective properties of cement paste are not considered in the calculation of diffusion potentials, etc. Nevertheless, the proposed algorithm leads to accurate results.

In this case, diffusion potentials are relatively low. However, in the presence of higher concentration gradients, i.e., pH gradients or combined chloride and pH gradients, as expected in field conditions, their quantification is highly important. Thus, the electrode system and the calculation procedure proposed in this work appears to be essential.

6.4 Achievement of objectives

This work aimed to develop three types of long-term stable electrodes to be embedded in concrete: an electrode that is able to provide a long-term stable and well-defined potential (i.e., a reference potential), a chloride sensor, and a pH sensor.

A long-term stable and well-defined potential is obtained by embedding several Ag/AgCl ion-selective electrodes and several Iridium/Iridium oxide (IrO_x) electrodes at different locations. A calculation procedure is developed that allows obtaining a well-defined potential response for each embedded electrode. The main objective of this calculation procedure is to take into account diffusion potentials arising from chloride ingress or carbonation. The proposed electrode system has the advantage that reference potential, chloride profiles and pH profiles can be obtained even if chloride and pH conditions are changing over time at each electrode location.

Chloride sensors used in this work are Ag/AgCl ion-selective electrodes, which have already been used in concrete providing satisfactory results. In this thesis, the main sources of error that could impair the functionality of these sensors have been identified. It is concluded that these electrodes can be satisfactorily used in concrete with the exception of materials with mid-high content of sulfide, such as slag cement.

The pH sensors were self-produced by thermal oxidation of iridium wires. The results regarding the use of these sensors in solution and when embedded in concrete show that

these electrodes can be used to monitor any pH value, at least in a pH range between 13.5 and 9, as long as they are properly produced and conditioned.

7 CONCLUSIONS

In this thesis, an embeddable electrode system for concrete was developed. This system is composed of several Iridium/Iridium oxide (IrO_x) electrodes, used as pH sensors, and several Ag/AgCl ion-selective electrodes, used as chloride sensors, embedded at different depths in concrete. While the potentiometric response of IrO_x electrodes is dictated by the pore solution pH, the Ag/AgCl electrodes respond to chloride concentrations in the pore solution. None of the electrodes are sensitive to oxygen. Together with an algorithm that takes into account diffusion potentials, this system is able to provide a long-term stable reference potential at all times and at different locations – even if pH and chloride concentration are changed over time. This is a major achievement, considering that all existing approaches for embeddable reference electrodes are sensitive to these changes. The proposed electrode system can be used as a stable reference electrode both for monitoring steel potential and for the potentiometric measurements of Ag/AgCl ISEs and IrO_x electrodes. Thus, the proposed approach, does not only serve as reference electrode, but also as a means to monitor the ingress of chloride and carbonation into concrete over time.

The proposed algorithm forms an essential part of the electrode system. This algorithm was developed on the basis of the theory of diffusion potentials and validated against experimental work. While the impact of diffusion potentials for potentiometric measurements is well known, there are hardly approaches in the literature that explicitly attempt to correct for this effect. The proposed combination of electrodes system and algorithm permits to accurately distinguish between diffusion potentials and actual electrode potentials.

The use of IrO_x electrodes permits, for the first time, the continuous, in situ monitoring of the pH in the concrete pore solution over a range of at least pH 9 to 13.5. These electrodes have to be conditioned in alkaline media for sufficient time, e.g., 3-4 months, to exhibit a well-defined and drift-free potential response. It is also recommended that they are individually calibrated before use.

New results regarding the carbonation process were obtained by applying these new pH sensors to OPC mortar specimens subjected to accelerated carbonation. It was observed that the pH of the pore solution first decreases down to ca. pH 12.5 and remains constant at that pH for a long time; this can be explained by the buffering action of $Ca(OH)_2$. Afterwards, the pH rapidly decreases down to ca. pH 9. The main finding is that pH 12.5 (“early carbonation

front") is reached at least 3 times faster than the "full carbonation front" at pH 9. The possibility to continuously monitor pH in the concrete pore solution has high scientific relevance, e.g. the carbonation of blended cements or pozzolanic reactions of supplementary cementitious materials can be studied in real time and in situ. These findings have also implications in corrosion engineering: at pH 12.5, the critical chloride content to initiate localized corrosion is much lower than at pH 13.5. Thus, the risk of chloride-induced corrosion of the steel in structures exposed to the atmosphere (and to carbonation) might be much higher than usually expected if the carbonation front at pH 12.5 reached the reinforcement level. Variations of the pH at the reinforcement level might be an explanation for the large scatter in the reported critical chloride contents.

8 OUTLOOK AND FUTURE RESEARCH

From the results presented in this thesis, the following recommendations for future research are given in this section.

Diffusion potentials

Correction of the measured potentials for diffusion potentials is important for both the functionality of the electrode system and the accuracy of the chloride and pH sensors proposed in this thesis. In this work, diffusion potentials were calculated with the data on ion mobility reported for aqueous solution. Permselective properties of the cement paste were thus not considered, as the mortar used in all the experiments was relatively porous (w/c=0.5) and one week of curing. However, it is possible that denser mortars with lower water-to-cement ratio or exposed to low relative humidity exhibit this permselective behavior, resulting in larger diffusion potentials [34, 36-38]. Thus, the influence of the permselective properties of cement paste on the ion mobility needs to be studied further.

pH and chloride sensors

The pH sensors used in this work (IrO_x electrodes) likely consist of a dense hydrated oxide layer. Thus, the functionality of these electrodes might be affected when concrete or mortar is exposed to environments with low moisture content. The IrO_x electrodes provided satisfactory results in a relatively dry environment (65% RH), but the effect of lower RH and of variable humidity conditions needs to be further studied. Additionally, the effect of temperature on the potential response should be studied.

The potential response of the Ag/AgCl ion-selective electrodes is not well defined in absence of chlorides, probably due to the transformation of the AgCl membrane into Ag_2O. Nevertheless, the results obtained in this work showed that after ca. 60 days immersed in alkaline solution without chlorides, these electrodes exhibit the expected potential response from the calibration curve upon addition of chlorides. For the long-term application in concrete, the potential response of these electrodes for longer exposure times, i.e., in the order of months to years, in absence of chlorides needs to be addressed in further studies. Additionally, it has been shown that in presence of sulfides, the Ag/AgCl ion-selective electrodes would lead to erroneous results due to the interference of this ion, e.g., addition of 0.006 $mol \cdot L^{-1}$ of sulfides in 0.01 $mol \cdot L^{-1}$ NaCl solution caused a significant potential shift in the electrode potential response. In this case, the use of other Ag/AgCl ion-selective with modified

membranes (see section 4.3.1) could be a solution and further studies with these types of electrodes should be performed for the use in concrete with for example, slag cements.

Corrosion of the reinforcement

Both the pH and the concentration of free chlorides at the steel surface play a role in corrosion initiation. However, reliable data on these parameters are often hardly available. The combination of the pH and chloride sensors developed in this thesis can thus enhance research dealing with reinforcement corrosion. It may be particularly interesting to study the impact of pH drops in the alkaline range, such as carbonation down to 12.5 (which it has been found to occur much earlier than the traditional carbonation (pH<10) that is currently detected (with indicator spray test)) on the chloride content necessary for inducing localized corrosion.

Study of blended cements

In this work, the use of IrO_x electrodes embedded in mortar allowed following the carbonation process continuously and in situ. The results regarding the evolution of pH vs. time can give substantial insight into the process of carbonation. The Portlandite ($Ca(OH)_2$ phase) content in blended cements is usually lower and it is thus possible that these cements have a lower buffer capacity, as Portlandite is the main source of the alkali reservoir at pH≈12.5. The use of the studied pH sensors in these cements could provide a better understanding of the kinetics and resistance against carbonation, e.g., the time to resist a pH drop below 12.5.

Additionally, the possibility to non-destructively monitor the pH of the pore solution with the studied IrO_x electrodes may be further applied to study the hydration processes of pozzolanic materials. In this case, the pH of the pore solution is reduced owing to the pozzolanic reaction, which may slowly proceed during years after casting.

Cathodic protection in soil and in concrete

In cathodic protection systems in soil and in concrete, relatively low protection current densities are applied, which leads to a significant increase in pH at the steel surface and provides effective cathodic protection. In order to validate the effectiveness of this method, the pH at the steel surface should be known. The newly developed and tested pH sensors based on IrO_x electrodes are feasible and can contribute to resolving open questions related to the mechanism of cathodic protection in research or the protection criteria in practice.

Validation of models to predict carbonation and chloride ingress

There are many models that aim to predict chloride ingress and carbonation penetration in concrete. Detailed knowledge of pH and chloride as a function of both time and depth for different materials and exposure conditions can be obtained with the pH and chloride sensors developed in this work. This will allow obtaining input data and validating the results obtained with these models, resulting in a more accurate prediction of the service life of concrete structures.

9 REFERENCES

1. A. Poursaee (2016), Corrosion of Steel in Concrete Structures, ed., Amsterdam, Elsevier.
2. O. Klinghoffer, P. Goltermann, R. Bäßler (2002), *Smart structures: embeddable sensors for use in the integrated monitoring systems of concrete structures* in *First International Conference on Bridge Maintenance, Safety and Management*, Barcelona.
3. R. Polder, O. Klinghoffer, J. Eri, J. Leggedoor (2007), Use of advanced corrosion monitoring for risk based management of concrete structures, HERON, 52 (4), 239-250.
4. G.H. Koch, M.P.H. Brongers, N.G. Thomson, Y.P. Virmani, J.H. Payer (2002), Corrosion cost and preventive strategies in the united states, No. FHWA-RD-01-156.
5. Strassenrechnung der Schweiz 2011, Bundesamt für Statistik (http://www.bfs.admin.ch/).
6. http://www.g2mtlabs.com/cost-of-corrosion.
7. L. Bertolini, B. Elsener, P. Pedeferri, E. Redaelli, R.P. Polder (2013), Corrosion of steel in concrete, second ed., Weinheim, Wiley.
8. G. Koch, J. Varney, N. Thompson, O. Moghissi, M. Gould, J. Payer (2016), International measures of prevention, application, and economics of corrosion technologies study, NACE International IMPACT Report.
9. R. Myrdal (2007), The electrochemistry and characteristics of embeddable reference electrodes for concrete, ed., Cambridge, European Federation of Corrosion Publication no. 43, Woodhead Publishing Ltd.
10. H.F.W. Taylor (1997), Cement chemistry, 2nd ed., London, Thomas Telford Publishing.
11. A.M. Neville (2011), Properties of Concrete, 5th ed., Harlow, Pearson Education Limited.
12. U. Angst, B. Elsener, C.K. Larsen, Ø. Vennesland (2009), Critical chloride content in reinforced concrete - A review, Cem. Concr. Res., 39, 1122-1138. 10.1016/j.cemconres.2009.08.006.
13. A. Hidalgo, G.D. Vera, M.A. Climent, C. Andrade, C. Alonso (2001), Measurements of chloride activity coefficients in real portland cement paste pore solutions, J. Am. Ceram. Soc., 84, 3008-3012. 10.1111/j.1151-2916.2001.tb01128.x.
14. J. Tritthart (1989), Chloride binding in cement I. Investigations to determine the composition of porewater in hardened cement, Cem. Concr. Res, 19, 586-594. 10.1016/0008-8846(89)90010-0.
15. J. Tritthart (1989), Chloride binding in cement II. The influence of the hydroxide concentration in the pore solution of hardened cement paste on chloride binding, Cem. Concr. Res, 19, 683-691. 10.1016/0008-8846(89)90039-2.
16. M.C.G. Juenger, F. Winnefeld, J.L. Provis, J.H. Ideker (2011), Advances in alternative cementitious binders, Cem. Concr. Res., 41, 1232-1243. 10.1016/j.cemconres.2010.11.012.
17. R.J. Flatt, N. Roussel, C.R. Cheeseman (2012), Concrete: An eco material that needs to be improved, J. Eur. Ceram. Soc., 32, 2787-2798. 10.1016/j.jeurceramsoc.2011.11.012.
18. European Standard EN 197-1. Cement—Part 1: Composition, specification and conformity criteria for common cements. European Committee for Standardization, Brussels, Belgium; 2000.
19. T.C. Powers (1958), Structure and physical properties of hardened Portland cement paste, J. Am. Ceram. Soc., 41, 1-6. 10.1111/j.1151-2916.1958.tb13494.x.

20. K.L. Scrivener, A.K. Crumbie, P. Laugesen (2004), The interfacial transition zone (ITZ) between cement paste and aggregate in concrete, Interface Sci., 12, 411-421. 10.1023/B:INTS.0000042339.92990.4c.
21. C.L. Page (2009), Initiation of chloride-induced corrosion of steel in concrete: role of the interfacial zone, Mater. Corros., 60, 586-592. 10.1002/maco.200905278.
22. P. Lambert, C.L. Page, P.R.W. Vassie (1991), Investigations of reinforcement corrosion. 2. Electrochemical monitoring of steel in chloride-contaminated concrete, Mater. Struct., 24, 351-358. 10.1007/BF02472068.
23. M.R. Nokken, R.D. Hooton (2004), Discontinuous capillary porosity in concrete–does it exist. IN J. Weiss, K. Kovler, J. Marchand, S. Mindess (Eds.) Int. RILEM Symp. on Concrete Science and Engineering, Illinois.
24. E. Bardal (2007), Corrosion and protection, ed., London, Springer.
25. A.J. Bard, L.R. Faulkner (2001), Electrochemical methods: fundamentals and applications, second ed., New York, Willey.
26. M. Pourbaix (1974), Atlas of electrochemical equilibria in aqueous solutions, Pergamon Press, 2nd ed.
27. A.J. Bard, M. Stratmann, E. Gileadi, M. Urbakh, E.J. Calvo, P.R. Unwin, G.S. Frankel, D. Macdonald, S. Licht, H.J. Schäfer, G.S. Wilson, I. Rubinstein, M. Fujihira, P. Schmuki, F. Scholz, C.J. Pickett, J.F. Rusling: "Encyclopedia of electrochemistry", Willey, Vol. 1, (2002).
28. M. Pourbaix (1973), Lectures on electrochemical corrosion, ed., New York/London, Plenum Press.
29. E. McCafferty (2010), Introduction to corrosion science, ed., New York (USA), Springer.
30. R. Myrdal (1997), Potential gradients in concrete caused by charge separations in a complex electrolyte, Corrosion/97, NACE International, Paper No.278.
31. R. Myrdal (1996), Phenomena that disturb the measurement of potentials in concrete, Corrosion/96, NACE International, Paper No.339.
32. U. Angst, Ø. Vennesland, R. Myrdal (2009), Diffusion potentials as source of error in electrochemical measurements in concrete, Mater. Struct., 42, 365-375. 10.1617/s11527-008-9387-5.
33. Y. Schiegg, M. Büchler, M. Brem (2009), Potential mapping technique for the detection of corrosion in reinforced concrete structures: Investigation of parameters influencing the measurement and determination of the reliability of the method, Mater. Corros., 60, 79-86. 10.1002/maco.200805042.
34. S. Chatterji (1994), Transportation of ions through cement based materials.Part 3. Experimental evidence for the basic equations and some important deductions, Cem. Concr. Res., 24, 1229-1236. 10.1016/0008-8846(94)90107-4.
35. SHRP-S-337 (1993), Cathodic protection of reinforced concrete bridge elements: a state of the art report, Strategic Highway Research Program, National Research Council.
36. S. Goto, D.M. Roy (1981), Diffusion of ions through hardened cement paste, Cem. Concr. Res., 11, 751-757. 10.1016/0008-8846(81)90033-8.
37. U. Angst, B. Elsener, R. Myrdald, Ø. Venneslanda (2010), Diffusion potentials in porous mortar in a moisture state below saturation, Electrochim. Acta, 55, 8545–8555. 10.1016/j.electacta.2010.07.085.
38. A. Atkinson, A.K. Nickerson (1984), The diffusion of ions through water-saturated cement, J. Mater. Sci., 19, 3068–3078. 10.1007/BF01026986.
39. U. Angst, B. Elsener, C.K. Larsen, Ø. Vennesland (2010), Potentiometric determination of the chloride ion activity in cement based materials, J. Appl. Electrochem., 40, 561-573. 10.1007/s10800-009-0029-6.

40. U. Angst, Ø. Vennesland (2009), Detecting critical chloride content in concrete using embedded ion selective electrodes - Effect of liquid junction and membrane potentials, Mater. Corros., 60, 638-643. 10.1002/maco.200905280.
41. J. Janata (1989), Principles of chemical sensors, second ed., New York, Plenum Press.
42. J. Koryta, J. Dvorák, L. Kavan (1993), Principles of electrochemistry, second ed., Chichester, Willey.
43. G. Inzelt, A. Lewenstam, F. Scholz (2013), Handbook of reference ectrodes, ed., Berlin, Springer.
44. J. Koryta, K. Stulik (1983), Ion-selective electrodes, second ed., Cambridge, Cambridge Univ. Press.
45. J. Wang (2006), Analytical Electrochemistry, third ed., New Jersey, Willey.
46. W.E. Morf (1981), The principles of ion-selective electrodes and of membrane transport, ed., New York, Elsevier.
47. P. Kurzweil (2009), Metal oxides and on-exchanging surfaces as pH sensors in liquids: state-of-the-art and outlook, Sensors, 9, 4955-85. 10.3390/s90604955.
48. W.T. Grubb, L.H. King (1980), Palladium-palladium oxide pH electrodes, Anal. Chem., 52, 270–273. 10.1021/ac50052a013.
49. J.Y.Kim, Y.H.Lee (1989), Pd-PdO pH microprobe for local pH measurement, Biotechnol. Bioeng., 34, 131-136. 10.1002/bit.260340118.
50. F. Contu, M. Vega-Arroyo, R. Taylor (2014), The fabrication and calibration of an iridium pH micro-sensor for biological applications, Int. J. Mat. Sci., 4, 8. 10.14355/ijmsci.2014.0401.02.
51. S.A.M. Marzouk, S. Ufer, R.P. Buck, T.A. Johnson, L.A. Dunlap, W.E. Cascio (1998), Electrodeposited iridium oxide pH electrode for measurement of extracellular myocardial acidosis during acute ischemia, Anal. Chem., 70, 5054-5061. 10.1021/Ac980608e.
52. H.A. Elsen, C.F. Monson, M. Majda (2009), Effects of electrodeposition conditions and protocol on the properties of iridium oxide pH sensor electrodes, J. Electrochem. Soc., 156, F1-F6. 10.1149/1.3001924.
53. C. Terashima, T.N. Rao, B.V. Sarada, N. Spataru, A. Fujishima (2003), Electrodeposition of hydrous iridium oxide on conductive diamond electrodes for catalytic sensor applications, J. Electroanal. Chem., 544, 65-74. 10.1016/s0022-0728(03)00066-4.
54. W. Olthuis, M.A.M. Robben, P. Bergveld, M. Bos, W.E.V.d. Linden (1990), pH sensor properties of electrochemically grown iridium oxide, Sens. Actuators, B, 2, 247-256. 10.1016/0925-4005(90)80150-X.
55. W.-D. Huang, H. Cao, S. Deb, M. Chiao, J.C. Chiao (2011), A flexible pH sensor based on the iridium oxide sensing film, Sens. Actuators, A, 169, 1-11. 10.1016/j.sna.2011.05.016.
56. W.-D. Huang, J. Wang, T. Ativanichayaphong, M. Chiao, J.C. Chiao (2008), *Development of an IrOx micro pH sensor array on flexible polymer substrate* in *SPIE Nanosensors and Microsensors for Bio-Systems Conference* California. 10.1117/12.775856.
57. S. Yao, M. Wang, M. Madou (2001), A pH electrode based on melt-oxidized iridium oxide, J. Electrochem. Soc., 148, H29-H36. 10.1149/1.1353582.
58. S. Kakooei, M.C. Ismail, B. Ari-Wahjoedi (2013), An overview of pH sensors based on iridium oxide: fabrication and application, Int. J. Mat. Sci Innovations, 1, 62-72.
59. M. Wang, S. Yao, M. Madou (2002), A long-term stable iridium oxide pH electrode, Sens. Actuators, B, 81, 313-315. 10.1016/S0925-4005(01)00972-8.
60. M. Wang, S. Yao (2003), Carbonate-Melt Oxidized Iridium Wire for pH Sensing, Electroanalysis, 15, 1606-1615. 10.1002/elan.200302723.

61. F. Huang, Y. Jin, L. Wen, D. Mu, M. Cui (2013), Effects of Thermal Oxidation Cycle Numbers and Hydration on IrOx pH Sensor, J. Electrochem. Soc., 160, B184-B191. 10.1149/2.006310jes.
62. S.A.M. Marzouk (2003), Improved electrodeposited iridium oxide pH sensor fabricated on etched titanium substrates, Anal. Chem., 75, 1258-1266. 10.1021/ac0261404.
63. T.Y. Kim, S. Yang (2014), Fabrication method and characterization of electrodeposited and heat-treated iridium oxide films for pH sensing, Sens. Actuators, B, 196, 31-38. 10.1016/j.snb.2014.02.004.
64. G.S. Duffó, S.B. Farina, C.M. Giordano (2009), Characterization of solid embeddable reference electrodes for corrosion monitoring in reinforced concrete structures, Electrochim. Acta, 54, 1010-1020. 10.1016/j.electacta.2008.08.025.
65. S. Trasatti (1991), Physical electrochemistry of ceramic oxides, Electrochim. Acta, 36, 225-241. 10.1016/0013-4686(91)85244-2.
66. B. Lee (2003), Review of the present status of optical fiber sensors, Opt. Fiber Technol., 9, 57-79. 10.1016/s1068-5200(02)00527-8.
67. K. Fidanboylu, H.S. Efendioğlu (2009), Fiber optic sensors and their applications, 5th International Advanced Technologies Symposium (IATS'09), 6.
68. E.-H. Kang, J.-K. Ham, J.-M. Shim, J.-K. Lee, M.-R. Kim (2006), Applications of pH sensor Using a Covalent Bond Indicator Based on Containing Functional Group Copolymer, Mol. Cryst. Liq. Cryst. Sci., 445, 285/[575]-290/[580]. 10.1080/15421400500366779.
69. C. Vimer, S. Yu, Masoud Ghandehari (2009), Probing pH levels in civil engineering materials, J. Mater. Civ. Eng., 21, 51-57. 10.1061/ ASCE 0899-1561 2009 21:2 51.
70. R. Srinivasan, T.E. Phillips, C.B. Bargeron, M.A. Carlson, E.R. Schemm, H.M. Saffarian (2000), *Embedded micro-sensor for monitoring pH in concrete structures* in *Proc. SPIE 3988, Smart Systems for Bridges, Structures, and Highways*.
71. T.H. Nguyen, T. Venugopala, S. Chen, T. Sun, K.T.V. Grattan, S.E. Taylor, P.A.M. Basheer, A.E. Long (2014), Fluorescence based fibre optic pH sensor for the pH 10–13 range suitable for corrosion monitoring in concrete structures, Sens. Actuators, B, 191, 498-507. 10.1016/j.snb.2013.09.072.
72. M. Blumentritt, K. Melhorn, J. Flachsbarth, M. Kroener, W. Kowalsky, H.-H. Johannes (2008), A novel fabrication method of fiber-optical planar transmission sensors for monitoring pH in concrete structures, Sens. Actuators, B, 131, 504-508. 10.1016/j.snb.2007.12.034.
73. G.E. Khalil, P. Daddario, K.S. Lau, S. Imtiaz, M. King, M. Gouterman, A. Sidelev, N. Puran, M. Ghandehari, C. Bruckner (2010), meso-Tetraarylporpholactones as high pH sensors, Analyst, 135, 2125-31. 10.1039/c0an00018c.
74. P. Bergveld (1970), Development of an ion-sensitive solid-state device for neurophysiological measurements IEEE Trans. Biomed. Eng., 17, 70-71. 10.1109/TBME.1970.4502688.
75. W. Olthuis, J.G. Bomer, P. Bergveld (1991), Iridium oxide as actuator material for the ISFET-based sensor-actuator system, Sens. Actuators, B, 5, 47-52. 10.1016/0925-4005(91)80218-9.
76. W. Olthuis, P. Bergveld (1995), Integrated coulometric sensor-actuator devices, Microchim. Acta, 121, 191–223. 10.1007/BF01248251.
77. A.J.J. van der Zanden, A. Taher, T. Arends (2015), Modelling of water and chloride transport in concrete during yearly wetting/drying cycles, Constr. Build. Mater., 81, 120-129. 10.1016/j.conbuildmat.2015.02.012.
78. M. Durand-Charre (2003), Microstructure of steels and cast irons, ed., Berlin, Springer.
79. N. Singh, S.P. Singh (2016), Reviewing the carbonation resistance of concrete, J. Mater. Eng. Struct., 3, 35-57.

80. T.Y. Lo, A. Nadeem, W.C.P. Tang, P.C. Yu (2009), The effect of high temperature curing on the strength and carbonation of pozzolanic structural lightweight concretes, Constr. Build. Mater. , 23, 1306-1310. 10.1016/j.conbuildmat.2008.07.026.
81. D.W.S. Ho, R.K. Lewis (1987), Carbonation of concrete and its prediction, Cem. Concr. Res, 17, 489-504. 10.1016/0008-8846(87)90012-3.
82. M. Manera, Ø. Vennesland, L. Bertolini (2008), Chloride threshold for rebar corrosion in concrete with addition of silica fume, Corros. Sci., 50, 554-560. 10.1016/j.corsci.2007.07.007.
83. H. Justnes (1998), A review of chloride binding in cementitious systems, Nordic Concr. Res., 21, 1–6.
84. F. Adenot, M. Buil (1992), Modelling of the corrosion of the cement paste by deionized water, Cem. Concr. Res, 22, 489-496. 10.1016/0008-8846(92)90092-A.
85. J.L. García Calvo, A. Hidalgo, C. Alonso, L. Fernández Luco (2010), Development of low-pH cementitious materials for HLRW repositories, Cem. Concr. Res, 40, 1290-1297. 10.1016/j.cemconres.2009.11.008.
86. K. Byfors (1987), Influence of silica fume and flyash on chloride diffusion and pH values in cement paste, Cem. Concr. Res, 17, 115-130. 10.1016/0008-8846(87)90066-4.
87. C.L. Page, Ø. Vennesland (1983), Pore solution composition and chloride binding capacity of silica-fume cement pastes, Mater. Struct., 16, 19–25. 10.1007/BF02474863.
88. J.A. Larbi, A.L.A. Fraay, J.M.J.M. Bijen (1990), The chemistry of the pore fluid of silica fume-blended cement systems, Cem. Concr. Res, 20, 506-516. 10.1016/0008-8846(90)90095-F.
89. S. Diamond (1981), Effects of two danish fly ashes on alkali contents of pore solutions of cement-fly ash pastes, Cem. Concr. Res, 11, 383-394. 10.1016/0008-8846(81)90110-1.
90. O. Skjolsvold (1986), Carbonation depths of concrete with and without condensed silica fume, ACI Special Publications, 91, 1031-1048.
91. J. Khunthongkeaw, S. Tangtermsirikul, T. Leelawat (2006), A study on carbonation depth prediction for fly ash concrete, Constr. Build. Mater., 20, 744–753. 10.1016/j.conbuildmat.2005.01.052.
92. B. Lothenbach, G. Le Saout, M. Ben Haha, R. Figi, E. Wieland (2012), Hydration of a low-alkali CEM III/B–SiO2 cement (LAC), Cem. Concr. Res, 42, 410-423. 10.1016/j.cemconres.2011.11.008.
93. R.B. Polder, T.G. Nijland, M.R.d. Rooij (2014), Blast furnace slag cement concrete with high slag content (CEM III/B) – Experiences with the durability in The Netherlands since the 1920's, NPRA report SVV 270.
94. H.W. Song, V. Saraswathy (2006), Studies on the corrosion resistance of reinforced steel in concrete with ground granulated blast-furnace slag--An overview, J. Hazard. Mater., 138, 226-33. 10.1016/j.jhazmat.2006.07.022.
95. J.L. García Calvo, M.C. Alonso, A. Hidalgo, L. Fernández Luco, V. Flor-Laguna (2013), Development of low-pH cementitious materials based on CAC for HLW repositories: Long-term hydration and resistance against groundwater aggression, Cem. Concr. Res, 51, 67-77. 10.1016/j.cemconres.2013.04.008.
96. S. Lamberet (2004), Durability of ternary binders based on Portland cement, calcium aluminate cement and calcium sulfate (PhD thesis). 10.5075/epfl-thesis-3151.
97. K. Sisomphon, L. Franke (2007), Carbonation rates of concretes containing high volume of pozzolanic materials, Cem. Concr. Res, 37, 1647–1653. 10.1016/j.cemconres.2007.08.014.
98. V.G. Papadakis (2000), Effect of supplementary cementing materials on concrete resistance against carbonation and chloride ingress, Cem. Concr. Res, 30, 291–299. 10.1016/S0008-8846(99)00249-5.

99. K. Tuutti (1982), Corrosion of steel in concrete, Swedish Cement and Concrete Research Institute.
100. V.G. Papadakis, Costas G. Vayenas, M.N. Fardis. (1991), Fundamental modeling and experimental investigation of concrete carbonation, ACI Mater. J., 88, 363-373. 10.14359/1863.
101. S.-J. Kwon, H.-W. Song (2010), Analysis of carbonation behavior in concrete using neural network algorithm and carbonation modeling, Cem. Concr. Res, 40, 119–127. 10.1016/j.cemconres.2009.08.022.
102. S. Kashef-Haghighi, Y. Shao, S. Ghoshal (2015), Mathematical modeling of CO2 uptake by concrete during accelerated carbonation curing, Cem. Concr. Res, 67, 1-10. 10.1016/j.cemconres.2014.07.020.
103. P.J. Parrott (1994), Design for avoiding damage due to carbonation-induced corrosion, ACI Special Publications, 145, 283-298.
104. L. Shreir (1994), Metal/environment reactions. IN L. Shreir, R. A. Jarman, G. T. Burstein (Eds.) Corrosion, Oxford, Butterworth-Heinemann Ltd.
105. G.S. Frankel (1998), Pitting corrosion of metals. A review of the critical factors, J. Electrochem. Soc., 148, 2186-2198. 10.1149/1.1838615.
106. H.-H. Strehblow, P. Marcus (2011), Mechanisms of pitting corrosion. IN P. Marcus (Eds.) Corrosion mechanisms in theory and practice, New York, CRC Press.
107. C. Alonso, C. Andrade, M. Castellote, P. Castro (2000), Chloride threshold values to depassivate reinforcing bars embedded in a standardized OPC mortar, Cem. Concr. Res, 30, 1047-1055. 10.1016/S0008-8846(00)00265-9.
108. (2003), 46-COST 521, Corrosion of Steel in Reinforced Concrete Structures, Final report. IN R. Cigna, C. Andrade, U. Nürnberger, R. Polder, R. Weydert, E. Seitz (Eds.) Luxembourg, European Communities EUR 20599.
109. U. Angst, A. Rønnquist, B. Elsener, C.K. Larsen, Ø. Vennesland (2011), Probabilistic considerations on the effect of specimen size on the critical chloride content in reinforced concrete, Corros. Sci., 53, 177-187. 10.1016/j.corsci.2010.09.017.
110. G.K. Glass, N.R. Buenfeld (1997), The presentation of the chloride threshold level for corrosion of steel in concrete, Corros. Sci., 39, 1001-1013. 10.1016/S0010-938X(97)00009-7.
111. L.O. Nilsson, Poulsen, E., Sandberg, P., Sørensen, H. E., & Klinghoffer, O. (1996), HETEK. Chloride penetration into concrete. State of the Art, Transport processes, corrosion initiation, test methods and prediction models., Denmark, ISSN/ISBN, 0909-4288.
112. C.L. Page, P. Lambert, P.R. Vassie (1991), Investigations of reinforcement corrosion. 1. The pore electrolyte phase in chloride-contaminated concrete, Mater. Struct., 24, 243-252. 10.1007/BF02472078.
113. D.A. Hausmann (1967), Corrosion of steel in concrete. How does it occur?, J. Mater. Prot., 6, 19-23.
114. J.S. Ryou, K.Y. Ann (2008), Variation in the chloride threshold level for steel corrosion in concrete arising from different chloride sources, Mag. Concr. Res., 60, 177-187. 10.1680/macr.2008.60.3.177.
115. M. Thomas (1996), Chloride thresholds in marine concrete, Cem. Concr. Res, 26, 513-519. 10.1016/0008-8846(96)00035-X.
116. J. Xu, L. Jiang, W. Wang, Y. Xu, Y. Jiang (2011), Chloride threshold value for reinforcement corrosion in concrete with additions of silica fume or fly ash, Mag. Concr. Res., 63, 905-913. 10.1680/macr.10.00101.
117. M.V.A. Marinescu, H.J.H. Browners (2010), Free and bound chloride contents in cementitious materials, 8th fib PhD Symposium in Kgs. Lyngby, Denmark.

118. T. Luping, L.O. Nilsson (1993), Chloride binding capacity and binding isotherms of OPC pastes and mortars, Cem. Concr. Res., 23, 247-253. 10.1016/0008-8846(93)90089-R.
119. C. Arya, Y. Xu (1995), Effect of cement type on chloride binding and corrosion of steel in concrete, Cem. Concr. Res, 25, 893-902. 10.1016/0008-8846(95)00080-V.
120. C. Arya (1990), Factors influencing chloride-binding in concrete, Cem. Concr. Res, 20, 291-300. doi.org/10.1016/0008-8846(90)90083-A.
121. P. Suraneni, V.J. Azad, B.O. Isgor, W.J. Weiss (2016), Calcium oxychloride formation in pastes containing supplementary cementitious materials: thoughts on the role of cement and supple- mentary cementitious materials reactivity, RILEM Tech. Lett., 1, 24–30. 10.21809/rilemtechlett.2016.7.
122. A.K. Suryavansh, J.D. Scantlebury, S.B. Lyon (1998), Corrosion of reinforcement steel embedded in high water-cement ratio concrete contaminated with chloride, Cem. Concr. Res, 20, 263-281. 10.1016/S0958-9465(98)00018-3.
123. Rasheeduzzafar, S.S. Al-Saadoun, A.S. Al-Gahtan, F.H. Dakhil (1990), Effect of tricalcium aluminate content of cement on corrosion of reinforcing steel in concrete, Cem. Concr. Res, 20, 723-738. 10.1016/0008-8846(90)90006-J.
124. S.E. Hussain, Rasheeduzzafar, A. Al-Musallam, A.S. Al-Gahtani (1995), Factors affecting threshold chloride for reinforcement corrosion in concrete, Cem. Concr. Res, 25, 1543-1555. 10.1016/0008-8846(95)00148-6.
125. K. Sakr (2005), Effect of cement type on the corrosion of reinforcing steel bars exposed to acidic media using electrochemical techniques, Cem. Concr. Res, 35, 1820-1826. 10.1016/j.cemconres.2004.10.015.
126. C.L. Page, N.R. Short., W.R. Holden (1986), The influence of different cements on chloride-induced corrosion of reinforcing steel, Cem. Concr. Res, 16, 79-86. 10.1016/0008-8846(86)90071-2.
127. T. Ishida, S. Miyahara, T. Maruya (2008), Chloride binding capacity of mortars made with various portland cements and mineral admixtures, J. Adv. Concr. Technol., 6, 287-301. 10.3151/jact.6.287.
128. N. Benkemoun, M.N. Hammood, O. Amiri (2017), Embedded finite element formulation for the modeling of chloride diffusion accounting for chloride binding in meso-scale concrete, Finite Elem. Anal. Des., 130, 12-26. 10.1016/j.finel.2017.03.003.
129. W.Z. Taffese, E. Sistonen (2017), Significance of chloride penetration controlling parameters in concrete: Ensemble methods, Constr. Build. Mater., 139, 9-23. 10.1016/j.conbuildmat.2017.02.014.
130. S. Pradelle, M. Thiéry, V. Baroghel-Bouny (2017), Sensitivity analysis of chloride ingress models: Case of concretes immersed in seawater, Constr. Build. Mater., 136, 44-56. 10.1016/j.conbuildmat.2017.01.019.
131. K.Y. Yeau, E.K. Kim (2005), An experimental study on corrosion resistance of concrete with ground granulate blast-furnace slag, Cem. Concr. Res, 35, 1391-1399. 10.1016/j.cemconres.2004.11.010.
132. J. Koryta (1972), Theory and applications of ion-selective electrodes, Anal. Chim. Acta, 61, 329–411. 10.1016/S0003-2670(01)95071-8.
133. J.R.D. Frank J. Ansuini (2001), Long-term field tests of reference electrodes for concrete - ten year results, Corrosion.
134. R. Myrdal, K. Videm (1995), Evaluation of corrosion of steel reinforcement in concrete from potential measurements of embedded reference electrodes, Corrosion/95, NACE International, Paper No.512.
135. S. Muralidharan, T.H. Ha, J.H. Bae, Y.C. Ha, H.G. Lee, K.W. Park, D.K. Kim (2006), Electrochemical studies on the performance characteristics of solid metal–metal oxide reference sensor for concrete environments, Sens. Actuators, B, 113, 187-193. 10.1016/j.snb.2005.02.052.

136. S. Muralidharan, V. Saraswathy, A. Madhavamayandi, K. Thangavel, N. Palaniswamy (2008), Evaluation of embeddable potential sensor for corrosion monitoring in concrete structures, Electrochim. Acta, 53, 7248-7254. 10.1016/j.electacta.2008.04.078.
137. G.S. Duffó, S.B. Farina, C.M. Giordano (2009), Embeddable reference electrodes for corrosion monitoring of reinforced concrete structures, Mater. Corros., 61, 480-489. 10.1002/maco.200905346.
138. Y. Abbas, W. Olthuis, A. van den Berg (2015), Activated carbon as a pseudo-reference electrode for electrochemical measurement inside concrete, Constr. Build. Mater., 100, 194-200. 10.1016/j.conbuildmat.2015.10.001.
139. R. Myrdal (1997), Evaluation of electrochemical techniques for assessing corrosion of steel in concrete (PhD thesis), Department of Chemistry, University of Oslo.
140. S.-G. Dong, C.-J. Lin, R.-G. Hu, L.-Q. Li, R.-G. Du (2011), Effective monitoring of corrosion in reinforcing steel in concrete constructions by a multifunctional sensor, Electrochim. Acta, 56, 1881-1888. 10.1016/j.electacta.2010.08.089.
141. C.P. Atkins, J.D. Scantlebury, P.J. Nedwell, S.P. Blatch (1996), Monitoring chloride concentrations in hardened cement pastes using ion selective electrodes, Cem. Concr. Res., 26, 319-324. 10.1016/0008-8846(95)00218-9.
142. Miguel A. Climent-Llorca, E. Viqueira-Pérez, M.M. López-Atalaya (1996), Embeddable Ag/AgCl sensors for in-situ monitoring chloride contents in concrete, Cem. Concr. Res., 26, 1157-1161. 10.1016/0008-8846(96)00104-4.
143. B. Elsener, L. Zimmermann, H. Böhni (2003), Non destructive determination of the free chloride content in cement based materials, Mater. Corros., 54, 440–446. 10.1002/maco.200390095.
144. M.F. Montemor, J.H. Alves, A.M. Simões, J.C.S. Fernandes, Z. Lourenço, A.J.S. Costa, A.J. Appleton, M.G.S. Ferreira (2006), Multiprobe chloride sensor for in situ monitoring of reinforced concrete structures, Cem. Concr. Compos., 28, 233-236. 10.1016/j.cemconcomp.2006.01.005.
145. V. Garcia, R. François, M. Carcasses, P. Gegout (2013), Potential measurement to determine the chloride threshold concentration that initiates corrosion of reinforcing steel bar in slag concretes, Mater. Struct., 47, 1483-1499. 10.1617/s11527-013-0130-5.
146. C.P. Atkins, M.A. Carter, J.D. Scantlebury (2001), Sources of error in using silver/silver chloride electrodes to monitor chloride activity in concrete, Cem. Concr. Res., 31, 1207–1211. 10.1016/S0008-8846(01)00544-0.
147. G. de Vera, M.A. Climent, C. Antón, A. Hidalgo, C. Andrade (2010), Determination of the selectivity coefficient of a chloride ion selective electrode in alkaline media simulating the cement paste pore solution, J. Electroanal. Chem., 639, 43-49. 10.1016/j.jelechem.2009.11.010.
148. M.A. Climent, C. Antón, G.d. Vera, A. Hidalgo, C. Andrade (2011), *The interference of OH- ions in the potentiometric determination of free Cl- in cement paste pore solution* in *Proceedings of the International RILEM Conference on Advances in Construction Materials Through Science and Engineering*, Hong Kong, China, RILEM Publications, Bagneux, France.
149. R.-G. Du, R.-G. Hu, R.-S. Huang, C.-J. Lin (2006), In situ measurement of Cl^- concentrations and pH at the reinforcing steel: concrete interface by combination sensors, Anal. Chem., 78, 3179-3185. 10.1021/ac0517139.
150. G. Biedermann, L.G. Sillén (1960), Studies on the hydrolysis of metal ions. Part 30. A critical survey of the solubility equilibria of Ag_2O., Acta Chem. Scan., 14, 717-725. 10.3891/acta.chem.scand.14-0717.
151. F. Pargar, D.A. Koleva, E.A.B. Koenders, K.V. Breugel (2014), *The importance of chloride sensors stability in monitoring ageing phenomena in concrete structures:*

Ag/AgCl electrodes performance in simulated pore-water environment in *AMS 14: 1st Ageing of Materials & Structures Conference*, Delft.
152. S. Karthick, S.-J. Kwon, H.S. Lee, S. Muralidharan, V. Saraswathy, R. Natarajan (2017), Fabrication and evaluation of a highly durable and reliable chloride monitoring sensor for civil infrastructure, RSC Adv., 7, 31252-31263. 10.1039/c7ra05532c.
153. Y. Abbas, D.B. de Graaf, W. Olthuis, A. van den Berg (2014), No more conventional reference electrode: transition time for determining chloride ion concentration, Anal. Chim. Acta, 821, 81-88. 10.1016/j.aca.2014.03.013.
154. Y. Abbas, W. Olthuis, A. van den Berg (2013), A chronopotentiometric approach for measuring chloride ion concentration, Sens. Actuators, B, 188, 433-439. 10.1016/j.snb.2013.07.046.
155. D.B. de Graaf, Y. Abbas, J. Gerrit Bomer, W. Olthuis, A. van den Berg (2015), Sensor-actuator system for dynamic chloride ion determination, Anal. Chim. Acta, 888, 44-51. 10.1016/j.aca.2015.06.047.
156. D.O. McPolin, P.A.M. Basheer, K.T.V. Grattan, A.E. Long, T. Sun, W. Xie (2011), Preliminary Development and Evaluation of Fiber-Optic Chemical Sensors, J. Mater. Civ. Eng., 23, 1200-1210. 10.1061/(asce)mt.1943-5533.0000290.
157. J.-L. Tang, J.-N. Wang (2007), Measurement of chloride-ion concentration with long-period grating technology, Smart Mater. Struct., 16, 665-672. 10.1088/0964-1726/16/3/013.
158. A. Behnood, K.V. Tittelboom, N.D. Belie (2016), Methods for measuring pH in concrete: A review, Constr. Build. Mater., 105, 176–188. 10.1016/j.conbuildmat.2015.12.032.
159. W.R. Habel, K. Krebber (2011), Fiber-optic sensor applications in civil and geotechnical engineering, Photonic Sensors, 1, 268-280. 10.1007/s13320-011-0011-x.
160. P.A.M. Basheer, K.T.V. Grattan, T. Sun, A.E. Long, D. McPolin, W. Xie (2004), *Fiber optic chemical sensor systems for monitoring pH changes in concrete* in *Proceedings of the International Society for Optical Engineering*. 10.1117/12.601198.
161. J.I. Goldstein, D.E. Newbury, P. Echlin, D.C. Joy, J. A. D. Romig, C.E. Lyman, C. Fiori, E. Lifshin (1992), Scanning electron microscopy and X-Ray microanalysis, 2nd ed., New York, Plenum.
162. P.W. Hawkes, J.C.H. Spence (2007), Science of microscopy, ed., New York, Springer.
163. M.-Y. Yu, J.-Y. Lee, C.-W. Chung (2010), The application of various indicators for the estimation of carbonation and pH of cement based materials, J. Test. Eval., 38, 534-540.
164. DIN, EN 14629 (2007), Produkte und Systeme für den Schutz und die Instandsetzung von Betontragwerken - Prüfverfahren - Bestimmung des Chloridgehalts von Festbeton, Deutsches Institut für Normung, Berlin.
165. C. Boschmann Käthler, U.M. Angst, M. Wagner, B. Elsener (2017), Image analysis for determination of cement content in concrete to improve accuracy of chloride analyses, Cem. Concr. Res, 99, 1-7. 10.1016/j.cemconres.2017.04.007.
166. ASTM C1152/C1152M-04-e1: "Standard test method for acid-soluble chloride in mortar and concrete".
167. ASTM C114-15: "Standard test methods for chemical analysis of hydraulic cement".

PAPER I

Y. Seguí Femenias, U. Angst, F. Caruso, B. Elsener (2016)

Ag/AgCl ion-selective electrodes in neutral and alkaline environments containing interfering ions

Materials and Structures 49, 2637–265. doi: 10.1617/s11527-015-0673-8.

Materials and Structures (2016) 49:2637–2651
DOI 10.1617/s11527-015-0673-8

ORIGINAL ARTICLE

Ag/AgCl ion-selective electrodes in neutral and alkaline environments containing interfering ions

Yurena Seguí Femenias · Ueli Angst · Francesco Caruso · Bernhard Elsener

Received: 13 April 2015 / Accepted: 4 July 2015 / Published online: 10 July 2015

Abstract Chloride ingress can lead to serious degradation of various materials and structures. Continuous measurements of local chloride concentrations is thus of uttermost importance for laboratory research, monitoring of structures, and predictions of the residual life span for the most common building materials. This work investigates the applicability of Ag/AgCl ion-selective electrodes for the non-destructive continuous measurement of local chloride concentrations in concrete and stone when exposed to chloride-bearing environments such as seawater. The work studies the stability of Ag/AgCl ion-selective electrodes in neutral and alkaline solutions and the sensitivity to the main interfering ions coming from the environment and from the material itself. The results indicate negligible interference from fluoride, sulfate, and hydroxyl but considerable from bromide and sulfide. In chloride-free alkaline solutions, Ag/AgCl ion-selective electrodes are not stable over time, but—upon chloride arrival—they permit again reliable measurements of the chloride concentration. The results concerning interference are discussed by taking into account typical exposure environments and it is concluded that the ion-selective electrodes can satisfactorily be used to monitor chloride concentrations in built structures made out of concrete or stone.

Keywords Chloride monitoring · Ion-selective electrode · Interfering species · Sensitivity · Long-term stability · Selectivity coefficient

Y. Seguí Femenias (✉) · U. Angst · F. Caruso · B. Elsener
ETH Zürich, Institute for Building Materials (IfB), Stefano-Franscini-Platz 3, 8093 Zurich, Switzerland
e-mail: syurena@ethz.ch

U. Angst
Swiss Society for Corrosion Protection (SGK), Technoparkstrasse 1, 8005 Zurich, Switzerland

B. Elsener
Department of Chemical and Geological Sciences, University of Cagliari, 09100 Monserrato, CA, Italy

1 Introduction

Chloride ingress can lead to deterioration of various materials and structures. In non-carbonated reinforced concrete, when the chloride concentration reaches the so-called critical chloride content at the steel surface, depassivation of the steel occurs and chloride-induced corrosion initiates [1]. Natural stone can also be damaged by chloride ingress. When local chloride content reaches a certain level, supersaturation and crystallization of various salts can occur. Salt crystallization in the stone porosity may then exert substantial expansive stresses and seriously deteriorate the stone microstructure [2–5]. For similar reasons, structural degradation can also result from chloride ingress in masonry [6, 7]. In addition, when combined with other external constraints such as, for instance, freeze–thaw cycles, it is known that the presence of

chlorides can enhance the resulting damage in both stone and concrete [4, 8, 9].

In this context, the measurement of local chloride concentrations appears essential in building materials and structures. This is further enhanced by the latest advances and research in science, engineering, and technology. From a scientific point of view, the concept of the critical chloride content in concrete is at the origin of large debates [10–12]. Non-destructive and local measurements of chloride concentrations at the surface of the embedded reinforcement steel play an important role in research on this matter. From an engineering point of view, service life prediction models are increasingly used, in the design or in the infrastructure management stage. These models are based on predicting chloride ingress into concrete [13–15]. Therefore, continuous measurements of local chloride concentrations in laboratory specimens or in field structures are needed for their validation. Furthermore, the ever-increasing awareness for environmental concerns and sustainability resulted in a growing market share of blended cements [16, 17], which raised new questions on durability and mass transfer properties of these non-traditional materials [18, 19]. These questions cannot be answered using the existing one-century experience from Portland cement. However, they need to be quickly solved to bring these new binders from laboratory research to practice and improve the environmental performance of concrete [17].

The current methods for determining the local chloride contents in concrete and stone traditionally require destructive sampling (drilling, grinding, etc.) and do not allow obtaining continuous information at an identical location over time [4, 20, 21]. Non-destructive techniques for chloride detection are therefore being developed [22–28]. Some of the proposed techniques are able to measure relative variations in local chloride contents rather than the absolute local chloride contents [26, 28]. In this regard, it is considered that the use of Ag/AgCl ion-selective electrodes (ISEs) may be a promising solution [29–33]. Potentiometric measurement of chloride with ISEs is a well-established method that has mostly been limited to laboratory conditions. However, some attempts of in situ use of Ag/AgCl ISE have been recently made for the specific case of concrete [22–25, 27]. Nevertheless, surfaces of ISEs are notably sensitive to chemical species other than chloride [27, 34–37]. The applicability of Ag/AgCl ISE in complex chemical environments can thus be impaired by the presence of interfering species, coming either from the considered structure environment or from the material itself (for instance, hydroxyl interference in concrete). This paper investigates the applicability of the Ag/AgCl ISE for monitoring chloride concentrations in built structures made out of concrete or stone and exposed to chloride-bearing environments such as seawater. Therefore, it studies the long-term stability of Ag/AgCl ISE at high pH values and the possible interference arising from the presence of bromide, sulfate, sulfide, fluoride, and hydroxyl. From the obtained results, the ability of Ag/AgCl ISE to monitor the local chloride content in the pore solutions of concrete and stone is here discussed.

2 Theoretical background

2.1 The silver/silver chloride ion-selective electrode

The Ag/AgCl ISE used in this work belongs to the category of ion-selective electrodes with solid ion exchangers [29–31]. The Ag/AgCl ISE used here consists of silver covered by a layer of silver chloride. Since the AgCl coating has a low solubility, the electrolyte around the ISE is easily saturated with it and the potential E of the ISE is given by the Nernst equation:

$$E = E^0_{\mathrm{Ag/AgCl}} - \frac{RT}{F}\ln a_{\mathrm{Cl^-}} \quad (1)$$

where R is the gas constant, F the Faraday constant, T the absolute temperature, $a_{\mathrm{Cl^-}}$ the activity of the chloride, and $E^0_{\mathrm{Ag/AgCl}}$ expresses the standard potential of the Ag/AgCl electrode. $E^0_{\mathrm{Ag/AgCl}}$ is defined by the following equation [38]:

$$E^0_{\mathrm{Ag/AgCl}} = E^0_{\mathrm{Ag/Ag^+}} + \frac{RT}{F}\ln K_{S\_\mathrm{AgCl}} \quad (2)$$

where $E^0_{\mathrm{Ag/Ag^+}}$ is the standard potential of the $\mathrm{Ag/Ag^+}$ electrode and K_{S_AgCl} is the solubility product of AgCl.

The Ag/AgCl ISE responds to the primary ion (chloride ion) with a Nernstian behavior only above a

minimum concentration of it, the detection limit [31, 32, 39, 40]. Furthermore, the ISE is also sensitive to other species that can form precipitates of lower solubility with the constituent ionic species [27, 34–37]. This interference is traditionally considered with the selectivity coefficient, $K^{pot}_{Cl^-,Y}$ (with Y standing for the interfering species), included in the Nikolsky–Eisenman equation [31, 32, 41]:

$$E = E^0_{Ag/AgCl} - \frac{RT}{F}\ln\left(a_{Cl^-} + \sum\left(K^{pot}_{Cl^-,Y} \times a_Y^{-1/z_Y}\right)\right) \quad (3)$$

where a_Y is the activity of the interfering ionic species and z_Y its charge.

2.2 Influencing parameters

The ISE potential E depends on the chloride activity, the temperature, and the sensitivity to other species [Eq. (3)].

2.2.1 Chloride activity

In concentrated solutions, the high ionic strength causes large differences between activity and concentration. This phenomenon is taken into account by the use of the ionic activity a_X, which is related to the concentration c_X of a species X by the activity coefficient γ_X [38]:

$$a_X = \gamma_X \cdot {c_X}/{c^0} \quad (4)$$

where c^0 is the standard state composition (chosen as 1 mol L^{-1}).

2.2.2 Interfering species

Many silver salts have very low solubilities [38]; therefore, in their presence, the ISE is likely to be affected. The AgCl membrane responds mainly to Cl^-, Br^-, I^-, OH^-, and S^{2-} [27, 32, 35, 40, 41]. According to Eq. (3), the potential of the ISE will exhibit a Nernstian behavior when the following relation is satisfied [27]:

$$a_{Cl^-} \gg \sum\left(K^{pot}_{Cl^-,Y} \times a_Y^{-1/z_Y}\right) \quad (5)$$

2.2.3 Temperature

Both the Ag/AgCl electrode standard potential $E^0_{Ag/AgCl}$ and the *RT/F* term in Eq. (1) depend on temperature. Concerning $E^0_{Ag/AgCl}$, the effect of temperature has been addressed in detail in other studies and data is available to make the appropriate corrections; temperature coefficients between −0.6 and −0.65 mV $°C^{-1}$ have been reported [27, 42]. As an example, a decrease in temperature by 10 °C would thus lead to a decrease of ca. 6 mV in $E^0_{Ag/AgCl}$ and of ca. 3 mV in the *RT/F* term. Nevertheless, these errors can be corrected by always taking into account the temperature when applying the sensors under temperature fluctuating conditions. Furthermore, temperature effects can be reduced by using silver/silver chloride based reference electrodes (e.g. Ag/AgCl/sat. KCl) since in this case, the reference electrode and the ISE have the same standard potential, $E^0_{Ag/AgCl}$ and thus temperature only affects the *RT/F* term in Eq. (1).

Finally, it should be noticed that when a potentiometric measurement is performed the potentials of both the chloride ISE and the reference electrode against which the measurement is performed, depend on temperature [27]. When a temperature difference between the ISE and the reference electrode exists, errors in the measurement arise. Atkins et al. [35] showed that small temperature differences can lead to significant errors. Therefore, it is recommended that ISE and reference electrode are placed as close as possible (see also Sect. 4.3.3).

3 Materials and protocols

3.1 Electrodes, instruments and materials

3.1.1 The Ag/AgCl ion-selective electrode (ISE)

The Ag/AgCl ISE used is a commercially available ISE (Metrohm AG, Zofingen, Switzerland) consisting of Ag wire coated with AgCl deposited by anodizing. The tip of the ISE was additionally dipped in a melt of AgCl in order to achieve a more stable membrane [24, 27]. A stereomicroscopy image of the Ag/AgCl electrode is shown in Fig. 1.

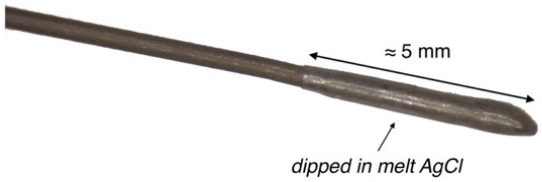

Fig. 1 Stereomicroscopy image of the Ag/AgCl ISE used in this work consisting of a Ag wire coated with AgCl

3.1.2 *Instruments for the potentiometric measurements*

The potential of the ISEs was measured against the silver/silver chloride/saturated potassium chloride (Ag/AgCl/sat. KCl) reference electrode (+0.197 V vs. SHE). A Luggin capillary (filled with the test solution) was used when the reference electrode was immersed in the test solution to avoid chloride contamination derived from the contact between test solution and KCl from the reference electrode.

It should be noted that, when the reference electrode is immersed in the test solution, liquid junction potential [40] establishes at the test solution/reference electrode interface and adds arithmetically to the measured potential. The situation is schematically depicted in Fig. 2.

The measurements were performed with a PGSTAT 30 Autolab potentiostat/galvanostat (Metrohm Autolab, Utrecht, the Netherlands) with high input impedance (>100 GΩ) connected to a Windows PC for data acquisition. The program for data acquisition was Autolab Nova v.1.10. All the experiments were carried out at room temperature (20–21 °C).

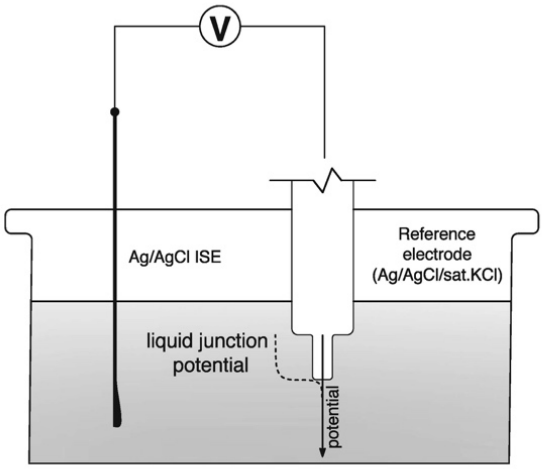

Fig. 2 Set-up for the potentiometric measurements with the schematic representation of the liquid junction potential established at the interface of the reference electrode and the solution

3.1.3 *Materials*

The sodium chloride (ACS, ISO Reag. Ph. Eur. grade) used for the preparation of the solutions was purchased from Merck (Merck KGaA, Darmstadt, Germany). The chemicals used for the preparation of interfering species solutions were: sodium hydroxide (≥99.0 %, Merck), potassium bromide (99.999 %, Fluka, Sigma-Aldrich Chemie GmbH, Buchs, Switzerland), potassium sulfate (≥99.0 %, Fluka), sodium fluoride (≥99.0 %, Sigma-Aldrich), and sodium sulfide nonahydrate (≥98.0 %, Sigma-Aldrich). All the solutions were prepared with de-ionized water (conductivity ≈ 2 μS/cm).

3.2 Methods

3.2.1 *Calibration in solution*

The Ag/AgCl ISEs were calibrated in neutral and alkaline solutions that contained known concentrations of sodium chloride ranging from 0.002 to 4 mol L^{-1}.

Liquid junction potentials E_{junction} [40] at the interface between the reference electrode and the calibration solution were calculated according to the Henderson equation [40]. For this calculation, it is considered that the concentration of KCl is 4.16 mol L^{-1} when saturated in water at room temperature (20 °C) [38].

The used solutions and the liquid junction potentials calculated are presented in Table 1.

The chloride activity was calculated according to Eq. (4). The activity coefficients of the chloride ion (γ_{Cl^-}) were interpolated from the data given by de Vera et al. [43]. For the alkaline solutions, the effect of the accompanying ions was neglected and activity coefficients were calculated considering the total hydroxyl concentration. The data is provided in Table 2.

The calibration curves were obtained by linear regression analysis:

$$E = E_{\text{measured}} - E_{\text{junction}} = m \cdot \log a_{Cl^-} + b \qquad (6)$$

Table 1 Calibration solutions and corresponding liquid junction potentials for the Ag/AgCl/sat. KCl

NaCl concentration (mol L^{-1})	NaOH concentration (mol L^{-1})	$E_{junction}$ at 20 °C (mV)
0.002	–	−3.7
0.01	–	−2.9
0.1	0.01	−1.2
0.1	0.1	0.7
0.1	1	8.4
0.5	–	0.1
0.5	0.01	0.3
0.5	0.1	1.5
0.5	1	8.4
1	–	1.2
1.5	–	1.9
4	–	4.2

Table 2 Activity coefficients of the chloride ion γ_{Cl^-} used in this work. Values of pH other than 7 were obtained by addition of sodium hydroxide. The values of γ_{Cl^-} are interpolated from the data given by de Vera et al. [43]

NaCl concentration (mol L^{-1})	pH	γ_{Cl^-}
0.002	7	0.958
0.01	7	0.901
0.1	7	0.767
0.5	7	0.648
1	7	0.603
1.5	7	0.587
2	7	0.572
4	7	0.576
5	7	0.591
0.1	≈12	0.740
0.1	≈13	0.727
0.1	≈14	0.603
0.5	≈12	0.642
0.5	≈13	0.637
0.5	≈14	0.585

3.2.2 Sensitivity to interfering species

The interference was investigated for hydroxyl, bromide, sulfate, fluoride, and sulfide. These were considered the main species that could cause interference to the Ag/AgCl ISEs response in concrete, stone, and seawater exposure [4, 24, 35, 44, 45]. It should be noted (Table 4) that iodide might be a potentially serious contaminant. However, iodide is not expected in relevant concentrations in the exposure regimes considered in this work. Moreover, it has been previously reported that iodide interference is actually smaller than generally assumed [41] and therefore, it is not addressed in this study.

With the exception of hydroxyl interference, the Ag/AgCl ISEs were first immersed in NaCl solutions without containing interfering species. Regarding the hydroxyl interference, experiments were always started with 0.1 mol L^{-1} sodium hydroxide solutions to simulate the alkalinity of the concrete pore solution. In this case, experiments were also carried out avoiding exposure to daylight as this may affect the results [46]. This would be an artifact because when the sensors are embedded in building materials, they are not exposed to daylight.

The concentration of the interfering species was increased stepwise as soon as the potential became stable over time (from a few minutes—for the addition of hydroxyl, sulfate, and fluoride—up to a few days—for the addition of bromide and sulfide). Ag/AgCl ISEs were immersed in the solutions containing increasing amounts of the possible interfering species for a total of 2 months.

The used solutions and the concentration ranges of interfering species are given in Table 3. The selected concentration ranges and their relation to practice for the case of stone and concrete are discussed in Sect. 4.2.

Once the experiments were finished, the Ag/AgCl ISEs that were immersed in the solutions containing bromide, fluoride, sulfate, and sulfide were immersed back into the initial NaCl solutions without interfering

Table 3 Solutions used for the study of the sensitivity to interfering species of the Ag/AgCl ISE

NaCl concentration (mol L^{-1})	Concentration range of interfering species (mol L^{-1})	Interfering species
0.05	0.1–1.7	OH^-
0.1	0.1–1.6	OH^-
0.2	0.1–1.5	OH^-
0.3	0.1–1.6	OH^-
0.5	0.1–1.6	OH^-
0.01	0–0.4	Br^-
0.1	0–0.3	Br^-
0.01	0–0.04	F^-
0.01	0–0.04	SO_4^{2-}
0.1	0–0.01	S^{2-}
1	0–0.008	S^{2-}

species. The potential was then measured after 1 month of immersion in the chloride solutions. The aim of this last experiment was to check whether prolonged exposure to the interfering species could compromise the functionality of Ag/AgCl ISEs once they are exposed again only to chlorides.

3.2.3 Long-term stability at high pH

The stability of the Ag/AgCl ISEs at high pH in the absence of chloride was investigated over a period of 60 days. Erlenmeyer flasks were filled to the very top with sodium hydroxide solutions and closed with a rubber plug through which the ISEs were inserted via drilled holes. The flasks were additionally sealed with silicon grease to avoid evaporation and/or carbonation of the solution.

The solutions used for the long-term stability were: 0.01 mol L^{-1} NaOH, 0.1 mol L^{-1} NaOH, and 1 mol L^{-1} NaOH. For comparison, 0.1 mol L^{-1} NaOH solution that contained always 0.1 mol L^{-1} NaCl was also used in this experiment.

After 60 days of immersion, sodium chloride was added to the chloride-free alkaline solutions up to a concentration of 0.1 mol L^{-1}.

4 Results and discussion

4.1 Calibration in solution

The calibration curve according to Eq. (6) is shown in Fig. 3.

The Ag/AgCl ISEs exhibit a Nernstian behavior with a slope of −59 mV/decade, in good agreement with the values reported in previous works [24, 27]. Furthermore, the standard deviation of the ten individual potential readings is always below 2 mV.

The ISEs exhibit Nernstian behavior in the interference-free solutions for the whole range of chloride concentrations tested (Fig. 3). It can be then concluded that the detection limit of the chloride ion in aqueous neutral solution is lower than 0.002 mol L^{-1}, in agreement with the results reported by Angst et al. [27].

4.2 Sensitivity to interfering species

4.2.1 Zones of interference

Figure 4 schematically illustrates the effect of the interfering species on the Ag/AgCl ISE response by dividing the diagram ISE potential versus activity of interfering species in three different regions.

In zone "a" (Fig. 4), the Ag/AgCl ISE behaves as an ideal chloride sensor. It exhibits a stable potential, determined by the chloride ion activity and independent on the interfering species [27, 29, 47]. It is in this range where the Ag/AgCl ISE is suitable for field measurements—namely, where it acts as "pure chloride sensor"—without interference. The effect on the chloride activity of the other ions present in the solution should however be taken into account.

When the concentration of interfering species increases (zone "b" in Fig. 4), the response of the ISE is altered and it shows a potential determined by the simultaneous action of primary (chloride) and

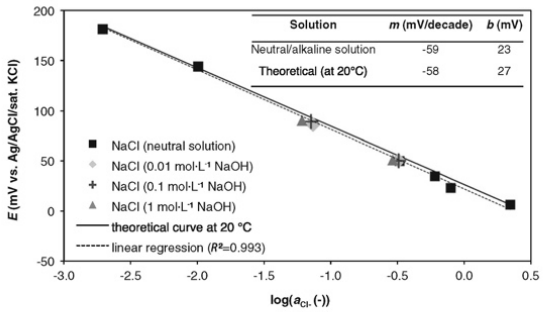

Fig. 3 Calibration curve for the Ag/AgCl ISE in neutral and alkaline solutions (mean values obtained from ten individual readings). The standard deviation is always less than 2 mV (smaller than the symbols). The parameters of the linear regression analysis are also given together with the theoretical values [42] (considering a constant room temperature of 20 °C)

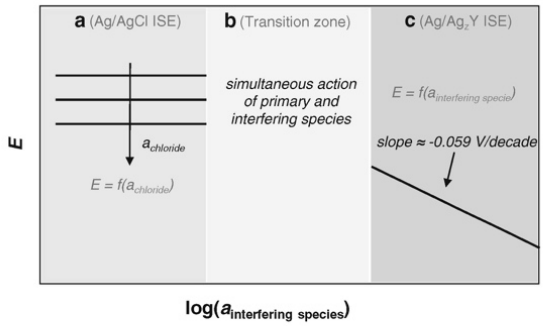

Fig. 4 Schematic Ag/AgCl ISE potential E as a function of the activity of the interfering species (at room temperature)

interfering species. This interference is reported to be due to the replacement of the chloride by the interfering species on the surface of the ISE [29, 47]. Different concentrations of primary and interfering species would lead to different stages in surface coverage of the precipitate formed between silver and interfering species [47]. No line was drawn for this region in Fig. 4 because the potential of the ISE is here depending on a number of factors, including time effects (see Appendix 1).

At sufficiently high concentrations of interfering species, the ISE surface becomes totally covered by the salt formed between silver and interfering species and then the ISE is only sensitive to this species [47, 48] (zone "c" in Fig. 4).

The response of the Ag/AgCl ISE will be in one of the three zones of Fig. 4 depending on how severe is the interference is and on the experimental conditions [29, 33, 47, 48]. In addition, it should also be noted that once the interfering species is removed from the solution, the Ag/AgCl ISE should ideally behave again as an ideal chloride sensor [35] (zone "a" in Fig. 4).

4.2.2 *Sensitivity to hydroxyl, bromide, fluoride, sulfate and sulfide*

In this work, the ideal ISE behavior shown in zone "a" in Fig. 4 is found for hydroxyl, fluoride, and sulfate for almost the whole range of tested concentrations.

Figure 5 gives the potential E of the Ag/AgCl ISEs immersed in alkaline solutions containing NaCl as a function of the hydroxyl concentration. The potential E of the Ag/AgCl ISEs was corrected for the liquid junction potential [Eq. (6)].

From Fig. 5, it can be seen that the Ag/AgCl ISEs do not significantly deviate from the potential registered in absence of hydroxyl (empty markers in Fig. 5). The maximum deviation with respect to this value is 8 mV and it is found for the ISEs immersed in the solution containing 0.05 mol L^{-1} NaCl. The difference between the largest and smallest observed potentials is 10 mV and it is also found for the ISEs immersed in the solution containing 0.05 mol L^{-1} NaCl.

Figure 6 gives the potential E of the Ag/AgCl ISEs immersed in 0.01 mol L^{-1} NaCl solution with increasing amount of fluoride and sulfate as a function of the concentration of these species. The potential

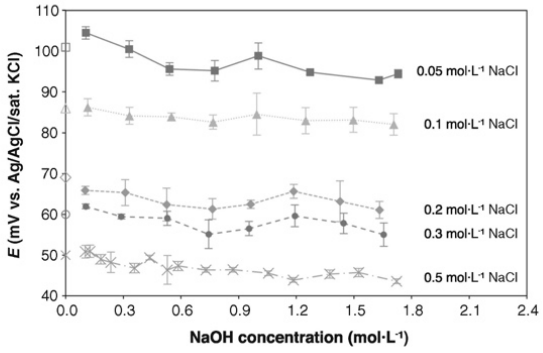

Fig. 5 Ag/AgCl ISE mean potential values (from five individual readings) as a function of the NaOH concentration. The *empty markers* (*left side* of the graph) indicate the potential at zero NaOH concentration obtained for the corresponding chloride concentration (calibration curve). The *error bars* indicate the standard deviation from the individual readings

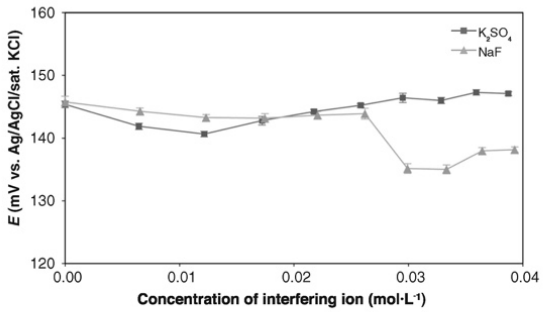

Fig. 6 Ag/AgCl ISE mean potential values (from ten individual readings) as a function of the NaF and K_2SO_4 concentrations in 0.01 mol L^{-1} NaCl solution. The potentials of both curves at zero NaF and K_2SO_4 concentration correspond to the mean value for the chloride concentration obtained from the calibration curve (Sect. 4.1). The *error bars* indicate the standard deviation from the individual readings

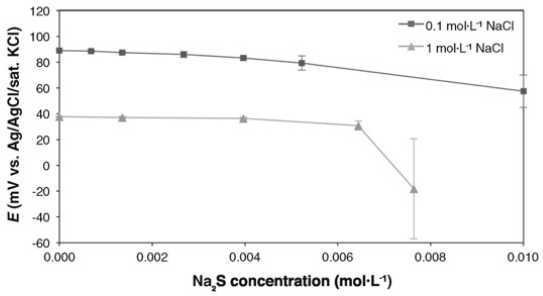

Fig. 7 Ag/AgCl ISE mean potential values (from ten individual readings) as a function of the Na_2S concentration. The potentials of both curves at zero Na_2S concentration correspond to the mean value for the chloride concentration obtained from the calibration curve (Sect. 4.1). *Error bars* indicate the standard deviation from the individual readings

E of the Ag/AgCl ISEs was also corrected for the liquid junction potential [Eq. (6)].

Regarding the fluoride interference, it is observed that up to a fluoride concentration of 0.02 mol L^{-1}, the ISE potential can be considered to be unaffected (Fig. 6). At fluoride concentrations higher than 0.025 mol L^{-1}, however, a small decrease in the potential is observed. For sulfate, the potential remains almost unaffected to—at least—a concentration of 0.04 mol L^{-1} (fourfold chloride concentration). Moreover, when returned back to the original NaCl solution (fluoride- and sulfate-free), the ISEs exhibit potentials equal to those initially registered in the absence of the interfering species within a few minutes.

For bromide and sulfide, the interference is more severe. Figure 7 shows the potential E of the Ag/AgCl ISEs immersed in 0.1 and 1 mol L^{-1} NaCl solutions with increasing amounts of sulfide. For the bromide interference, the potential E is plotted against the logarithm of the bromide concentration. This is shown in Fig. 8. The potential E of the Ag/AgCl ISEs shown in Figs. 7 and 8 was also corrected for the liquid junction potential [Eq. (6)].

In the presence of bromide and sulfide, the ISE exhibits the ideal behavior depicted in zone "a" in Fig. 4 only at low bromide and sulfide concentrations ($c_{KBr} < 0.01$ mol L^{-1} for the ISEs immersed in the solution containing 0.1 mol L^{-1} NaCl and $c_{Na_2S} < 0.006$ mol L^{-1} for both tested chloride solutions).

Relatively small amounts of sulfide and bromide cause high potential shifts. For sulfide concentrations above 0.006 mol L^{-1}, the registered ISE potential decreases more than 20 mV for the ISEs immersed in the 0.1 mol L^{-1} NaCl solution and more than 50 mV for the ISEs immersed in the 1 mol L^{-1} NaCl solution. The standard deviation also increases significantly at this sulfide concentration (Fig. 7), with values higher than 12 mV in both cases. For the bromide interference, strong potential shifts are observed at bromide concentrations higher than 0.01 and 0.02 mol L^{-1} for the ISEs immersed in the solutions containing 0.01 and 0.1 mol L^{-1} NaCl, respectively. The standard deviation is also high in this range, reaching values up to 25 mV. It should also be noted that the immersed tip of the ISEs turned green upon the addition of bromide. The same phenomenon was observed for the ISEs

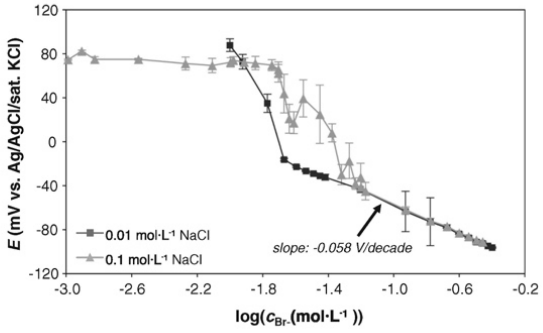

Fig. 8 Ag/AgCl ISE mean potential values (from ten individual readings) as a function of the KBr concentration. The potentials of both curves at zero KBr concentration correspond to the mean value for the chloride concentration obtained from the calibration curve (Sect. 4.1). *Error bars* indicate standard deviation between the individual readings

immersed in the solutions containing sulfide but, in this case, the tip of the ISEs turned black and it also decreased its thickness.

The significant potential decrease (at constant chloride concentration) and the high standard deviation for the sensors immersed in the same solution are an indication of the mentioned surface coverage process (Sect. 4.1) when both primary and interfering species act simultaneously (zone "b" in Fig. 4). The color change of the tip of the ISEs also evidences the surface coverage of the ISE with the salt formed with the interfering species.

For bromide concentrations higher than 0.05 mol L^{-1}, the potential E is governed by the bromide concentration for both tested chloride concentrations (Fig. 8). The slope in this part of the graph is -0.058 V/decade, thus exhibiting a Nernstian behavior. This corresponds to the zone "c" depicted in Fig. 4.

When returned back to the original NaCl solutions, the ISEs immersed in the solutions containing increasing amounts of bromide and sulfide did not regain the potential values that they initially exhibited for the given chloride solution. As pointed out in Sect. 4.1, once the interfering species is removed from the solution, the Ag/AgCl ISE should respond again to the chloride with Nernstian behavior (zone "a" depicted in Fig. 4). This was already reported by Atkins et al. [35] for the bromide interference. However, in this study, the ISEs were immersed in the solutions containing bromide for about 2 months, whereas Atkins et al. immersed them for only 15 min [35]. It is believed that this disagreement is due to the kinetics of the transformation of AgBr back into AgCl. In fact, Rhodes et al. [47] reported that the kinetics of the transformation of the AgBr back into AgCl is at least 200 times slower than the conversion of AgCl into AgBr. Thus, prolonged exposure to bromide and sulfide in the absence of significant amounts of chlorides may significantly impair the applicability of Ag/AgCl ISEs for field measurements.

4.3 Applicability of the Ag/AgCl ion-selective electrode in practical situations

As explained in Sect. 2.1, the interference from external species on the ISEs response is usually quantified with the selectivity coefficients. However, the kinetics of the reactions of the interfering species with the ISE surface is normally not considered. This issue is discussed in the Appendix 1 of this paper. Therefore, the use of selectivity coefficients appears not to be appropriate for evaluating interference at mid-long term exposure (see Appendix 1). In this work, the exposure time of the ISE to the possible interfering species was 2 months. From the obtained results, the applicability of the Ag/AgCl ISE for in situ measurements in concrete and stone is discussed in this section.

4.3.1 Concrete

Upon hydration of cement, high hydroxyl concentrations are typically present in the concrete pore solution. When it comes to chloride-induced corrosion of the reinforcement steel, a concentration ratio chloride to hydroxyl $c_{Cl^-}/c_{OH^-} = 0.6$ may as a fist-hand estimate be considered as threshold value for corrosion initiation [49]. As it is apparent from Fig. 5, no interference is found even for clearly lower ratios c_{Cl^-}/c_{OH^-}. Thus, the Ag/AgCl ISEs are feasible to monitor chloride ingress into concrete for the purpose of corrosion studies. It will allow detecting chloride concentrations much below levels considered critical for corrosion initiation even at high pH.

If concrete structures are exposed to seawater, bromide interference could be a potential issue. The bromide/chloride ratio in seawater is approximately 0.002 [50]. At a bromide/chloride ratio of 0.1 (for the ISEs immersed in 0.1 mol L^{-1} NaCl), no interference is here observed. Furthermore, from Fig. 8, it becomes apparent that the ISEs can tolerate slightly higher bromide concentrations when the chloride content is also higher. The chloride concentration in seawater is around 0.5 mol L^{-1} NaCl. Thus, no significant interference from bromide is expected in this case.

On the contrary, because of the severity of its interference, it is strongly suggested that the Ag/AgCl ISEs are not used when sulfide can be present in high amounts as, for example, in slag cement [44, 51, 52]. Moreover, slag cement is not a well-defined product, showing great variations of sulfide content in the different production plants and cement binders [44, 51–54]. Therefore, the influence on the sulfide concentration in the pore solution is difficult to predict and the question of whether the Ag/AgCl ISE can be used in the concretes containing mid-low amounts of blast furnace slag (for example, CEM III/A) seems

unclear and it has been already questioned by the authors [55].

The instability of the Ag/AgCl ISE at high pH with no or low presence of chlorides has also been questioned [24, 27, 45]. For this reason, the stability of the Ag/AgCl ISEs at high pH in absence of chloride was also investigated in this work. Figure 9 shows the potential E of as a function of time, before and after addition of chloride (at $t = 60$ days) for the chloride-free solutions. The potential E was corrected for the liquid junction potential [Eq. (6)].

In absence of chloride, the potential of the Ag/AgCl ISEs shows high scatter between the individual sensors (Fig. 9). In addition, the color of the solutions turned brown-black with time. This color change was more pronounced for the solutions that contained higher NaOH concentrations.

In alkaline environments in absence or low content of chlorides, the AgCl precipitate undergoes the following reaction [56]:

$$2AgCl_{(s)} + 2OH^- \rightleftarrows Ag_2O_{(s)} + H_2O + 2Cl^- \quad (7)$$

For the case of the Ag/AgCl ISEs immersed in chloride-free alkaline solutions (Fig. 9), the measured potential values were initially higher than 140 mV and they decreased to approximately 120 mV after 60 days of immersion. This suggests that the continuous formation of Ag_2O shifts the potential of the sensors to more negative values; potentials of $\sim$100 mV (vs. Ag/AgCl/sat. KCl) at room temperature and pH 14 are reported in the literature [27, 57]. The change of color observed can also be related to the transformation of AgCl into Ag_2O. This was already observed by Angst et al. [27]. The possible formation of Ag_2O [Eq. (7)] could explain the oscillations in the Ag/AgCl ISE potential shown in Fig. 5, especially at the lowest chloride concentrations.

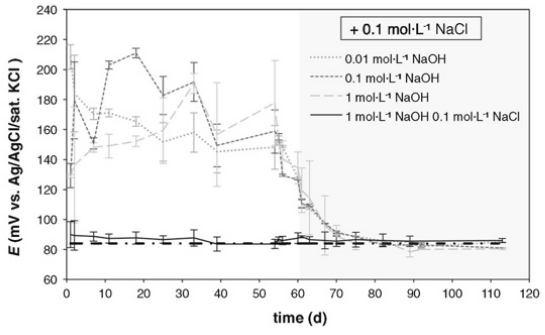

Fig. 9 Ag/AgCl ISE mean potential values (from ten individual readings) as a function of time. The *dash dot thick line* indicates the potential 0.1 mol L^{-1} NaCl solution (calibration curve). The *error bars* indicate the standard deviation from the individual readings. The beginning of the *grey shaded area* marks the addition of potential 0.1 mol L^{-1} NaCl

Upon addition of chloride, however, the ISEs exhibit the potential expected from the calibration curve within less than 8 days. The temporal scatter and instability are also considerably reduced. Thus, the possible formation of silver oxide is fully reversible, as it was already stated by Angst et al. [27] and Pargar et al. [57]. The adherence of the Ag_2O to the ISE surface (questioned by Angst et al. [27]) could however be an issue for the long-term stability because of the reversibility of the AgCl formation. This aspect should deserve further attention.

4.3.2 Stone

Silicates are the most common minerals in igneous, metamorphic and many sedimentary rocks [4]. However, stones may also contain other minerals in smaller quantities; the ones that can potentially interfere the response of the Ag/AgCl ISE are: galena (PbS), sphalerite (ZnS), fluorite (CaF_2), gypsum ($CaSO_4 \cdot 2H_2O$) and anhydrite ($CaSO_4$). On the basis of the values of solubility product at 25 °C (or equilibrium constant for the case of sulfide) reported in literature [38], the maximum amount of each species is here calculated and the possible interference discussed.

The maximum concentration of fluoride that can be found from the dissolution of pure fluorite is $c_{F^-} \approx 2 \times \left(\frac{K_{S\_CaF_2}}{4}\right)^{1/3} = 4 \times 10^{-4}$ mol L^{-1}. From Fig. 6, no interference is expected at such low concentrations. Following the same reasoning, the maximum amount of sulfate deriving from the dissolution of pure gypsum ($CaSO_4 \cdot 2H_2O$) and pure anhydrite ($CaSO_4$) is estimated to be 1.2×10^{-2} and 1.5×10^{-2} mol L^{-1}, respectively. From Fig. 6, no interference is found at those sulfate concentrations.

Regarding the presence of sulfide, it should be noted that S^{2-} is not present in significant concentrations due to the hydrolysis reaction of this ion with water [38, 58]. In this case, the solubility product of compounds containing sulfides Y_xS_z is replaced by the equilibrium constant K_{YS} of the following reaction:

$$Y_xS_z + zH^+ \rightleftarrows xY^{(2z/x)+} + zHS^- \quad (8)$$

Thus, the concentration c_{HS^-} of hydrogen sulfide ion derived from the dissolution of pure galena and pure sphalerite can be estimated as: $c_{HS^-} \approx \sqrt{K_{YS} \times c_{H^+}}$. In absence of carbonates, it can be assumed that the pH of the pore water in stone is neutral ($c_{H^+} \approx 10^{-7}$ mol L^{-1}). Therefore, the maximum concentrations of hydrogen sulfide ion are 8×10^{-12} and 1.4×10^{-8} mol L^{-1}, respectively, when pure galena (PbS) and pure sphalerite (ZnS) are present. From the obtained results (Fig. 7), no effect on the ISE response is expected at such low concentrations.

The data obtained in this study show that the above-listed minerals possibly present in stone should not interfere with the Ag/AgCl ISE response. The above-mentioned considerations are, however, valid for pure minerals and are given as general indications. A more complex environment (like the natural one) could substantially change these values due to the contemporary presence of other equilibria with the surrounding environment. For example, iodide may be expected in some organic-rich sedimentary rocks [59]. The possible interference in these cases should be then further tested and studied.

In addition, experience on the applicability of the Ag/AgCl in stone is very limited and more research in this field should be done.

4.3.3 Additional remarks on the applicability of the Ag/AgCl ISE for field measurements

Similar to the liquid junction potentials taken into account in this work, any concentration differences present between the ISE and the reference electrode will give rise to diffusion potentials that add arithmetically to the measured potential [60]. In porous systems such as concrete, stone, or soil, concentration gradients are likely to be present and maintained over long periods, due to the restricted mass transport in the tortuous pore systems. Thus, depending on the position of the reference electrode with respect to the ISE, these diffusion potentials may present a serious error source. This has been treated in detail elsewhere [60]. In general, to minimize these errors, the reference electrode should be placed as close to the ISE as possible.

5 Conclusions

The Ag/AgCl ISEs studied in this work responded to chloride, as expected from Nernst's law and previous studies.

The sensitivity of the Ag/AgCl ISE to other interfering species has been carefully studied in this work. While negligible interference was found for fluoride, sulfate, and hydroxyl, the interference is relatively severe for bromide and sulfide. Nevertheless, due the high chloride/bromide concentration ratio in seawater, the interference of bromide is considered negligible for applications in seawater exposure.

In completely chloride-free alkaline solutions, the ISEs were not stable over time, probably due to transformation reactions with the environment. Upon addition of chloride, however, the sensors responded again according to Nernst's law.

Based on the current experimental observations, it is concluded that the studied Ag/AgCl ISEs are feasible for practical monitoring of the chloride concentration in inorganic porous building materials, such as stone or concrete exposed to chloride-containing environments. A notable exception is concrete with high blast furnace slag content, where the presence of sulfides could strongly disturb the measurements.

Acknowledgments The financial support from the Swiss National Science Foundation (SNF) is kindly acknowledged. The authors would also like to thank Dr. Nicolas Roussel for his valuable comments to improve the manuscript.

Appendix 1

Limitations of the concept of selectivity coefficients (time effect)

The severity of the interference of external species with the ISE is commonly taken into account with the selectivity coefficients [see Eq. (3)] [30–33, 39]. The theoretical models for estimating selectivity coefficients are traditionally based on the assumption that thermodynamic equilibrium is established. In these models, the kinetics of the reactions is normally neglected.

Table 4 lists the selectivity coefficients $K^{pot}_{Cl^-,Y}$ of the Ag/AgCl ISE to other species reported in

Table 4 Values of selectivity coefficients $K^{pot}_{Cl^-,Y}$ for the Ag/AgCl ISE reported in literature and maximum allowable chloride to interfering species ratio not causing interference

Interfering species	Minimum allowable chloride to interfering species ratio [61]	Selectivity coefficient $K^{pot}_{Cl^-,Y}$	Exposure time to the solution with interfering species	Reference for the reported selectivity coefficient $K^{pot}_{Cl^-,Y}$
OH^-	1.25×10^{-2}	4×10^{-3}	>6 months	[27]
		2×10^{-3}–9.1×10^{-3}	<1 day	[62, 63]
		2.4×10^{-2}	Not specified	[29]
		9.33×10^{-3}	Theoretical model	Calculated from [39]
		$\approx 10^{-2}$	Theoretical model	[30]
		$\approx 10^{-2}$	Not specified	[36]
Br^-	3.33×10^{2}	2.1–3.3×10^{2}	<1 day	[64]
		1.1×10^{2}–3.5×10^{2}	<1 day	[62, 63]
		1.2	Not specified	[29]
		3.63×10^{2}	Theoretical model	Calculated from [39]
		1–3.5×10^{2}	Theoretical model	[30]
I^-	2×10^{6}	3–14	<1 day	[41]
		1.8×10^{2}–2.2×10^{6}	<1 day	[62, 63]
		86.5–1.8×10^{6}	<1 day	[64]
		86.5	Not specified	[29]
		2.9×10^{6}	Theoretical model	Calculated from [39]
		1–2.1×10^{6}	Theoretical model	[30]
S^{2-}	$>10^{6}$	2.04×10^{15}	–	Calculated from [39]
SO_4^{2-}		4.73×10^{-8}	–	Calculated from [39]

literature. Information about the theoretical or experimental calculation of the selectivity coefficients and the exposure time of the ISE in the solution containing interfering species (in the case of experimental calculation) is also given here. The values of the solubility products for the calculation of the theoretical selectivity coefficient according to Morf et al. [39] were obtained from the data reported by Haynes [38]. Table 4 also provides the minimum chloride to interfering species ratio tolerated without causing interferences reported by Kaland et al. [61].

In general, there is a large variability in the reported selectivity coefficients (Table 4). As a comparison, Eq. (3) is solved for the selectivity coefficient for the case of the bromide interference, yielding:

$$K^{pot}_{Cl^-,Br^-} = \frac{e^{\frac{\left(E^0_{Ag/AgCl} - E\right)F}{RT}}}{a_{Br^-}} - a_{Cl^-} \quad (9)$$

From the experiments performed in this study, all the parameters on the right side of Eq. (9) are known for each step of the increasing interference concentration. The values of chloride and bromide activity coefficients were obtained with the PHREEQC Interactive v. 3.1.4 software. Its computational routine is based on the specific ion interaction theory (SIT) and it models well chloride-based systems with ionic strength up to 1 mol L^{-1} [62]. Figure 10 shows the computed selectivity coefficient according to Eq. (9) as a function of the bromide concentration.

When the ISE acts as an ideal Ag/AgCl ISE (zone "a" in Figs. 4 and 10), the selectivity coefficient is relatively small, indicating that the contribution of the bromide is low and that the potential exhibited by the ISE is governed by the chloride content.

When the ISE acts only as AgBr ISE (zone "c" in Figs. 4 and 10), the values of the selectivity coefficient obtained for both tested chloride concentrations are similar and relatively constant. They are also in the same order of magnitude as most of the values reported in literature (Table 4). It should be noted, however, that, in this zone, the ISE is no longer a Ag/

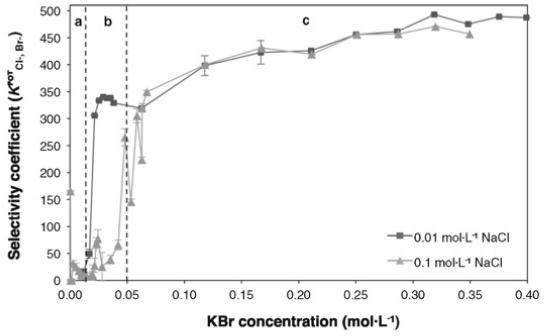

Fig. 10 Selectivity coefficient $K^{pot}_{Cl^-,Br^-}$ as a function of the bromide concentration calculated according to Eq. (9). The standard deviation (*error bars*) from the ten individual potential readings is always below 30 mV. The zones defined in Fig. 4 are here divided by *dashed lines*: *a* Ag/AgCl ISE, *b* transition zone, *c* Ag/AgBr ISE

AgCl ISE, but rather a Ag/AgBr ISE. Thus, the selectivity coefficient $K^{pot}_{Cl^-,Br^-}$—as it appears in Eq. (3)—does in principle not make sense.

When the chloride and bromide act simultaneously (zone "b" in Figs. 4 and 10), the selectivity coefficient suddenly rises, indicating the increasing interference of the bromide in this case. It is believed that, in this case, the ISE response is influenced by other parameters, such as the surface coverage, diffusion processes, membrane morphology, etc. [33, 41, 47, 48, 63–65]. This might also be the reason for the high variability of the selectivity coefficients found in literature.

In case of short-term exposures, as in the case of applications in analytical chemistry, the protocol described by the IUPAC [33] is recommended. However, it is believed that both thermodynamics and kinetics contribute to the selectivity of ion-selective electrodes. This has already been suggested by other authors [64, 66]. Therefore, it appears that the theoretical models for predicting the Ag/AgCl ISE response in presence of interfering ions are not suitable for mid to long-term exposure.

References

1. Elsener B, Bertolini L, Pedeferri P, Polder RP (2013) Corrosion of steel in concrete, 2nd edn. Wiley-VCH, Weinheim
2. Scherer GW (2004) Stress from crystallization of salt. Cem Concr Res 34:1613–1624. doi:10.1016/j.cemconres.2003.12.034
3. Angeli M, Benavente D, Bigas J-P, Menéndez B, Hébert R, David C (2007) Modification of the porous network by salt crystallization in experimentally weathered sedimentary stones. Mater Struct 41:1091–1108. doi:10.1617/s11527-007-9308-z
4. Siegesmund S, Snethlage R (2011) Stone in architecture: properties, durability, 4th edn. Springer, Berlin
5. Flatt RJ, Caruso F, Sanchez AM, Scherer GW (2014) Chemo-mechanics of salt damage in stone. Nat Commun 5:4823. doi:10.1038/ncomms5823
6. Ottosen LM, Rörig-Dalgaard I (2008) Desalination of a brick by application of an electric DC field. Mater Struct 42:961–971. doi:10.1617/s11527-008-9435-1
7. Bourgès A, Vergès-Belmin V (2010) Application of fresh mortar tests to poultices used for the desalination of historical masonry. Mater Struct 44:1233–1240. doi:10.1617/s11527-010-9695-4
8. Valenza JJ, Scherer GW (2006) Mechanism for salt scaling of a cementitious surface. Mater Struct 40:259–268. doi:10.1617/s11527-006-9104-1
9. Shi X, Fay L, Peterson MM, Yang Z (2009) Freeze–thaw damage and chemical change of a Portland cement concrete in the presence of diluted deicers. Mater Struct 43:933–946. doi:10.1617/s11527-009-9557-0
10. Angst U, Elsener B, Larsen CK, Vennesland Ø (2009) Critical chloride content in reinforced concrete—a review. Cem Concr Res 39:1122–1138. doi:10.1016/j.cemconres.2009.08.006
11. RILEM technical committee 235-CTC (2009) Corrosion initiating chloride threshold concentrations in concrete. http://www.rilem.org/gene/main.php?base=8750&gp_id=237
12. RILEM technical committee SCI (2014) Characteristics of the steel/concrete interface and their effect on initiation of chloride-induced reinforcement corrosion. http://www.rilem.org/gene/main.php?base=8750&gp_id=331
13. Geiker M, Nielsen EP, Herfort D (2006) Prediction of chloride ingress and binding in cement paste. Mater Struct 40:405–417. doi:10.1617/s11527-006-9148-2
14. Wall H, Nilsson L-O (2007) A study on sampling methods for chloride profiles: simulations using data from EPMA. Mater Struct 41:1275–1281. doi:10.1617/s11527-007-9325-y
15. Zheng JJ, Zhou XZ, Wu ZM (2009) A simple method for predicting the chloride diffusivity of cement paste. Mater Struct 43:99–106. doi:10.1617/s11527-009-9473-3
16. Juenger MCG, Winnefeld F, Provis JL, Ideker JH (2011) Advances in alternative cementitious binders. Cem Concr Res 41:1232–1243. doi:10.1016/j.cemconres.2010.11.012
17. Flatt RJ, Roussel N, Cheeseman CR (2012) Concrete: an eco material that needs to be improved. J Eur Ceram Soc 32:2787–2798. doi:10.1016/j.jeurceramsoc.2011.11.012
18. Chidiac SE, Panesar DK, Zibara H (2012) The effect of short duration NaCl exposure on the surface pore structure of concrete containing GGBFS. Mater Struct 45:1245–1258. doi:10.1617/s11527-012-9831-4
19. Kaminskas R, Barauskas I (2013) Influence of pozzolana on sulfate attack of cement stone affected by chloride ions. Mater Struct 47:1901–1910. doi:10.1617/s11527-013-0159-5

20. Vennesland Ø, Climent MA, Andrade C (2012) Recommendation of RILEM TC 178-TMC: testing and modelling chloride penetration in concrete. Mater Struct 46:337–344. doi:10.1617/s11527-012-9968-1
21. Cheewaket T, Jaturapitakkul C, Chalee W (2013) Concrete durability presented by acceptable chloride level and chloride diffusion coefficient in concrete: 10-year results in marine site. Mater Struct 47:1501–1511. doi:10.1617/s11527-013-0131-4
22. Atkins CP, Scantlebury JD, Nedwell PJ, Blatch SP (1996) Monitoring chloride concentrations in hardened cement pastes using ion selective electrodes. Cem Concr Res 26:319–324. doi:10.1016/0008-8846(95)00218-9
23. Climent-Llorca Miguel A, Viqueira-Pérez E, López-Atalaya MM (1996) Embeddable Ag/AgCl sensors for in situ monitoring chloride contents in concrete. Cem Concr Res 26:1157–1161. doi:10.1016/0008-8846(96)00104-4
24. Elsener B, Zimmermann L, Böhni H (2003) Non destructive determination of the free chloride content in cement based materials. Mater Corros 54:440–446. doi:10.1002/maco.200390095
25. Montemor MF, Alves JH, Simões AM, Fernandes JCS, Lourenço Z, Costa AJS, Appleton AJ, Ferreira MGS (2006) Multiprobe chloride sensor for in situ monitoring of reinforced concrete structures. Cem Concr Compos 28:233–236. doi:10.1016/j.cemconcomp.2006.01.005
26. Hugenschmidt J, Loser R (2007) Detection of chlorides and moisture in concrete structures with ground penetrating radar. Mater Struct 41:785–792. doi:10.1617/s11527-007-9282-5
27. Angst U, Elsener B, Larsen CK, Vennesland Ø (2010) Potentiometric determination of the chloride ion activity in cement based materials. J Appl Electrochem 40:561–573. doi:10.1007/s10800-009-0029-6
28. Garcia V, François R, Carcasses M, Gegout P (2013) Potential measurement to determine the chloride threshold concentration that initiates corrosion of reinforcing steel bar in slag concretes. Mater Struct 47:1483–1499. doi:10.1617/s11527-013-0130-5
29. Koryta J (1972) Theory and applications of ion-selective electrodes. Anal Chim Acta 61:329–411. doi:10.1016/S0003-2670(01)95071-8
30. Morf WE (1981) The principles of ion-selective electrodes and of membrane transport. Elsevier, New York
31. Koryta J, Stulik K (1983) Ion-selective electrodes, 2nd edn. Cambridge University Press, Cambridge
32. Janata J (1989) Principles of chemical sensors, 2nd edn. Plenum Press, New York
33. Lindner E, Umezawa Y (2008) Performance evaluation criteria for preparation and measurement of macro- and microfabricated ion-selective electrodes (IUPAC technical report). Pure Appl Chem. doi:10.1351/pac200880010085
34. Hidalgo A, Vera GD, Climent MA, Andrade C, Alonso C (2001) Measurements of chloride activity coefficients in real Portland cement paste pore solutions. J Am Ceram Soc 84:3008–3012. doi:10.1111/j.1151-2916.2001.tb01128.x
35. Atkins CP, Carter MA, Scantlebury JD (2001) Sources of error in using silver/silver chloride electrodes to monitor chloride activity in concrete. Cem Concr Res 31:1207–1211. doi:10.1016/S0008-8846(01)00544-0
36. de Vera G, Climent MA, Antón C, Hidalgo A, Andrade C (2010) Determination of the selectivity coefficient of a chloride ion selective electrode in alkaline media simulating the cement paste pore solution. J Electroanal Chem 639:43–49. doi:10.1016/j.jelechem.2009.11.010
37. Climent MA, Antón C, de Vera G, Hidalgo A, Andrade C (2011) The interference of OH^- ions in the potentiometric determination of free Cl^- in cement paste pore solution. In: Proceedings of the international RILEM conference on advances in construction materials through science and engineering, Hong Kong, China. RILEM Publications, Bagneux
38. Haynes WM (2013–2014) Handbook of chemistry & physics, 94th edn. CRC Press, Boca Raton
39. Morf WE, Kahr G, Simon W (1974) Theoretical treatment of the selectivity and detection limit of silver compound membrane electrodes. Anal Chem 46(11):1538–1543. doi:10.1021/ac60347a014
40. Bard AJ, Faulkner LR (2001) Electrochemical methods: fundamentals and applications, 2nd edn. Wiley, New York
41. Klasens HA, Goossen J (1977) The iodide interference with silver chloride electrodes. Anal Chim Acta 88(1):41–46
42. Shreir L (1994) Corrosion control. In: Shreir LL, Jarman RA, Burstein GT (eds) Corrosion, 3rd edn. Butterworth-Heinemann, Oxford
43. de Vera G, Hidalgo A, Climent MA, Andrade C, Alonso C (2000) Chloride-ion activities in simplified synthetic concrete pore solutions: the effect of the accompanying ions. J Am Ceram Soc 83(3):640–644. doi:10.1111/j.1151-2916.2000.tb01245.x
44. Chen W (2006) Hydration of slag cement—theory, modeling and application. PhD thesis, Enschede, University of Twente
45. Švegl F, Kalcher K, Kolar M (2006) In-situ detection of chlorides in capillary water of cementitious materials with potentiometric sensors. Eighth CANMET/ACI International Conference on Recent Advances in Concrete Technology. doi:10.14359/15913
46. Crowell RA, Lian R, Shkrob IA, Bartels DM, Chen X, Bradforth SE (2004) Ultrafast dynamics for electron photodetachment from aqueous hydroxide. J Chem Phys. doi:10.1063/1.1739213
47. Rhodes RK, Buck RP (1980) Competitive ion-exchange evaluation of the bromide interference on anodized silver/silver chloride electrodes. Anal Chim Acta 113:67–78. doi:10.1016/S0003-2670(01)85115-1
48. Hulanicki A, Lewenstam A (1977) Interpretation of selectivity coefficients of solid-state ion-selective electrodes by means of the diffusion-layer model. Talanta 24:171–175. doi:10.1016/0039-9140(77)80084-2
49. Hausmann DA (1967) Corrosion of steel in concrete. How does it occur? J Mater Prot 6:19–23
50. Dickson AG, Goyet C (1994) Handbook of methods for the analysis of the various parameters of the carbon dioxide system in sea water. US Department of Energy, Washington
51. Gollop RS, Taylor HFW (1996) Microstructural and microanalytical studies of sulfate attack: IV. Reactions of a slag cement paste with sodium and magnesium sulfate solutions. Cem Concr Res 26:1013–1028. doi:10.1016/0008-8846(96)00089-0

52. Taylor HFW (1997) Cement chemistry, 2nd edn. Thomas Telford, London
53. Lothenbach B, Le Saout G, Ben Haha M, Figi R, Wieland E (2012) Hydration of a low-alkali CEM III/B–SiO_2 cement (LAC). Cem Concr Res 42:410–423. doi:10.1016/j.cemconres.2011.11.008
54. Gruskovnjak A, Lothenbach B, Winnefeld F, Figi R, Ko SC, Adler M, Mäder U (2008) Hydration mechanisms of super sulphated slag cement. Cem Concr Res 38:983–992. doi:10.1016/j.cemconres.2008.03.004
55. Seguí-Femenias Y, Angst U, Elsener B (2015) Monitoring chloride concentrations in concrete by means of Ag/AgCl ion-selective electrodes. In: ICCRRR—international conference on concrete repair, rehabilitation and retrofitting (accepted), Leipzig
56. Biedermann G, Sillén LG (1960) Studies on the hydrolysis of metal ions. Part 30. A critical survey of the solubility equilibria of Ag_2O. Acta Chem Scand 14:717–725. doi:10.3891/acta.chem.scand.14-0717
57. Pargar F, Koleva DA, Koenders EAB, Breugel KV (2014) The importance of chloride sensors stability in monitoring ageing phenomena in concrete structures: Ag/AgCl electrodes performance in simulated pore-water environment. In: AMS 14: 1st ageing of materials & structures conference, Delft
58. Licht S (1988) Aqueous solubilities, solubility products and standard oxidation–reduction potentials of the metal sulfide. J Electrochem Soc 135:2971–2975. doi:10.1149/1.2095471
59. Nicholson K (1993) Geothermal fluids—chemistry and exploration techniques. Springer, Berlin
60. Angst U, Vennesland Ø, Myrdal R (2008) Diffusion potentials as source of error in electrochemical measurements in concrete. Mater Struct 42:365–375. doi:10.1617/s11527-008-9387-5
61. Kaland F, Hakli U, Ruoff P (1986) Use of an ion-selective electrode for determination of free chloride ions in water-based drilling fluids. SPE Drill Eng 1:365–368. doi:10.2118/15147-PA
62. Parkhurst DL, Appelo CAJ (2013) Description of input and examples for PHREEQC version 3—a computer program for speciation, batch-reaction, one-dimensional transport, and inverse geochemical calculations. U.S. Geological Survey Techniques and Methods, Denver
63. Moody GJ, Rigdon LP, Meisenheimerand RG, Frazer JW (1981) Selectivity parameters of homogeneous solid-state chloride ion-selective electrodes and the surface morphology of silver chloride-silver sulphide discs under simulated interference conditions. Analyst 106:547–556. doi:10.1039/AN9810600547
64. Hulanicki A, Lewenstam A (1982) Variability of selectivity coefficients of solid-state ion-selective electrodes. Talanta 29:671–674. doi:10.1016/0039-9140(82)80072-6
65. Radu A, Peper S, Bakker E, Diamond D (2007) Guidelines for improving the lower detection limit of ion-selective electrodes: a systematic approach. Electroanalysis 19:144–154. doi:10.1002/elan.200603741
66. Reinsfelder RE, Schultz FA (1973) Anion selectivity studies on liquid membrane electrodes. Anal Chim Acta 65:425–435. doi:10.1016/S0003-2670(01)82509-5

PAPER II

Y. Seguí Femenias, U. Angst, B. Elsener (2015)

Monitoring chloride concentrations in concrete by means of Ag/AgCl ion-selective electrodes

in *ICCRRR - International Conference on Concrete Repair, Rehabilitation and Retrofitting*, Leipzig

Monitoring chloride concentrations in concrete by means of Ag/AgCl ion-selective electrodes

Yurena Seguí Femenias, Ueli Angst & Bernhard Elsener
ETH Zürich, Institute for Building Materials (IfB), Stefano-Franscini-Platz 3, 8093 Zurich, Switzerland

ABSTRACT: This work investigates the applicability of Ag/AgCl ion-selective electrodes for the non-destructive measurement of chloride concentrations in concrete.

Sensitivity to potential interfering ions and stability of the Ag/AgCl membrane in neutral and alkaline solutions are presented. The results indicate negligible interference by fluoride, sulfate, and hydroxide, but considerable interference by bromide and sulfide. In completely chloride-free alkaline solutions, the ion-selective electrodes are not stable over time, but they become again functional as soon as chlorides arrive at the sensor.

It is concluded that the studied ion-selective electrodes are applicable for monitoring the free chloride concentration in the pore solution of concrete structures exposed to chloride-bearing environments. The applicability in concrete containing blast furnace slag or other sulfide sources is however questioned.

1 INTRODUCTION

In non-carbonated concrete with low or no presence of chlorides, the steel reinforcement is passive due to the alkaline environment provided by the hydration of cement. The passive layer protects the steel from corrosion. However, this passive layer can be destroyed when a certain concentration of chlorides reaches the reinforcement (chloride-induced corrosion). Chloride-induced corrosion is the principal cause of premature failure in reinforced concrete structures worldwide (Elsener et al., 2004).

Common methods for determining chloride content in concrete are based on destructive sampling and do thus not allow continuous information at identical locations over time (Elsener et al., 2003, Atkins et al., 1996); therefore, a non-destructive technique that permits continuous measurement of the chloride content is of high interest. For this purpose, the use of Ag/AgCl ion-selective electrodes (ISEs) is a promising solution. The Ag/AgCl exhibit a Nernstian electrochemical potential as a function of the chloride ion activity in solution (Koryta, 1972, Janata, 1989, Bard et al., 2002); thus, for concrete, the Ag/AgCl ISE allows measuring the free chloride content in the pore solution. However, ISEs are also sensitive to other species that can form compounds normally of lower solubility with the constituent ion (Ag^+ for the Ag/AgCl ISE).

The sensitivity in environments containing interfering species and the stability at high pH of Ag/AgCl ISEs are thus two crucial factors regarding the applicability of the Ag/AgCl ISEs in concrete. This paper investigates the stability of the Ag/AgCl ISE at high pH values and the interference arising from the presence of bromide, sulfate, sulfide, fluoride, and hydroxide. The use of the Ag/AgCl ISE in concrete is discussed.

2 THEORETICAL BACKGROUND

2.1 *The silver/silver chloride ion-selective electrode*

The Ag/AgCl ISE used in this work consists of silver covered by a layer of silver chloride. The Ag/AgCl ISE used belongs to the category of ion selective electrodes with solid ion exchangers (Koryta, 1972).

The potential E of the Ag/AgCl ISE is given by the Nernst law as a function of the chloride ion activity in solution (Angst et al., 2009). However, the Ag/AgCl ISE responds to the primary ion (chloride ion) with a Nernstian behavior only above a minimum concentration of it (i.e. detection limit) (Koryta and Stulik, 1983, Morf et al., 1974). Furthermore, the ISE is also sensitive to other species that can form precipitates of lower solubility with the constituent ionic specie (Koryta and Stulik, 1983, Atkins et al., 2001). This interference is traditionally considered with the selectivity coefficients, $K^{pot}_{Cl-,Y}$ (with Y standing for the interfering specie) included in the Nikolsky-Eisenman equation (Koryta and Stulik, 1983, Janata, 1989):

$$E = E^0_{Ag/AgCl} - \frac{RT}{F}\ln\left(a_{Cl^-} + \sum\left(K^{pot}_{Cl^-,Y}\cdot a_Y^{-1/z_Y}\right)\right) \quad (1)$$

where R is the gas constant, T the absolute temperature, F the Faraday constant, a_{Cl^-} the activity of the chloride ion, $E^0_{Ag/AgCl}$ the standard potential of the silver/silver chloride electrode (Haynes, 2013-2014), a_Y is the activity of the interfering ionic specie and z_Y its charge.

2.2 *Influencing parameters*

The potential E of the Ag/AgCl ISE depends on the chloride activity, the temperature and the sensitivity to other species.

- Chloride activity.

In concentrated solutions, ions deviate from ideality as a consequence of the high ionic strength. This phenomenon is taken into account by the use of the ionic activity a_X, which is related to the concentration c_X of a specie X by the activity coefficient γ_X (Haynes, 2013-2014):

$$a_X = \gamma_X \cdot c_X / c_0 \quad (2)$$

where c_0 is the standard state composition (generally chosen as 1 mol·L^{-1} (Haynes, 2013-2014)).

- Interfering species

Many silver salts have very low solubilities (Haynes, 2013-2014); therefore, in their presence, the ISE is likely to be affected . The AgCl membrane responds mainly to Cl^-, Br^-, I^-, OH^-, and S^{2-} (Angst et al., 2009, Janata, 1989, Atkins et al., 2001, Klasens and Goossen, 1977). According to equation (1), the potential of the ISE will exhibit a Nernstian behavior when the following relation is satisfied (Angst et al., 2009):

$$a_{Cl^-} >> \sum\left(K^{pot}_{Cl^-,Y}\cdot a_Y^{-1/z_Y}\right) \quad (3)$$

- Temperature

The effect of temperature has in detail been addressed in other studies and data is available to make corrections in this regard (Angst et al., 2009, Shreir, 1994).

3 EXPERIMENTAL

3.1 *Electrodes, instruments and materials*

3.1.1 Silver/silver chloride ion-selective electrode

The used Ag/AgCl ISE is an industrial ISE consisting of a silver wire coated with silver chloride deposited by anodizing. The tip of the ISE was additionally dipped in a melt of AgCl in order to achieve a more stable membrane (Angst et al., 2009, Elsener et al., 2003).

3.1.2 Potentiometric measurements

The potential of the ISEs was measured versus the silver/silver chloride/saturated potassium chloride (Ag/AgCl/sat. KCl) reference electrode (+0.197 V versus SHE).

The measurements were performed with a PGSTAT 30 Autolab potentiostat/galvanostat (Metrohm Autolab, Utrecht, the Netherlands) with high input impedance (> 100 GΩ) connected to a Windows PC for data acquisition. The program for data acquisition was Autolab Nova v.1.10. All the experiments were carried out at room temperature (20-21 °C).

3.2 *Methods*

3.2.1 Calibration in solution

The Ag/AgCl ISEs were calibrated in neutral and alkaline solutions that contained known concentrations of sodium chloride ranging from 0.002 to 4 mol·L^{-1}.

It should be noted that when the reference electrode is immersed in the measured solution, a liquid junction potential $E_{junction}$ (Bard et al., 2002) establishes at its interface and adds arithmetically to the measured potential. In this work, liquid junction potentials $E_{junction}$ were calculated according to the Henderson equation (Bard et al., 2002) to correct the measured potential $E_{measured}$. For this calculation, it is considered that the KCl concentration is 4.16 mol·L^{-1} when saturated in water at room temperature (Haynes, 2013-2014). The used solutions and the liquid junction potentials calculated are presented in Table 1.

Table 1. Calibration solutions and corresponding liquid junction potentials for the Ag/AgCl/sat. KCl.

NaCl concentration (mol·L^{-1})	NaOH concentration (mol·L^{-1})	$E_{junction}$ at 20°C (mV)
0.002	-	-3.7
0.010	-	-2.9
0.100	0.010	-1.2
0.100	0.100	0.7
0.100	1.000	8.4
0.500	-	0.1
0.500	0.010	0.3
0.500	0.100	1.5
0.500	1.000	8.4
1.000	-	1.2
1.500	-	1.9
4.000	-	4.2

The chloride activity was calculated according to equation (2). Mean activity coefficients ($\gamma_{NaCl\pm}$) for sodium chloride in neutral solution were obtained from the data provided by Haynes *et al.* (Haynes,

2013-2014). The activity coefficients of the chloride ion (γ_{Cl^-}) in the solutions containing sodium hydroxide were interpolated from the data given by Hidalgo *et al.* (Vera et al., 2000). In this case, the effect of the accompanying ions was neglected and activity coefficients were calculated considering the total hydroxide concentration. The data are provided in table 2.

The calibration curves were obtained by linear regression analysis:

$$E = E_{\text{measured}} - E_{junction} = m \cdot \log a_{Cl^-} + b \qquad (4)$$

For the case of pH neutral solutions, it was assumed that $\gamma_{NaCl\pm} \approx \gamma_{Cl^-}$ (Angst et al., 2009).

Table 2. Mean activity coefficients $\gamma_{NaCl\pm}$ and activity coefficients of the chloride ion γ_{Cl^-} used in this work. Values of pH other than 7 were obtained by addition of sodium hydroxide. The values of $\gamma_{NaCl\pm}$ are taken or interpolated from (Haynes, 2013-2014). The values of γ_{Cl^-} are interpolated from (Vera et al., 2000).

	Value	NaCl concentration ($mol \cdot L^{-1}$)	pH
$\gamma_{NaCl\pm}$	0.952	0.002	7
$\gamma_{NaCl\pm}$	0.903	0.01	7
$\gamma_{NaCl\pm}$	0.770	0.1	7
$\gamma_{NaCl\pm}$	0.681	0.5	7
$\gamma_{NaCl\pm}$	0657	1	7
$\gamma_{NaCl\pm}$	0.663	1.5	7
$\gamma_{NaCl\pm}$	0.668	2	7
$\gamma_{NaCl\pm}$	0.815	4	7
$\gamma_{NaCl\pm}$	0.874	5	7
γ_{Cl^-}	0.740	0.1	≈12
γ_{Cl^-}	0.727	0.1	≈13
γ_{Cl^-}	0.603	0.1	≈14
γ_{Cl^-}	0.642	0.5	≈12
γ_{Cl^-}	0.637	0.5	≈13
γ_{Cl^-}	0.585	0.5	≈14

3.2.2 Sensitivity to interfering species

The effect of the possible interfering species was investigated for the case of hydroxide, bromide, sulfate, fluoride and sulfide. These were considered the main species that could cause interference to the Ag/AgCl ISEs response in concrete pore solution and seawater exposure (Elsener et al., 2003, Atkins et al., 2001, Chen, 2006, Švegl et al., 2006).

The Ag/AgCl ISEs were first immersed in NaCl solutions. The concentration of the interfering specie was increased stepwise when the potential became stable over time (few minutes – for the addition of hydroxide, sulfate, and fluoride – or few days – for the addition of bromide, and sulfide). For the study of the fluoride, sulfate and bromide interference, the experiments were started in 0.01 $mol \cdot L^{-1}$ NaCl solutions, and the concentration of interfering specie was increased up to 0.04 $mol \cdot L^{-1}$ The addition of bromide caused the Ag/AgCl ISE potential to significantly decrease, and the experiments were repeated with the sensors immersed in 0.1 $mol \cdot L^{-1}$ NaCl solution.

The silver sulfide has an especially low solubility (Haynes, 2013-2014). It was thus expected that the Ag/AgCl ISE potential would be affected in presence of already little sulfide with respect to chloride, and the experiments were done with the sensors immersed in 0.1 $mol \cdot L^{-1}$ and 1 $mol \cdot L^{-1}$ NaCl solutions.

The use of Ag/AgCl ISE in concrete seems to be a promising solution to monitor chloride changes and some studies have already been done (Angst et al., 2009, Elsener et al., 2003, Atkins et al., 1996). For this reason, the hydroxide inference was treated separately and in more detail. The experiments were always started with 0.1 $mol \cdot L^{-1}$ NaOH solutions to simulate the alkalinity of the concrete pore solution. It has been reported that light may have an effect on the kinetics reactions of hydroxide (Crowell et al., 2004). The experiments were thus carried out avoiding exposure to daylight to simulate the concrete pore solution.

The ISEs were immersed in the solutions containing increasing amounts of the possible interfering species for a total of two months. The solutions used and the concentration ranges of interfering specie are given in Table 3.

Table 3. Solutions used for the study of the sensitivity to interfering species of the Ag/AgCl ISE.

NaCl concentration ($mol \cdot L^{-1}$)	Concentration range of interfering specie ($mol \cdot L^{-1}$)	Interfering specie
0.05	0.1-1.7	OH^-
0.1	0.1-1.6	OH^-
0.2	0.1-1.5	OH^-
0.3	0.1-1.6	OH^-
0.5	0.1-1.6	OH^-
0.01	0-0.4	Br^-
0.1	0-0.3	Br^-
0.01	0-0.04	F^-
0.01	0-0.04	SO_4^{2-}
0.1	0-0.01	S^{2-}
1	0-0.008	S^{2-}

The measured potential, E_{measured}, was corrected according to equation (4) with regard to the liquid junction potential, E_{junction}.

Once the experiments were finished, the Ag/AgCl ISEs that were immersed in the solutions containing bromide, fluoride, sulfate, and sulfide were returned to the original NaCl solutions, i.e. without the interfering specie present. The potential was measured again after one month of immersion in the interfering ion-free solution.

3.2.3 Long-term stability at high pH

The stability of the Ag/AgCl ISEs at high pH in the absence of chloride was investigated over a period of 60 days. Erlenmeyer flasks were filled to the very top with NaOH solutions and closed with a rubber

tween 140 mV and 120 mV vs. $Ag/AgCl_{sat}$ after 60 days of immersion.

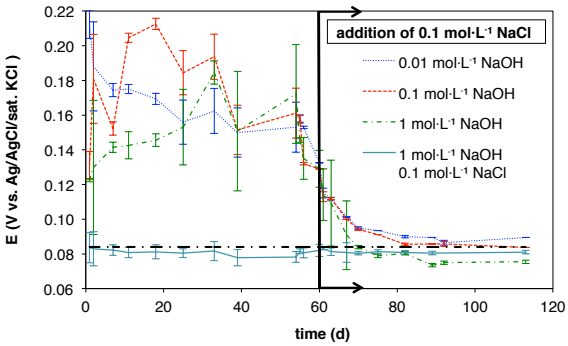

Figure 3. Ag/AgCl ISE mean potential values (from ten individual readings) as a function of time. The dot dash thick line represents the potential for a solution 0.1 mol·L^{-1} NaCl obtained from the calibration curve (section 4.1). The error bars indicate the standard deviation from the individual readings

In alkaline environments in absence or low content of chlorides, the AgCl precipitate undergoes the following reaction (Biedermann and Sillén, 1960):

$$AgCl_{(s)} + OH^- \rightleftarrows \tfrac{1}{2}\, Ag_2O_{(s)} + \tfrac{1}{2}\, H_2O + Cl^- \qquad (5)$$

The potential shift observed to more negative values is probably due to the continuous formation of Ag_2O; potentials of ~144 mV vs. $Ag/AgCl_{sat}$ at room temperature and pH ≈ 14 are reported in the literature if the ISE membrane is considered to be completely covered with Ag_2O (Angst et al., 2009, Pargar et al., 2014, Biedermann and Sillén, 1960).

It is also worth mentioning that the color of the solutions turned brown-black with time, being more pronounced for the solutions that contained higher NaOH concentrations. This color change may also be related to the transformation of AgCl into Ag_2O. This was already observed by Angst *et al.* (Angst et al., 2009).

The possible formation of Ag_2O (equation (5)) could also explain the oscillations in the Ag/AgCl ISE potential shown in figure 2, especially at the lowest chloride concentrations.

It was finally observed that the ISEs recover fast as soon as they come into contact with chloride (right part in Figure 3). The temporal scatter and instability are also considerably reduced. Thus, the possible formation of silver oxide is reversible, as already reported by other authors (Angst et al., 2009, Pargar et al., 2014). The adherence of the Ag_2O to the ISE surface (questioned by Angst *et al.* (Angst et al., 2009)) could however be an issue for the long-term stability because of the reversibility of the AgCl formation. This aspect should deserve further attention.

4.2.1 Exposure in environments containing interfering species

Figure 4 shows the potential *E* of the Ag/AgCl ISEs immersed in 0.01 mol·L^{-1} NaCl (bromide, fluoride and sulfate) and in 0.1 mol·L^{-1} NaCl (bromide) as a function of the logarithm of the concentration of the possible interfering specie (bromide, fluoride, and sulfate).

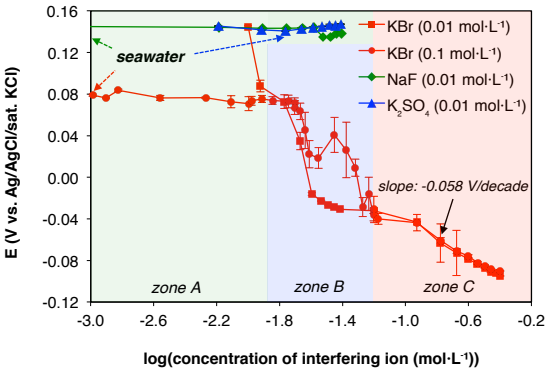

Figure 4. Ag/AgCl ISE mean potential values (from ten individual readings) as a function of the logarithm of the interfering specie in 0.01 mol·L^{-1} NaCl solution (for bromide, fluoride and sulfate) and 0.1 mol·L^{-1} NaCl solution (bromide). The error bars indicate the standard deviation from the individual readings. The zones defined in the graph (zone A, zone B, zone C) schematically represent the effect of the different interfering species on the Ag/AgCl ISE response (compare text).

Regarding the bromide interference, it can be seen that for very small bromide concentrations, the Ag/AgCl ISEs exhibit an overall stable potential independent on the bromide content (figure 4). However, small amounts of bromide exert a large effect on the response of the Ag/AgCl ISE; the potential shifts to more negative values and the standard deviation increases, reaching values up to 25 mV. For bromide concentrations higher than 0.05 mol·L^{-1}, the potential *E* linearly depends on the bromide concentration for both chloride concentrations tested.

When returned back to the original NaCl solutions, the ISEs did not regain the initial potential values. It has also to be noted that the immersed tip of the ISEs turned green after the bromide addition.

Concerning the fluoride and sulfate interference, up to a fluoride concentration of 0.02 mol·L^{-1}, the ISE potential can be considered to be unaffected. At fluoride concentrations higher than 0.025 mol·L^{-1}, however, a small decrease in the potential is observed. For sulfate, the potential remains almost unaffected to – at least – a concentration of 0.04 mol·L^{-1}. Moreover, when returned back to the original NaCl solution (fluoride- and sulfate-free), the ISEs exhibited potentials equal to those initially registered

plug through which the ISEs were inserted via drilled holes. The flasks were additionally sealed with silicon grease to avoid evaporation and/or carbonation of the solution.

After 60 days of immersion, 0.1 mol·L^{-1} NaCl was added to the chloride-free alkaline solutions. The solutions used for the long-term stability experiments are given in table 4.

Table 4. Solutions used for the study of the long-term stability at high pH of the Ag/AgCl ISE.

NaCl initial concentration (mol·L^{-1})	NaOH concentration (mol·L^{-1})	NaCl addition after 60 days (mol·L^{-1})
0	0.01 (pH ≈ 12)	0.1mol·L^{-1}
0	0.1 (pH ≈ 13)	0.1mol·L^{-1}
0	1 (pH ≈ 14)	0.1mol·L^{-1}
0.1	0.01 (pH ≈ 14)	-

The measured potential, $E_{measured}$, was corrected according to equation (4) with regard to the liquid junction potential, $E_{junction}$.

4 RESULTS AND DISCUSSION

4.1 *Calibration in solution*

The calibration curve according to equation (4) is shown in figure 1.

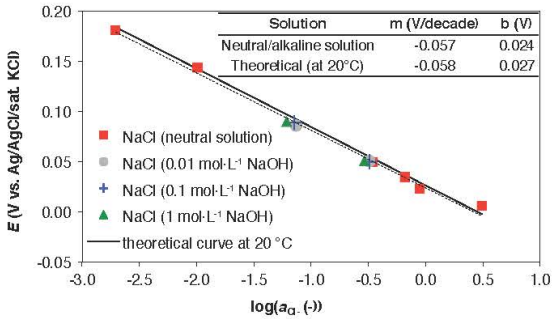

Figure 1. Calibration curve of the Ag/AgCl ISE in neutral and alkaline solutions. The mean values were obtained form ten individual readings. The standard deviation is always less than 2 mV, thus, smaller than the symbols. The parameters of the linear regression analysis are also given with the theoretical values (considering constant room temperature of 20°C (Angst et al., 2009, Shreir, 1994)).

The Ag/AgCl ISEs exhibited a Nernstian behavior with slope of –57 mV (figure 1), in good agreement with the values reported in previous works (Elsener et al., 2003, Angst et al., 2009). The ISE exhibits a Nernstian behavior in the interference-free solutions for the whole range of chloride concentrations tested; it can be then concluded that the detection limit of the chloride ion in aqueous neutral solution is lower than 0.002 mol·L^{-1}, in agreement with the results reported by Angst *et al* (Angst et al., 2009). Furthermore, the standard deviation of the ten individual potential readings is always below 2 mV.

4.2 *Applicability of Ag/AgCl ISEs in concrete*

Figure 2 shows the potential E of the Ag/AgCl ISEs immersed in alkaline solutions containing sodium chloride as a function of the logarithm of the hydroxide concentration.

From figure 2, it can be seen that the potential E of the Ag/AgCl ISEs is overall plateau for the whole range of concentrations tested. The range (difference between the largest and smallest observed potentials) is 10 mV and it is found for the ISEs immersed in the solution containing 0.05 mol·L^{-1} NaCl.

When it comes to chloride-induced corrosion, a concentration ratio chloride to hydroxide c_{Cl^-}/c_{OH^-} =0.6 is sometimes considered as threshold value for corrosion initiation (Hausmann, 1967). As it is apparent from figure 2, no interference is expected even for clearly lower ratios c_{Cl^-}/c_{OH^-} . Thus, the Ag/AgCl will permit to detect chloride concentrations much below levels considered critical for corrosion initiation even at high pH.

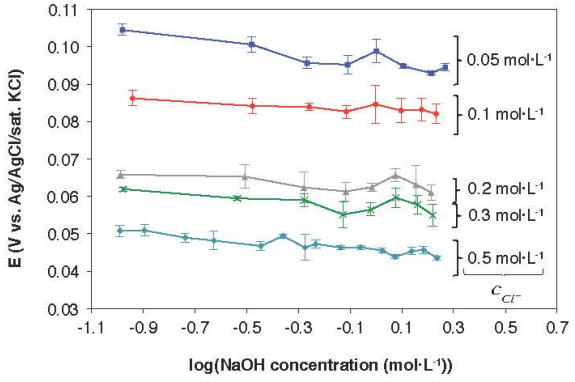

Figure 2. Ag/AgCl ISE mean potential values (from five individual readings) as a function of the logarithm of the NaOH concentration. The error bars indicate the standard deviation (≤ 5 mV) from the individual readings.

Nonetheless, the instability of the Ag/AgCl ISE at high pH with no or low amount of chlorides has also been questioned (Elsener et al., 2003, Angst et al., 2009, Švegl et al., 2006). Figure 3 shows the potential E of as a function of time, before and after addition of chloride (at t = 60 days) for the chloride-free solutions.

In absence of chloride, the potential of the Ag/AgCl ISEs shows high scatter between the individual sensors (figure 3). For the Ag/AgCl ISEs immersed in chloride-free alkaline solutions (figure 3), the measured potential values were comprised be-

in the absence of the interfering specie within a few minutes.

To illustrate the effect of the interfering species on the ISE response, figure 4 is schematically divided in three different zones (zone A, zone B, and zone C).

In zone A (figure 4), the Ag/AgCl ISE behaves as an ideal chloride sensor; it exhibits a stable potential independent of the interfering specie (Angst et al., 2009, Koryta, 1972, Rhodes and Buck, 1980). This is the case for fluoride and sulfate (for the whole range of concentrations tested) and for very low concentrations of bromide (plateau part). It is in this range where the Ag/AgCl ISE is suitable for field measurements without interference. The effect of the ions in solution on the chloride activity should however be taken into account (compare Figure 1).

When the concentration of the interfering specie increases (zone B in figure 4), the response of the ISE is altered and it shows a potential determined by the simultaneous action of the primary (chloride) and interfering ion. The interference is due to the replacement of the chloride by the interfering specie on the surface of the ISE (Rhodes and Buck, 1980, Koryta, 1972). This phenomenon can be clearly seen for the case of bromide: the significant potential decrease and the high standard deviation are an indication of the above-mentioned surface coverage process. The color change of the tip of the ISEs also evidences the surface coverage with silver bromide (green).

At sufficiently high concentrations of interfering specie, the ISE surface becomes totally covered by the salt formed between the silver and the interfering specie and acts as an ISE sensitive to this specie (Rhodes and Buck, 1980, Hulanicki and Lewenstam, 1977) (zone C in figure 4). This can be observed for the case of bromide. The ISEs virtually exhibit Nernstian slope after a certain threshold of concentration.

In addition, once the interfering specie is removed from the solution, the Ag/AgCl ISE should ideally behave again as a pure chloride sensor (zone A in figure 10). For the bromide interference, this was reported by Atkins *et al.* (Atkins et al., 2001). However, the ISEs tested in this work did not completely recover. In this study, the ISEs were immersed in the solutions containing bromide for about 2 months, whereas Atkins *et al.* immersed them for only 15 minutes (Atkins et al., 2001). It is believed that the disagreement with respect to the results reported by Atkins *et al.* (Atkins et al., 2001) is due to the kinetics of the transformation of AgBr back into AgCl. In fact, Rhodes *et al.* (Rhodes and Buck, 1980) reported that the kinetics of the transformation of the AgBr back into AgCl is at least 200 times slower than the conversion of AgCl into AgBr. Thus, prolonged exposure to the interfering specie may significantly impair the functionality of Ag/AgCl ISEs.

The response of the Ag/AgCl ISE will be on one of the three zones of figure 4 depending on how severe is the interference and the experimental conditions (Koryta, 1972, Lindner and Umezawa, 2008, Hulanicki and Lewenstam, 1977, Rhodes and Buck, 1980). The severity of the interference is commonly taken into account with the selectivity coefficients (see equation (1)) (Lindner and Umezawa, 2008, Janata, 1989, Koryta and Stulik, 1983, Morf et al., 1974, Morf, 1981). The theoretical models for estimating selectivity coefficients are traditionally based on the assumption that thermodynamic equilibrium is established and the kinetics of the reactions are neglected. However, it is believed that both thermodynamics and kinetics contribute to the selectivity of ion-selective electrodes. This has already been suggested by other authors (Hulanicki and Lewenstam, 1982, Reinsfelder and Schultz, 1973).

Therefore, it appears that the theoretical models for predicting the Ag/AgCl ISE response in presence of interfering ions are not suitable for mid to long-term exposure. In this work, the exposure time of the ISE to the possible interfering species was two months. Although this is clearly longer than in other laboratory studies, field exposure times will be even far longer. Currently, we do not have any data indicating whether exposure times on the order of a few months (this work) are sufficiently long to represent field exposure times (in order of years or decades). Nevertheless, given the actual results, the following can be concluded.

If concrete structures are exposed to seawater, bromide, sulfate, and fluoride interference could be a potential error source. The bromide, sulfate and fluoride concentrations in seawater are approximately $8.7 \cdot 10^{-4}$, $2.9 \cdot 10^{-2}$ and $7 \cdot 10^{-5}$ $mol \cdot L^{-1}$ respectively (Dickson and Goyet, 1994). At those concentrations (shown with arrows in figure 4), no interference was found for the ISEs immersed in 0.1 $mol \cdot L^{-1}$ NaCl (bromide) and in 0.01 $mol \cdot L^{-1}$ NaCl (fluoride, sulfate). Furthermore, from figure 4, it becomes apparent (for the bromide interference) that the ISEs can tolerate slightly higher concentrations of interfering specie when the chloride content is also higher. The chloride concentration in seawater is around 0.5 $mol \cdot L^{-1}$ NaCl. Thus, no significant interference from bromide is expected for seawater exposure.

4.2.2 Blast furnace slag

The ions present in pore solution of hydrating slag cement are principally the same as those in Portland cement, with a remarkable amount of sulfide ion in the pore solution (Chen, 2006, Gruskovnjak et al., 2008, Lothenbach et al., 2012). The sulfide interference is thus discussed in this section.

Figure 5 shows the potential E of the Ag/AgCl ISEs immersed in 0.1 $mol \cdot L^{-1}$ and in 1 $mol \cdot L^{-1}$ NaCl

as a function of the logarithm of the sulfide concentration.

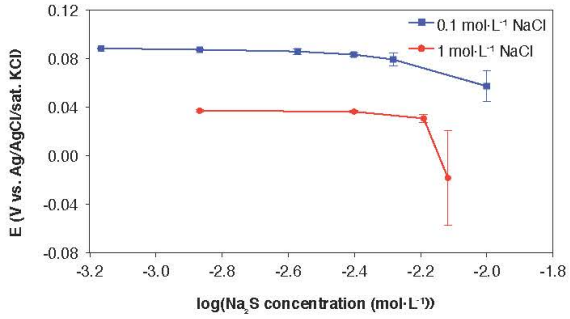

Figure 5. Ag/AgCl ISE mean potential values (from ten individual readings) as a function of the logarithm of the Na_2S concentration. The error bars indicate the standard deviation from the individual readings.

Sulfide interference is particularly severe. Relatively small amounts of sulfide cause high potential shifts (figure 5). For sulfide concentrations above 0.006 $mol \cdot L^{-1}$, the potential of the ISEs significantly decreased for both tested chloride concentrations ($\Delta E >$ 20 mV for 0.1 $mol \cdot L^{-1}$ NaCl and $\Delta E >$ 50 mV for 1 $mol \cdot L^{-1}$ NaCl). The standard deviation also increased significantly at this sulfide concentration.

When returned back to the original NaCl solutions, the ISEs did not regain the initial potential values. It has also to be noted that the immersed tip of the ISEs turned black and decreased its thickness after the addition of sulfide for both tested chloride concentrations. The significant potential decrease, the high standard, and the color change of the tip of the ISEs evidences the progressive surface coverage with silver sulfide (black), as it was similarly observed for the bromide interference.

Lothenbach *et al.* (Lothenbach et al., 2012) observed that the sulfide concentration in CEM III/B 42.5 L containing 59% of slag increases during the first month of reaction and remains rather constant thereafter; concentration of about 0.008 $mol \cdot L^{-1}$ of sulfide were found after one month of reaction. From figure 5, it can be seen that the ISE potential is strongly affected at those concentrations.

In super sulfated cements (SSC) (Lothenbach et al., 2012, Gruskovnjak et al., 2008), even higher sulfide concentrations are found. Gruskovnjak *et al.* (Gruskovnjak et al., 2008) reported concentrations of about 0.1 $mol \cdot L^{-1}$ of sulfide after approximately one month of reaction.

Therefore, it seems that the applicability of the Ag/AgCl ISE in concretes with mid-high amounts of slag will be impaired by the presence of sulfide. For the concretes containing mid-low amounts of blast furnace slag (CEM III/A), it could be possible that the amount of sulfide in solution remained low enough. However, the hydration of cement containing slag is not well understood (Gollop and Taylor, 1996, Taylor, 1997).

It is also important to notice that the ISEs probably tolerate higher concentrations of interfering specie when the chloride content is also higher (figure 4); thus, in absence of chloride, the ISEs potential shown in figure 5 is probably shifted to more negative values at lower sulfide concentrations. Moreover, it should be noted that part of the chlorides will be bound by some of the hydrated cement phases (Luping and Nilsson, 1993) and the ratio chloride/sulfide can be reduced as the amount of Portland cement is increased.

In addition, the decrease in the thickness of the Ag/AgCl ISEs after the sulfide addition questions the adherence of the potential formation silver sulfide on the ISE membrane and the later reaction back into AgCl. Thus, the sensors could be damaged before chloride arrival.

5 CONCLUSIONS

The Ag/AgCl ISEs measure the free chloride content in the concrete pore solution by exhibiting a Nernstian electrochemical potential as a function of the chloride ion activity.

The sensitivity of the Ag/AgCl ISE to interfering species has been carefully studied: while negligible interference was found for fluoride, sulfate, and hydroxide, the interference is relatively severe for bromide and sulfide. Nevertheless, due the high chloride/bromide concentration ratio in seawater, the interference of bromide is considered negligible for applications related to seawater exposure.

In chloride-free alkaline solutions, the ISEs were unstable over time – probably due to transformation reactions with the environment. Upon addition of chloride, however, the sensors responded again according the Nernst's law.

Based on the current experimental observations, it was concluded that the studied Ag/AgCl ISEs are feasible for practical monitoring of the chloride concentration in concrete exposed to chloride-containing environments. An exception is concrete with high contents of blast furnace slag, where the presence of sulfide could strongly disturb the measurements. For the case of low to mid content of blast furnace slag, further research regarding the kinetics and the hydration is needed to evaluate the severity of the sulfide interference. Another open question is the long-term time evolution. If the sulfide concentration decreases with time and embedded ISEs are able to recover, they may after years/decades be functional again when chlorides start arriving at depths corresponding to common reinforcement steel cover depths.

6 REFERENCES

European Standard EN 197-1. Cement—Part 1: Composition, specification and conformity criteria for common cements. European Committee for Standardization, Brussels, Belgium; 2000.

Angst, U., Elsener, B., Larsen, C. K. & Vennesland, Ø. (2009) Potentiometric determination of the chloride ion activity in cement based materials. J. Appl. Electrochem., 40, 561-573.

Atkins, C. P., M.A. Carter & Scantlebury, J. D. (2001) Sources of error in using silver/silver chloride electrodes to monitor chloride activity in concrete. Cem. Concr. Res., 31, 1207–1211.

Atkins, C. P., Scantlebury, J. D., Nedwell, P. J. & Blatch, S. P. (1996) Monitoring chloride concentrations in hardened cement pastes using ion selective electrodes. Cem. Concr. Res., 26, 319-324.

Bard, A. J., Stratmann, M., Gileadi, E., Urbakh, M., Calvo, E. J., Unwin, P. R., Frankel, G. S., Macdonald, D., Licht, S., Schäfer, H. J., Wilson, G. S., Rubinstein, I., Fujihira, M., Schmuki, P., Scholz, F., Pickett, C. J. & Rusling, J. F. (2002) Encyclopedia of electrochemistry. IN WILLEY (Ed.

Biedermann, G. & Sillén, L. G. (1960) Studies on the hydrolysis of metal ions. Part 30. A critical survey of the solubility equilibria of Ag_2 O. Acta Chem. Scan., 14, 717-725.

Chen, W. (2006) Hydration of slag cement – Theory, modeling and application (PhD thesis). Enschede, University of Twente, The Netherlands.

Crowell, R. A., Lian, R., Shkrob, I. A., Bartels, D. M., Chen, X. & Bradforth, S. E. (2004) Ultrafast dynamics for electron photodetachment from aqueous hydroxide. J. Chem. Phys., 120.

Dickson, A. G. & Goyet, C. (1994) Handbook of methods for the analysis of the various parameters of the carbon dioxide system in sea water, Washington.

Elsener, B., Bertolini, L., Pedeferri, P. & Polder, R. P. (2004) Corrosion of steel in concrete, Weinheim.

Elsener, B., Zimmermann, L. & Böhni, H. (2003) Non destructive determination of the free chloride content in cement based materials. Mater. Corros., 54, 440–446.

Gollop, R. S. & Taylor, H. F. W. (1996) Microstructural and microanalytical studies of sulfate attack: IV. Reactions of a slag cement paste with sodium and magnesium sulfate solutions. Cem. Concr. Res, 26, 1013–1028.

Gruskovnjak, A., Lothenbach, B., Winnefeld, F., Figi, R., Ko, S. C., Adler, M. & Mäder, U. (2008) Hydration mechanisms of super sulphated slag cement. Cem. Concr. Res, 38, 983-992.

Hausmann, D. A. (1967) Corrosion of steel in concrete. How does it occur? J. Mater. Prot., 6, 19-23.

Haynes, W. M. (2013-2014) Handbook of chemistry & physics, Boca Raton.

Hulanicki, A. & Lewenstam, A. (1977) Interpretation of selectivity coefficients of solid-state ion-selective electrodes by means of the diffusion-layer model. Talanta, 24, 171–175.

Hulanicki, A. & Lewenstam, A. (1982) Variability of selectivity coefficients of solid-state ion-selective electrodes. Talanta, 29, 671–674.

Janata, J. (1989) Principles of chemical sensors, New York, Plenum Press.

Klasens, H. A. & Goossen, J. (1977) The iodide interference with silver chloride electrodes. Anal. Chim. Acta , 88 (1), 41–46.

Koryta, J. (1972) Theory and applications of ion-selective electrodes. Anal. Chim. Acta, 61, 329–411.

Koryta, J. & Stulik, K. (1983) Ion-selective electrodes, Cambridge.

Lindner, E. & Umezawa, Y. (2008) Performance evaluation criteria for preparation and measurement of macro- and microfabricated ion-selective electrodes (IUPAC Technical Report). Pure Appl. Chem., 80.

Lothenbach, B., Le Saout, G., Ben Haha, M., Figi, R. & Wieland, E. (2012) Hydration of a low-alkali CEM III/B–SiO2 cement (LAC). Cem. Concr. Res, 42, 410-423.

Luping, T. & Nilsson, L. O. (1993) Chloride binding capacity and binding isotherms of OPC pastes and mortars. Cem. Concr. Res., 23, 247-253.

Morf, W. E. (1981) The principles of ion-selective electrodes and of membrane transport, New York.

Morf, W. E., Kahr, G. & Simon, W. (1974) Theoretical treatment of the selectivity and detection limit of silver compound membrane electrodes. Anal. Chem. , 46 (11), 1538–1543.

Pargar, F., Koleva, D. A., Koenders, E. A. B. & Breugel, K. V. (2014) The importance of chloride sensors stability in monitoring ageing phenomena in concrete structures: Ag/AgCl electrodes performance in simulated pore-water environment. AMS 14: Proceedings of the 1st Ageing of Materials & Structures Conference, Delft, The Netherlands.

Reinsfelder, R. E. & Schultz, F. A. (1973) Anion selectivity studies on liquid membrane electrodes. Anal Chim Acta, 65, 425–435.

Rhodes, R. K. & Buck, R. P. (1980) Competitive ion-exchange evaluation of the bromide interference on anodized silver/silver chloride electrodes. Anal. Chim. Acta, 113, 67–78.

Shreir, L. (1994) Corrosion control. IN SHREIR, L., JARMAN, R. A. & BURSTEIN, G. T. (Eds.) Corrosion. third ed. Oxford.

Švegl, F., Kalcher, K. & Kolar, M. (2006) In-situ detection of chlorides in capillary water of cementitious materials with potentiometric sensors. Eighth CANMET/ACI International Conference on Recent Advances in Concrete Technology, 235.

Taylor, H. F. W. (1997) Cement chemistry, London.

Vera, G. D., Hidalgo, A., Climent, M. A., Andrade, C. & Alonso, C. (2000) Chloride-ion activities in simplified synthetic concrete pore solutions: the effect of the accompanying ions. J. Am. Ceram. Soc., 83 [3], 640-644.

PAPER III

Y. Seguí Femenias, U. Angst, B. Elsener (2017)

Monitoring pH in corrosion engineering by means of thermally-produced iridium oxide electrodes

Materials and Corrosion, 1-13. doi: 10.1002/maco.201709715.

Received: 27 June 2017 | Accepted: 20 July 2017
DOI: 10.1002/maco.201709715

ARTICLE

Materials and Corrosion

Monitoring pH in corrosion engineering by means of thermally produced iridium oxide electrodes

Y. Seguí Femenias[1] | U. Angst[1] | B. Elsener[1,2]

[1] ETH Zürich, Institute for Building Materials (IfB), Stefano-Franscini-Platz 3, 8093 Zurich, Switzerland

[2] Department of Chemical and Geological Sciences, University of Cagliari, 09100 Monserrato (CA), Italy

Correspondence
B. Elsener, ETH Zürich, Institute for Building Materials (IfB), Stefano-Franscini-Platz 3, 8093 Zurich, Switzerland and Department of Chemical and Geological Sciences, University of Cagliari, 09100 Monserrato (CA), Italy.
Email: elsener@ethz.ch

Funding information
Schweizerischer Nationalfonds zur Förderung der Wissenschaftlichen Forschung

A pH sensor to be used in highly alkaline media under continuous long-term immersion conditions is crucial in various engineering applications. This work develops the production protocol and posterior conditioning of thermally oxidized iridium (IrO_x) electrodes to be used as potentiometric pH sensors embedded in highly alkaline environments such as concrete or cathodically protected steel in soil. The main investigated aspects for the desired applications are the potential-pH response, its reproducibility, accuracy, and oxygen dependency. The stability during long-term immersion is also studied in detail. The studied IrO_x electrodes responded to pH changes with slopes between −50 and −68 mV/pH unit, even after continuous immersion in alkaline solutions for almost 2 years. Additionally, the electrodes response did not show oxygen dependency. Our results highlight the importance of sufficient conditioning in alkaline media prior to use. When properly produced, conditioned, and pre-calibrated the electrodes reproducibly permit measuring the pH with a maximum error of 0.5 pH units over a range of at least pH 9–13.5. Preliminary results show that the studied electrodes are promising sensors for monitoring pH changes in concrete.

KEYWORDS
alkaline environment, cathodic protection in soil, long-term stability, reinforcing steel corrosion in concrete, thermally oxidized iridium pH sensor

1 | INTRODUCTION

The pH (negative logarithm of the H^+ activity) is one of the most important parameters in many fields, from life science (biological, environmental, medical) to engineering (civil, nuclear, energy).[1–6] Therefore, many different electrochemical and non-electrochemical techniques have been developed for measuring the pH.[7]

Applications in corrosion engineering require permanent long-term monitoring of pH (in the order of years) in highly alkaline media (pH up to 13.5). In these applications, long-term stability of the method is of outmost importance. On the other hand, as the processes leading to a change in pH are relatively slow, the requirements to sensor response time are far less strict than in analytical chemistry.

The most important corrosion engineering application for in situ long-term pH measurement is steel reinforced concrete, which is the most used construction material world-wide. In the highly alkaline pore solution of concrete (pH 12.5–13.5), steel is protected from corrosion by the formation of an oxide layer (passive film). Due to the reaction of alkaline components in the concrete pore solution with CO_2 from the atmosphere, a process called carbonation, the pH decreases to levels lower than 9[8,9] and

the steel reinforcement is depassivated. In presence of oxygen and humidity, corrosion of the reinforcement occurs, leading to loss of durability and finally structural deterioration.[8] Therefore, knowledge of the pH in the concrete is essential. The different methods tested and used for pH measurements in concrete are presented in a recent review.[10] From this review, it emerges that most of the available methods are destructive, time consuming, and do not allow continuous pH monitoring. Regarding the latter, fiber optic sensors were tested but showed serious limitations such as chemical instability at high pH, dye leaching, and short life span. Embedded potentiometric electrodes based on several metal oxides for measuring pH in concrete were also studied. Among them, iridium/iridium oxide electrodes (IrO_x) were the most promising.[11]

Iridium/iridium oxide electrodes have been reported to perform well in aqueous solutions over wide range of pH and temperature.[1,6,12–17] Preparation methods of IrO_x electrodes include electrochemical deposition,[12–14,18] sputtering deposition,[3] sol–gel processes,[15,16] and electrochemical[1,14] or thermal oxidation.[17,19,20] Table 1 collects the main features of iridium oxides electrodes reported in literature.

From Table 1, it emerges that most studies were performed in research works of analytical chemistry, thus in solutions with pH < 12 and with relatively short immersion times in the order of days; the longest immersion time was in fact 10 days.[1,17,19,20] The differences in potential-pH response reported in literature (Table 1) were usually associated to differences in structure and composition of the oxide layer depending on the fabrication methods.[25]

In this work, thermally oxidized iridium oxide (IrO_x) electrodes were prepared and tested as potentiometric pH sensors in highly alkaline solutions (pH between 9 and 13.5) up to almost 2 years of immersion times. The main features studied are the response to pH changes, together with the reproducibility and accuracy of the potential response for the individual IrO_x electrodes. The influence of the oxygen content in solutions and the long-term stability when continuously immersed in alkaline solution were also studied.

2 | MATERIALS AND METHODS

2.1 | Materials and solutions

For the preparation of the IrO_x electrodes (section 2.2), iridium wires (0.5 mm diameter, 99.9% purity) and gold wires (0.25 mm diameter, 99.99% purity) were obtained from Goodfellow, lithium carbonate (anhydrous powder, purity >99%) from Alfa Aesar, and epoxy coating (ASTORIT PUR 105) from Astorit.

Exposure solutions were prepared by mixing defined amounts of orthoboric acid (H_3BO_3) (≥99.5%, Sigma–Aldrich) and sodium hydroxide (≥99.5%, Merck KGaA) with de-ionized water (conductivity ≈ 2 μS/cm). The pH of the solutions was periodically measured with a standard glass cell pH electrode with silver–silver chloride (Ag/AgCl) reference electrode. The pH values of the solutions and the concentrations of orthoboric acid and sodium hydroxide used for their preparation are listed in Table 2.

TABLE 1 Influence of the production method on oxide thickness, hydrous/anhydrous oxide, potential-pH slope, and response time, together with the longest immersion time and tested pH-range of iridium oxide electrodes reported in literature

Method	Oxide thickness (nm)	Hydrous/ anhydrous	Potential-pH slope (V/ pH unit)	Response time (s)	Longest immersion	Tested pH-range	Ref.
Sol–gel	≈400	Anhydrous	≈−0.051	<2	<1 day	≈1.5–12	[15]
	400–600	Anhydrous	≈-0.071	≈6	<1 day	≈3–11	[16]
	–	Anhydrous	≈-0.059	<10	<1 day	≈1–13	[21]
Electrochem. oxidation	–	Hydrous	≈−0.047	<60	10 days	≈2–12	[1]
	≈200	Hydrous	−0.090 ÷ −0.06	<300	5 days	≈3–9	[22]
Sputtering	≈100	Anhydrous	−0.060 ÷ −0.055	–	<1 day	≈2–12	[23]
Electrochem. deposition	–	Hydrous	−0.070 ÷ −0.064	≈30	<1 day	≈2–12	[24]
	3500	Hydrous	−0.084 ÷ −0.070	<60	<1 day	≈2–12	[13]
	≈200	Hydrous	−0.080 ÷ −0.060	≈60	5 days	≈2–11	[14]
Thermal oxidation	2000	Anhydrous	≈−0.059	<1	2–10 days (2.5 years)[a]	≈1–13	[17,19,20]

[a]The electrodes were tested several times up to an age of 2.5 years; the immersion times were 2–10 days

TABLE 2 pH values of the four solutions prepared for the potentiometric measurements, together with the concentrations of orthoboric acid (H_3BO_3) and sodium hydroxide used for their preparation

Solution	Concentration H_3BO_3 ($mol \cdot L^{-1}$)	Concentration NaOH ($mol \cdot L^{-1}$)	Measured pH after production (at 20 °C)
Borate 1	0.50	0.30	9.3
Borate 2	0.50	0.48	10.6
Borate 3	0.05	0.60	11.9
Borate 4	0.05	1.20	13.5

2.2 | Preparation of the IrO_x electrode

Iridium metal wires (0.5 mm diameter and 10–15 mm length) were ultrasonically cleaned in 6 $mol \cdot L^{-1}$ HCl solution for 10 min and afterwards washed with de-ionized water (conductivity $\approx 2\ \mu S/cm$) for 10 min to ensure that no impurities were left on the wires surface. The wires were then dried in air at 20 °C and positioned in a ceramic crucible lined with a gold foil and covered with lithium carbonate on both sides. They were then heated up to 870 °C in 3 h in a furnace (Nabertherm, model B180) under air atmosphere, maintained at 870 °C for 5 h and cooled down. A fast (1 h) and a slow (14 h) cooling process were investigated. In the fast cooling process, the crucible with the sample was taken out from the furnace; in the slow cooling process, the crucible with the oxidized Ir wires was left inside the furnace until ambient temperature (20–21 °C) was reached. In both cases, the cooling process had an asymptotic behavior with respect to time. For the fast cooling, the sample needed 20 min to cool down to half of the oxidation temperature (870 °C), whereas for the slow cooling time, 2 h were needed.

Once reached room temperature, the solid carbonate in the crucible was dissolved with 6 $mol \cdot L^{-1}$ HCl solution. Two different cleaning procedures were then investigated in order to remove any attached soluble components and to ensure that there was no chloride left on the electrodes surface: (a) 10 min ultrasonic cleaning in de-ionized water and (b) several times careful rinsing with de-ionized water. As a result, a black oxide layer was formed on the surface of the iridium wires. Information regarding the mechanism of metal oxide film growth in carbonate melt can be found in literature.[17,19,26,27] To remove the water not bound to the oxide layer formed, the cleaned wires were heated up to 120 °C, maintained at that temperature for 11 h and cooled down inside the furnace until they reached ambient temperature (approximately 10 h). A small area at the end of the oxidized wire was then scraped off until pure iridium was exposed. A thin gold wire (0.25 mm diameter and approximately 5 mm length) was tightly wrapped around the exposed iridium and fixed with crimping pliers to form a good physical and electrical connection. Finally, an epoxy coating was applied to cover the area of the exposed iridium and gold connection to provide electric insulation. Epoxy coating was also applied on the tip of the electrode because it was suspected that some adherence problems of the IrO_x could happen on the edges. A schematic representation and stereomicroscopy image of the IrO_x electrode produced and used in this study is shown in Figure 1.

In total, eight different batches (denoted I–VIII) of 3–9 IrO_x electrodes (denoted 1-n for each batch) were produced. This production procedure is based on the one reported in Yao et al. and Wang et al.[17,19] However, we modified the cooling and cleaning processes.

2.3 | Microscopic characterization of the IrO_x electrodes

Selected IrO_x wires were cast in epoxy and the cross section was polished. Optical and scanning electron microscopy (SEM) was performed. Based on the backscattered electron SEM images, the thickness and the percentage of pores (porosity) of the oxide layer formed on the iridium wires were determined.

The average and standard deviation of the oxide layer thickness was obtained from ten measurements.

The oxide porosity was defined as the percentage of pores (black spots in the SEM image) of the oxide layer (gray area in the SEM image). The SEM images were analyzed with the GIMP image analysis software, which enables to adjust the black/white contrast of the image selected and to quantify the pore area (black area). The percentage of pores of the oxide layer was then calculated as the average of five image analyses of 20–30 μm-long areas of the oxide layer.

2.4 | Set-up and instruments for the potentiometric measurements

The potential E of the IrO_x electrodes produced was measured versus a silver/silver chloride/saturated potassium chloride (Ag/AgCl/sat. KCl) reference electrode (+0.197 V vs. the

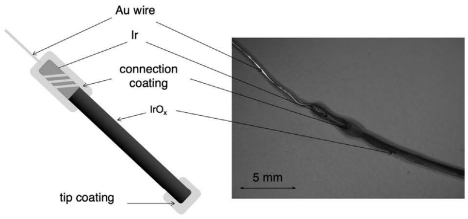

FIGURE 1 Schematic representation and stereomicroscopy image of the IrO_x electrode produced and used in this study

standard hydrogen electrode, SHE). A Luggin capillary (filled with the test solution) was used when the reference electrode was immersed in the test solution to avoid contamination of the test solution with KCl and of the reference electrode with the test solution. The set-up is schematically depicted in Figure 2.

The liquid junction potential established when immersing the reference electrode in the test solution was estimated to maximum 5 mV for the pH values considered in this study[28] and was thus neglected.

The measurements were performed with a Keithley multimeter and multiplexer (Keithley Instruments Inc.) connected to a computer for data acquisition, which allowed recording the potential of several IrO_x versus the reference electrode over time. All the experiments were carried out at room temperature (20–21 °C).

2.5 | Measurement procedures

2.5.1 | Determination of potential-pH response

After production, the IrO_x electrodes were immersed in one of the four test solutions used (Table 2). The exposure solution was changed several times in order to investigate the influence of the pH exposure history on the final potential-pH response. These pH exposure variations lasted between 2 and 6 months. After this, the exposure solution was exchanged to pH ≈ 13.5 and the potential-pH response of the produced IrO_x electrodes was then investigated by applying a pH sweep from high pH (pH ≈ 13.5) to low pH (pH ≈ 9.5) with the set-up described in section 2.4. Changes in the pH of the solution were performed either stepwise or continuously:

- Stepwise pH changes were achieved by exchanging the exposure solution (Table 2) or by adding given quantities of alkalinity or acidity. Between steps, the pH was kept constant (frequently monitored with a commercial glass pH-electrode and corrected if needed). Steps in pH were made after exposure of at least 4 days to the same pH and once a potential drift lower than 0.5 mV/day was reached.
- Gradual (slow) pH changes were achieved by leaving the solution exposed to air and allowing to react with CO_2 from the atmosphere (natural carbonation). The pH of the solution over time was controlled with a commercial glass electrode.

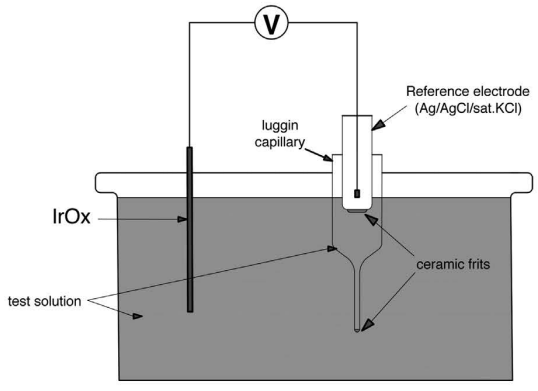

FIGURE 2 Set-up for the potentiometric measurements of the IrO_x electrodes

After these measurements, the electrodes were preserved in pH ≈ 13.5.

For some IrO_x electrodes, stepwise pH changes were applied 2–3 times, i.e., the pH was decreased from pH ≈ 13.5 to pH ≈ 9.3 and then brought back to pH ≈ 13.5, in order to study the reproducibility and reversibility of the potential response. The time difference between two consecutive measurements at a given pH was between 20 and 30 days. Afterwards, the pH of the solution was also kept constant at pH ≈ 13.5.

The pH exposure history will be indicated together with the results.

2.5.2 | Influence of conditioning on the potential-pH response

With "conditioning" we mean the duration of the initial exposure of the electrodes to alkaline solutions, i.e., prior to being subjected to the procedure described in section 2.5.1 for measuring the *E-pH* response. In order to study the influence of conditioning, the IrO_x electrodes of batch VIII were directly tested after being produced (without previous exposure to solution) during short time in solutions of different pH: the electrodes were initially immersed at pH ≈ 13.5 ("Borate 4," Table 2) for <1 min, and then they were washed and transferred to the next solution also for <1 min and so on (following the sequence Borate 4→Borate 3→Borate 2→Borate 1, Table 2). For all these measurements, the potential drift was always less than 2 mV/min. After these measurements, the electrodes were preserved in pH ≈ 13.5 ("Borate 4," Table 2) and the procedure described in section 2.5.1 was later applied.

This relatively fast protocol of measurements at different pH values was repeated with the electrodes of batch VIII after 8 and 23 days of immersion in "Borate 4" (pH ≈ 13.5, Table 2).

2.5.3 | Oxygen dependency

The aim of this experiment is to evaluate whether the potential response of the IrO_x electrodes is influenced by the oxygen concentration in solution. For this test, both an IrO_x

electrode and a stainless steel bar were immersed in the test solutions (Table 2) according to the set-up described in section 2.4. When the potential of the IrO_x electrode and stainless steel stabilized (potential drift lower than 5 mV/min), nitrogen was bubbled into the solution in order to remove the oxygen. A decrease in the potential of the stainless steel electrode was used as an indicator of the decrease in oxygen concentration[8] during nitrogen bubbling. The experiment lasted between 2 and 3 h and it was performed for several IrO_x electrodes immersed in the test solutions (Table 2).

3 | RESULTS

3.1 | Influence of fabrication protocol on electrode morphology

Figure 3 shows representative examples of the SEM analysis of the cross sections of the produced IrO_x electrodes obtained with the different cooling times and cleaning processes described in section 2.2.

The IrO_x electrodes formed by thermal oxidation generally exhibited a columnar structure with high aspect ratio grains, but there were significant differences in the oxide thickness and porosity depending on the cooling time and the type of cleaning performed (Figure 3). Table 3 provides all data on thickness and porosity of the oxide layer for all the batches produced with different cooling and cleaning processes.

From the data in Table 3, it can be deduced that overall thicker oxide layers are obtained for the slow cooling process (14 h). IrO_x electrodes with lower porosity and more homogeneous oxide layer thicknesses were obtained by rinsing with ultrapure water, avoiding ultrasonic cleaning. Optical microscopy also showed that after ultrasonic cleaning, part of the oxide was occasionally detached and iridium metal was exposed.

As a consequence of these results, only IrO_x electrodes based on the slow cooling process (14 h) with a careful posterior rinsing of the wires (no ultrasonic cleaning) were used for the electrochemical measurements presented in the following sections.

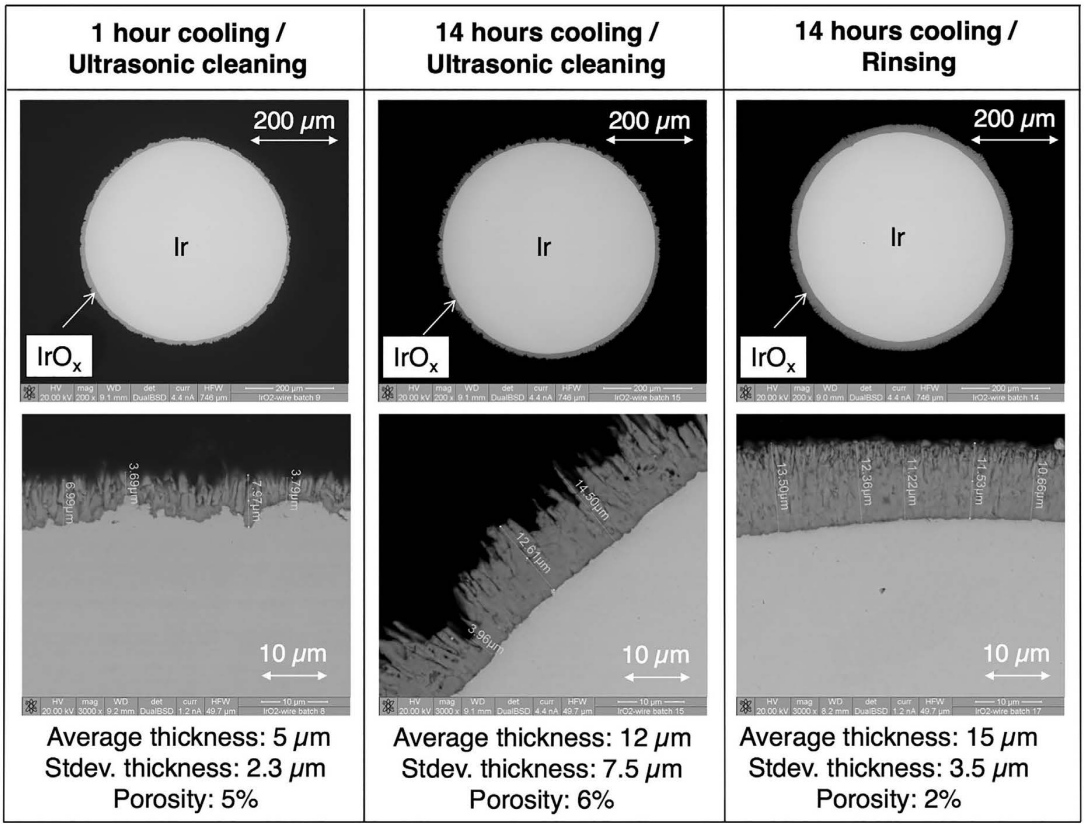

FIGURE 3 SEM images of the cross section of IrO_x electrodes produced with different cooling times (1 and 14 h) and cleaning processes (ultrasonic cleaning vs. rinsing). The average thickness (together with the standard deviation) and the porosity of the oxide layer are also provided for each IrO_x

TABLE 3 Average thickness, standard deviation of the thickness, and porosity of the iridium oxide layer formed with different cooling and cleaning processes (ultrasonic cleaning vs. rinsing)

Cleaning process	Cooling process	Average thickness (µm)	SD thickness (µm)	Porosity (%)
Ultrasonic	Fast (1 h)	5[a]	2.3	5
		7	2.5	7
	Slow (14 h)	20	6	7
		12[a]	7.5	6
		11	4.2	6
Rinsing	Fast (1 h)	6	2	3
	Slow (14 h)	22	2.5	2.5
		15[a]	3.5	2

SD, standard deviation.
[a]Shown in Figure 3

3.2 | Potential-pH response

3.2.1 | Influence of conditioning on *E-pH* slope

Figure 4 shows the average *E-pH* response curves obtained directly after production (no conditioning) and after 8 and 23 days of conditioning in pH ≈ 13.5 of the electrodes produced in batch VIII. These results were obtained with the protocol described in section 2.5.2. The fitting coefficients for the potential-pH response curves shown in Figure 4 are given in Table 4.

TABLE 4 Fitting coefficients, together with the standard deviation, for the *E-pH* response curves (average of five individual IrO_x electrodes) obtained with the protocol described in section 2.5.2 (for batch VIII, at different conditioning times in pH ≈ 13.5) shown in Figure 4

Conditioning time (days)	Slope (V/pH)	SD slope (V/pH)	Intercept (V vs. Ag/AgCl/sat. KCl)	SD intercept (V vs. Ag/AgCl/sat. KCl)
0	−0.031	0.007	0.503	0.068
8	−0.050	0.005	0.693	0.052
23	−0.052	0.003	0.723	0.042

SD, standard deviation.

It can be seen that the values of *E-pH* slope and *E-pH* intercept increase (in absolute value) with conditioning time. The results after 8 and 23 days of conditioning are similar.

3.2.2 | Influence of conditioning on response time

The time from immersion, once the pH was changed, until the potential drift was <2 mV/day was considered the response time.

Figure 5 shows the potential ΔE versus time response of IrO_x electrodes when exposed to a certain pH (here pH = 13.5). The potential difference ΔE is defined as the difference between IrO_x response E_{IrO_x} ($t = t_{response}$) when the potential changed <2 mV/day and the IrO_x response E_{IrO_x} (t) at a given time.

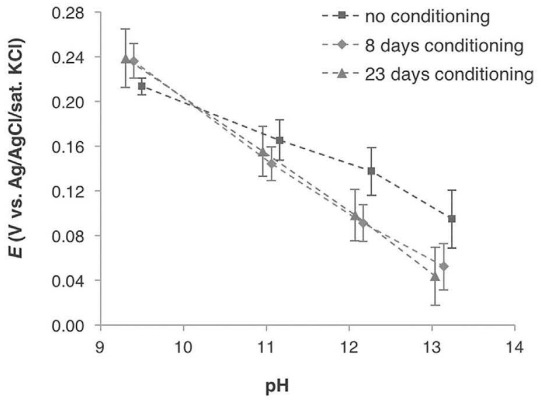

FIGURE 4 Average and standard deviation of the potential—pH response of five individual IrO_x electrodes (produced in batch VIII) after different conditioning times in pH ≈ 13.5 (measurements at each pH exposure lasted <1 min, i.e., protocol described in section 2.5.2). The pH values from the curves "no conditioning" and "8 days conditioning" were slightly shifted in the graph for the sake of clarity

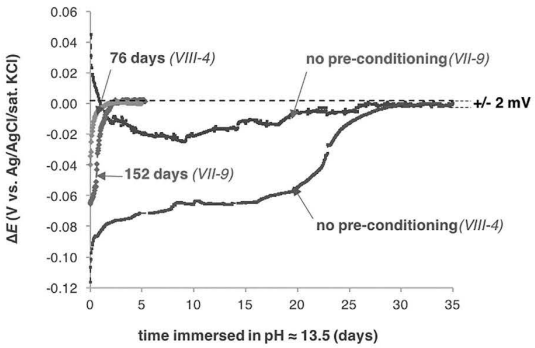

FIGURE 5 Potential difference ΔE (Eq. (1)) as a function of the immersion time in pH ≈ 13.5 for different conditioning times in alkaline solution (indicated in the graph) of two IrO_x electrodes (IrO_x 9 from Batch VII and IrO_x 4 from batch VIII); response time = time to reaching a potential drift <2 mV/day. The potential change over time (2 mV/day) accepted is also indicated in the graph

$$\Delta E(t) = E_{\mathrm{IrO_x}}\left(t = t_{\mathrm{response}}\right) - E_{\mathrm{IrO_x}}(t) \qquad (1)$$

In Figure 5, two different cases are shown (no pre-conditioning vs. conditioning for a certain time, indicated in the graph). For each scenario, two representative examples of IrO_x electrodes were selected (IrO_x 9 from batch VII and IrO_x 4 from batch VIII). For the two electrodes that were not pre-conditioned, the response time was approximately 1 month. In contrast, for the two electrodes that were conditioned in alkaline solutions for 76 and 152 days, respectively, the response time became much shorter, namely in the order of days. The same trend was observed for the other produced IrO_x electrodes.

3.2.3 | Potential-pH response — after conditioning

This section presents the *E-pH* response of the IrO_x electrodes, determined after sufficient conditioning (protocol described in section 2.5.1). Figure 6 shows the average of potential responses of the IrO_x electrodes produced in each batch as a function of the pH of the solution. For each batch, the linear fit for the relationship between potential and pH is also plotted, together with the theoretical *E-pH* response according to Pourbaix.[29] The fitting coefficients of the *E-pH* curves of each individual IrO_x electrodes (38 in total), together with the information regarding the pH-range exposure history is provided in Table S1 (Supplementary Material).

Figure 6 shows that the potential-pH slopes of the IrO_x electrodes are generally in good agreement with the theoretical potential-pH response according to Pourbaix.[29] The *E-pH* slopes of individual electrodes are between −0.050 V/pH and −0.068 V/pH and the standard deviation is between 0.002 and 0.007 V/pH (Table S1).

The *E-pH* intercepts of individual electrodes are between 0.605 and 0.863 V versus Ag/AgCl/sat. KCl and the standard deviation is between 0.019 and 0.075 V versus

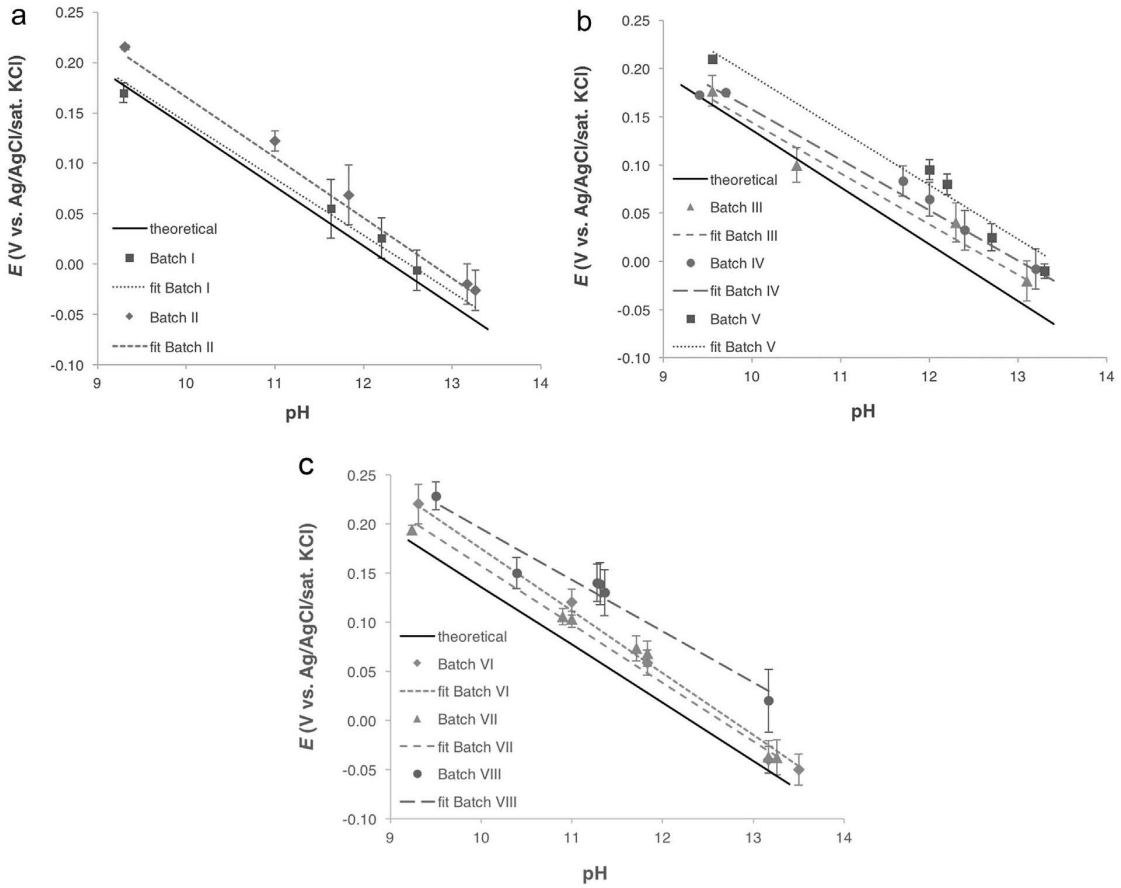

FIGURE 6 Average of potential responses of the IrO_x electrodes of batches: I and II (a), III–V (b), VI–VIII (c). Immersion time at each pH lasted at least 4 days. For each batch, the linear fit for the *E-pH* relationship is given (differentiated by line and color), together with the standard deviation (error bars) of the individual readings (of 3–9 individual IrO_x electrodes). The theoretical *E-pH* response according to Pourbaix is also plotted [29]

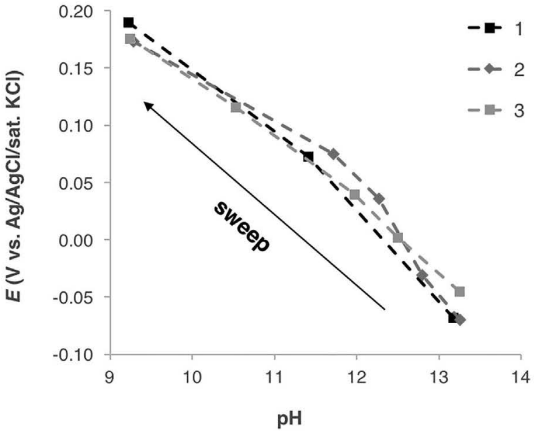

FIGURE 7 Reproducibility of the *E-pH* response of sufficiently conditioned electrodes (representative example; electrode 1, batch I). Each time, the electrode was first exposed to pH 13.5 and then the pH was stepwise decreased to 9.3. A pH sweep from 13.5 to 9.3 took 20–30 days. The numbers indicated in the graph (1–3) refer to the order in which the measurements were performed

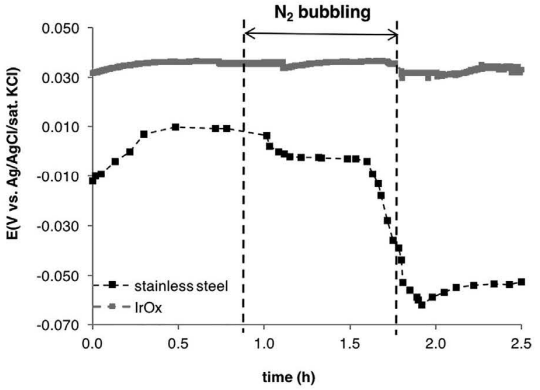

FIGURE 8 Potential of an IrO_x (IrO_x 1 from Batch III) and stainless steel bar immersed in pH ≈ 13 as a function of time while oxygen content is decreased due to nitrogen bubbling into the solution (indicted in the graph)

Ag/AgCl/sat. KCl (Table S1). Interestingly, almost all measured potentials were more positive than the values suggested by Pourbaix.[29]

Note that the electrodes produced in batches I–V had different exposure histories within the range of pH between 9.3 and 13.5 over more than 1 year. Nevertheless, their *E-pH* response curve is in agreement with the rest of the results.

3.2.4 | Reproducibility and reversibility

For several individual IrO_x electrodes, the protocol described in 2.5.1 (stepwise pH changes) was repeated 2–3 times to study the reproducibility of the *E-pH* response of a single electrode (once they were sufficiently conditioned). A representative example of three *E-pH* response curves repeatedly obtained for the same electrode (electrode 1, batch I) is shown in Figure 7. The order of the measurements is also indicated in the graph. The complete set of results (for 29 IrO_x out of the 38 produced) is provided in Table S2 (Supplementary Material).

From Figure 7, it can be noted that the potential response can be considered reversible and reproducible; only small differences between the different curves can be observed. The same behavior was found for the rest of electrodes produced (Table S2 in the Supplementary Material). The maximum difference between potential readings for the same electrode measured at the same pH, but at different periods in time was typically in the range of 20 mV. Concerning the potentiometric determination of the pH, this would correspond to an error of maximum 0.5 pH units for pre-calibrated IrOx electrodes.

3.2.5 | Oxygen dependency

A representative example of the potential of the IrO_x electrode and the stainless steel immersed in solution of pH 13 is shown in Figure 8. The same trend was observed for the other produced IrO_x electrodes immersed in the other test solutions (Table 2). From Figure 8, it can be seen that while nitrogen was bubbled into the test solution, the potential of steel significantly decreased while the potential of the IrO_x electrode remained essentially unaffected (maximum changes within a few millivolts). It thus becomes apparent that the oxygen concentration in solution does not affect the potential of the IrO_x electrodes produced in this study, which is in agreement with other works.[6,12]

3.3 | Long-term stability

For engineering applications, long-term stability is the most important property for the IrO_x electrodes. Figure 9a shows the potential response of an IrO_x (electrode 1, batch II) as a function of time while undergoing an exposure history to varying pH for 1.5 years. Figure 9b, shows the magnified area of the graph when the pH of the solution was kept constant at pH ≈ 13.5 after 540 days of exposure.

Several aspects in the results presented in Figure 9 deserve attention. First of all, this IrO_x was subjected to a history of variable pH for more than 1 year before the *E-pH* curves were obtained (Figure 9a). Nevertheless, the potential-pH response curves measured are in agreement with the rest of results (see Tables S1 and S2 in the Supplementary Material).

Secondly, it can be observed that as long as the pH was kept constant, the potential response varied less than ±2 mV over 80 days, thus without potential drift. In addition, the

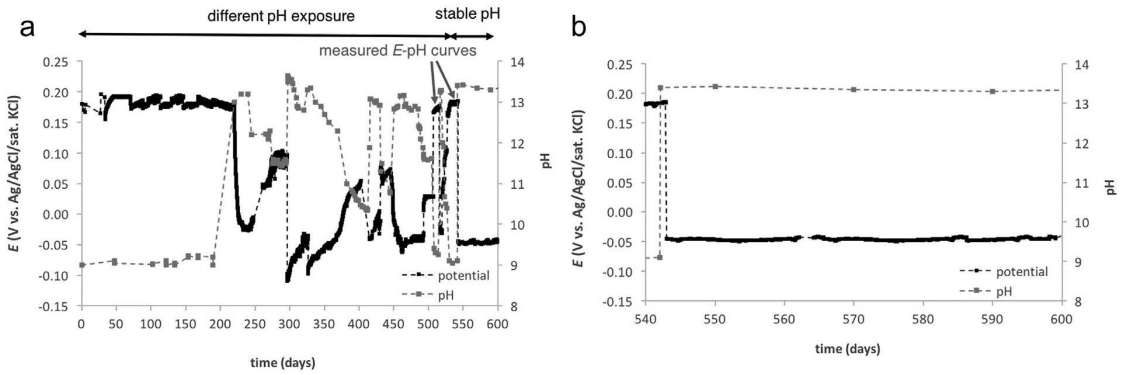

FIGURE 9 (a) Potential response of an IrO_x (electrode 1, batch II) as a function of time while undergoing a history of variable pH exposure. (b) Magnified area of the graph after 540 days of immersion and when the pH is kept constant at 13.5

response time was very short (ca. 1 day) when the pH was increased from 9.3 to 13.5 after 540 days of immersion in alkaline solution (Figure 9b), in agreement with the results presented in section 3.1.2.

The same behavior was observed for the rest of the electrodes immersed in the different solutions, always after "sufficient" conditioning time (see section 4.2). Table S3 in the Supplementary Material reports the total immersion time in alkaline solution, the immersion time in pH ≈ 13.5 when the potential drift was <0.5 mV/day, and the potential response in pH ≈ 13.5 (when the potential drift was <0.5 mV/day).

4 | DISCUSSION

4.1 | Potential-pH response

It was observed that each produced IrO_x electrode responds slightly different (section 3.2.3) and that its response is also influenced by the conditioning time (sections 3.2.1 and 4.2). It is thus recommended that previous conditioning and pre-calibration of each IrO_x electrode is performed before use. Given the variability within all electrodes, this will enhance the accuracy of the measurements of the single electrode compared to simply using general (average) slope and standard potential.

- Slope: The range of *E-pH* slopes values obtained, after sufficient conditioning, was between −0.050 and −0.068 V/pH (Table S1, Figure 6), i.e., relatively close to the −0.059 V/pH slope reported for IrO_x electrodes produced by thermal oxidation [17,19,20] and in agreement with Pourbaix.[29] It is believed that the differences in slope obtained in this study with respect to the reported −0.059 V/pH may be due to the porosity of the exposed oxide layer, which may influence ion exchange.[15,30] It should be also noted that the total immersion time of the electrodes in this work is much longer (months–years) than in other studies (generally minutes to days, see Table 1). Different immersion times, i.e., conditioning times (section 4.2), could also explain the reported differences in pH-slopes in literature.[1,12–16,22]
- Standard potential: IrO_x electrodes formed by thermal oxidation have been reported to be (*semi*)-anhydrous[17,19,20] with intercept values of the *E-pH* relationship similar to the value according to Pourbaix,[29] i.e., 0.736 V versus Ag/AgCl/sat. KCl. In this work, the average value is close to theory (0.733 V vs. Ag/AgCl/sat. KCl) but the variability among the intercept values obtained is high (average 0.733 V with scatter between 0.605 and 0.863 V vs. Ag/AgCl/sat. KCl (Tables S1 and S2 in the Supplementary Material)). From Figure 6 it can be seen that the potential responses of many electrodes at a given pH are higher than the theoretical curve for $Ir_2O_3 \cdot nH_2O/IrO_2$ nH_2O (theoretical potential-pH response according to Pourbaix[29]); this could be explained by the presence of other (hydrated) iridium oxides other than the $Ir_2O_3 \cdot nH_2O/IrO_2$ nH_2O couple.[31] For example, Wang et al.,[19] reported that the electrode produced with a method similar to the present one was $Li_{0.86}IrO_{2.34}(OH)_{0.76} \cdot 0.39H_2O$. However, the electrodes produced in this case were stored in neutral solution (4 KCl mol $\cdot L^{-1}$) or in air between the measurements. Therefore, the hydration state of the present electrodes is likely different, since they had been continuously immersed in alkaline solution.

4.2 | Influence of conditioning

4.2.1 | Influence of conditioning on potential-pH response

According to the present results, the total immersion time in alkaline solution (conditioning time) plays an important role

in obtaining a reproducible and stable potential reading upon exposure to a certain pH (section 3.2.1).

The values of *E-pH* slope and *E-pH* intercept change with conditioning time. When not properly conditioned, the potential response of the studied electrodes changes over time (Figure 4), but after "sufficient" conditioning time, the individual IrO_x electrodes exhibit a reproducible potential response, regardless of the previous exposure (section 3.2.4).

Figure S2 in the Supplementary Material gives the average total immersion time in alkaline solution until obtaining reproducible potential response when immersed in pH ≈ 13.5, differentiated by batch. The data in Figure S2 show that in order to obtain a reproducible response, sufficient conditioning time is needed. For some electrodes, this may be the case already after 50 days, while for others, it may take up to 250 days.

In section 4.1, it was suggested that the oxide layer formed is probably composed by oxide forms other than the $Ir_2O_3 \cdot nH_2O$/ $IrO_2\,nH_2O$; most likely hydrated as the studied IrO_x in this study are continuously immersed in alkaline solution.[1,12–16,22] It is believed that the time needed until obtaining a reproducible potential response at a given pH is due to the "hydration" of the oxide layer formed. Trasatti[32] suggested that the "wetting" of dry oxide films may take more than 2 months.

4.2.2 | Influence of conditioning and morphology on response time

The IrO_x electrodes formed by thermal oxidation exhibit a columnar structure with high aspect ratio grains, as previously observed in other studies.[17,19,20] Table 3 shows that overall thicker oxide layers were obtained for the longer cooling time in the production protocol. This may be explained by increased oxidation times when slower cooling was permitted.[26,27]

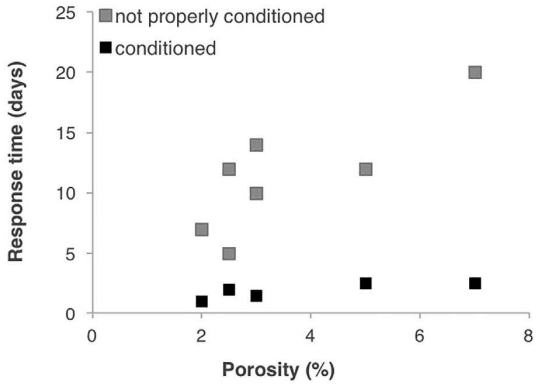

FIGURE 10 Response time as a function of the porosity of the oxide layer, differentiated by electrodes with sufficient/insufficient conditioning time (response time = time to reaching a potential drift <2 mV during 1 day)

The thickness of the oxide layer does not seem to influence the response time (Figure S1 in the Supplementary Material). Nevertheless, we consider thicker oxide layers as beneficial for the application for long-term pH monitoring because higher thickness increases the robustness of the electrodes.

In section 3.1, it was shown that the oxide layers can exhibit some very narrow pores (Figure 3 and Table 3); this could explain why response times in the order of days were obtained in some cases (Figure 5), as increased porosity may be translated into longer response times.[15,30] Nevertheless, the results presented in Figure 5 show that the response time strongly decreases when the electrodes were immersed in alkaline solution for a certain conditioning time.

Figure 10 shows the response time (see section 3.1.2) as a function of the porosity of the oxide layer, differentiated by electrodes conditioning.

The response time of the electrodes strongly decreases if they were conditioned for a sufficient time. Furthermore, the response time increases with the porosity for the electrodes that were not properly conditioned.

4.2.3 | Sufficient conditioning

In conclusion, it appears that the produced iridium oxide electrodes need to be conditioned in alkaline solution in order to provide both a reproducible potential-pH response and relatively short response time. Based on the current results, we suggest that the electrodes need 3–4 months of immersion in alkaline solution until they provide fully reproducible potentials at a given pH.

5 | APPLICATION IN RESEARCH AND ENGINEERING

5.1 | Concrete structures

Corrosion of steel reinforcement is the most frequent cause of failure in reinforced concrete structures.[33] The pH of the concrete pore liquid and solid alkaline components such as $Ca(OH)_2$ play a major role in the ability of reinforced concrete to withstand corrosion — both for carbonation-induced and for chloride-induced corrosion.[8]

Common methods to determine the pH in concrete used in science and engineering of concrete durability are destructive and can thus not provide continuous information at a certain location.[34,35] The most established method in practice is based on spraying an indicator solution on a freshly exposed concrete surface.[35] Only a few indicator solutions have proven applicable to concrete, the most common ones are phenolphthalein (changing color between pH 8 and 9) or thymolphthalein (changing color between pH 9 and 10). This approach for pH measurements basically provides a yes/no

answer and gives no information about the pH changes above and below the characteristic pH at which the used indicator solution changes color. The accuracy is roughly one pH unit. Other approaches to determine the pH of concrete are based on crushing concrete samples and exposing them to a leaching agent.[34] While this may yield more finely graded results than the indicator spray test, the methods are laborious and time-consuming. Additionally, leaching methods do not permit measuring the pH in the concrete at moisture states below saturation.

In contrast to these approaches, the IrO_x electrodes used as pH sensors presented in this work provide relatively highly resolved pH measurements. As the method is non-destructive, embedded electrodes allow measurements over time (with a high time resolution) for given locations in the concrete, which is not possible with destructive measurements. These are considered important advantages for various applications.

One example is all research aiming at studying the penetration of the carbonation front through the concrete cover. If embedded at certain depths, the IrO_x electrodes can provide detailed insight in the kinetics of the carbonation and the time evolution of the solution pH, which is, depending on the type and amounts of solid phases, buffered at different pH levels. It may be particularly interesting to study non-Portlandite binders that likely exhibit very different shapes in evolution of pH versus time.[36–38] Additionally, the IrO_x electrodes permit measuring the pH in the concrete at the exposure conditions favorable for carbonation, which are below saturation state.[39]

These electrodes may in principle be applied also in monitoring of engineering structures, i.e., embedded in the concrete cover zone at different depths. This would permit measuring the pH as a function of time and cover depth. On this basis, the time until the pH becomes depressed to a certain value at the steel surface could be extrapolated and allow for a prediction of the time to depassivation.

Another possible application of the sensors could be the validation of the existing carbonation models.[40–42] These models are typically calibrated against experimental data determined with the indicator solution spray test. In this regard, detailed knowledge of the pH as a function of both time and cover depth permits refining and validating carbonation models for different exposure conditions and for different binders.

In order to study the previously mentioned applications, the performance of the studied IrO_x electrodes when embedded in concrete is currently under investigation. The experiments are based on embedding the electrodes at different depths in mortar and exposing them to one-dimensional carbonation by placing the sample in a carbonation chamber (65% RH, 21 °C and 4% CO_2) while the potential response of the pH sensor is recorded. Preliminary results show that the electrodes can be used to monitor changes pH in situ in the concrete pore solution of reinforced concrete.[39] Table 5 gives the potential response of an IrO_x electrode embedded in mortar at a cover depth = 15 mm, before and after the sample was carbonated, together with the days of exposure to carbonation.[39] The pH was calculated from averaged *E-pH* response curves obtained for the corresponding IrO_x electrode (Table S2).

From Table 5, it can be seen that the pH of uncarbonated concrete is ca. pH ≈ 13, while it decreases down to ca. pH ≈ 10 when it is carbonated, in agreement with literature.[8] Carbonation after 5 months at this depth was validated with the phenolphthalein spraying method. It is also interesting to note that even after more than 5 months of exposure to CO_2 ingress and under relatively dry environment (65% RH), the electrode functionality is still given.[39]

Finally, we would like to note that concrete is typically exposed to different exposure conditions, e.g., seasonal changes, that may lead to marked variations in the moisture content in the concrete. It has been indicated in this study that produced electrodes consist of a dense hydrated oxide layer. While the preliminary results reported in Table 5 indicated that dry environments do not impair the pH sensors, the effect of variable humidity conditions needs to be addressed in further studies.

TABLE 5 Potential response of an IrO_x electrode (IrO_x 4 produced in Batch VI) embedded in mortar (at cover depth = 15 mm), before and after the sample was carbonated, together with the days of exposure to carbonation.[39] The pH was calculated from averaged *E-pH* response curves obtained for the corresponding IrO_x electrode.

	IrO_x embedded in mortar	
pH	Days in the carbonation chamber	*E* (V vs. Ag/AgCl/sat. KCl)
13.2	5	−0.022
9.7	160	0.170

5.2 Cathodic protection in soil

In laboratory studies, it has been shown that relatively low protection current densities lead to a significant increase in pH at the steel surface.[43] Only a few mA/m^2 appear to be sufficient to raise the pH at the steel surface to values above 10 and provide effective cathodic protection.

However, determining the pH at the very surface of steel embedded in soil is difficult, mainly because of the pronounced change in pH with increasing distance from the metal surface.

The solution (soil) volume relevant in the measurement is thus extremely small, which limits the use of commercial pH sensors that typically are too large. As a result, researchers either use highly specialized test set-ups, which may be

limited in terms of being representative for practice, or rely on indirect measurements to estimate the pH. To validate the existing literature data and to broaden knowledge (e.g., studying different soil types, chemical composition of the soil solution, and other experimental conditions) a more simple and direct method is thus desirable.

In this regard, the IrO_x electrodes studied in this work are feasible. They are small, work well in the relevant range of pH (>9), and have response times that are sufficiently fast for the application in CP studies in soil. Considering the long-standing controversy about CP criteria based on potentials,[43] being able to measure the pH in situ in the soil would contribute to resolving open questions in research and practice.

6 | CONCLUSIONS

Based on the major conclusions below, we consider the studied IrO_x electrodes feasible for long-term continuous monitoring purposes in corrosion engineering in concrete or soil. When properly produced, conditioned, and pre-calibrated, they permit measuring the pH with a maximum error of 0.5 pH units in a range of at least pH 9 to 13.5.
The main findings obtained in this work are:

- Conditioning: in order to provide accurate and reproducible potential-pH responses, the produced IrO_x electrodes need conditioning in highly alkaline solutions for at least 3–4 months.
- Response time: given sufficient conditioning, the response time of the electrodes varied between a few hours to a few days. This is sufficiently fast for monitoring pH changes in concrete or soil.
- Oxygen dependency: the potential exhibited by the produced iridium oxide electrodes was found to be independent on the oxygen concentration dissolved in the solution.
- Long-term stability: after immersion in different alkaline solutions for up to almost 2 years, the electrodes were still capable of responding reliably to pH changes. The oxide layers formed with the suggested procedure were relatively thick (10–25 μm); we consider this beneficial for the long-term stability in concrete or soil.
- Response in concrete: preliminary results show that the studied electrodes permit monitoring pH changes when embedded in concrete.

ACKNOWLEDGEMENT

The financial support from the Swiss National Science Foundation (SNF) is kindly acknowledged.

ORCID

Y. Seguí Femenias http://orcid.org/0000-0002-9150-4305

REFERENCES

[1] F. Contu, M. Vega-Arroyo, R. Taylor, *Int. J. Mat. Sci.* **2014**, *4*, 8.
[2] M. Pikulski, W. Gorski, *Anal. Chem.* **2000**, *72*, 2696.
[3] K. Kreider, *Sens. Actuators, B* **1991**, *5*, 165.
[4] A. N. Bezbaruah, T. C. Zhang, *Anal. Chem.* **2002**, *74*, 5726.
[5] I. A. Ges, B. L. Ivanov, D. K. Schaffer, E. A. Lima, A. A. Werdich, F. J. Baudenbacher, *Biosens. Bioelectron.* **2005**, *21*, 248.
[6] S. A. M. Marzouk, S. Ufer, R. P. Buck, T. A. Johnson, L. A. Dunlap, W. E. Cascio, *Anal. Chem.* **1998**, *70*, 5054.
[7] W. Vonau, U. Guth, *J. Solid State Electrochem.* **2006**, *10*, 746.
[8] B. Elsener, L. Bertolini, P. Pedeferri, R. P. Polder *Corrosion of Steel in Concrete*, Wiley, Weinheim **2013**.
[9] D. A. Hausmann, *J. Mater. Prot.* **1967**, *6*, 19.
[10] A. Behnood, K. V. Tittelboom, N. D. Belie, *Constr. Build. Mater.* **2016**, *105*, 176.
[11] R.-G. Du, R.-G. Hu, R.-S. Huang, C.-J. Lin, *Anal. Chem.* **2006**, *78*, 3179.
[12] H. A. Elsen, C. F. Monson, M. Majda, *J. Electrochem. Soc.* **2009**, *156*, F1.
[13] C. Terashima, T. N. Rao, B. V. Sarada, N. Spataru, A. Fujishima, *J. Electroanal. Chem.* **2003**, *544*, 65.
[14] W. Olthuis, M. A. M. Robben, P. Bergveld, M. Bos, W. E. V. d. Linden, *Sens. Actuators, B* **1990**, *2*, 247.
[15] W.-D. Huang, H. Cao, S. Deb, M. Chiao, J. C. Chiao, *Sens. Actuators, A* **2011**, *169*, 1.
[16] W.-D. Huang, J. Wang, T. Ativanichayaphong, M. Chiao, J. C. Chiao, presented at *SPIE Nanosensors and Microsensors for Bio-Systems Conference, California*, 9–13 March, **2008**, 693104.
[17] S. Yao, M. Wang, M. Madou, *J. Electrochem. Soc.* **2001**, *148*, H29.
[18] K. Yamanaka, *Jpn. J. of Appl. Phys.* **1989**, *28*, 632.
[19] M. Wang, S. Yao, *Electroanalysis* **2003**, *15*, 1606.
[20] M. Wang, S. Yao, M. Madou, *Sens. Actuators, B* **2002**, *81*, 313.
[21] G. M. da Silva, S. G. Lemos, L. A. Pocrifka, P. D. Marreto, A. V. Rosario, E. C. Pereira, *Anal. Chim. Acta* **2008**, *616*, 36.
[22] J. E. Baur, T. W. Spaine, *J. Electroanal. Chem.* **1998**, *443*, 208.
[23] M. J. Tarlov, S. Semancik, K. G. Kreider, *Sens. Actuators, B* **1990**, *1*, 293.
[24] C. C. M. Martinez, R. E. Madrid, C. J. Felice, *IEEE Trans. Educ.* **2009**, *52*, 133.
[25] S. Kakooei, M. C. Ismail, B. Ari-Wahjoedi, *Int. J. Mat. Sci Innov.* **2013**, *1*, 62.
[26] M. J. O'Malley, P. M. Woodward, H. Verweij, *J. Mater. Chem.* **2012**, *22*, 7782.
[27] M. O'Malley, Ph.D. *Thesis*, The Ohio State University (United States) **2008**.
[28] U. Angst, Ø. Vennesland, R. Myrdal, *Mater. Struct.* **2008**, *42*, 365.
[29] M. Pourbaix, *Atlas of Electrochemical Equilibria in Aqueous Solutions*, Pergamon Press, New York **1974**.
[30] M. Hüppauff, B. Lengeler, *J. Electrochem. Soc.* **1993**, *140*, 598.
[31] J. Juodkazytė, B. Šebeka, I. Valsiunas, K. Juodkazis, *Electroanalysis* **2005**, *17*, 947.

[32] S. Trasatti, *Electrochim. Acta* **1991**, *36*, 225.
[33] *State-of-art report*, International Federation of Structural Concrete (FIB), Task group 5.8.
[34] G. Plusquellec, M. R. Geiker, J. Lindgård, J. Duchesne, B. Fournier, K. D. Weerdt, *Cem. Concr. Res.* **2017**, *96*, 13.
[35] M.-Y. Yu, J.-Y. Lee, C.-W. Chung, *J. Test. Eval.* **2010**, *38*, 534.
[36] J. Khunthongkeaw, S. Tangtermsirikul, T. Leelawat, *Constr. Build. Mater.* **2006**, *20*, 744.
[37] K. Sisomphon, L. Franke *Cem. Concr. Res.* **2007**, *37*, 1647.
[38] V. G. Papadakis, *Cem. Concr. Res.* **2000**, *30*, 291.
[39] Y. Seguí Femenias, U. Angst, B. Elsener, presented at *SMAR 2017 – International Conference on Smart Monitoring, Assessment and Rehabilitation of Civil Structures*, Zürich, **2017**.
[40] V. G. Papadakis, C. G. Vayenas, M. N. Fardis, *ACI Mater. J.* **1991**, *88*, 363.
[41] S.-J. Kwon, H.-W. Song, *Cem. Concr. Res.* **2010**, *40*, 119.
[42] S. Kashef-Haghighi, Y. Shao, S. Ghoshal, *Cem. Concr. Res.* **2015**, *67*, 1.
[43] U. Angst, M. Büchler, B. Martin, H. G. Schöneich, G. Haynes, S. Leeds, F. Kajiyama, *Mater. Corros.* **2016**, *67*, 1135.

SUPPORTING INFORMATION

Additional Supporting Information may be found online in the supporting information tab for this article.

How to cite this article: Seguí Femenias Y, Angst U, Elsener B. Monitoring pH in corrosion engineering by means of thermally produced iridium oxide electrodes. *Materials and Corrosion*. 2017;1–13. https://doi.org/10.1002/maco.201709715

WILEY-VCH

Article type: Article

Monitoring pH in corrosion engineering by means of thermally-produced iridium oxide electrodes

Y. Seguí Femenias[1], U. Angst[1], B. Elsener[1,2]

[1] **ETH** Zürich, Institute for Building Materials (IfB), Stefano-Franscini-Platz 3, 8093 Zurich, Switzerland
[2] University of Cagliari, Department of Chemical and Geological Sciences, 09100 Monserrato (CA), Italy

Correspondence
B. Elsener, **ETH** Zürich, Institute for Building Materials (IfB), Stefano-Franscini-Platz 3, 8093 Zurich, Switzerland
University of Cagliari, Department of Chemical and Geological Sciences, 09100 Monserrato (CA), Italy
Email: elsener@ethz.ch

Fig. S 1 Response time as a function of the average thickness of the oxide layer, together with the standard deviation (error bars) of ten individual readings. IrO_x electrodes immersed in pH ≈9.3 (Borate 1, Table 2; response time=time to reaching a potential drift <2 mV during one day).

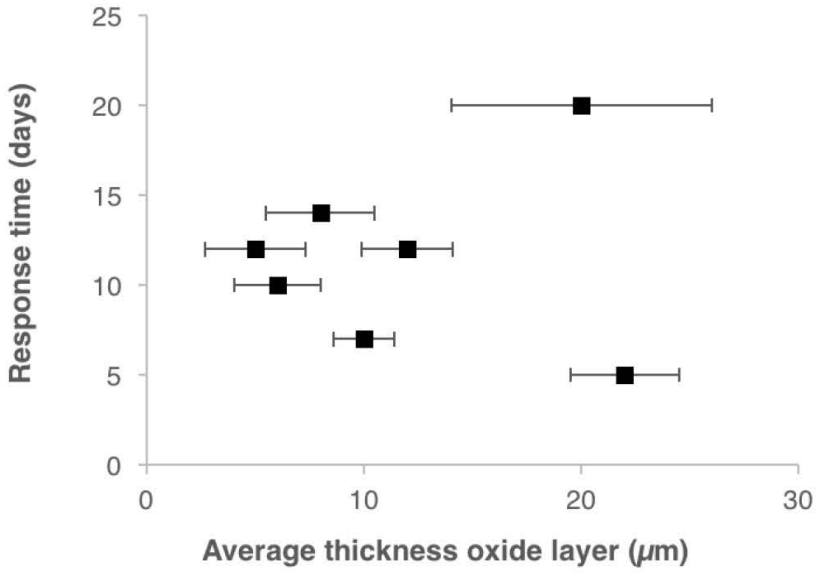

Fig. S 2 Average total immersion time in alkaline solution until obtaining reproducible potential response when immersed in pH≈13.5, differentiated by batch. The error bars indicate the standard deviation from the individual IrO_x produced in each batch.

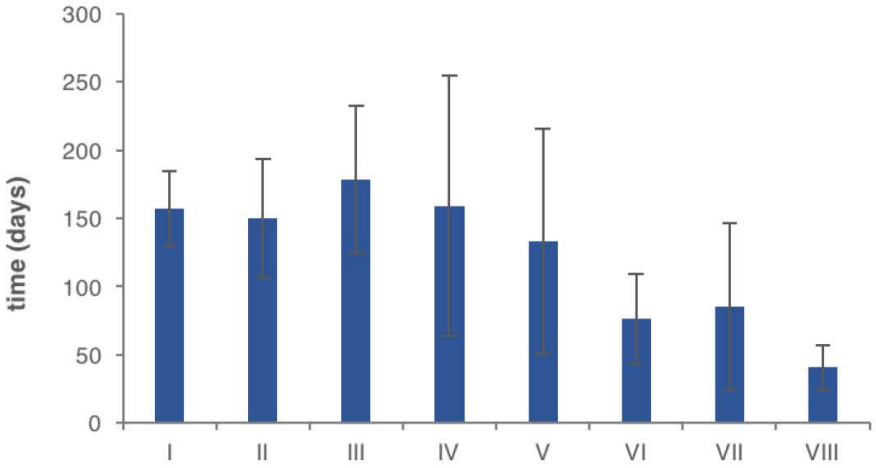

Table S 1 Fitting coefficients for the *E-pH* response curves shown in Fig. 6 for the individual IrO_x electrodes, previous pH range exposure and exposure time to solution before *E-pH* curves were obtained.

Batch	Electrode	Previous pH range exposure	Previous exposure time [days]	Slope [V/pH]	Intercept [V vs. Ag/AgCl/sat. KCl]
I	1	9-13.5	475	-0.065	0.806
	2	9-13.5	500	-0.054	0.661
	3	9-13.5	530	-0.051	0.646
	Average	-	-	**-0.057**	**0.663**
	Standard deviation	-	-	**0.007**	**0.019**
II	1	9-13.5	480	-0.059	0.718
	2	9-13.5	480	-0.064	0.815
	3	9-13.5	480	-0.053	0.696
	4	9-13.5	480	-0.064	0.834
	Average			**-0.060**	**0.766**
	Standard deviation			**0.005**	**0.069**
III	1	9-13.5	470	-0.052	0.653
	2	9-13.5	470	-0.056	0.698
	3	9-13.5	470	-0.05	0.661
	Average	-	-	**-0.053**	**0.671**
	Standard deviation	-	-	**0.003**	**0.024**
IV	1	9-13.5	450	-0.053	0.685
	2	9-13.5	450	-0.051	0.651
	3	9-13.5	450	-0.050	0.652
	4	9-13.5	450	-0.054	0.721
	Average	-	-	**-0.052**	**0.670**
	Standard deviation	-	-	**0.002**	**0.043**
V	1	10-13.5	370	-0.054	0.731
	2	10-13.5	370	-0.059	0.784
	Average			**-0.057**	**0.758**
	Standard deviation			**0.004**	**0.037**
VI	1	9-13.5	260	-0.056	0.761

	2	9-13.5	260	-0.051	0.711
	3	9-13.5	240	-0.068	0.832
	4	9-13.5	240	-0.065	0.826
	5	9-13.5	240	-0.064	0.775
	6	9-13.5	240	-0.066	0.832
	7	9-13.5	240	-0.068	0.863
	8	9-13.5	240	-0.067	0.845
	Average	-	-	**-0.063**	**0.806**
	Standard deviation	-	-	**0.006**	**0.051**
VII	1	9-13.5	180	-0.063	0.807
	2	9-13.5	180	-0.057	0.722
	3	9-13.5	180	-0.061	0.774
	4	9-13.5	180	-0.061	0.736
	5	10-13.5	160	-0.056	0.721
	6	10-13.5	160	-0.059	0.748
	7	10-13.5	160	-0.064	0.787
	8	10-13.5	160	-0.054	0.706
	9	10-13.5	160	-0.06	0.762
	Average	-	-	**-0.059**	**0.751**
	Standard deviation	-	-	**0.003**	**0.034**
VIII	1	13	50	-0.050	0.605
	2	13	50	-0.054	0.798
	3	13	50	-0.050	0.707
	4	13	50	-0.055	0.748
	5	13	50	-0.052	0.727
	Average			**-0.052**	**0.717**
	Standard deviation			**0.002**	**0.071**
	Average	-	-	**-0.057**	**0.731**
	Standard deviation	-	-	**0.004**	**0.047**
Theoretical (Pourbaix [29])				**-0.059**	**0.730**

Table S 2 Fitting coefficients for the potential-pH dependency curves obtained 2-3 consecutive times for the individual IrO_x according to the described protocol in 2.3.2

		First measurement		Second measurement		Third measurement	
Batch	**Electrode**	**Slope [V/pH]**	**Intercept [V vs. Ag/AgCl/sat. KCl]**	**Slope [V/pH]**	**Intercept [V vs. Ag/AgCl/sat. KCl]**	**Slope [V/pH]**	**Intercept [V vs. Ag/AgCl/sat. KCl]**
I	1 [a]	-0.065	0.806	-0.053	0.674	-0.055	0.67
	2	-0.054	0.661				
	3	-0.051	0.646				
	Average	**-0.057**	**0.663**				
	Standard deviation	**0.007**	**0.019**				
II	1	-0.059	0.718	-0.05	0.638		
	2	-0.064	0.815				
	3	-0.053	0.696				
	4	-0.064	0.834	-0.05	0.656		
	Average	**-0.060**	**0.766**	**-0.050**	**0.647**		
	Standard deviation	**0.005**	**0.069**	**0.000**	**0.013**		
III	1 [b]	-0.052	0.653	-0.051	0.698		
	2	-0.056	0.698	-0.056	0.762		
	3	-0.05	0.661	-0.050	0.692		
	Average	**-0.053**	**0.671**	**-0.052**	**0.717**		
	Standard deviation	**0.003**	**0.024**	**0.003**	**0.039**		
IV	1	-0.053	0.685	-0.052	0.666		
	2	-0.051	0.651	-0.053	0.668		
	3	-0.050	0.652	-0.050	0.67		
	4	-0.054	0.721	-0.056	0.724		
	Average	**-0.052**	**0.670**	**-0.026**	**0.682**		
	Standard deviation	**0.002**	**0.043**	**0.053**	**0.028**		
V	1	-0.054	0.731	-0.055	0.755		
	2	-0.059	0.784	-0.059	0.801		
	Average	**-0.057**	**0.758**	**-0.057**	**0.778**		

	Standard deviation	**0.004**	**0.037**	**0.003**	**0.033**		
VI	1	-0.056	0.761	-0.059	0.79		
	2	-0.051	0.711	-0.054	0.751		
	3	-0.068	0.832	-0.059	0.745	-0.054	0.642
	4	-0.065	0.826	-0.059	0.768	-0.055	0.714
	5	-0.064	0.775	-0.060	0.748	-0.054	0.685
	6	-0.066	0.832	-0.058	0.750	-0.055	0.714
	7	-0.068	0.863	-0.060	0.781	-0.055	0.718
	8	-0.067	0.845	-0.059	0.760	-0.053	0.694
	Average	**-0.063**	**0.806**	**-0.058**	**0.762**	**-0.054**	**0.695**
	Standard deviation	**0.006**	**0.051**	**0.002**	**0.017**	**0.001**	**0.029**
VII	1	-0.063	0.807	-0.060	0.785		
	2	-0.057	0.722	-0.053	0.768		
	3	-0.061	0.774	-0.057	0.828		
	4	-0.061	0.736	-0.053	0.770		
	5	-0.056	0.721	-0.053	0.693	-0.05	0.662
	6	-0.059	0.748	-0.052	0.682	-0.06	0.759
	7	-0.064	0.787	-0.057	0.728	-0.05	0.632
	8	-0.054	0.706	-0.051	0.663	-0.055	0.702
	9	-0.06	0.762	-0.055	0.716	-0.051	0.678
	Average	**-0.059**	**0.751**	**-0.054**	**0.737**	**-0.053**	**0.687**
	Standard deviation	**0.003**	**0.034**	**0.003**	**0.054**	**0.004**	**0.048**
VIII	1	-0.050	0.605				
	2	-0.054	0.798				
	3	-0.050	0.707				
	4	-0.055	0.748				
	5	-0.052	0.727				
	Average	**-0.052**	**0.717**				
	Standard deviation	**0.002**	**0.071**				
	Average	**-0.057**	**0.731**	**-0.054**	**0.720**	**-0.054**	**0.695**

Standard deviation	**0.004**	**0.047**	**0.003**	**0.049**	**0.001**	**0.012**

[a] shown in Figure 7

[b] shown in Figure 8

Table S 3 Total immersion time in alkaline solution and immersion time in pH≈13.5, together with the potential response, when the potential drift was <0.5 mV/day for the individual IrO_x electrodes produced (after being conditioned).

Batch	Electrode	Total immersion time (days)	Total immersion time when <0.5 mV/day (days)	*E* response in pH≈13.5 (V vs. Ag/AgCl/sat. KCl)
I	1	640	60	-0.053
	2	640	80	-0.050
	3	640	60	-0.035
II	1 [a]	620	80	-0.045
	2	620	80	-0.050
	3	620	80	-0.025
	4	620	80	-0.028
III	1	610	70	-0.005
	2	610	70	-0.013
	3	610	70	0.016
IV	1	580	50	-0.029
	2	580	50	-0.029
	3	580	50	-0.005
	4	580	50	-0.030
V	1	510	50	0.013
	2	510	50	0.002
VI	1	410	50	0.001
	2	410	50	0.027

	3	410	50	-0.062
	4	410	50	-0.030
	5	410	50	-0.049
	6	410	50	-0.034
	7	410	50	-0.032
	8	410	50	-0.037
	1	320	40	-0.025
	2	320	40	-0.018
	3	320	40	-0.009
	4	320	40	-0.033
VII	5	320	40	-0.019
	6	320	40	-0.032
	7	320	40	-0.039
	8	320	40	-0.021
	9	320	40	-0.015
	1	150	65	-0.060
	2	150	65	0.011
VIII	3	150	65	0.023
	4	150	65	0.001
	5	150	65	-0.010

[a] shown in Fig. 8

PAPER IV

Y. Seguí Femenias, U. Angst, B. Elsener (2017)

PH-monitoring in mortar with thermally-oxidized iridium electrodes

RILEM Technical Letters (submitted)

Author's version of the prepared manuscript.

PH-monitoring in mortar with thermally-oxidized iridium electrodes

Yurena Seguí Femenias[a,], Ueli Angst[a], Bernhard Elsener[a,b]*

[a] ETH Zürich, Institute for Building Materials (IfB), Stefano-Franscini-Platz 3, 8093 Zurich, Switzerland

[b] University of Cagliari, Department of Chemical and Geological Sciences, 09100 Monserrato (CA), Italy

***Corresponding author:** Phone: +41 44 633 76 68, Email: syurena@ethz.ch

Abstract:

The pH of the concrete pore solution plays a vital role in protecting the reinforcing steel from corrosion. Here, we present results from embeddable pH sensors that permit the continuous, in-situ monitoring of the pH in the concrete pore solution. These are potentiometric sensors, based on thermally-oxidized Iridium/Iridium oxide (IrO_x) electrodes. We propose an iterative calculation algorithm taking into account diffusion potentials arising from pH changes, thus permitting the reliable, non-destructive determination of the pore solution pH over time. This calculation algorithm forms an essential part of the method using IrO_x electrodes. Mortar samples were exposed to accelerated carbonation and the pH was monitored at different depths over time. Comparative tests were also performed using thymolphthalein pH-indicator. The results from the pH sensors give insight in the carbonation process, and can, in contrast to thermodynamic modelling and titration experiments, give insight in kinetic processes such as transport and phases transformations. Additionally, it was found that the front at which the pH is decreased from initially 13-14 down to 12.5 can be significantly ahead of the common carbonation front corresponding to pH 9-10. This has major implications for laboratory testing and engineering practice.

Keywords: iridium/iridium oxide electrode; pH sensor; carbonation monitoring, non-destructive technique.

1. Introduction

Reinforced concrete is the most common building material used in civil engineering. Durability of this material can, however, be compromised due to the corrosion of reinforcement steel. In fact, this is the most frequent cause of failure in reinforced concrete structures [1].

The pH of the concrete pore solution is in the range pH 13-14 due to the alkalinity provided by the dissolved sodium and potassium oxides present in Portland cement [2]. At these high pH values, reinforcing steel is protected from corrosion by a thin oxide layer, i.e., the passive layer, spontaneously formed on the steel surface [3]. However, the reaction of CO_2 from the atmosphere with the alkaline components in the concrete pore solution and the $Ca(OH)_2$ (Portlandite) in the cement paste, decreases the pH to levels below 9 [3, 4]. As a result, when the carbonation front reaches the steel, it may be depassivated and in presence of oxygen and humidity reinforcement corrosion starts. This is known as carbonation-induced corrosion [3].

As carbonation-induced corrosion is accompanied by a decrease in the alkalinity of the concrete pore solution, knowledge of the pH in concrete is essential. Common methods to determine the pH in concrete are destructive, do not provide continuous information over time and have limited resolution in terms of both space and pH [5, 6]. The most established method in practice is based on spraying an indicator solution [7], such as phenolphthalein or thymolphthalein, on a freshly exposed concrete surface. This test indicates the depth of carbonation, which is defined as the depth at which the pH gradient meets the indicator's characteristic pH. Typically, the carbonation front is understood as the front at which the pH drops below pH 9 or 10. The indicator spray test does not give any information about the pH distribution behind and in front of the "carbonation front". Thus, this method does not indicate a decrease in pH from the initial value (typically pH 13-14) until pH 9-10 is reached. Only recently, by using several indicators, the spatial distribution of pH levels between pH 13.5 and 11 was mapped [8]. However, this approach is laborious. Other methods to determine the pH of concrete are pore solution expression or crushing concrete samples and exposing them to a leaching agent [5, 6]. While these approaches may provide more accurate results than indicator tests, they are time consuming and present difficulties at low moisture levels as well as in the presence of sharp pH gradients, where limitations regarding the minimum sample volume needed render the application of these methods impossible.

Embedded, non-destructive pH sensors in concrete, however, would allow the permanent monitoring of pH and its space and time-dependent variations in-situ. Different sensors have been developed for this purpose; among them, fibre-optic sensors and metal oxide potentiometric sensors emerge as the most promising [6]. Fibre optic sensors have low price and general chemical stability, but they present severe limitations for applications in concrete including short life spans, narrow pH-range that can accurately be measured, leaching effects, and chemical instability at high pH values. Moreover, few studies exist where the pH>13 has been measured [6].

Concerning potentiometric sensors, iridium/iridium oxide (IrO_x) electrodes showed promising results in aqueous solution [9-12] in terms of high stability in a broad pH range, accuracy, and insensitivity to the oxygen content. However, only a few studies regarding the use of IrO_x embedded in mortar or concrete have been made [13, 14]. Despite the promising results in the reported works, the pH values measured were always above pH 11.5 and no data regarding the pH evolution while cement paste is carbonated was presented.

In this work, we report the pH response of IrO_x electrodes embedded at different depths in mortar samples that were exposed to accelerated carbonation. These sensors allowed monitoring the pH of the pore solution continuously while the cement paste was carbonated. Comparative tests were also conducted using thymolphthalein pH-indicator. The findings have major implications for research and practice.

2. Materials and methods

2.1 pH determination using thymolphthalein pH-indicator

Mortar cubes (4 x 4 x 4 cm^3) were produced with mix proportions cement/water/sand 1: 0.5: 2 with CEM I 52.5 and sand size <1mm. They were cured for one week at 95%RH and 21°C. After one week of exposure to laboratory conditions (ca. 50%RH and 21°C), all the surfaces (except one) were painted with an epoxy-resin. The samples were then placed in a carbonation chamber (65%RH, 21°C and 4% CO_2) so one-dimensional carbonation occurred though the non-coated surface.

Mortar cubes were taken from the carbonation chamber after different exposure times and split perpendicular to the surface of CO_2 ingress. The carbonation depth was then determined by means of the indicator spray test. For that, thymolphthalein solution was prepared by dissolving 0.04 gr of thymolphthalein in 50 mL of 95% ethanol, diluted to 100 mL of deionized

water. The prepared thymolphthalein solution was sprayed on the two freshly broken mortar surfaces. The carbonation depth was determined from the average of 8 measurements of the depth of color change (4 measurements for each exposed surface).

2.2 pH monitoring with embedded iridium/iridium oxide (IrO_x) electrodes

2.2.1 Iridium/Iridium oxide (IrO_x) electrodes

Thermally oxidized iridium wires were produced based on the procedure reported in [9, 15, 16]. After production, the IrO_x electrodes were conditioned in alkaline solution (pH 13.5 - pH 9) for 2-6 months and then individually calibrated in solution of pH values ranging from 13.5 to 9. The potential response to pH of the produced IrO_x electrodes can be written as:

$$E_{\mathrm{IrO_x}} = E^0_{\mathrm{IrO_x}} - b \cdot pH \qquad (1)$$

where $E^0_{\mathrm{IrO_x}}$ is the electrode standard potential and *b* the potential-pH (*E-pH*) slope. Note that each electrode's standard potential and *E-pH* slope was obtained from separate individual pre-calibration. More details regarding the production protocol, conditioning and potential response are given in Ref. [17].

Each IrO_x electrode was mounted inside a rigid stainless steel tube (ca. 5 cm long and 2 mm in diameter), leaving only approx. 5 mm length of the IrO_x electrode protruding from the steel tube (Fig. 1). This ensures accurate positioning of the pH-sensor at the desired cover depth. The stainless steel tube and the IrO_x wire were electrically isolated with a Teflon tube (ca. 6 cm long and 1 mm in diameter) slightly longer than the steel tube. Front and back ends were sealed with an epoxy resin. Epoxy resin had also been applied, after production, to the tip of the IrO_x electrode because it was suspected that some adherence problems of the oxide layer could happen on the edges [17].

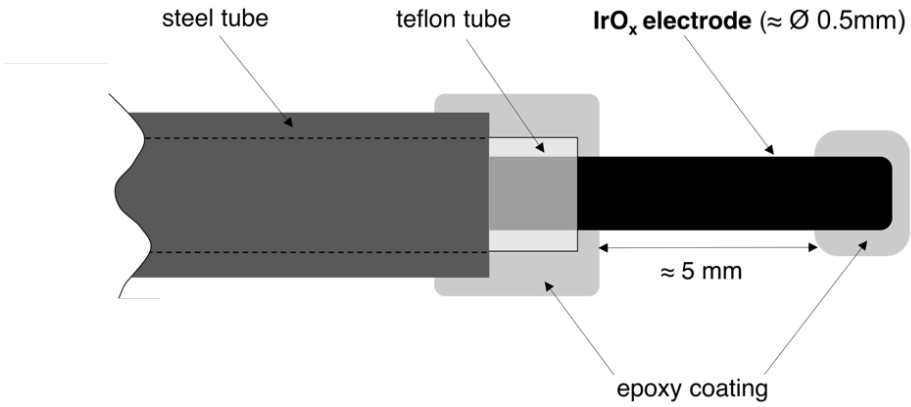

Fig. 1 Schematic representation of IrO_x sensors embedded in mortar. The pH sensitive part (IrO_x electrode) is mounted in a stainless steel tube (outer diameter approx. 2 mm) to enable accurate positioning in the mortar/concrete. A Teflon tube electrically separates the steel and the IrO_x. The ends are coated with an epoxy resin for sealing purposes.

2.2.2 Set-up and measurement procedure

Three rectangular mortar prisms (5 x 7.5 x 7.5 cm^3) with embedded IrO_x sensors were produced (Fig. 2). In total, six IrO_x sensors were embedded at different cover depths of 4, 6, 10, 15 and 20 mm (in different samples). The mortar mix proportions were the same as indicated in section 2.1. One hour after the mortar prisms (with the embedded IrO_x sensors) were cast, another 2.5 cm thick mortar layer with an embedded Ag/AgCl ion-selective electrode was cast on top of the previous samples. This match-cast part contained 4% of admixed chlorides by weight of cement to ensure that the Ag/AgCl electrode exhibits a stable potential [18] and thus could serve as internal reference electrode. The distance between the IrO_x sensor embedded at "depth 2" (Fig. 2) and the Ag/AgCl electrode was always higher than 4 cm. Thus, it was not expected that significant amounts of chlorides would reach the IrO_x sensors within the time of the current experiments.

The mortar prisms were cured for one week at 95%RH and 21°C. Subsequently, they were exposed for one week to laboratory conditions (ca. 50%RH and 21°C). Afterwards, all the surfaces (except one) were painted with an epoxy-resin and the samples were then placed in a carbonation chamber (65%RH, 21°C and 4% CO_2) so one- dimensional carbonation occurred though the non-coated surface (Fig. 2).

The potential of the internal reference electrode (Ag/AgCl ISE) was periodically checked with an Ag/AgCl/sat. KCl external reference electrode that was inserted in the upper opening ("hole for contact with external RE" in Fig. 2). A drop of simulated pore solution (0.15 $mol \cdot L^{-1}$ NaOH

0.2 mol·L^{-1} KOH and sat. $Ca(OH)_2$) was used to establish electrolytic contact between the reference electrode and the mortar surface. The liquid junction potential was estimated to ca. 5 mV and the measured potential was corrected accordingly [19]. Between measurements, the upper opening was closed with a rubber plug to avoid carbonation of the mortar located in the hole. The main features of the set-up are shown in Fig. 2.

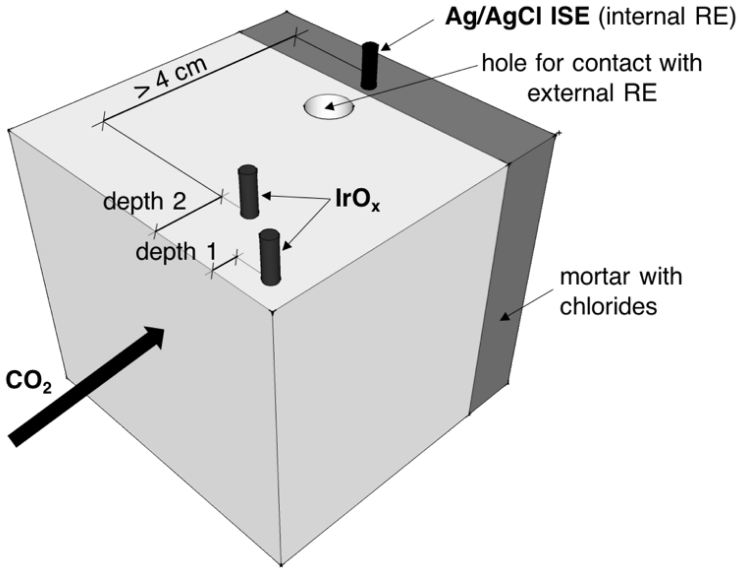

Fig. 2 Illustration of the mortar samples used to monitor carbonation propagation with embedded IrO_x sensors. All the surfaces were coated with epoxy resin with the exception of the surface of CO_2 ingress. Each sample contained 2 IrO_x sensors at different depths. A chloride containing layer of mortar with an embedded Ag/AgCl electrode was used to provide an embedded reference electrode (see text for explanation).

The potential of the embedded IrO_x sensors was continuously measured (with a time interval of 1 hour) versus the embedded reference electrode (Ag/AgCl ISE) with a Campbell data logger with 1MΩ input impedance, which was connected to a computer for data acquisition. When the calculated pH (see section 2.2.3) at a certain selected sensor location was pH≈9.7, the sample was split perpendicular to the surface of CO_2 ingress and thymolphthalein indicator solution (see section 2.1) was sprayed on both freshly broken surfaces. The carbonation depth was determined from the average of 10 measurements of the depth of color change (5 measurements for each exposed surface).

2.2.3 Algorithm for pH determination

In concrete, diffusion potentials can be present due to internal concentration gradients, such as differences in pH or chloride concentration [19-21]. In this work, diffusion potentials were established between the internal reference electrode and IrO_x sensors due to differences in chloride concentration (as the mortar with embedded Ag/AgCl ISE contains chlorides, see

section 2.2.2) and due to pH gradients (due to the progressive carbonation of the cement paste). Diffusion potentials thus varied as the pH of the pore solution changed due to carbonation. The potential measured $E_{measured}$ for each IrO_x sensor is:

$$E_{\text{measured}} = E_{\text{IrO}_x}(pH) + E_{\text{diffusion}}(pH) - E_{\text{Ag/AgCl ISE}} \quad (2)$$

where $E_{Ag/AgCl\ ISE}$ is the potential of the Ag/AgCl ISE internal reference electrode [18].

The diffusion potential $E_{diffusion}$ was calculated with the Henderson equation as described elsewhere [22]. For the calculation, the mobility of chloride and hydroxide ions was taken from the data reported in aqueous solution [22]. The concentration of hydroxide ions was related to the pH through the activity coefficient, obtained from the reported values in aqueous solution [23]. More information on the diffusion potentials in concrete and its evaluation can be found in literature [19-21, 24, 25].

Due to the interdependence of pH, $E_{\text{IrO}_x}(pH)$ and $E_{\text{diffusion}}(pH)$ (Eq. (2)), no closed solution can be given and an iterative calculation procedure (Fig. 3) was used. In this calculation, $E_{\text{IrO}_x}(pH)$ was initially calculated assuming that $E_{\text{diffusion}}(pH) = 0$. The pH was then determined from the calibration curve of the IrO_x electrode (Eq. (1)). Subsequently, $E_{\text{diffusion}}(pH)$ was calculated with this pH value and $E_{\text{IrO}_x}(pH)$ was re-calculated according to Eq. (2). This procedure was repeated until the pH difference between two consecutive iterations became < 0.1.

Note that the pH at the Ag/AgCl ISE $pH_{Ag/AgCl\ ISE}$ ($pH_{Ag/AgCl\ ISE} \approx 13.5$) was obtained from the first measurement (assuming that the pH of the pore solution was initially homogeneous for all the sample)when the mortar sample was placed in the carbonation chamber, i.e., <1 hour in the carbonation chamber.

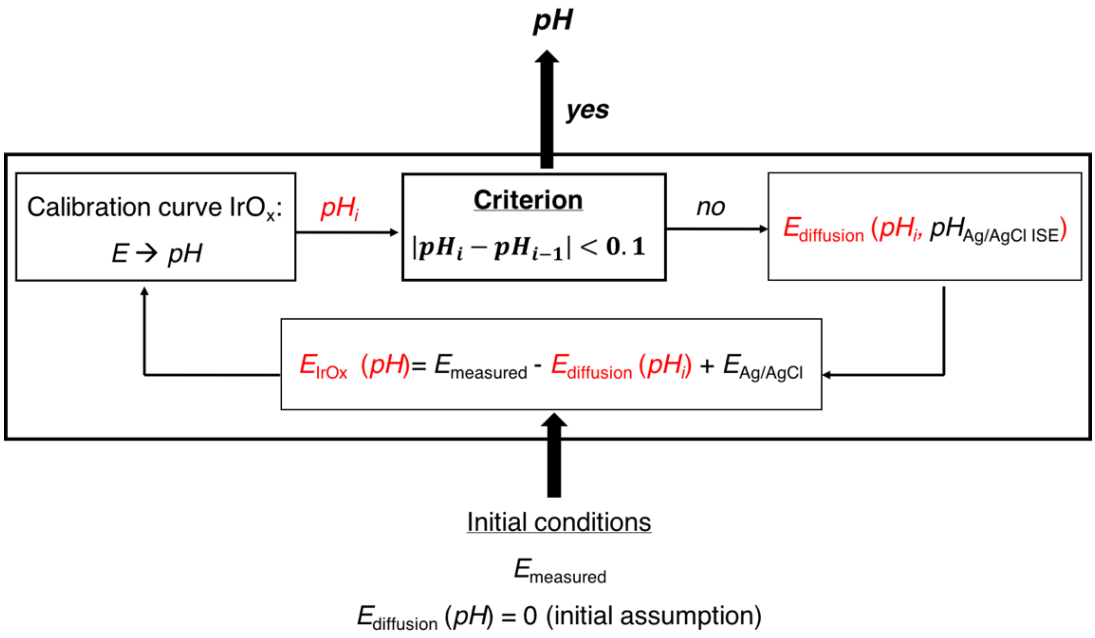

Fig. 3 Representation of the iterative calculation procedure used to determine the pH of the pore solution with embedded IrO_x sensors as the mortar sample carbonates. The parameters changed in each iteration are indicated in red. The calculated pH in each iteration (pH_i) is specifically indicated in the diagram

As an example, the calculated diffusion potential as a function of the pH for the IrO_x sensor embedded at 15 mm cover depth is shown in Fig. 4.

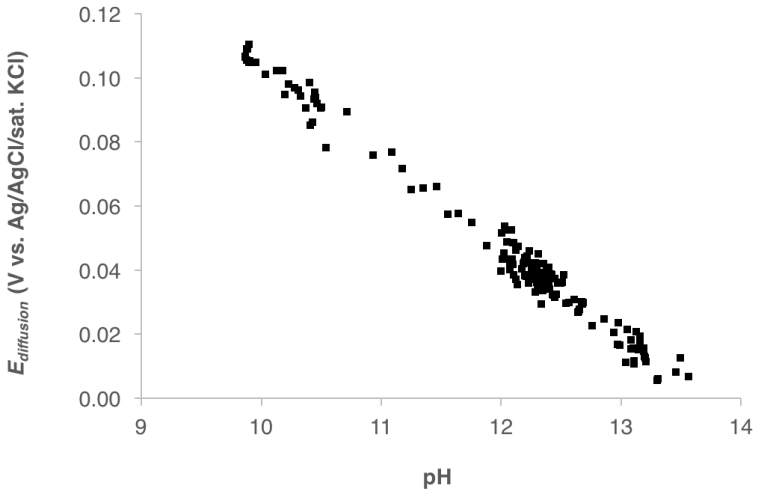

Fig. 4 Example of calculated diffusion potential as a function of pH for the IrO_x electrode embedded at 15 mm cover depth.

The diffusion potential increases as the pH gradient (between IrO_x sensor and embedded reference electrode Ag/AgCl ISE) increases, reaching potentials up to ca. 100 mV (Fig. 4). Considering a theoretical *E-pH* slope of -0.059 V/pH for the IrO_x electrode, it can be deduced

that relying on the experimentally measured potential without corrections, the real pH decrease from 13.5 to 9 would only be registered as a drop of ca. 2 pH units. Thus, taking into account diffusion potentials in the calculation procedure forms an essential part of the pH measurement methodology in mortar or concrete.

3. Results

3.1 Carbonation of concrete measured with embedded iridium/iridium oxide (IrO_x) sensors

Fig. 5a shows the calculated pH as a function of the square root of time in the carbonation chamber for six IrO_x sensors embedded at cover depths 4, 5, 6, 10, 15 and 20 mm. Note that curves with same color correspond to the same mortar sample. Fig. 5b shows a representative example (IrO_x embedded at depth 6 mm) of the pH decrease from pH≈14 down to pH≈12 as a function of time in the carbonation chamber.

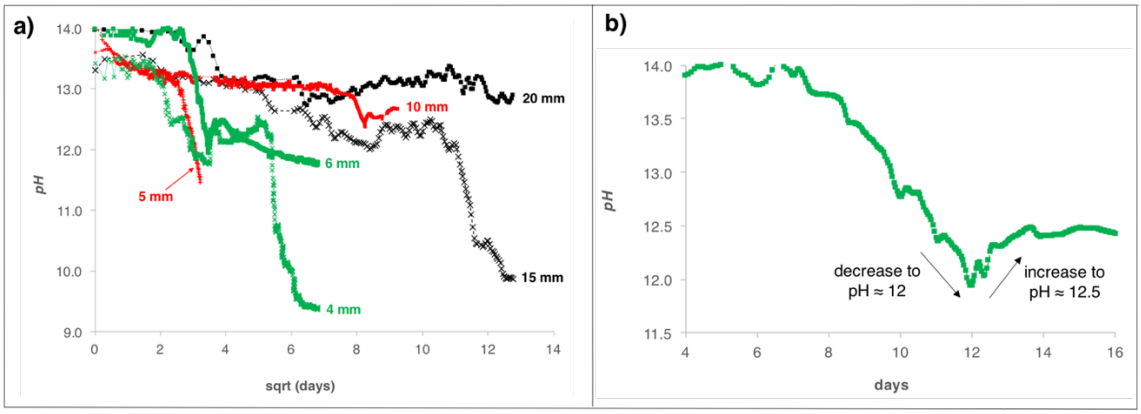

Fig. 5 (a) Calculated pH as a function of the square root of time in the carbonation chamber for six IrO_x sensors embedded at cover depths 4, 5, 6, 10, 15 and 20 mm. The curves with same color correspond to the same mortar sample (b) Representative example (IrO_x sensor embedded at 6 mm cover depth) showing the decrease from pH≈14 down to pH≈12, followed by a fast increase to pH 12.5.

From Fig. 5a, it can be observed that for the sensors embedded at depths 4, 5 and 6 mm, the pH decreased from 13.5 to ca. 12.5 with a relatively sharp drop. In contrast, the sensors embedded at higher cover depths (10,15, and 20 mm) showed a gradual pH decrease. In all cases, the pH initially decreased from its initial value to ca. pH≈12, with a subsequent increase back to ca. pH 12.5 within a few days (Fig. 5b) and remained constant at that pH for some time. Afterwards, the pH rapidly decreased down to pH ≈9.5, as it can be observed for the results obtained for the sensors embedded at 4 and 15 mm cover depths (Fig. 5a).

3.2 Comparison between pH determined with embedded IrO_x sensors and with pH-indicator solution

One of the main advantages of the sensors used in this work is that they permit measuring the pH evolution of the pore solution continuously. Thus, the time needed to reach a certain pH (e.g. 12.5) at a given depth during the carbonation process can be determined – a big advantage over the traditional indicator spray method. Fig. 6 compares the relationship between depth and time for pH 12.5 and pH≈9.7 determined with the sensor, together with the relationship between depth and time for pH 9-10 determined with the indicator. These two values were selected because pH 12.5 is a characteristic value (see Fig 5) at which the pH remains constant for some time (at least in Portland cement systems); and because pH 9-10 corresponds to the value detected with help of the indicator spray test (thymolphthalein). Additionally, from thermodynamic calculations, pH 9.7 corresponds to a complete reaction of $Ca(OH)_2$, ettringite and Ca-C-S-H with CO_2 forming $CaCO_3$ [26]. Note that both cases can be approximated by a linear relationship between depth to reach a given pH and the square root of time.

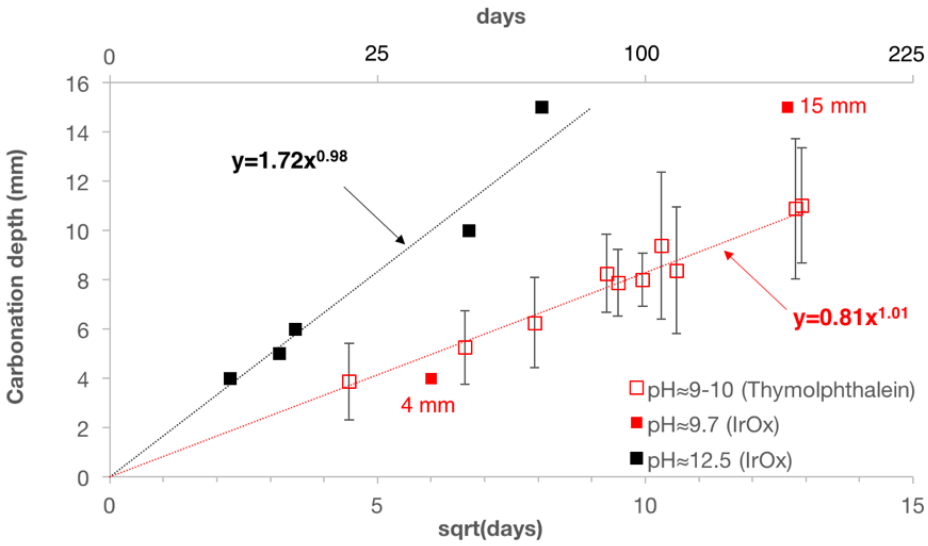

Fig. 6 Carbonation depth at pH≈12.5 and pH≈9.7(obtained with the embedded IrO_x sensors) and at pH 9-10 (average of the individual measurements of the thymolphthalein spraying test, together with the standard deviation, indicated with the error bars) as a function of the square root of time in the carbonation chamber. The linear regression curves for the carbonation front at pH≈12.5 and at pH≈9-10 (obtained with the pH indicator) are indicated with dotted lines.

From Fig. 6, it can be seen that the carbonation front corresponding to pH≈12.5, determined with the sensor, propagates significantly faster than the carbonation front at pH 9-10, determined with the indicator. Additionally, Fig. 6 shows that the IrO_x sensors indicate the carbonation at very similar times (result from the IrO_x sensor embedded at 4 mm cover depth,

which is within the standard deviation of the indicator spray test) or at earlier times (result from the IrO_x sensor embedded at 15 mm cover depth) compared to the indicator spray test.

4. Discussion

4.1 pH evolution during carbonation process – the carbonation mechanism

The studied IrO_x sensor permits, for the first time, studying in-situ the evolution of the pore solution pH during carbonation of the cement paste (Fig. 5). Our results revealed several features that are discussed here. First, the pH drops stepwise, at least at shallow depths, and remains for a long time on pH approx. 12.5. At higher cover depths, this drop in pH occurs more gradually. Additionally, the propagation of the carbonation front associated with pH 12.5, determined with IrO_x sensors, seems to be much faster than the propagation of the front associated with pH 9-10 that is determined with the indicator spray test (Fig. 6).

It is believed that the observed differences regarding carbonation propagation at pH 12.5 and at pH 9-10 are due to differences in the process of carbonation and due to the measuring method (embedded IrO_x sensors vs. pH-indicator test, described in section 4.2).

In the carbonation process of cement paste, the CO_2 from the gas phase is first dissolved in the water film on the pore wall:

$$CO_2 + H_2O \rightarrow H_2CO_3 \quad (3)$$

The following equilibrium is then established:

$$H_2CO_3\ (aq) \leftrightarrow H^+\ (aq) + HCO_3^-\ (aq) \leftrightarrow 2H^+ + CO_3^{2} \quad (4)$$

The resulting protons react with the OH^- ions of the pore solution, leading to the observed initial pH decrease from pH ≈13.5 to pH ≈12.5 (Fig. 5). The products of this early reaction are soluble Na^+ or K^+ carbonates (CO_3^{2-}), the formation of which does not hinder further ingress of CO_2. However, the fact that part of the CO_2 in the gas phase is dissolved in the water film on the pore walls will lead to a decrease of the CO_2 concentration at larger distances from the surface (filter effect). Replenishment of the CO_2 concentration in the pores would then be governed by diffusion processes, resulting in the $\sqrt{t}$ law (Fig. 6).

During the long time where the pH of the pore solution remains constant at pH≈12.5 (Fig. 5), the CO_3^{2-} ions react with the dissolved Ca^{2+} ions forming sparingly soluble $CaCO_3$ (solubility product $K_{sp}=3.36\cdot10^{-9}$ at 25°C [23]). As a consequence the Ca^{2+} concentration in the pore solution decreases and, in turn, $Ca(OH)_2$ (Portlandite, solubility product $K_{sp}=5.02\cdot10^{-6}$ at 25°C [23]) is dissolved. The possible formation of the $CaCO_3$ coating on the Portlandite crystals [27, 28] can however, act as a barrier and hinder further Portlandite dissolution. In this regard, it may also be possible that the dissolution of $Ca(OH)_2$ may be partially diffusion-controlled [29]. Thus, the kinetically limited dissolution of Portlandite, specially under conditions of accelerated carbonation, may be the reason why the pH of the pore solution initially decreased down to pH ≈12 before it increased and remained constant at pH ≈12.5 (Fig. 5).

Once all the $Ca(OH)_2$ is consumed, the pH of the pore solution decreases down to pH ≈10. In this case, the reactions involve other cement phases, e.g. mainly C–S–H [27, 28]. Measurements with the IrO_x sensors results, at least, in a factor of 3 for the time needed to reach pH 9.7 compared to the time needed to reach pH 12.5 (compare results regarding the sensors embedded at 4 and 15 mm, Fig. 6). For the sensors embedded at 5, 6, 10 and 20 mm cover depths, it can be seen that pH 9.7 has not been reached yet (Fig. 5). From the above described carbonation mechanism, it is believed that early carbonation with the first pH decrease from pH≈13.5 to pH≈12.5 is mainly governed by the kinetics of CO_2 transport into the pore system (diffusion-controlled), while the second pH decrease from 12.5 to about 9 is additionally determined by the kinetics of reaction of CO_2 with the solid alkali reserve of the cement paste, resulting in much longer times. In this case, the pH drop is expected to occur later for higher amounts of Portlandite.

Additionally, it is known that carbonation propagation becomes slower with time, e.g. due to a densification of the pore structure over time [3], and possibly due to changes in cement microstructure during carbonation [30]. This may result into slower diffusion of CO_2 and longer times to reach pH 12.5. This could explain slower and gradual carbonation propagation at pH≈12.5 at larger cover depths (e.g. sensors embedded at 10, 15 and 20 cover depths in Fig. 5) and stepwise and faster propagation at shallow cover depths (e.g. sensor embedded at 4, 5 and 6 cover depths in Fig. 5), as observed by Glass et al. [31] when studying the acid neutralization behavior of cement paste by adding different amounts of acid stepwise.

4.2 Comparison between pH determined with embedded IrO_x sensors and by means of pH-indicator solution

From Fig. 6, clear differences can be observed regarding carbonation propagation measured with the sensor at pH≈12.5 and with the indicator test at pH 9-10. Apart from differences in the carbonation process (section 4.1), it is believed that these differences are also due to the measuring method. We believe that the electrode detects the pH locally in the pore solution, whereas the indicator sprayed on a freshly split surface can become blue (pH>9-10) when not yet fully carbonated Portlandite particles react with the indicator solution. Thus, the sensor may show a pH drop earlier than or at the same time as the indicator, but in principle never later.

Additionally, it should be noted that the differences may also be due to the accuracy of the method used. The maximum error for the pH expected is ca. 0.5 pH units [17], whereas the accuracy of the pH indicator is roughly 1 pH unit and the carbonation front determined with the indicator on OPC mortar is quite blurry (see the high standard deviations in Fig. 6), a fact that can be associated to a transition zone (thickness of about 2 - 3 mm) where $CaCO_3$ and $Ca(OH)_2$ are coexisting [27, 28].

4.3 Implications and outlook of the obtained results

4.3.1 Relation to natural carbonation

The relationship between the carbonation depth *d* and the square root of time, shown in Fig. 6, can be described with a linear law, in the form [3]:

$$d = K_{\mathrm{acc,\ 4\%}} \cdot \sqrt{\mathrm{t}} \qquad (5)$$

where $K_{acc,4\%}$ is the carbonation coefficient in the present accelerated conditions. For the carbonation front determined with the indicator test (pH≈9-10), $K_{acc,4\%}$ is equal to approx. 16 mm/year$^{1/2}$ (corresponding to 0.81 mm/day$^{1/2}$), in agreement with values reported in the literature for porous concrete [32]. For the carbonation front at pH 12.5 determined with the sensor, $K_{acc,4\%}$ is approx. 31 mm/year$^{1/2}$ (corresponding to 1.72 mm/day$^{1/2}$), thus much higher than the results of the indicator test.

Based on the experimentally determined carbonation coefficients, an extrapolation to much longer times can be made. The result is shown in Fig 7a both for the carbonation front associated with pH 12.5 and the carbonation front determined with the indicator test at pH 9-

10. In Fig. 7b, a schematic representation of the different carbonation fronts at pH 12.5 and at pH 9-10 is shown.

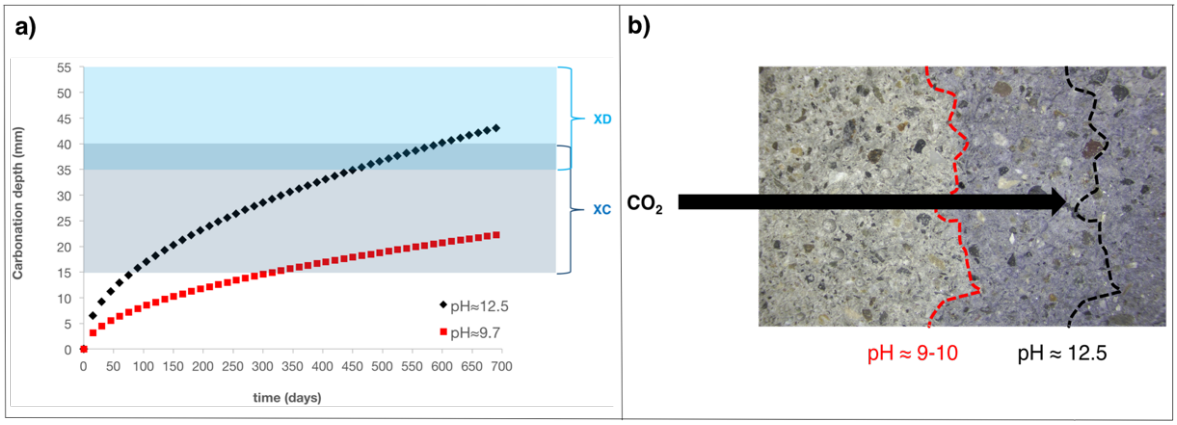

Fig. 7 (a) Carbonation front associated with pH 12.5 (IrO_x sensor) and with pH≈9-10 (indicator spray test) from the fitted curves obtained from accelerated carbonation tests (Fig. 6). The range of minimum cover depth for XC (carbonation-induced-corrosion) and for XD (chloride induced corrosion) exposure classes according to EN 206-1 [33] are also indicated in the graph (b) Schematic representation of the carbonation front in concrete at a certain point in time.

From Fig. 7a, it can be seen that for the present experimental conditions, the carbonation depth at pH≈12.5 will reach a cover depth of 15 mm (minimum cover depth for exposure condition XC3) in about 3 months, whereas it will take about one year to detect a pH below 10 at the same cover depth with the indicator spray test. For natural carbonation in sheltered outdoor conditions, the carbonation coefficients have been found to be about 6-8 times lower compared to accelerated carbonation with 4% CO_2 (for relatively porous Portland cement concrete (w/c = 0.65)) [32]. With lower w/c ratio, this factor increased. As a first-hand estimate for our case, with a relatively porous mortar (Portland cement, w/c=0.5, only one week curing), this factor may be approx. 10. Thus, to reach pH 12.5 at 15 mm, about 23 years would be necessary, whereas this time would be extended to about 100 years to reach full carbonation at pH 9-10 (detectable with the indicator spray test). Denser concrete pore structures and exposure to unsheltered conditions might significantly increase these times. Nevertheless, this indicates that after only a few decades (long before the designed service life), the concrete is carbonated down to pH 12.5 at cover depths in agreement with EN 206-1 for XC exposure conditions.

4.3.2. Implication on corrosion of the reinforcement

The significantly shorter time for the concrete to be carbonated down to pH 12.5 (from initially about 13.5) than down to pH 9-10 has implications for the corrosion of the embedded reinforcing steel bars. The indicator test used in condition assessment of structure [34] with a

colour change in the range of pH 9-10 is usually believed to confirm that the reinforcement is still in alkaline concrete (tacitly assumed as about 13.5 in OCP concrete). However, the level of alkalinity may play a crucial role in the presence of even low amounts of chloride, where a difference between pH 13.5 and 12.5 can be decisive. Based on the critical ratio of chloride and hydroxide ions needed to trigger corrosion, as proposed by Hausmann [4] ($Cl^-/OH^- = 0.6$), a pH of about 13.5 corresponds to a critical chloride concentration for corrosion initiation of about 0.2 mol·L^{-1}. At pH 12.5, on the other hand, the tolerable chloride concentration is one order of magnitude lower, that is only about 0.02 mol·L^{-1}. This value might be reached due to chlorides in the raw materials or as free chloride content when 0.4% total chloride ions by weight of cement are present as is apparent from various studies investigating chloride binding in concrete [35, 36]. Thus, chloride-induced corrosion of the reinforcement in structures exposed to carbonation might occur at much lower chloride concentrations than usually considered for “uncarbonated” concrete. However, this situation is usually not studied in laboratory testing of chloride induced corrosion; due to the comparatively short durations of testing, the pH at the steel surface may still be above 13.

4.3.3 Outlook: study of blended cements

Another possible application of the pH sensors presented in this work could be the study of the kinetics of carbonation of blended cements. In these cements, the Portlandite content ($Ca(OH)_2$ phase) is lower due to the substitution of the clinker by SCMs. While this may have only a small influence on the pH of the pore solution, the pH buffer capacity around pH≈12.5 may be significantly impaired. Our sensors permit directly characterizing this by measuring the time during which a certain system resists a decrease in pH below 12.5. In contrast to titration methods or thermodynamic modeling, our sensors, being embedded at different depths, permit assessing the combined effects of transport of CO_2 through the increasingly carbonated and thus microstructurally affected cover as well as the kinetics of the carbonation reactions in a given real system. This is expected to increase considerably the practice-relevance of the results.

5. Conclusions

In this work, we used embedded IrO_x sensors to continuously monitor in-situ the pH in mortar specimens subjected to accelerated carbonation. To this aim, we suggested an iterative calculation algorithm that takes into diffusion potentials and thus permits determining the pH at any depth; this algorithm forms an essential part of the pH measuring method.

The main implications from the obtained results are:

- The shape of the pH vs time curve upon carbonation was found to exhibit a number of characteristic features including a pH decrease in steps, with the pH remaining on certain levels for different amounts of times, and a dependency on the cover depth. These pH vs time measurements can give substantial insight in to the process of carbonation;

- The stepwise decrease was found in agreement with literature data, e.g. from “titration tests” or thermodynamic modeling. In contrast to these approaches, however, the used pH sensors also permit considering time-dependent processes, such as CO_2 transport or the kinetics of phase transformations in the cement paste;

- We suggest that the measurement of the time during which the pH of the pore solution remains constant at pH 12.5 while cement paste carbonates may present a novel means to characterize blended cements (with lower Porlandite content);

- The carbonation front at pH 12.5 is much ahead of the front at pH 9-10, which is the carbonation front usually determined with common indicator spray tests. At pH 12.5, the risk of chloride-induced corrosion greatly increases, but this situation is usually not detected in the field and rarely studied in laboratory testing. The possibility to monitor pH evolution over time under field conditions has major implications for the durability of reinforced concrete structures.

6. References

1. Condition control and assessment of reinforced concrete structures exposed to corrosive environments (2011), State-of-art report, International Federation of Structural Concrete (FIB), Task group 5.8.
2. A.M. Neville (2011), Properties of Concrete, 5th ed., Harlow, Pearson Education Limited.
3. L. Bertolini, B. Elsener, P. Pedeferri, E. Redaelli, R.P. Polder (2013), Corrosion of steel in concrete, second ed., Weinheim, Wiley.
4. D.A. Hausmann (1967), Corrosion of steel in concrete. How does it occur?, J. Mater. Prot., 6, 19-23.
5. G. Plusquellec, M.R. Geiker, J. Lindgård, J. Duchesne, B. Fournier, K.D. Weerdt (2017), Determination of the pH and the free alkali metal content in the pore solution of concrete: Review and experimental comparison, Cem. Concr. Res, 96, 13–26. doi: 10.1016/j.cemconres.2017.03.002.
6. A. Behnood, K.V. Tittelboom, N.D. Belie (2016), Methods for measuring pH in concrete: A review, Constr. Build. Mater., 105, 176–188. doi: 10.1016/j.conbuildmat.2015.12.032.

7. M.-Y. Yu, J.-Y. Lee, C.-W. Chung (2010), The application of various indicators for the estimation of carbonation and pH of cement based materials, J. Test. Eval., 38, 534-540.
8. E. Liu, M. Ghandehari, C. Brückner, G. Khalil, J. Worlinsky, W. Jin, A. Sidelev, M.A. Hyland (2017), Mapping high pH levels in hydrated calcium silicates, Cem. Concr. Res, 95, 232-239. doi: 10.1016/j.cemconres.2017.02.001.
9. S. Yao, M. Wang, M. Madou (2001), A pH electrode based on melt-oxidized iridium oxide, J. Electrochem. Soc., 148, H29-H36. doi: 10.1149/1.1353582.
10. W.-D. Huang, H. Cao, S. Deb, M. Chiao, J.C. Chiao (2011), A flexible pH sensor based on the iridium oxide sensing film, Sens. Actuators, A, 169, 1-11. doi: 10.1016/j.sna.2011.05.016.
11. S.A.M. Marzouk, S. Ufer, R.P. Buck, T.A. Johnson, L.A. Dunlap, W.E. Cascio (1998), Electrodeposited iridium oxide pH electrode for measurement of extracellular myocardial acidosis during acute ischemia, Anal. Chem., 70, 5054-5061. doi: 10.1021/Ac980608e.
12. W. Olthuis, M.A.M. Robben, P. Bergveld, M. Bos, W.E.V.d. Linden (1990), pH sensor properties of electrochemically grown iridium oxide, Sens. Actuators, B, 2, 247-256. doi: 10.1016/0925-4005(90)80150-X.
13. R.-G. Du, R.-G. Hu, R.-S. Huang, C.-J. Lin (2006), In situ measurement of Cl^- concentrations and pH at the reinforcing steel: concrete interface by combination sensors, Anal. Chem., 78, 3179-3185. doi: 10.1021/ac0517139.
14. S.-G. Dong, C.-J. Lin, R.-G. Hu, L.-Q. Li, R.-G. Du (2011), Effective monitoring of corrosion in reinforcing steel in concrete constructions by a multifunctional sensor, Electrochim. Acta, 56, 1881-1888. doi: 10.1016/j.electacta.2010.08.089.
15. M. Wang, S. Yao, M. Madou (2002), A long-term stable iridium oxide pH electrode, Sens. Actuators, B, 81, 313-315. doi: 10.1016/S0925-4005(01)00972-8.
16. M. Wang, S. Yao (2003), Carbonate-Melt Oxidized Iridium Wire for pH Sensing, Electroanalysis, 15, 1606-1615. doi: 10.1002/elan.200302723.
17. Y. Seguí Femenias, U. Angst, B. Elsener (2017), Monitoring pH in corrosion engineering by means of thermally-produced iridium oxide electrodes, Mater. Corros. (accepted).
18. Y. Seguí Femenias, U. Angst, F. Caruso, B. Elsener (2016), Ag/AgCl ion-selective electrodes in neutral and alkaline environments containing interfering ions, Mater. Struct., 49, 2637–2651. doi: 10.1617/s11527-015-0673-8.
19. U. Angst, Ø. Vennesland, R. Myrdal (2009), Diffusion potentials as source of error in electrochemical measurements in concrete, Mater. Struct., 42, 365-375. doi: 10.1617/s11527-008-9387-5.
20. R. Myrdal (1996), Phenomena that disturb the measurement of potentials in concrete, Corrosion/96, NACE International, Paper No.339.
21. R. Myrdal (1997), Potential gradients in concrete caused by charge separations in a complex electrolyte, Corrosion/97, NACE International, Paper No.278.
22. A.J. Bard, L.R. Faulkner (2001), Electrochemical methods: fundamentals and applications, second ed., New York, Willey.
23. W.M. Haynes (2013-2014), Handbook of chemistry & physics, ninety fourth ed., Boca Raton, CRC Press.
24. U. Angst, B. Elsener, R. Myrdald, Ø. Venneslanda (2010), Diffusion potentials in porous mortar in a moisture state below saturation, Electrochim. Acta, 55, 8545–8555. doi: 10.1016/j.electacta.2010.07.085.
25. A. Atkinson, A.K. Nickerson (1984), The diffusion of ions through water-saturated cement, J. Mater. Sci., 19, 3068–3078. doi: 10.1007/BF01026986.
26. Z. Shi, B. Lothenbach, M.R. Geiker, J. Kaufmann, A. Leemann, S. Ferreiro, J. Skibsted (2016), Experimental studies and thermodynamic modeling of the carbonation of

Portland cement, metakaolin and limestone mortars, Cem. Concr. Res, 88, 60-72. doi: 10.1016/j.cemconres.2016.06.006.
27. M. Thiery, G. Villain, P. Dangla, G. Platret (2007), Investigation of the carbonation front shape on cementitious materials: Effects of the chemical kinetics, Cem. Concr. Res, 37, 1047-1058. doi: 10.1016/j.cemconres.2007.04.002.
28. Geoffrey W. Groves, Adrian Brough, Ian G. Richardson, C.M. Dobson (1991), Progressive changes in the structure of hardened C3S cement pastes due to carbonation, J. Am. Ceram. Soc., 74, 2891-2896. doi: 10.1111/j.1151-2916.1991.tb06859.x.
29. D.E.Giles, I.M.Ritchie, B.-A.Xu (1993), The kinetics of dissolution of slaked lime, Hydrometallurgy, 32, 119-128. doi: 10.1016/0304-386X(93)90061-H.
30. A. Hidalgo, C. Domingo, C. Garcia, S. Petit, C. Andrade, C. Alonso (2008), Microstructural changes induced in Portland cement-based materials due to natural and supercritical carbonation, J. Mater. Sci., 43, 3101-3111. doi: 10.1007/s10853-008-2521-5.
31. G.K. Glass, B. Reddy, N.R. Buenfeld (2000), Corrosion inhibition in concrete arising from its acid neutralisation capacity, Corros. Sci., 42, 1587–1598. doi: 10.1016/S0010-938X(00)00008-1.
32. A. Leemann, F. Moro (2016), Carbonation of concrete: the role of CO2 concentration, relative humidity and CO2 buffer capacity, Mater. Struct., 50. doi: 10.1617/s11527-016-0917-2.
33. CEN/TC-104 (2000), EN 206-1 Concrete – Part 1: Specification, performance, production and conformity. doi:
34. SHRP-S-337 (1993), Cathodic protection of reinforced concrete bridge elements: a state of the art report, Strategic Highway Research Program, National Research Council.
35. T. Luping, L.O. Nilsson (1993), Chloride binding capacity and binding isotherms of OPC pastes and mortars, Cem. Concr. Res., 23, 247-253. doi: 10.1016/0008-8846(93)90089-R.
36. J. Tritthart (1989), Chloride binding in cement I. Investigations to determine the composition of porewater in hardened cement, Cem. Concr. Res, 19, 586-594. doi: 10.1016/0008-8846(89)90010-0.

PAPER V

Y. Seguí Femenias, U. Angst, B. Elsener (2017)

Durability monitoring of reinforced concrete

In *SMAR 2017 - International Conference on Smart Monitoring, Assessment and Rehabilitation of Civil Structures*, Zürich (accepted).

SMAR 2017 – Fourth Conference on Smart Monitoring,
Assessment and Rehabilitation of Civil Structures

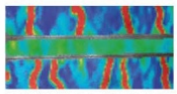

Durability monitoring of reinforced concrete

Yurena Seguí Femenias[1], Ueli Angst[1], and Bernhard Elsener[1,2]

[1] ETH Zürich, Institute for Building Materials (IfB), Stefano-Franscini-Platz 3, 8093 Zurich, Switzerland
[2] University of Cagliari, Department of Chemical and Geological Sciences, 09100 Monserrato (CA), Italy

ABSTRACT: Corrosion is the main cause of failure in steel reinforced concrete structures. In a non-carbonated chloride-free concrete, the steel reinforcement stays passive; however, this passivity can be destroyed due to ingress of chloride ions or carbonation of the cement paste. In this work, Ag/AgCl ion-selective electrodes (Ag/AgCl ISE), used as chloride sensor, and thermally oxidized iridium electrodes (IrO_x), used as pH sensor, have been developed to be embedded in concrete. Both sensors were calibrated in solutions simulating the concrete environment and tested in mortar samples in the laboratory. The results obtained show that the studied electrodes can be successfully used to monitor chloride concentrations and changes in pH in the concrete pore solution.

1 INSTRODUCTION

Reinforced concrete is the most common building material used in public infrastructures and private buildings. In the alkaline concrete environment, reinforcing steel is protected from corrosion by a thin oxide film (passive film). The reinforcing steel can, however, be depassivated when the concrete carbonates (carbonation-induced corrosion) (Elsener et al., 2013) or when a certain concentration of chlorides reach the reinforcement (chloride-induced corrosion) (Elsener et al., 2013).

Concrete structures damaged by reinforcement corrosion have to be repaired in order to reach their expected service life. In order to apply protective and repair techniques in the most simple and cost-effective way, detection of corrosion risk and/or determination of the rate of deterioration are important (Gulikers, 2016). In fact, most of the current monitoring methods in concrete structures aim at measuring the relevant parameters regarding corrosion risk and propagation. For example, the so-called anode-ladder system is based on the measurement of a macrocell current (established between steel reinforcement and anode-ladder) and it allows monitoring the time to depassivation (Raupach et al., 1997, Raupach et al., 2001). There are also several sensors based on in-depth resistivity measurements, such as the so- called multi-ring electrode (Schiessl et al., 1995), that provide information on the corrosion risk. Other techniques are based on embedded reference electrodes. Their use permit obtaining electrochemical data (such as steel potential and linear polarization resistance), from which the time to depassivation and corrosion rate is calculated (Elsener et al., 2013).

In this work, Ag/AgCl ion-selective electrodes (Ag/AgCl ISE) and thermally oxidized iridium electrode IrO_x, to be used as chloride and pH sensors respectively, have been developed. Whereas the use of the Ag/AgCl ion-selective electrode (Ag/AgCl ISE) is a well-established method to measure the free chloride concentration in the concrete pore solution (Angst et al.,

2010, Jin et al., 2017, Seguí Femenias et al., 2015), a reliable pH sensor to be embedded in concrete still does not exist (Plusquellec et al., 2017).

These sensors are used for the non-destructive in-situ measurement (monitoring) of the two most relevant parameters for corrosion, i.e., the chloride concentration and pH of the pore solution. This would permit predicting the service life of the structure in a non-destructive and more accurate way.

2 THEORETICAL BACKGROUND

2.1 The silver/silver chloride ion-selective electrode

The silver/silver chloride ion-selective electrode (Ag/AgCl ISE) used in this work is a commercial electrode consisting of a silver wired covered by a layer of silver chloride. In presence of chlorides, the potential response of the Ag/AgCl ISE is (Koryta, 1972):

$$E_{Ag/AgCl\ ISE} = E^0_{Ag/AgCl\ ISE} - \frac{RT}{F} \ln a_{Cl^-} \quad (1)$$

where R is the gas constant, F the Faraday constant, T the absolute temperature, and $E^0_{Ag/AgCl\ ISE}$ is the electrode standard potential ($E^0_{Ag/AgCl}$ =225.6 mV vs. Ag/AgCl/sat. KCl at 20 °C (Shreir, 1994). The Ag/AgCl ISE potential also depends on temperature (Shreir, 1994) and other ions that may be dissolved in the test solution (Seguí Femenias et al., 2015). Regarding the interference of other ions, the Ag/AgCl ISEs have been shown to be feasible for monitoring of chloride concentrations in concrete structures, except in presence of sulfide ions (Seguí Femenias et al., 2015).

2.2 The iridium oxide electrode

Thermally oxidized iridium wires were produced based on the procedure reported in (Yao et al., 2001). The details of the production protocol are reported in the following work (Seguí Femenias et al., 2017). The most common accepted pH-sensing mechanism of thermally oxidized iridium is based on the transition between Ir (IV) to Ir (III), involving the participation of one proton H^+. The Nernst equation that dictates the potential of the IrO_x is written as (Pourbaix, 1974):

$$E_{IrO_x} = E^0_{IrO_x} - \frac{RT}{F} pH \quad (2)$$

Different electrode standard potentials $E^0_{IrO_x}$ and slopes for the E_{IrO_x}-pH response are obtained depending on the production method and exposure conditions (Kakooei et al., 2013, Olthuis et al., 1990, Trasatti, 1991). In this work, the IrO_x electrodes were immersed in alkaline solution (pH values between 9 and 13.5) for months to simulate the concrete environment. The iridium oxide pH-sensors (IrO_x electrodes) were then calibrated in pH values between 13.5 and 9.

2.3 Potential response of the electrodes

The electrodes used in this work (silver/silver chloride ISE and iridium oxide electrode IrO_x) were calibrated in solution before being embedded in concrete. Figure 1a shows experimental data on the potential $E_{Ag/AgCl\ ISE}$ of the Ag/AgCl ISE as a function of the logarithm of the chloride activity as reported in previous works (Seguí Femenias et al., 2015). Figure 1b shows

experimental data on the potential E_{IrO_x} of an iridium oxide electrode IrO_x as a function of the pH of the solution. The obtained values (from the linear fit) for the E_{IrO_x}-pH intercept ($E^0_{IrO_x}$) and for the E_{IrO_x}-pH slope are 0.723 V (vs. Ag/AgCl/sat. KCl) and -0.053 V/pH respectively.

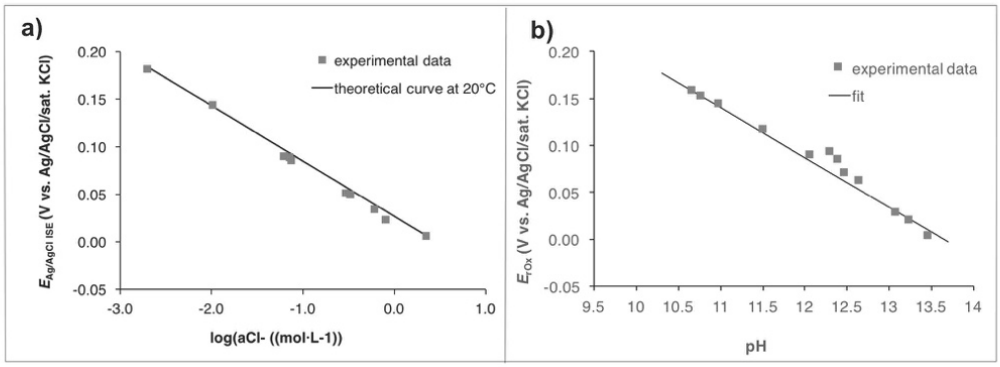

Figure 1. (a) Potential $E_{Ag/AgCl\ ISE}$ of the Ag/AgCl ISE as a function of the logarithm of the chloride activity, together with the theoretical curve at 20°C (Seguí Femenias et al., 2015) (b) Potential E_{IrO_x} of an IrO_x electrode (IrO_x 2, in Figure 3) as a function of the pH of the solution, together with the calculated linear fit.

3 METHODS

Two rectangular mortar prism were produced with embedded Ag/AgCl ISEs and IrO_x electrodes in each case. The mortar mix proportions were cement/water/sand 1: 0.5: 2 with CEM I 52.5, with sand size <1mm. For the first sample, three Ag/AgCl ISEs (ISE 1, ISE 2 and ISE 3 in Figure 2a) and three structural steel rods (steel 1, steel 2 and steel 3 in Figure 2a) were embedded. For the second sample, three IrO_x electrodes (IrO_x 1, IrO_x 2 and IrO_x 3 in Figure 2b) were embedded. In both cases, an internal reference electrode was also embedded (Figure 2a and 2b).

The samples were cured for one week at 95%RH and 21°C and then all the surfaces (with the exception of one surface, parallel to the embedded sensors) were painted with an epoxy-resin. The surface of the cube with embedded ISEs that was not coated was put in contact with synthetic pore solution (0.2 mol·L^{-1} KOH 0.15 mol·L^{-1} NaOH sat. $Ca(OH)_2$) containing 2 mol·L^{-1} NaCl, so one-dimensional chloride transport process occurred. The sample with the embedded IrO_xs was placed in a carbonation chamber (65%RH, 21°C and 4% CO_2) so one-dimensional carbonation occurred though the non-coated surface. The main features of the two set-ups are shown in Figure 2. In both cases, the mentioned sensors were embedded in the mortar at different cover depths, in order to monitor the penetration of the corrosive agent.

In both cases, a reference electrode was embedded in the mortar in order to be used as internal reference electrode (Figure 2a and 2b). The potential of the ISEs, steel rods (Figure 2a) and IrO_x electrodes (Figure 2b) was continuously measured versus this embedded reference electrode. In both cases, the potential of the internal reference was periodically measured (and corrected for the liquid junction potential (Angst et al., 2008)) with an external reference electrode that was

inserted in the upper opening ("hole for contact with external RE" in Figure 2a and 2b) on the sample surface.

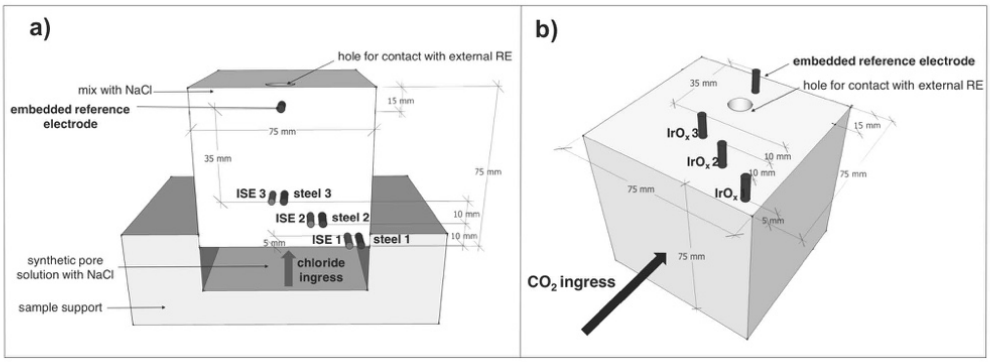

Figure 2. Main features of the set-up used to monitor (a) chloride ingress and corrosion state with embedded Ag/AgCl ISEs and steel rods respectively (b) carbonation propagation with embedded IrO_x electrodes. All the surfaces were coated with epoxy resin with the exception of the surface of chloride ingress (a) and CO_2 ingress (b).

All the experiments were carried out at room temperature (20-21 °C). After ca. 140 days, the experiment with embedded ISEs ended and slices of approximately 5mm-thick containing each embedded ISE/steel rod were cut and grinded. Approximately 20 g of mortar powder were taken from each slice and the total chloride content was determined by the acid digestion / potentiometric titration method. The experiment with embedded IrO_x electrodes was finished after ca. 170 days. The sample was then split in half (perpendicular to the surface of CO_2 ingress) and the carbonation front was determined by spraying thymolphthalein pH-indicator.

4 RESULTS AND DISCUSSION

4.1 Ag/AgCl ISEs embedded in concrete to monitor chloride ingress and corrosion state

Figure 3a shows the chloride concentration as a function of time for the Ag/AgCl ISE at each cover depth. Figure 3b shows the chloride concentration as a function of cover depth for some selected times (20, 60, 100, and 140 days). Figure 3c shows the chloride concentration (from the last potentiometric measurement performed) as a function of the total chloride content. Note that the for the calculation of the concentrations, the activity coefficients of chloride ions in cement paste were taken from (Vera et al., 2000).

From Figure 3a, the chloride concentration increased with time, especially during the first 60 days. The chloride concentration is markedly higher for the smaller cover depths. This can be clearly seen in Figure 3b.

Figure 3c shows the relation between the chloride concentration measured with the ISEs (free chlorides) and the results obtained from the total chloride content. The total chloride content includes both the free (dissolved in the pore solution) and the bound chlorides (i.e., those bound to the hydration products of the binder in concrete). In the present study, relatively high chloride concentrations were achieved within short exposure time, mostly due to the low cover depth. The high concentrations may explain the observed linearity in the relationship between free and

total chlorides. At low to moderate chloride concentrations, this relationship is well-known to be nonlinear (Luping et al., 1993).

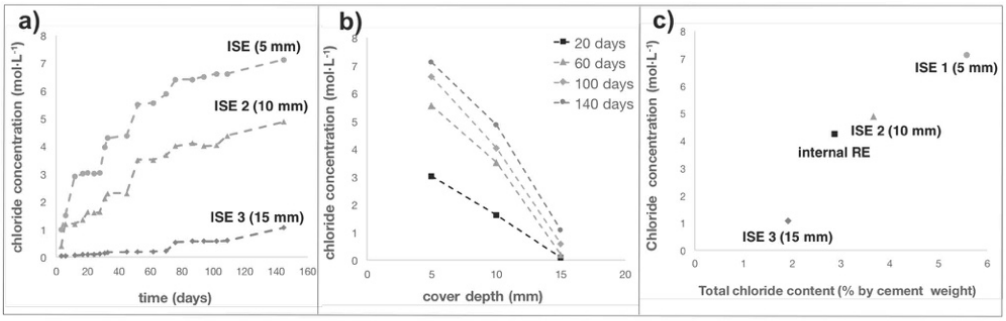

Figure 3. (a) Chloride concentration as a function of time for the Ag/AgCl ISE at each cover depth (5, 10 and 15 mm) (b) Chloride concentration as a function of cover depth for some selected times (20, 60, 100, and 140 days) (c) Chloride concentration (from the last potentiometric measurement performed) as a function of the total chloride content at each ISE location (Figure 2).

Figure 4 shows the steel potential versus the chloride concentration at each cover depth.

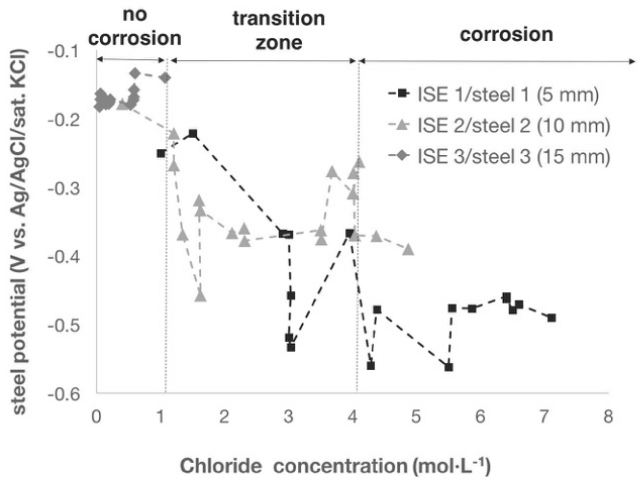

Figure 4. Steel potential vs. chloride concentration at each cover depth (5, 10, and 15 mm). The zones defined in the graph (no corrosion, transition zone, corrosion) schematically represent the corrosion state of the steel (compare text).

From Figure 4, it can be seen that for chloride concentrations below 1 mol·L^{-1} (no corrosion), the steel potential was relatively constant; variations in potential were smaller than 50 mV. For chloride concentrations between 1 and 4 mol·L^{-1}(transition zone), the steel potential overall decreased but it occasionally increased. Transition from passive to active state is not immediate and it is believed that this behaviour was due to local depassivation and further repassivation. At

chloride concentrations above 4 mol·L^{-1} (corrosion zone) the steel potential had decreased at least 200 mV with respect to the initial value. Such potential differences are usually related to corrosion initiation (Elsener et al., 2013).

From the results presented in this test, it can be seen that the combined measurement of steel potential and chloride concentration provide reliable data for assessing the corrosion risk of the reinforcement.

4.2 IrO_x embedded in concrete to monitor carbonation propagation

Figure 5 shows the potential of the IrO_x electrode embedded at 15 mm cover depth (IrO_x 2 in Figure 2b) and the pH as a function of exposure time in the carbonation chamber. The potential measured was corrected for the diffusion potential (Angst et al., 2008) established between IrO_x and internal reference electrode due to the pH gradient. The pH was calculated from the calibration curve shown in Figure 1b.

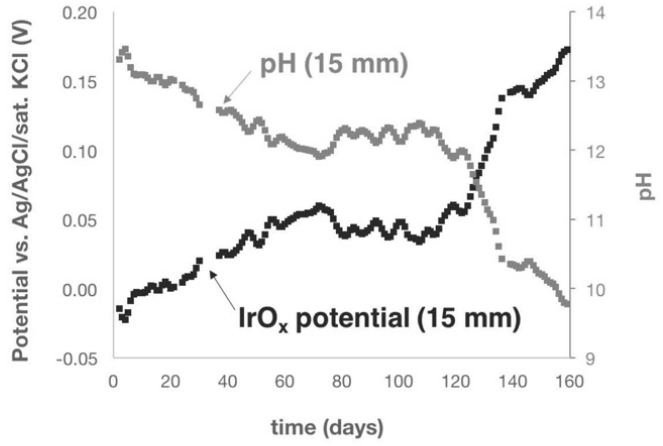

Figure 5. Potential of the IrO_x electrode embedded at 15 mm cover depth (IrO_x 2 in Figure 2b) and the calculated pH as a function of time of exposure in the carbonation chamber.

With this experimental approach, combining an embedded reference electrode and an embedded pH sensor, it was possible to follow for the first time the change of the pore solution pH in the mortar sample continuously and in-situ (directly in the carbonation chamber), showing interesting results on the carbonation process. The IrO_x potential increased by 50 mV during the first 60 days, corresponding to a pH decrease from 13.4 to approximately 12.5 (Figure 5). For the following 60 days, the pH remained quite stable at 12.5. Then a rapid drop of pH was observed: after 160 days in the carbonation chamber, the pH decreased to ca. 10 (Figure 5).

The interpretation of these results is similar to a titration curve. The initial pH decrease down to ca. 12.5 was due to the consumption of the alkalinity from the KOH and NaOH in the pore solution. The constant pH registered afterwards is due to the gradual consumption of the alkaline reserve provided by $Ca(OH)_2$, calcium hydroxide being the hydration product providing the buffer capacity of the concrete pore solution (Glass et al., 2000). The marked pH decrease observed afterwards is probably due to the rapid consumption of the pore solution alkalinity in the absence of a buffer. The results from the thymolphthalein test, performed at the end of the

exposure testing showed a carbonation front of ca. 12-15 mm; thus, in agreement with the results of the sensors.

5 CONCLUSIONS AND OUTLOOK

The results obtained in this work show that the Ag/AgCl ISE and the IrO_x electrodes can be successfully used to monitor changes in chloride content and pH continuously and in-situ in the concrete pore solution of reinforced concrete. The sensors have shown to work reliably also at relative humidity of 65%. The possible applications are:

a) *Research*: the pH sensor can be applied to study the carbonation rate of new binders with lower clinker content. In contrast to the laborious traditional, destructive tests with phenolphthalein spraying on the concrete surface that give only a yes/no answer, with the in-situ sensors the carbonation process can be followed more in detail. It will be possible to relate the time at pH 12.5 (consumption of the $Ca(OH)_2$ buffer) to the amount of clinker in the cement.

b) *Condition monitoring and assessment*: knowing the pH and/or the chloride concentration at different depths in reinforced concrete over time will allow predicting further propagation of the CO_2 or chloride ingress into concrete. This would be especially useful to predict residual service life of structures exposed to high chloride concentrations (de-icing salts) or high CO_2 concentrations (road tunnels). Figure 6 shows two examples of how the sensors may be applied in engineering structures.

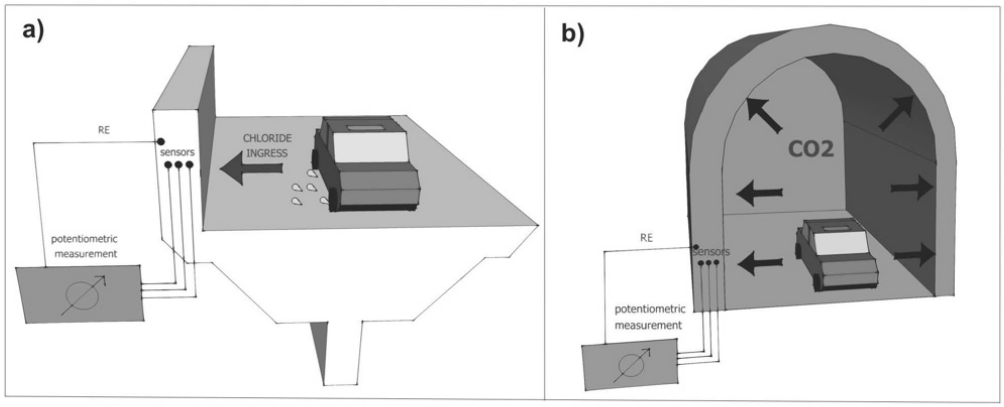

Figure 6. Schematic depiction of the set-up proposed to detect chloride ions and variations in pH in concrete structures exposed to (a) high chloride concentrations (e.g., as bridges exposed to deicing salts) (b) high CO_2 concentrations (e.g., tunnels).

6 REFERENCES

Angst, Elsener, Larsen and Vennesland, 2010, Potentiometric determination of the chloride ion activity in cement based materials, *J. Appl. Electrochem.*, 40, 561-573. doi: 10.1007/s10800-009-0029-6.

Angst, Vennesland and Myrdal, 2008, Diffusion potentials as source of error in electrochemical measurements in concrete, *Mater. Struct.*, 42, 365-375. doi: 10.1617/s11527-008-9387-5.

Elsener, Bertolini, Pedeferri and Polder, 2013, *Corrosion of steel in concrete, second ed.* Weinheim: Willey.

Gulikers, 2016, What are the benefits of corrosion monitoring in concrete structures from an owner's perspective?, *Concr. Solutions*, 19-24.

Jin, Jiang and Zhu, 2017, Monitoring chloride ion penetration in concrete with different mineral admixtures based on embedded chloride ion selective electrodes, *Constr. Build. Mater.*, 143, 1-15. doi: 10.1016/j.conbuildmat.2017.03.131.

Kakooei, Ismail and Ari-Wahjoedi, 2013, An overview of pH sensors based on iridium oxide: fabrication and application, *Int. J. Mat. Sci Innovations,* 1, 62-72.

Koryta, 1972, Theory and applications of ion-selective electrodes, *Anal. Chim. Acta,* 61, 329–411. doi: 10.1016/S0003-2670(01)95071-8.

Luping and Nilsson, 1993, Chloride binding capacity and binding isotherms of OPC pastes and mortars, *Cem. Concr. Res.*, 23, 247-253. doi: 10.1016/0008-8846(93)90089-R.

Olthuis, et al., 1990, pH sensor properties of electrochemically grown iridium oxide, *Sens. Actuators, B,* 2, 247-256. doi: 10.1016/0925-4005(90)80150-X.

Plusquellec, et al., 2017, Determination of the pH and the free alkali metal content in the pore solution of concrete: Review and experimental comparison, *Cem. Concr. Res,* 96, 13–26. doi: 10.1016/j.cemconres.2017.03.002.

Pourbaix, 1974, Atlas of electrochemical equilibria in aqueous solutions, *Pergamon Press,* 2nd ed.

Raupach and Schiessl, 1997, Monitoring system for the penetration of chlorides, carbonation and the corrosion risk for the reinforcement, *Constr. Build. Mater.*, 11, 207-214. doi: 10.1016/S0950-0618(97)00039-1.

Raupach and Schießl, 2001, Macrocell sensor systems for monitoring of the corrosion risk of the reinforcement in concrete structures, *NDT&E Int.*, 34, 435–442. doi: 10.1016/S0963-8695(01)00011-1.

Schiessl and Breit, 1995, Monitoring of the depth-dependent moisture content of concrete using multi-ring electrodes in *Concrete Under Severe Conditions: Environment and loading (Volume Two)*, United Kingdom.

Seguí Femenias, Angst, Caruso and Elsener, 2015, Ag/AgCl ion-selective electrodes in neutral and alkaline environments containing interfering ions, *Mater. Struct.* doi: 10.1617/s11527-015-0673-8.

Seguí Femenias, Angst and Elsener, 2017, Monitoring pH in corrosion engineering by means of thermally-produced iridium oxide electrodes, *(in preparation).*

Shreir, 1994, *Corrosion control* IN *Corrosion,* third ed. Oxford: Butterworth-Heinemann Ltd.

Trasatti, 1991, Physical electrochemistry of ceramic oxides, *Electrochim. Acta,* 36, 225-241. doi: 10.1016/0013-4686(91)85244-2.

Vera, et al., 2000, Chloride-ion activities in simplified synthetic concrete pore solutions: the effect of the accompanying ions, *J. Am. Ceram. Soc.*, 83 [3], 640-644. doi: 10.1111/j.1151-2916.2000.tb01245.x.

Yao, Wang and Madou, 2001, A pH electrode based on melt-oxidized iridium oxide, *J. Electrochem. Soc.*, 148, H29-H36. doi: 10.1149/1.1353582.

Appendix

Sensor system embedded in mortar exposed to chloride and CO_2 ingress

Sensor system embedded in mortar exposed to chloride and CO_2 ingress

1 Introduction and objectives

This project proposes an electrode system composed by several pH and chloride sensors embedded at different depths. This allows the simultaneous monitoring of steel potential and changes in pH and chloride concentration at the different locations. For that, an algorithm was developed so the diffusion potentials established between the electrodes can be calculated and the measured potential corrected accordingly.

The applicability of the pH sensors proved to be successful when embedded in mortar exposed to carbonation, i.e., by monitoring the decrease of pH of the pore solution, whereas the experiments with chloride sensors showed that that they can successfully be used to monitor chloride penetration in the concrete alkaline media. In this Appendix, the results from two experiments are reported. The first experiment aims at studying the potential response of the pH sensors when a mortar sample is exposed to chloride ingress and the pH is kept relatively constant. In the second experiment, the potential of embedded pH and chloride sensors is monitored while a mortar sample is carbonated. The potential response of the chloride sensors while cement paste is carbonated and in absence of chlorides is then evaluated.

2 Materials and methods

2.1 Electrodes used

2.1.1 Silver/silver chloride ion-selective electrode (Ag/AgCl ISE)

The chloride sensor used in this work is a silver/silver chloride ion-selective electrode (Ag/AgCl ISE), consisting of a silver wire covered by a layer of silver chloride. In presence of chlorides, the potential response of the Ag/AgCl ISE is [1]:

$$E_{\mathrm{Ag/AgCl\ ISE}} = E^{0}_{\mathrm{Ag/AgCl\ ISE}} - \frac{RT}{F}\ln a_{\mathrm{Cl^-}} \quad (1)$$

where R is the gas constant (8.314 J·mol-1·K-1), T is the temperature (K), F is the faraday constant (96.485·103 C·mol-1), $\mathrm{E}^{0}_{\mathrm{Ag/AgCl\ ISE}}$ is the electrode standard potential (225.6 mV vs. Ag/AgCl/sat. KCl at 20 °C [2]), and $a_{\mathrm{Cl^-}}$ is the activity of the chloride ions.

More information on the performance of these electrodes can be found in papers I-II and V.

2.1.2 Iridium/Iridium oxide (IrOx) electrodes

Iridium/iridium oxide (IrO_x) electrodes were produced by thermal oxidation of iridium wires, based on the protocol reported in [3-5]. The potential response of the produced IrO_x electrodes is a function of the pH of the exposure solution:

$$E_{\mathrm{IrO_x}} = E^0_{\mathrm{IrO_x}} - b \cdot pH \quad (2)$$

where $E^0_{\mathrm{IrO_x}}$ is the electrode standard potential and *b* is the$E_{\mathrm{IrO_x}}$-*pH* slope.

More details regarding the production protocol, conditioning and potential response (e.g. $E^0_{\mathrm{IrO_x}}$ and $E_{\mathrm{IrO_x}}$-*pH* slope) can be found in paper III.

2.1.3 Electrode set-up

Each electrode (both IrO_x and Ag/AgCl wires) was mounted inside a rigid stainless steel tube (ca. 50 mm long and 2 mm in diameter), leaving approx. 5 mm-length of the electrode wire protruding from the steel tube. This was done to minimize bending of the thin electrode wires and thus ensure accurate positioning at the desired cover depth. The steel tube and the electrode wire were galvanically separated with a Teflon tube (ca. 60 mm long and 1 mm in diameter), inserted between the steel tube and the electrode wire. To ensure that both steel and electrode wire would never be in contact, the Teflon tube was slightly longer than the steel tube and front and back ends were sealed with an epoxy resin. Fig. 1 shows a schematic representation of the set-up used to embed the electrode wires in mortar.

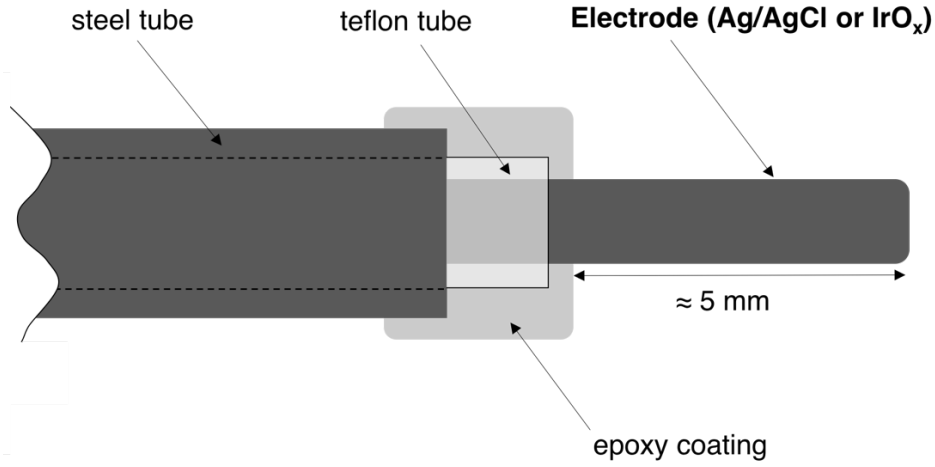

Fig. 1 Set-up used to embed the electrodes (both IrO_x and Ag/AgCl wires) in mortar.

Epoxy resin had also been applied to the tip of the IrO_x electrode after production, since it was suspected that some adherence problems of the oxide layer could happen on the edges (paper III).

2.2 Experimental set-up

2.2.1 Embedded IrOx electrodes and Ag/AgCl ISEs in mortar exposed to chloride ingress

One rectangular mortar prism was produced with three Ag/AgCl ISEs, three IrO_x electrodes and three structural steel bars (3 mm diameter) embedded at three different cover depths of 5, 8 and 12 mm. The mortar mix proportions were cement/water/sand 1: 0.5: 2 with CEM I 52.5, with sand size <1mm. One hour after the mortar prism was cast, another 25 mm thick match-cast mortar layer with an embedded Ag/AgCl ion-selective electrode was cast on top of the previous sample. In this case, the cast mortar contained 4% of admixed chlorides by weight of cement to ensure that the Ag/AgCl ISE exhibited a stable potential [6] and thus served as internal reference electrode (see section 6.1.1 of the thesis). The shortest distance between the embedded electrodes and the Ag/AgCl internal reference electrode was 40 mm. It was thus not expected that significant amounts of chlorides would diffuse from the mortar containing chlorides (with the embedded Ag/AgCl ISE) and reach the embedded electrodes (IrO_x electrodes, Ag/AgCl ISEs and steel bars).

The mortar prism was cured for one week at 95%RH and 21°C and then all the surfaces (with the exception of one surface, parallel to the embedded electrodes) were painted with an epoxy-resin. The surface of the cube that was not coated was placed in contact with simulated pore solution (0.2 mol·L^{-1} KOH 0.15 mol·L^{-1} NaOH sat. $Ca(OH)_2$) containing 0.5 mol·L^{-1} NaCl, so one-dimensional chloride transport would occur. One of the objectives of this experiment was to study the behavior of the IrO_x electrodes solely under chloride ingress and for that, gradients in pH were minimized by using the simulated pore solution. This experiment was carried out under laboratory conditions (ca. 50%RH, 21°C).

The main features of the set-up described are shown in Fig. 2. Note that the electrodes (IrO_x electrodes, Ag/AgCl ISEs and steel bars) were embedded at different cover depths in order to monitor the penetration of chlorides.

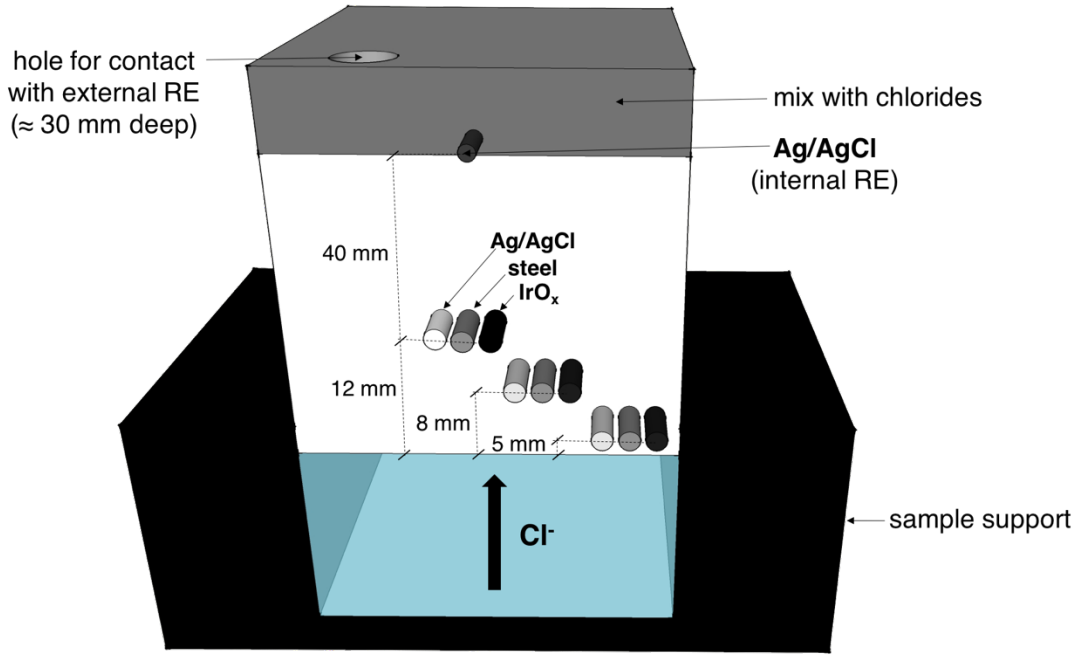

Fig. 2 Main features of the set-up used to monitor chloride ingress with embedded Ag/AgCl ISEs, IrO_x electrodes and steel rods at 5, 8 and 12 mm cover depths. All the surfaces were coated with epoxy resin with the exception of the surface of chloride ingress.

The potential of the Ag/AgCl ISEs, IrO_x electrodes, and steel bars (Fig. 2) was continuously measured versus the embedded Ag/AgCl ISE internal reference electrode. To obtain accurate measurements, the internal reference electrode was periodically calibrated. For that, the potential of the internal reference electrode $E_{\text{Ag/AgCl ISE RE}}$ was measured with a Ag/AgCl/sat. KCl external reference electrode that was inserted in an upper opening ("hole for contact with external RE" in Fig. 2) on the mortar surface. A drop of simulated pore solution (0.15 mol·L^{-1} NaOH 0.2 mol·L^{-1} KOH and sat. $Ca(OH)_2$) was used to establish electrolytic contact between the reference electrode and the mortar surface. The potential of the internal reference electrode $E_{\text{Ag/AgCl ISE RE}}$ is calculated with the following equation:

$$E_{\text{Ag/AgCl ISE RE}}(\text{Cl}^-) = E_{\text{measured}} - E_{\text{diffusion}}(\text{Cl}^-) - E_{\text{liquid junction}}(\text{Cl}^-) + E_{\text{RE}} \quad (3)$$

where E_{RE} is the potential of Ag/AgCl/sat. KCl reference electrode (0.199 V vs. SHE), $E_{\text{liquid junction}}$ is the liquid junction potential, and $E_{\text{diffusion}}$ is the diffusion potential established between the Ag/AgCl ISE internal reference electrode (located in the mortar with chlorides) and the mortar (without added chlorides) where the contact solution (0.15 mol·L^{-1} NaOH 0.2 mol·L^{-1} KOH and sat. $Ca(OH)_2$) was added.

The liquid junction potential is a diffusion potential established due to the gradient in chemical composition between the internal electrolyte of the external reference electrode (4.16 mol·L^{-1} KCl) and the test solution, i.e., contact solution (0.15 mol·L^{-1} NaOH 0.2 mol·L^{-1} KOH and sat. $Ca(OH)_2$ in this experiment. Both liquid junction potential and diffusion potential can be calculated with the Henderson equation [7]. The calculation procedure used for that is described in see section 2.3.

Between measurements, the upper opening was closed with a rubber plug to avoid carbonation of the mortar located in the hole. This experiment lasted approximately 100 days.

2.2.2 Embedded IrO_x electrodes and Ag/AgCl ISEs in mortar exposed to CO2 ingress

One rectangular mortar prism was produced with one embedded Ag/AgCl ISE (at 4 mm depth) and two embedded IrO_x electrodes (at 4 and 6 mm depths). The mortar mix proportions were cement/water/sand 1: 0.5: 2 with CEM I 52.5, with sand size <1mm. One hour after the mortar prism (with the embedded Ag/AgCl ISE and IrO_x electrodes) was cast, another 25 mm thick match-cast mortar layer with an embedded Ag/AgCl ion-selective electrode was cast on top of the previous sample. In this case, the cast mortar contained 4% of admixed chlorides by weight of cement to ensure that the Ag/AgCl ISE exhibited a stable potential [6] and thus served as internal reference electrode (see section 6.1.1 of the thesis). The shortest distance between embedded electrodes and the Ag/AgCl internal reference electrode was 50 mm. It was thus not expected that significant amounts of chlorides would diffuse from the mortar containing chlorides (with the embedded Ag/AgCl ISE) until the embedded electrodes (IrO_x electrodes and Ag/AgCl ISE).

The mortar prism was cured for one week at 95%RH and 21°C and then all the surfaces (with the exception of one surface, parallel to the embedded electrodes) were painted with an epoxy-resin. The mortar cube was then placed in a carbonation chamber (65%RH, 21°C and 4% CO_2) so one- dimensional carbonation occurred through the non-coated surface. The main features of the set-up are shown in Fig. 3. Note that the IrO_x electrodes were embedded at two different cover depths in order to monitor the carbonation front over time.

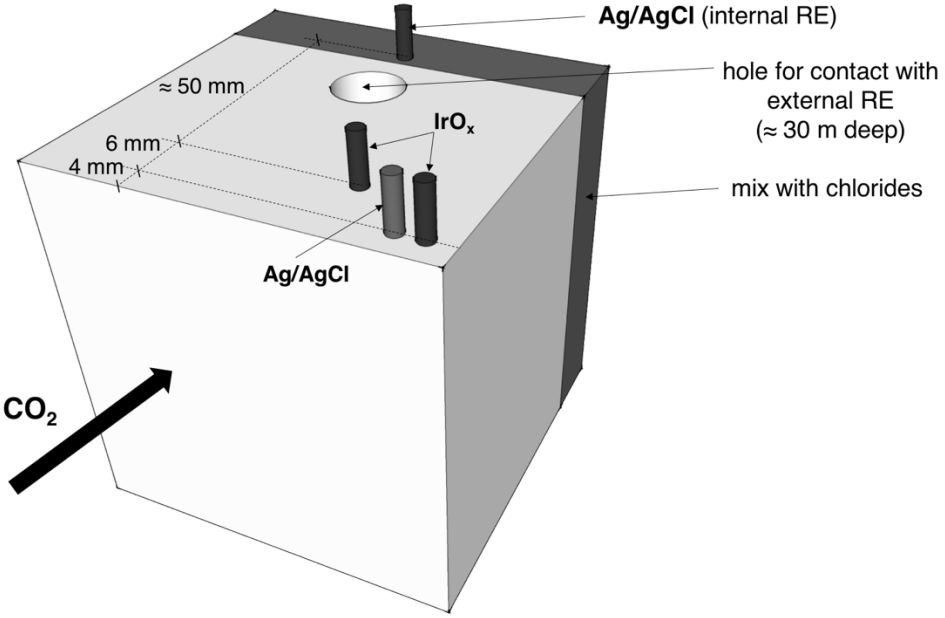

Fig. 3 Main features of the set-up used to monitor carbonation front with embedded IrO_x electrodes and Ag/AgCl ISE. All the surfaces were coated with epoxy resin with the exception of the surface of CO_2 ingress.

The potential of the IrO_x electrodes and Ag/AgCl ISE (Fig. 3) was continuously measured versus the embedded Ag/AgCl ISE internal reference electrode. To get accurate measurements, the internal reference electrode was periodically calibrated following the procedure described in section 2.2.1 (analogue for pH gradient). For this experiment, more data can be found in paper IV.

2.3 Algorithm for determination of the electrode potential

2.3.1 Mortar samples exposed to chloride ingress

As described in section 2.2.1, the potential of Ag/AgCl ISEs $E_{Ag/AgCl\ ISE}$, IrO_x electrodes E_{IrOx}, and steel bars E_{steel} (Fig. 2) was continuously measured versus the embedded Ag/AgCl ISE internal reference electrode.

In this experiment, chloride ingress was achieved by putting the sample in contact with simulated pore solution containing chlorides. The gradients in pH were minimized by using simulated pore solution and the calculations were then simplified by considering diffusion potentials only due to chloride gradients, i.e., by assuming constant pH. Thus, the measured electrode potential $E_{measured}$ versus the internal reference electrode (Ag/AgCl ISE RE) can be written as:

$$E_{\text{measured Ag/AgCl ISE}} = E_{\text{Ag/AgCl ISE}}(\text{Cl}^-) + E_{\text{diffusion}}(\text{Cl}^-) - E_{\text{Ag/AgCl ISE RE}} \quad (4)$$

$$E_{\text{measured IrO}_x} = E_{\text{IrO}_x} + E_{\text{diffusion}}(\text{Cl}^-) - E_{\text{Ag/AgCl ISE RE}} \quad (5)$$

$$E_{\text{measured steel}} = E_{\text{steel}} + E_{\text{diffusion}}(\text{Cl}^-) - E_{\text{Ag/AgCl ISE RE}} \quad (6)$$

where $E_{\text{diffusion}}$ is the diffusion potential established due to the difference in chloride concentration at the location of the Ag/AgCl ISE internal reference electrode and the chloride concentration at the working electrode location (IrO_x electrode, Ag/AgCl ISE or steel bar).

The diffusion potential $E_{\text{diffusion}}$ was calculated with the Henderson equation as described elsewhere [8]. For the calculation, it was assumed that the mortar pore solution was composed by 0.15 mol·L^{-1} NaOH 0.2 mol·L^{-1} KOH and sat. $Ca(OH)_2$ (same composition as the prepared solutions simulating the pore solution in the experiment, i.e., contact solution for the measurements with the external reference electrode and solution used for chloride ingress). The mobilites of the involved ions (K^-, OH^-, Ca^{2+}, Na^+, and Cl^-) were obtained from the data reported in aqueous solution [8]. More information on the diffusion potentials in concrete and its evaluation can be found in literature [7, 9-12].

Note that both the potential of the Ag/AgCl ISE and the diffusion potential depend on chloride concentration (Eq. (4)); thus, no closed solution can be given. Because of that, an algorithm, based on an iterative calculation, was used at each time step (Fig. 4). In this calculation, the potential of the Ag/AgCl ISE $E_{\text{Ag/AgCl ISE}}$ was initially determined assuming that $E_{\text{diffusion}}$=0 (initial conditions) and the chloride concentration in this iteration step was then determined from the calibration curve of the Ag/AgCl ISE (Eq. (1)). For this calculation, the concentration of chloride ions was related to the chloride activity through the activity coefficient obtained from [13]. Once the chloride concentration was determined, $E_{\text{diffusion}}$ was calculated and from this, $E_{\text{Ag/AgCl ISE}}$ was recalculated according to Eq. (4). This procedure was repeated until a chloride concentration difference between two consecutive iterations became < 0.01 mol·L^{-1}. Note that the potential of the Ag/AgCl ISE internal reference electrode had been previously calculated when this electrode was calibrated (section 2.2.1).

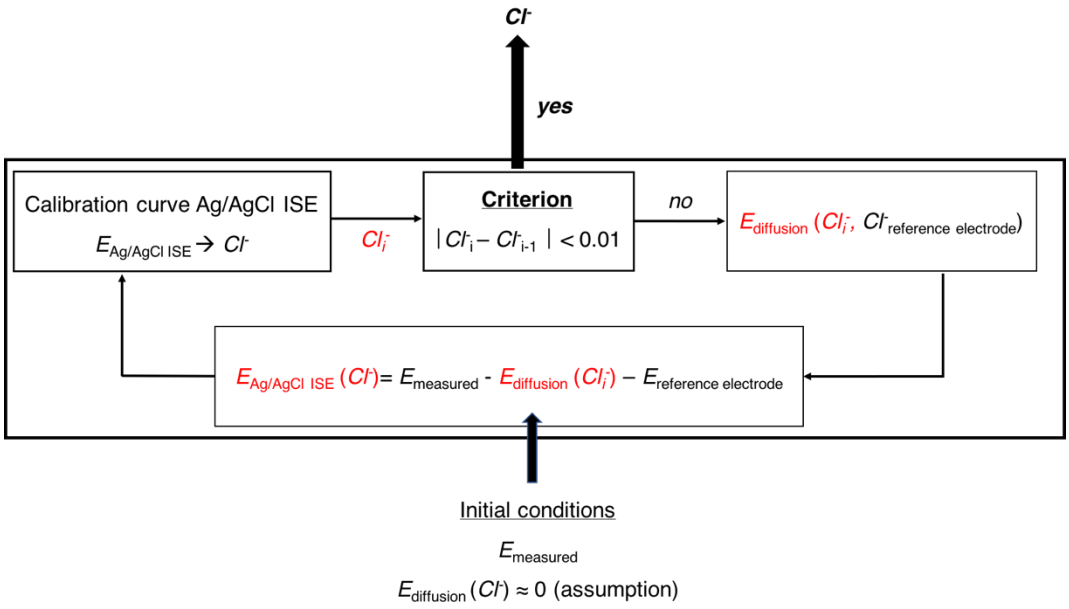

Fig. 4 Representation of the iterative calculation procedure used to determine the chloride concentration at each Ag/AgCl ISE location. The parameters changed in each iteration are indicated in red.

Once the chloride concentration was determined at the given Ag/AgCl ISE location, the potential of the IrO_x electrode and steel bars was determined according to Eqs. (5) and (6) respectively.

2.3.2 Mortar samples exposed to CO_2 ingress

As described in section 2.2.2, the potential of the Ag/AgCl ISE $E_{Ag/AgCl\ ISE}$ and IrO_x electrodes E_{IrOx} (Fig. 3) was continuously measured versus the Ag/AgCl ISE internal reference electrode. For each case, the measured potential $E_{measured}$ can be written as:

$$E_{\text{measured IrO}_x} = E_{\text{IrO}_x}(pH) + E_{\text{diffusion}}(pH) - E_{\text{Ag/AgCl ISE RE}} \quad (7)$$

$$E_{\text{measured Ag/AgCl ISE}} = E_{\text{Ag/AgCl ISE}}(\text{Cl}^-) + E_{\text{diffusion}}(pH) - E_{\text{Ag/AgCl ISE RE}} \quad (8)$$

Note that in this case, diffusion potentials were established between the internal reference electrode and IrO_x electrodes due to differences in chloride concentration (as the mortar with embedded Ag/AgCl ISE contained chlorides, section 2.2.2) and due to pH gradients (due to the progressive carbonation of the cement paste). Diffusion potentials thus varied as the pH of the pore solution changed due to carbonation. The algorithm to determine these diffusion potentials is described in paper IV. Note that the chloride concentration at the Ag/AgCl ISE internal reference electrode had been previously calculated with Eq. (3).

3 Results and discussion

3.1 Embedded IrO_x electrodes and Ag/AgCl ISEs in mortar exposed to chloride ingress

Fig. 5a shows the chloride concentration as a function of exposure time to chloride ingress for the Ag/AgCl ISEs located at each cover depth, together with the calculated chloride concentration at the Ag/AgCl ISE internal reference electrode. Figure 5b shows the chloride concentration as a function of depth for some selected times (6, 49, 82 and 99 days).

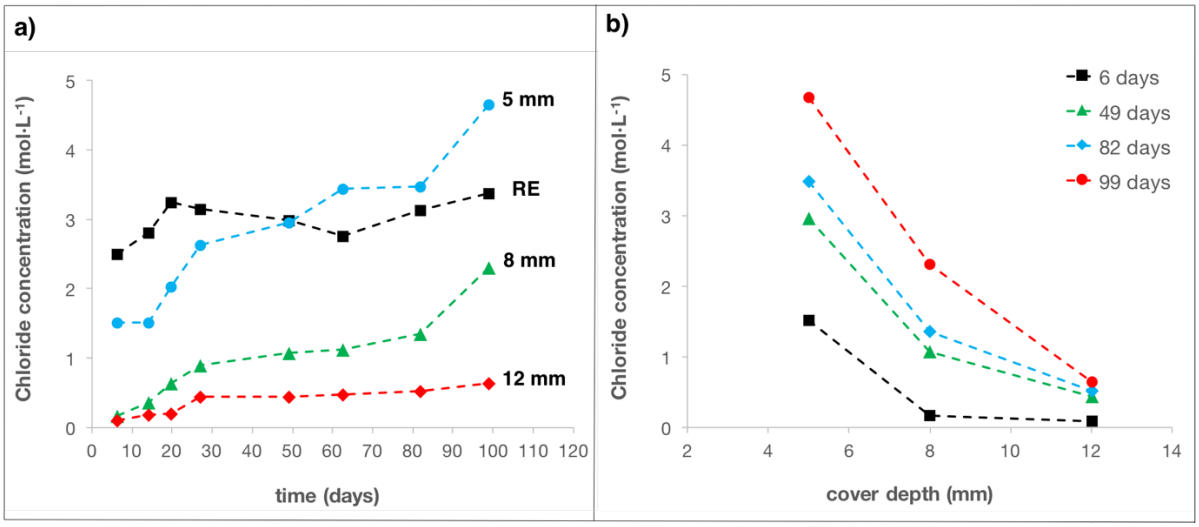

Fig. 5 (a) Chloride concentration as a function of exposure time for the Ag/AgCl ISEs at each cover depth (5, 8 and 12 mm), together with the calculated chloride concentration at the Ag/AgCl ISE internal reference electrode (RE) (b) Chloride concentration as a function of cover depth for some selected times (6, 49, 82 and 99 days)

The chloride concentration increases with time (Fig. 5a) and it is markedly higher for the shallower cover depths (Fig. 5a and Fig. 5b). The marked chloride increase at time>80 days for the electrodes embedded at 5 and 8 mm (Fig. 5) may be due to two reasons: i) the solution containing chlorides that was put in contact with the sample was refilled more often at those exposure times and ii) the assumption of constant pH when calculating chloride concentrations lead to small errors in the calculations (compare section 6.3.5 of the thesis).

The rate of chloride update in this experiment is especially fast and high chloride concentrations are reached at the electrodes located at the shallower depths, e.g., ca. 4 $mol \cdot L^{-1}$ for the electrode embedded at 5 mm; this is probably because the mortar sample used is very porous (w/c=0.5 and 1 week of curing).

The calculated chloride concentration at the Ag/AgCl ISE internal reference electrode oscillates between ca. 2.5 mol·L^{-1} and 3.3 mol·L^{-1}. This difference in concentration corresponds to only ca. 7 mV difference in the measured potential; it is thus possible that it is due to measurement errors or due to the simplifications made in the calculations (compare section 6.3.5 of this thesis). Note that the chloride concentration at this location generally increases over time (Fig. 5a); this may be due to partial drying, e.g., self-desiccation or due to contact with the dry laboratory atmosphere (this effect however should be minimum as the mortar surfaces were either coated or in contact with the chloride solution). These results are in agreement with the results reported in paper V.

Fig 6 shows the potential evolution over exposure time to chloride ingress of the steel bars (Fig. 6a) and of the IrO_x electrodes (Fig. 6b) at each depth (5, 8, and 12 mm).

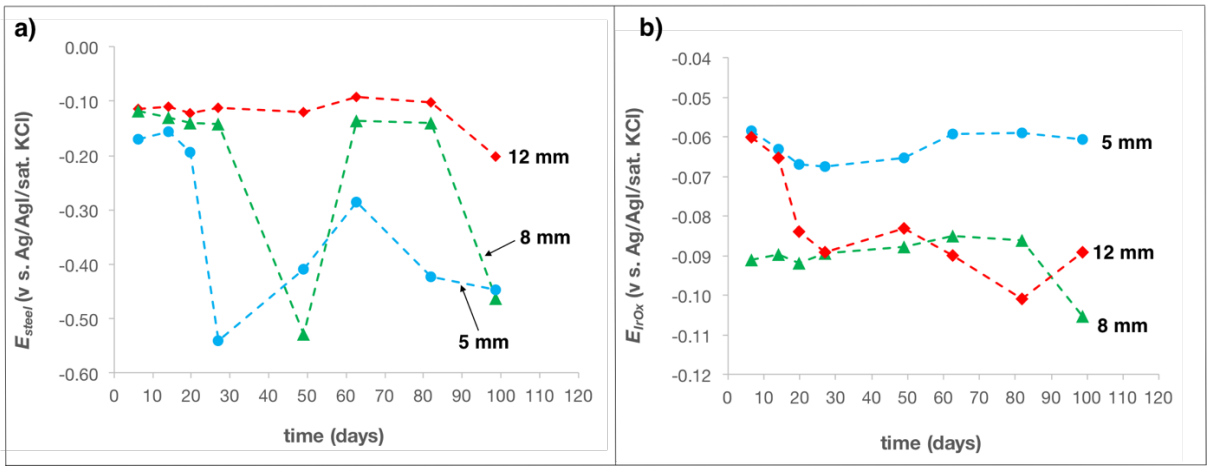

Fig. 6 (a) Steel potential vs. exposure time at each cover depth (5, 8, and 12 mm) (b) IrO_x electrode potential vs. exposure time at each cover depth (5, 8, and 12 mm).

The steel bar embedded at 12 mm exhibits a relatively constant potential (potential change <100 mV) for the whole exposure time. In contrast, the steel bars embedded at 5 and 8 mm exhibit relatively stable potential responses only during the first 20 and 50 days respectively. This corresponds to chloride concentrations below 1 mol·L^{-1} (Fig. 5a). After 20 and 50 days respectively, the potential of the steel bars embedded at 5 and 8 mm oscillates, showing potential differences up to 400 mV. This corresponds to local depassivation and further repassivation [14]. After ca. 60 days, the steel bar embedded at 5 mm depth had decreased significantly, i.e., at least 300 mV from the initial potential value. Such potential differences are related to active corrosion [15]. This corresponds to chloride concentrations above ca. 3.5 mol·L^{-1} (see Fig. 5a). These results are in agreement with the results reported in paper V;

nevertheless, it should be noted that typical chloride concentrations for corrosion initiation are usually below 1 mol·L^{-1} [16]. In this experiment, the steel bars exhibit significant potential oscillations at chloride concentrations of ≈1 mol·L^{-1}; thus, if given enough time, the steel may have a state of active corrosion at this chloride concentration. In any case, it should also be noted that high chloride threshold values are obtained in laboratory setups, e.g., associated with unrealistically good conditions during casting [14].

The potential of the IrO_x electrodes is relatively constant over time (Fig. 6b) and it can thus be concluded that it is independent of the chloride concentration. The highest potential change is observed for the IrO_x electrode embedded at 12 mm depth; the potential decreases ca. 40 mV compared to its initial value. This would correspond to an increase in pH of about 0.5 pH units. It is believed that this pH increase is caused by the chloride binding while chloride ingresses the sample, as reported by Tritthart [17]. This aspect is further explained in section 6.3.5 of the thesis.

3.2 Embedded IrO_x electrodes and Ag/AgCl ISEs in mortar exposed to CO_2 ingress

Fig. 7 shows the potential response of the Ag/AgCl ISE as a function of time in the carbonation chamber (Fig. 7), together with the pH evolution over time in the carbonation chamber. More details regarding the pH evolution over time, calculated with the embedded IrO_x electrodes, can be found in paper IV.

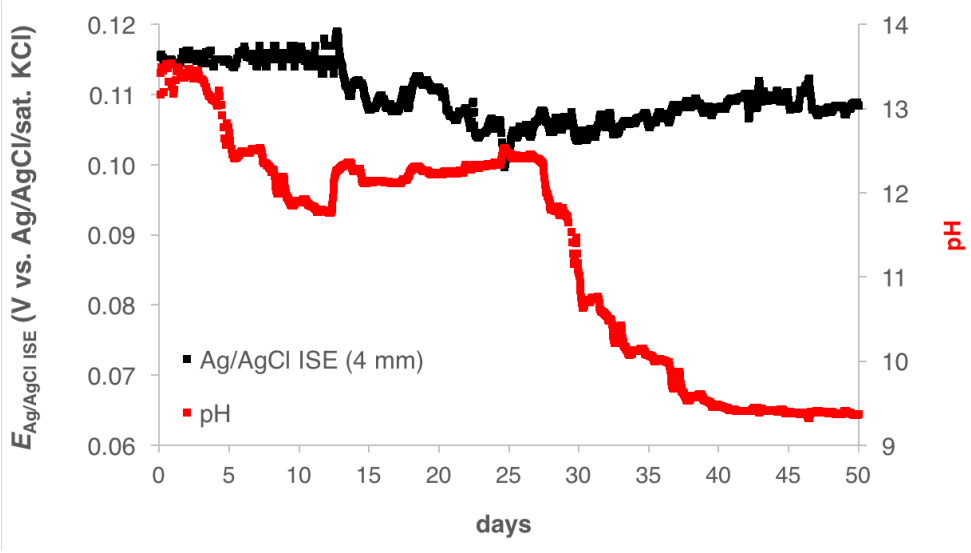

Fig. 7 Potential response of the Ag/AgCl ISE and calculated pH as a function of time in the carbonation chamber

The potential of the Ag/AgCl ISE is relatively constant while pH>12.5 (Fig. 8). In this case, the potential response of the Ag/AgCl ISE indicates a chloride concentration of ca. 0.03 mol·L^{-1}, which would correspond to ca. 0.3% chlorides by mass of cement [18]. It is likely that some chlorides are included in the raw materials, e.g. cement and aggregates, but it should be noted that this value is relatively high compared to the chloride content limit (0.4% chlorides by mass of cement) indicated in the EN 206-1 standard [19]. It is possible that this obtained value is overestimated; this may be due to simplifications made in the calculations (compare 6.3.5 of this thesis) or related to the accuracy of the IrO_x electrodes used, i.e., the error in the calculated pH can be up to 0.5 pH units (paper III), that results in different calculated diffusion and Ag/AgCl ISE potentials (Eqs. (7)-(8)). In order to evaluate the accuracy of the obtained results, a solution would be to determine the total chloride content, e.g., titration or spectrophotometry method [20].

When the pH of the pore solution decreases to ca. pH 12.5 (Fig. 7), the Ag/AgCl ISE potential slightly decreases ca. 12 mV, and it remains relatively constant at ca. 0.110 V (vs. Ag/AgCl/sat. KCl). This potential value corresponds to a chloride concentration of ca. 0.05 mol·L^{-1}. It is likely that this increase in chloride concentration is due to the release of bound chlorides as pH decreases [21, 22].

As indicated in section 6.2 of this thesis, diffusion potentials can significantly change in presence of both chloride and pH gradients. In this case, chloride gradients are relatively small but they may play a more important role in other situations, e.g., when concrete is exposed both to chloride ingress and to carbonation. The release of chlorides due to pH decrease in concrete could be especially important in evaluating the risk of chloride-induced corrosion, as the chloride threshold for corrosion initiation decreases with pH [23-25]. Simultaneous pH and chloride monitoring is thus important.

4 Conclusions

The results reported in this document show that both IrO_x electrodes and Ag/AgCl ISEs exhibit stable potential responses independently of chloride concentration and pH respectively.

Changes in chloride concentration and pH induce diffusion potentials that need to be corrected in order to evaluate properly the individual electrode potential. For that, simultaneous pH and chloride monitoring is important. It has been shown that chloride ingress may induce small changes in the pH of the pore solution and that a decrease in the pH of the pore solution, e.g.,

due to carbonation, may result in an increase in the chloride concentration due to the release of bound chlorides. In the latter case, the accurate electrode potential correction and evaluation becomes even more important, as pH decrease combined with an increase in chloride concentration greatly increase the risk of corrosion initiation.

5 References

1. J. Koryta (1972), Theory and applications of ion-selective electrodes, Anal. Chim. Acta, 61, 329–411. 10.1016/S0003-2670(01)95071-8.
2. L. Shreir (1994), Corrosion control. IN L. Shreir, R. A. Jarman, G. T. Burstein (Eds.) Corrosion, Oxford, Butterworth-Heinemann Ltd.
3. S. Yao, M. Wang, M. Madou (2001), A pH electrode based on melt-oxidized iridium oxide, J. Electrochem. Soc., 148, H29-H36. 10.1149/1.1353582.
4. M. Wang, S. Yao, M. Madou (2002), A long-term stable iridium oxide pH electrode, Sens. Actuators, B, 81, 313-315. 10.1016/S0925-4005(01)00972-8.
5. M. Wang, S. Yao (2003), Carbonate-Melt Oxidized Iridium Wire for pH Sensing, Electroanalysis, 15, 1606-1615. 10.1002/elan.200302723.
6. Y. Seguí Femenias, U. Angst, F. Caruso, B. Elsener (2016), Ag/AgCl ion-selective electrodes in neutral and alkaline environments containing interfering ions, Mater. Struct., 49, 2637–2651. 10.1617/s11527-015-0673-8.
7. U. Angst, Ø. Vennesland, R. Myrdal (2009), Diffusion potentials as source of error in electrochemical measurements in concrete, Mater. Struct., 42, 365-375. 10.1617/s11527-008-9387-5.
8. A.J. Bard, L.R. Faulkner (2001), Electrochemical methods: fundamentals and applications, second ed., New York, Willey.
9. U. Angst, B. Elsener, R. Myrdald, Ø. Venneslanda (2010), Diffusion potentials in porous mortar in a moisture state below saturation, Electrochim. Acta, 55, 8545–8555. 10.1016/j.electacta.2010.07.085.
10. A. Atkinson, A.K. Nickerson (1984), The diffusion of ions through water-saturated cement, J. Mater. Sci., 19, 3068–3078. 10.1007/BF01026986.
11. R. Myrdal (1996), Phenomena that disturb the measurement of potentials in concrete, Corrosion/96, NACE International, Paper No.339.
12. R. Myrdal (1997), Potential gradients in concrete caused by charge separations in a complex electrolyte, Corrosion/97, NACE International, Paper No.278.
13. A. Hidalgo, G.D. Vera, M.A. Climent, C. Andrade, C. Alonso (2001), Measurements of chloride activity coefficients in real portland cement paste pore solutions, J. Am. Ceram. Soc., 84, 3008-3012. 10.1111/j.1151-2916.2001.tb01128.x.
14. U. Angst, B. Elsener, C.K. Larsen, Ø. Vennesland (2011), Chloride-induced reinforcement corrosion: electrochemical monitoring of initiation stage and chloride threshold values, Corros. Sci., 53, 1451-1464. 10.1016/j.corsci.2011.01.025.
15. L. Bertolini, B. Elsener, P. Pedeferri, E. Redaelli, R.P. Polder (2013), Corrosion of steel in concrete, second ed., Weinheim, Wiley.
16. U. Angst, B. Elsener, C.K. Larsen, Ø. Vennesland (2009), Critical chloride content in reinforced concrete - A review, Cem. Concr. Res., 39, 1122-1138. 10.1016/j.cemconres.2009.08.006.
17. J. Tritthart (1989), Chloride binding in cement II. The influence of the hydroxide concentration in the pore solution of hardened cement paste on chloride binding, Cem. Concr. Res, 19, 683-691. 10.1016/0008-8846(89)90039-2.

18. T. Luping, L.O. Nilsson (1993), Chloride binding capacity and binding isotherms of OPC pastes and mortars, Cem. Concr. Res., 23, 247-253. 10.1016/0008-8846(93)90089-R.
19. CEN/TC-104 (2000), EN 206-1 Concrete – Part 1: Specification, performance, production and conformity.
20. DIN, EN 14629 (2007), Produkte und Systeme für den Schutz und die Instandsetzung von Betontragwerken - Prüfverfahren - Bestimmung des Chloridgehalts von Festbeton, Deutsches Institut für Normung, Berlin.
21. J. Geng, D. Easterbrook, Q.-F. Liu, L.-Y. Li (2016), Effect of carbonation on release of bound chlorides in chloride-contaminated concrete, Mag. Concr. Res, 68, 353-363. 10.1680/jmacr.15.00234.
22. S. Goñi, A. Guerrero (2003), Accelerated carbonation of Friedel's salt in calcium aluminate cement paste.pdf, Cem. Concr. Res, 33. 10.1016/S0008-8846(02)00910-9.
23. D.A. Hausmann (1967), Corrosion of steel in concrete. How does it occur?, J. Mater. Prot., 6, 19-23.
24. P. Lambert, C.L. Page, P.R.W. Vassie (1991), Investigations of reinforcement corrosion. 2. Electrochemical monitoring of steel in chloride-contaminated concrete, Mater. Struct., 24, 351-358. 10.1007/BF02472068.
25. C.L. Page, P. Lambert, P.R. Vassie (1991), Investigations of reinforcement corrosion. 1. The pore electrolyte phase in chloride-contaminated concrete, Mater. Struct., 24, 243-252. 10.1007/BF02472078.